Electrophoretic Separations of Small Molecules in Low Diffusion Environment

by

Pavisara Nanthasurasak

Applied Chemistry, B.Sc.

Submitted in fulfilment of the requirements for the degree of

Doctor of Philosophy (Chemical Sciences)

School of Natural Science (Chemistry)

University of Tasmania

June 2019

Statement and Declaration

Declaration of Originality

This thesis contains no material which has been accepted for a degree or diploma by the University or any other institution, except by way of background information and duly acknowledged in the thesis, and to the best of my knowledge and belief no material previously published or written by another person except where due acknowledgement is made in the text of the thesis, nor does the thesis contain any material that infringes copyright.

June 2019

Authority of Access

This thesis may be made available for loan and limited copying and communication in accordance with the Copyright Act 1968.

June 2019

Statement regarding published work contained in thesis

The publishers of the papers comprising Chapter 1 and 3 hold the copyright for that content, and access to the material should be sought from the respective journals. The remaining non- published content of the thesis may be made available for loan and limited copying and communication in accordance with the Copyright Act 1968.

June 2019

Statement of Co-authorship

The following people contributed to the publication of work undertaken as part of this thesis:

- Candidate: P. Nanthasurasak, Australian Research Centre on Separation Science (ACROSS), School of Natural Science – Chemistry, University of Tasmania, Australia.
- M.C. Breadmore, Australian Research Centre on Separation Science (ACROSS), School of Natural Science – Chemistry, University of Tasmania, Australia.
- R.M. Guijt, Centre for Rural and Regional Futures, School of Science, Engineering and Built Environment, Deakin University, Australia.
- H.H. See, Centre for Sustainable Nanomaterials, Ibnu Sina Institute for Scientific and Industrial Research, Universiti Teknologi Malaysia, Malaysia.
- M. Zhang, School of Life and Environmental Sciences, Guilin University of Electronic Technology, Guilin, Guangxi, China.
- J.M. Cabot, ARC Centre of Excellence for Electromaterials Science (ACES), School of Natural Science – Chemistry, University of Tasmania, Australia.

Authors details and roles

Paper 1, "Electrophoretic separations on paper: Past, present, and future – A review" – *referred to in chapter 1*

P. Nanthasurasak (50%), J.M. Cabot (20%), H.H. See (10%), R.M. Guijt (10%), M.C. Breadmore (10%)

- P. Nanthasurasak was a primary author with M.C. Breadmore and R.M. Guijt contributed to the idea and concept of the review as well as providing feedback on the review.
- J.M. Cabot was responsible for all the graphic presentation and provided feedback on the review.

- H.H. See assisted with literature and information gathering and provided feedback on the review.

Paper 2, "In-Transit electroextraction of small molecule pharmaceuticals from blood" – *referred to in chapter 3*

P. Nanthasurasak (70%), H.H. See (5%), M. Zhang (5%) R.M. Guijt (10%), M.C. Breadmore (10%)

- P. Nanthasurasak was a primary author with M.C. Breadmore and R.M. Guijt contributed to the idea and concept of the review as well as providing feedback, and storyline layout of the review.
- H.H. See assisted with extensive details and information gathering regarding the polymer inclusion membrane (PIM) as well as providing feedback on the review.
- M. Zhang provided assisted the candidate on calculations and graphic as well as providing feedback on the review.

List of publications and presentations

Reviews and original articles

1. 'Solid state' electrophoresis

   P. Nanthasurasak, H. See, R. Guijt, M. Breadmore, in 20th International Conference on Miniaturized Systems for Chemistry and Life Sciences, μTAS 2016, 2016, pp. 224-225.

2. Electrophoretic separations on paper: Past, present, and future-A review

   P. Nanthasurasak, J. M. Cabot, H. H. See, R. M. Guijt, M. C. Breadmore, Anal. Chim. Acta. 2017, 985, 7-23.

3. "In-Transit electroextraction of small molecule pharmaceuticals from blood"

   P. Nanthasurasak, H.H. See, M. Zhang, R.M. Guijt, M.C. Breadmore, In-Transit Electroextraction of Small-Molecule Pharmaceuticals from Blood, Angewandte Chemie International Edition, 58 (2019) 3790-3794.

Presentations at domestic and international conferences (presented author underlined)

1. "Solid-state" electrophoresis

   P. Nanthasurasak, H. See, R. Guijt, M. Breadmore, ***Oral presentation****, the 20th International Conference on Miniaturized Systems for Chemistry and Life Sciences (μTAS 2016), Dublin, Ireland, October 9th – 13th, 2016.*

2. Polymer inclusion membrane as solvent-free platform for electrophoresis

   P. Nanthasurasak, H. See, R. Guijt, M. Breadmore, ***Oral presentation****, The 16th Asia-Pacific International Symposium on Microscale Separations and Analysis (APCE 2016), Johor Bahru, Malaysia, November 7th – 10th, 2016.*

3. Polymer inclusion membrane as solvent-free platform for electrophoresis

   P. Nanthasurasak, H. See, R. Guijt, M. Breadmore, ***Oral presentation****, ACROSS International Symposium on Advances in Separation Science (ASASS 2), Tasmania, Australia, November 30th – December 2nd, 2016.*

4. "Solid state" electrophoresis

P. Nanthasurasak, H. See, R. Guijt, M. Breadmore, ***Oral presentation****, The 33rd International Symposium on Microscale Separations and Bioanalysis (MSB 2017), Noordwijkerhout, The Netherlands, March 26th- 29th, 2017.*

5. Polymer membranes for electrophoretic separations

   P. Nanthasurasak, H. See, R. Guijt, M. Breadmore, ***Oral presentation****, The 8th Australian New Zealand Nano-Microfluidics Symposium (ANZNMF 2017), Tasmania, Australia, June 26th – 29th, June 2017.*

6. Sending a SMS: Snail-mail Separations

   P. Nanthasurasak, H. See, R. Guijt, M. Breadmore, ***Oral presentation****, The 25th Annual Royal Australian Chemical Institute Research and Development Topics Conference (R&D Topics 2017), Tasmania, Australia, December 3rd – 6th, 2017.*

7. "Snail mail separations" - A portable, battery powered and solvent-less platform for electrophoresis

   P. Nanthasurasak, H. See, R. Guijt, M. Breadmore, ***Oral presentation****, The 9th Australian New Zealand Nano-Microfluidics Symposium (ANZNMF 2018), Auckland, New Zealand, June 27th – 29th, June 2018.*

8. "Snail Mail Separations (SMS)" - A Through-Mail Portable, Battery-Powered and Solvent-Less Platform for Electrophoresis

   P. Nanthasurasak, H. See, R. Guijt, M. Breadmore, ***Poster presentation****, the 22th International Conference on Miniaturized Systems for Chemistry and Life Sciences (µTAS 2018), Kaohsiung, Taiwan, November 11th – 15th, 2018.*

Statement of Ethical Conduct

The research associated with this thesis abides by the international and Australian codes on human and animal experimentation, the guidelines by the Australian Government's Office of the Gene Technology Regulator and the rulings of the Safety, Ethics and Institutional Biosafety Committees of the University.

June 2019

We the undersigned agree with the above stated “proportion of work undertaken” for each of the above published (or submitted) peer-reviewed manuscripts contributing to this thesis:

Signed:

Prof. Michael C. Breadmore

Supervisor

School of Natural Sciences

University of Tasmania

Date: 4 June 2019

Signed:

Prof. Mark Hunt

Dean

School of Natural Sciences

University of Tasmania

Date: 4 June 2019

Acknowledgements

First, I would like to express my deepest gratitude to Professor Michael Breadmore for giving me an opportunity to be one of his students and conducted this exciting research with him. I am very grateful not only for his creative ideas and guidance on my research but also for his humour, making my PhD journey at UTAS enjoyable. This thesis and degree would not have been successful without his kind supervision, support, and patience.

Furthermore, I would also like to deeply appreciate my co-supervisors, Professor Rosanne Guijt, Prof. Hong Heng See, and Prof. Min Zhang, for all the guidance and support alongside with Professor Michael Breadmore. Thanks to Prof. Hong Heng who initiated and originated this research with his expertise in membrane science as well as his continuous optimistic encouragement. Prof. Min Zhang, with his technical skill in electrochemistry, assisted me for the data validation and calculation and all electronic involvement in this work. Other than professionally guided me on my research, Professor Rosanne Guijt also mentally uplifted me with her kind spirit and cheerful character.

Most importantly, I would never able to show enough gratitude to my family who has been a very strong mental support to me. Their strong encouragement has been a powerful driving force for me in steps to complete my degree.

Additionally, I would like to also forward my gratitude to these following people:

- Dr. Sui Ching Phung and Dr. Soo Hyun Park, my officemates and best friends, for their warm welcome since the first day I have joined the office, giving me a friendly working environment every day and an invaluable friendship. Together with their experience with electrophoresis, their knowledge also helped me troubleshooting the problems with electrophoresis experiments.

- Dr. Petr Smejkal for his specialized technical skill in engineering and instrumentations, helping me in instrument and/or device designing build-up.
- Associate Professor Lito Joselito Quirino, for allowing us to use his high voltage supply, LabSmith HVS448-6000D for all the electrophoresis experiment performed in the laboratory throughout my last year of my PhD.
- Dr. William (Alex) Donald and Miss Liang Jiang, principal investigator and master student in Donald research group – Fundamental and Applied Mass Spectrometry at University of New South Wales (UNSW) Sydney, for their kindness in helping us with characterization and detection of pharmaceutical molecules on electrophoretic platform with Matrix Assisted Laser Desorption Ionization-Time of Flight Mass Spectrometry (MALDI-TOF).
- Dr. Joan Marc Cabot Canyelles for his interest in my research, together with his knowledge in different factors influencing electrophoretic separation performances, he kindly gave me advice and explanation on basic chemistries which was very helpful to my project.
- Mr. Liang Chen, together with Dr. Joan Marc Cabot Canyelles, for their help on characterization and detection of pharmaceutical molecules on electrophoretic platform with Desorption Electrospray Ionization-Mass Spectrometry (DESI-MS).
- Dr. Umme Kalsoom for her help with operation and data interpretation of Nitrogen adsorption characterization technique for determination of PIM porosity.
- Staffs from the Central Science Laboratory (CSL), University of Tasmania including Dr. Thomas Rodemann for Fourier Transform Infrared Spectroscopy (FT-IR) and Raman Spectroscopy, Dr. Karsten Goemann and Dr. Sandrin T. Feig for Scanning Electron Microscopy (SEM) for PIM characterizations.
- My colleagues in Professor Michael's Chippers and CEers group not only for their kindness in sharing their thoughts and discussion related to my research but also their precious friendship.
- All academics and colleagues from Australian Research Centre for Separation Science (ACROSS) for research facilities, support, advice, and ideas relating to my research.

- University of Tasmania for financial scholarships, Tasmania Graduate Research Scholarship (TGRS) and Dr. Ralph Bick Research Scholarship, which allowing me to start and complete my degree as well as living comfortably in Australia during my candidature.

List of Abbreviations and symbols

[EMIM][NTf_2]	1-ethyl-3-methylimidazolium bis(trifluoromethylsulfonyl)imide
2-DE	Two-dimensional electrophoresis
2-NPOE	Nitrophenyl octyl ether
3D	Three-dimensional
4-HCCA	α-Cyano-4-hydroxycinnamic acid
AF488	Alexa flour 488
AIDS	Acquired Immune Deficiency syndrome
Aliquat®336	Trioctylmethyl ammonium chloride
ART	Antiretroviral treatment
ATR	Attenuated total reflectance
BC	Berberine chloride
BDAC	Bisoctyldimethyl ammonium Chloride
bDNA	Branched DNA
BSA	Bovine serum albumin
BTAB	Butyltrimethyl ammonium bromide
BTAC	Butyltrimethyl ammonium chloride
BW	Buffer waste
C^4D	Capacitively coupled contactless conductivity detection
CA	Cellulose acetate
CAE	Capillary array electrophoresis
CB	Chelation boundary
CE	Counter electrode / Auxiliary electrode
CE	Capillary electrophoresis
CE-MS	Capillary electrophoresis-Mass spectrometry
cm	Centimetre
CNF	5(6)-Carboxynaphthofluorescein
CTA	Cellulose triacetate

CTAB	Cetyltrimethyl ammonium bromide
Cyanex 302	Bis (2,4,4-trimethylpentyl) monothiophosphinic acid
Cyanex 923	Trialkyl-phosphine oxides
CYPHOS® IL 104	Trihexyl(tetradecyl)phosphonium bis(2,4,4-trimethylpentyl)phosphinate
CZE	Capillary zone electrophoresis
D2EHPA	Di(2-ethylhexyl) phosphoric acid
Da	Dalton/Atomic mass unit
DBP	Dibutyl phthalate
DBS	Dried blood spot
DCM	Dichloromethane
DDAC	Didecyldimethyl ammonium chloride
DHB	2,5-dihydroxy benzoic acid
DI	Deionized water
DISC	Discontinuous electrophoresis
DNA	Deoxyribonucleic acid
DOP	Dioctyl phthalate
DoTAC	Dodecyltrimethyl ammonium Chloride
DTAB	Decyltrimethyl ammonium bromide
DTAC	Decyltrimethyl ammonium chloride
EDTA	Ethylenediaminetetraacetic acid
ELISA	Enzyme Linked Immunosorbent Assay
EME	Electromembrane extraction
EOF	Electroosmotic flow
FASS	Field-amplified sample stacking
FDA	Food and Drugs Administration
FESEM	Field emission analytical scanning electron microscope
FITC	Fluorescein Isothiocyanate
FT-IR	Fourier-transform infrared spectroscopy
g	Gram

GCE	Gel capillary electrophoresis
GDH	Glucose dehydrogenase
H	Height
HCCD	Chlorinated cobalt dicarbollide
hCG	Human chorionic gonadotropin
HEPES	4-(2-hydroxyethyl)-1-piperazineethanesulfonic acid
HIV	Human immunodeficiency viruses
HPLC	High performance liquid chromatography
HPLC-MS	High performance liquid chromatography-Mass spectrometry
HQ	8-hydroyquinaldine
Hr	Hour
i.d.	Internal diameter
IATA	International Air Transport Association
ICP	Ion concentration polarization
IEF	Isoelectric focussing
IMS	Ion-mobility spectroscopy
IPG	Immobilized pH gradient
IR	Infrared spectroscopy
ISE	Ion selective electrode
ITO	Indium tin oxide
ITP	Isotachophoresis
kV	Kilovolt
LC-MS	Liquid chromatography-Mass spectrometry
LE	Leading electrolyte
LFA	Lateral flow assay
LM	Liquid membrane
M	Mega
m	Metre
m/z	Mass per charge ratio

MALDI-TOF	Matrix assisted laser desorption/ionization-time of flight mass spectrometry
mbar	Millibar
MBE	Moving boundary electrophoresis
MCB	Moving chelation boundary
MEKC	Micellar electrokinetic chromatography
min	Minute
mL	Millilitre
mm	Millimetre
N/A	Not applicable
nm	Nanometre
NMR	Nuclear magnetic resonance
NTP	3-nitrophenol
o.d.	Outer diameter
o-NPPE	*o*-nitrophenyl pentyl ether
OTAB	Octyltrimethyl ammonium bromide
OTAC	Octyltrimethyl ammonium chloride
OTC	Over the counter
PAGE	Polyacrylamide gel electrophoresis
PDMS	Polydimethylsiloxane/Dimethicone
pI	Isoelectric point
PIM	Polymer inclusion membrane
PLA	Polylactic acid
pME	Paper-based microchip electrophoresis
PMMA	Polymethyl methacrylate
PMT	Photomultiplier tube
POC	Point-of-care / Point-of-collection
ppm	Part per million
PSI	Paper spray ionization
PTFE	Polytetrafluoroethylene

PVC	Polyvinyl chloride
PVP	Polyvinylpyrrolidone
R123	Rhodamine 123
R6G	Rhodamine 6G
RB	Rhodamine B
RE	Reference electrode
RNA	Ribonucleic acid
RTIL	Room temperature ionic liquid
s	Second
SDCS	Sodium decyl sulphate
SDCSF	Sodium decyl sulfonate
SDS	Sodium dodecyl sulphate
SEM	Scanning electron microscopy
SLC	Sodium laurate
SNC	Sodium nonanoate
SOC	Sodium octanoate
SOS	Sodium octyl sulphate
SOSF	Sodium octyl sulfonate
SPE	Solid polymer electrolyte
SW	Sample waste
TDM	Therapeutic drug monitoring
TE	Terminating electrolyte
TEHP	Tris(2-ethylhexyl) phosphate
TFA	Trifluoro acetic acid
TGA	Thermogravimetric analysis
TLC	Thin layer chromatography
Tris	Tris(hydroxymethyl)aminomethane
UV	Ultraviolet
V	Volt

VL	Viral load testing
vs	Versus
WE	Working electrode
WHO	World Health Organization
ZE	Zone electrophoresis
µL	Microlitre
µm	Micrometre
µPAD	Microfluidic paper-based analytical device
µTAS	Micro total analysis systems
"	Inch
°C	Degree Celsius
µ	Electrophoretic mobility
S_{BET}	Surface area
Vp	Pore volume
α	Alpha
β	Beta
γ	Gamma
λ	Wavelength
Ω	Ohm

Abstract

Portable analytical devices have been sought after heavily to support clinical diagnostics in lack-of-resource areas where access of advanced medical devices and specialists are restricted. Even though there are many commercially available portable Point-of-care (POC) devices allowing easy and rapid self-diagnostic, these POC were developed for generic infectious diseases such as diabetes or HIV and are not yet made for many common life-threatening disorders. In these cases, portable sample collection devices, such as Guthrie card, are employed for collection of biological samples including blood, urine, or saliva from patients off-hospital then the samples are sent to the centralized laboratory for analysis. However, several post-processing steps of the collected samples (i.e. extraction) upon arrival are required prior to the analysis and these are time-consuming steps that delay the turn-around-time of the result.

Electrophoresis, separation of molecules under application of electric field, is a powerful analytical and sample preparation technique mostly utilized in clinical diagnostics to isolate components in samples ready for analysis. Recently, there has been a large number of developments with electrophoresis into miniaturized formats; however, they are not yet fully integrated with a high voltage power supply and liquid electrolytes are needed to perform separation making it unsuitable as portable diagnostic device. In attempt to bring forward a practical platform for clinical sample collection and sample preparation, the main goal of this thesis is to create a portable electrophoretic platform capable of performing solvent-free electrophoresis under relatively low voltage addressing issues found in conventional clinical diagnostics and electrophoresis. In this research, a polymer inclusion membrane (PIM) embedded with a carrier was investigated as a separation medium for electrophoresis for the first time.

In chapter 2, PIM casting, dimension design, and electrophoresis apparatus are reported. A thin PIM was employed in this research in a lateral strip and electromigration studies

were performed of fluorescent dyes with different charges including Coumarin 334, Fluorescein, and Rhodamine 6G (R6G) as neutral, anionic, and cationic analytes, respectively. The electromigration was monitored and recorded using a portable fluorescence microscope. Three main components of PIM – cellulose triacetate (CTA) as polymer base, 2-nitrophenyl octyl ether (2-NPOE) as plasticizer, and 1-ethyl-3-methylimidazolium bis(trifluoromethylsulfonyl) imide ([EMIM][NTf_2]) as carrier – were optimized as the ratios were found to impact on the migration distance and the spot shape of the dyes. Under a voltage of 2000 V (500 V/cm), only migration of cationic R6G was observed in this PIM leading to further investigation of electrophoresis of several cationic dyes. Successful electrophoretic separation of cationic dyes then allowed the electrophoretic mobilities and diffusion constants to be estimated for each species. Additionally, physical characterization of the PIM and possible mechanism of electromigration were also elucidated.

Chapter 3 focuses on the potential of the PIM-based electrophoretic platform being useful in clinical application in the form of a portable electrokinetic device performing separation, as sample preparation, at low voltage while being transited to a central laboratory eliminating additional steps needed upon arrival. A positively charged alkaloid, Berberine chloride (BC), was used as a model analyte resembling small molecule pharmaceuticals spiked into the whole blood sample. Laboratory-based experiments revealed electromigration of BC but not dried drop of blood resulting in successful separation of BC from the blood matrix. To pursue the concept of in-transit separation, the PIM strip was fully assembled into a pocket-sized device with plastic housing equipped with two commercial batteries generating 6 V/cm (24 V) potential for separation. Separation real-time during transit was demonstrated by sending a portable device containing spiked BC in whole blood via internal mail and the analysis was performed once returned.

To investigate PIM selectivity towards anions, a different ionic liquid, Aliquat®336, was investigated as a carrier in chapter 4. It was found that not only electromigration of anionic species

was observed but neutral molecules also migrated presumably from heteroconjugation. The tunability of the PIM was further investigate using several cationic surfactants with a similar chemical structure to Aliquat®336, with different number of carbon units, number of chains, chain length and counter anions, as carriers and their influence on electromigration and selectivity of dyes were investigated. While most of the cationic surfactants were found to have similar selectivity towards anionic molecules to Aliquat®336, anionic surfactants investigated revealed selectivity towards cationic species similar to that observed with [EMIM][NTf_2].

In the last chapter, the possibility of integrating Matrix-assisted laser desorption ionization-time of flight mass spectrometry (MALDI-TOF) for detection of in-transit electrokinetic separations was explored. The experiment was performed to extend the applicability to non-coloured analytes as well as demonstrating for more powerful practical workflow allowing upon-arrival detection without additional labelling or derivatizing of analytes. PIM after in-transit separation was detached and taped on conductive Indium Tin oxide glass slide before being spray-coated with matrix α-Cyano-4-hydroxycinnamic acid (4-HCCA) and scanned using MALDI imaging. Colour intensity profile and distribution of BC molecules after electrophoretic separation from whole blood sample were graphically displayed in such case where the electrophoretic migration distance was unknown. The results showed promising potential for MALDI-TOF to be employed as detection method for in-transit electrokinetic platform concept where non-coloured analytes can be analyzed.

Table of contents

Table of contents (cont.)

Table of contents (cont.)

Table of contents (cont.)

Table of contents (cont.)

Table of contents (cont.)

Chapter 1

Introduction and Literature Review

1.1 History and evolution of electrophoresis

Many have recognized the breakthrough of electrophoresis –the migration of charged molecules in solution under the influence of electric field – from Tiselius's moving boundary electrophoresis (MBE) designed for separating components of blood plasma during 1930-1937 [1-5]. However, in 1807 by Ferdinand Frédérick Reuss, a Russian army officer, was the first to observe what is known today as electroosmotic flow (EOF) and the electrophoretic migration of charged colloidal particles from the clay solution in his U-tube under a microscope [5-8]. Even though there were many developments during the period between 1807-1930, the development of quartz U-tube with optical UV photography apparatus by Tiselius was proven as the most significant not only because of the technical apparatus but also the identification of four components in plasma, namely albumin, α-globulin, β-globulin, and γ-globulin [2, 5, 6]. Table 1.1 presents the chronological key events and/or developments contributing to modern electrophoresis from its origin.

Despite being the most innovative and practical technologies during this time, there were some drawbacks not only in term of labour and cost but also separation efficiency. The equipment was as large as five feet high and twenty feet wide and each assembly, especially the photography lens, Schlieren, used as detection component, was very expensive resulting in overall high cost to operate and maintain the instrument [3, 9]. Separation efficiency-wise, since Tiselius's MBE was dealing with large macromolecules in free solution by observing the movement and direction boundary, only two ends of the boundary representing the fastest and slowest molecules could be detected and partially collected as separation between the components could not be achieved. The boundaries observed were also very prone to be affected by the heat convection from the use of electric field causing it to become blurry once the component started to migrate; thus, impeding resolution [2, 4, 5, 7, 10]. To improve both the instrumentation and the efficiency,

an approach of having a “supporting medium” for electrophoresis was introduced as it was believed to be able to suppress the electrical convection and dispersion [6]. Cellulose in the form of filter paper, believed to be inspired from paper chromatography, was one of the very first supporting materials used for electrophoresis, not only was it cheap and small compared to the Tiselius’s apparatus but also simpler to prepare, operate, and visualise [5, 10, 11]. The very first report of electrophoresis on paper used a strip moistened with electrolyte, published in 1939 by Von Klobuzitsky and König, separating a yellow pigment in snake venom [7, 12]. Within about a decade, paper had been sufficiently improved and developed that a paper electrophoresis system was commercially available [13]. However, persisting issues of paper media were also being reported. Joule heating not only posed the risk of serum protein denaturation, but it also prohibited the separation from being conducted with a high voltage which would reduce analysis time. Electroosmotic flow of the bulk solution together with adsorption of proteins on the paper was found to cause tailing of detected bands or sometimes completely forbid mobility of the zones. Difficulty in sample loading into a defined narrow band was also mentioned as one of the drawbacks of paper due to diffusion decreasing the separating resolution [10, 13, 14]. Consequently, paper was slowly replaced by other supporting materials including glass powder [2, 15], agar gel [16], agarose gel [17, 18], starch gel [19], and polyacrylamide gel [20, 21]. Starch gel and polyacrylamide gel electrophoresis (PAGE) were the two most outstanding for electrophoresis as not only better separation was achieved compared to paper, but the separation of same charged proteins by size due to the sieving feature of the matrix was also observed during resulting in development of standard procedures for serum proteins and macromolecules [11, 13].

At the same time, the principle ion-mobility spectrometry (IMS) was also introduced by McDaniel as the first electrophoresis is gaseous media. The apparatus was coupled with a mass spectrometer designed to study the mobility of ions and molecules in the drift tube under electric field [22]. By mid to late 1960s, the popularity of paper electrophoresis began to fade as persisting issue of the system being only partial quantitative technique and new developments and

technologies were proposed to resolve the problems and gel-based electrophoresis remained in favoured for clinical practices for serum proteins [2]. Many other researchers continued to improve polyacrylamide gel with additional modifications such as the use of heterogeneous buffer system, named discontinuous electrophoresis or DISC in the 1960's, also known today as isotachophoresis (ITP) [23, 24]. Another successful modification made to PAGE was the use of sodium dodecyl sulphate (SDS) as an additive to the gel base for protein size estimation. This was based on a previous report on the possibility of protein sizing in starch gel in 1955 and the relationship between the molecular weight of the proteins and their mobilities in the gel media [25, 26]. Later, the improvement was made towards the two-dimensional electrophoresis (2-DE) combining isoelectric focussing (IEF), where the proteins were separated based on their charges, and SDS-PAGE, where proteins were separated based on their sizes [27]. By late 1970s, PAGE was exploited for the first time in determination of nucleotides in DNA which become a signature method for DNA sequencing today [28].

Alongside with developments of electrophoresis with supporting medium, free solution electrophoresis based on Tiselius's apparatus was still receiving some attention despite the pitfall in unresolved boundaries. Hjertén contributed to the new concept micro-moving boundary electrophoresis, the origin of modern-day capillary zone electrophoresis (CZE), involving the use of 1-3 mm (i.d.), horizontally rotating quartz capillary for a smaller and simpler to operate apparatus [29]. With a much smaller diameter, the convection was greatly reduced; therefore, not only more discrete boundaries or bands could be observed but it also allowed analysis of more dilute solutions, faster analysis times and higher voltage [2]. Hjertén also investigated and reported further reduction of electroosmotic flow within the capillary by coating the inner wall with a layer of polymer [29]. After the publications, it was quickly applied, by other researchers, for further study of ZE, Isoelectric focusing (IEF) and ITP throughout 1970s with the main focus in designing smaller i.d. of the capillary with the smallest i.d. reported to be 250 μm [2, 30]. In 1981, outstanding progress was reported by Jorgenson with steps to manufacture flexible, open tubing made from

borosilicate, fused silica, and Teflon with polymer protective coating with i.d. as small as 75 µm [31-33]. Variances and interfaces of CZE then started to grow rapidly including gel capillary electrophoresis (GCE) [34], micellar electrokinetic chromatography (MEKC) [35], coupling of capillary electrophoresis with mass spectrometry (CE-MS) [36].

While development of CE from the 1980s was blooming with publications, miniaturization of the system continued. In 1992, Manz and his team pioneered a concept with CE integrated on a glass chip, so-called Micro Total Analysis Systems (µTAS), which is considered a frontrunner of current microchip technology [37]. With this concept, necessary steps such as sample loading and transferring, chemical reaction, separation, and detection are performed simultaneously on a single platform. CE was transformed from long, open tubes into micro channels (approximately 30 µm) by etching the glass chip in which they successfully demonstrated electrophoresis of six fluorescent-labelled amino acids with optimal separation efficiency with lower voltage, shorter analysis time and smaller platform dimension [38]. After the breakthrough, many researchers and companies applied the concept of µTAS together with some improvement of various materials used for the chip until today; for example fused quartz [39], ceramic [40], plastic and polymer [41, 42], paper [43] and 3D printed materials [44] allowing for simpler and cheaper fabrication, flexibility of complex designs and application towards of point-of-care testing (POC) [14].

Considering variety of materials employed for µTAS concept, paper was known as one of the oldest and cheapest substrates used as supporting materials in electrophoresis [45-47]. With the research aim for electrophoresis in low diffusion environment together with expected end result of a platform complying with µTAS concept, reappearance of paper media developed in the form of µPADs was motivating. Hence, electrophoretic separation performed on paper media from past to present was extensively reviewed to better understand the evolution of existing technology and its potential for further development.

Table 1.1. Chronological history of electrophoresis

Year	*Researcher(s)*	*Key event(s) and/or development(s)*
1807	F.F. Reuss	Discovered electrophoresis from migration of clay colloid in water solution
		Discovered of EOF from migration of water in opposite direction
1892	H. Picton and S.E. Linder	Migration of inorganic colloids and hemoglobin in U-tube
1899	W.B. Hardy and W.C.D. Whetham	Migration of globulin and denatured proteins and observed the tunable apparent charge under suitable conditions
1905	W.B. Hardy	Study of migration of globulin in different solution conditions in U-tube
1909	L. Michaelis	Measured the migration of proteins and enzymes in different pH to determine their isoelectric point (pI)
1912	K. Ikeda and S. Suzuki	Discovered the basis of IEF of amino acids in membrane-separated electrophoresis chambers
1923	J. Kendall and E.D. Crittenden	Separation of rare earths metal isotopes by "ion migration method"
1928	J. Kendall	Improved ion migration method for separation of isotopes using colour spacer ions
1929	H.A. Abramson	Investigated the migration velocity of red blood cells in different mammals
1936	H.A. Abramson and L.S. Moyer	Estimation of surface electrical charges of mammalian red blood cells
1930	A.W.K. Tiselius	Discovered the MBE for separation of serum proteins in U-tube
1937	A.W.K. Tiselius	Improved U-tube apparatus for separation of serum proteins
1937	P. König	The first report on paper electrophoresis (published in foreign journal)
1939	T.B. Coolidge	Separation of proteins using column packed with ground glass wool
1939	L.G. Longsworth *et al.*	Improved Tiselius's U-tube apparatus and reported changes in protein patterns for nephritis-containing serum proteins
1939	H.H. Strain	First combination of electrophoresis and column chromatography for separation of coloured organic mixtures
1939	D. Von Klobusitzky and P. König	Paper electrophoresis for separation of yellow pigment in snake venom
1946	R. Consden *et al.*	First report on electrophoresis of small ions in silica jelly - "ionophoresis"
1948	T. Wieland and E. Fischer	Reported the use of paper electrophoresis for analysis of serum proteins and peptides
1949	L. Pauling *et al.*	Reported protein patterns using electrophoresis of serum proteins for sickle cell anaemia
1950	A.H. Gordon *et al.*	Electrophoresis of proteins in agar jelly

Year	*Researcher(s)*	*Key event(s) and/or development(s)*
1950	H. Haglund and A.W.K. Tiselius	Proposed electrophoresis apparatus with glass column packed with glass powder
1953	P. Grabar	First immune-electrophoresis in agar gel slab
1953	Beckman, Inc	First manufactured and sold commercial paper electrophoresis prototyped by Durrum
1954	A. Kolin	Applied the principle of IEF using artificial pH gradient for separation and concentration of proteins
1955	O. Smithies	Separation of serum proteins using starch gel
1956	R.L. Markham	First planar 2-DE of proteins in serum and urine on paper strip
1957	J. Kohn	Modified cellulose - Cellulose acetate sheet as a supporting media for electrophoresis of hemoglobin
1958	M.D. Poulik and O. Smithies	2-DE combining paper and starch gel medium for separation of human serum
1959	O. Smithies	Observed the possibility of proteins sizing in the starch gel
1959	S. Raymond and L. Weintraub	Introduction of PAGE using polyacrylamide gel as a support for zone electrophoresis of serum proteins
1961	S. Hjertén	First report of using agarose gel as a support for electrophoresis
1961	H. Svensson	Introduced various carrier ampholytes for proteins IEF
1962	E.W. McDaniel	Invented IMS - electrophoresis of ions in gas phase
1964	L. Ornstein	First report of using discontinuous electrolytes (DISC) for proteins separation in polyacrylamide gel
1964	R. Bachvaroff and P.R.B. McMaster	First electrophoresis of microsomal RNA in agar gel
1967	A.L. Shapiro	Modified PAGE with SDS and estimated the relationship between molecular size and migration of proteins
1967	S. Hjertén	Introduced "free zone electrophoresis" with 3mm i.d. rotating quartz capillary
1969	G. Dale and A.L. Latner	Combined IEF and PAGE for analysis of native serum proteins
1970	U.M. Laemmli	Developed a standard protocol for DISC electrophoresis for proteins
1974	L. Arlinger	First commercial automated ITP instrument manufactured by LKB Produkter
1975	P.H. O'Farrell	Combined IEF and SDS-PAGE for separation of proteins
1977	F. Sanger *et al.*	First electrophoresis of DNA on acrylamide gel - DNA sequencing
1977	L. Anderson and N.G. Anderson	First human plasma proteome map by 2-DE

Year	*Researcher(s)*	*Key event(s) and/or development(s)*
1979	F.E.P. Mikkers *et al.*	Electrophoresis using 0.2 mm i.d. polytetrafluoroethylene (PTFE) tube - high performance capillary electrophoresis (HPCE)
1981	J.W. Jorgenson and K.D. Lukacs	High voltage CZE with 75 µm i.d. open tubular glass capillary and on-tube detection
1982	B. Bjellqvist *et al.*	Introduced the immobilized pH gradient (IPG) "immobilines" for proteins separation
1983	S. Hjertén	Using gels as sieving matrices in capillary electrophoresis - Capillary gel electrophoresis (CGE)
1984	S. Terabe *et al.*	Developed MEKC as variant of CZE
1987	J.A. Olivares *et al.*	Introduced online CE-MS
1992	A. Manz *et al.*	First miniaturization of CE with planar chip technology - µTAS
1992	X.C. Huang	DNA sequencing using Capillary Array Electrophoresis (CAE)
1993	D.J. Harrison *et al.*	First µTAS electrophoresis of amino acid on glass microchip
1995	S.C. Jacobson	Fabrication and electrophoresis of metal complex on fused quartz microchip
1997	C.S. Effenhauser *et al.*	Analysis of single DNA molecules with integrated CE on PDMS microchip
1999	C. Heller	Electrophoresis of DNA using CZE with polymer matrix
1999	C.S. Henry *et al.*	µTAS electrophoresis using a microchip made from ceramic
2007	A.W. Martinez *et al.*	Recurrence of paper substrate for miniaturized microfluidic device - Microfluidic Paper-Based Analytical Devices (µPAD)
2014	L. Ge *et al.*	First electrophoretic separation on µPAD with on-device wireless electrogenerated detection
2016	K. Adamski *et al.*	CGE for DNA separation on 3D-printed microchip

1.2 Past, present, and future of paper-based platform for electrophoresis

Declaration: this section contains text which has been published in a review with the contribution for the published works was listed in the statement of co-authorship. Changes including paragraph layouts, numbering, and fonts are modified from original review paper to fit the format of this thesis. Minor adjustment to the content was made to link different sections and minimize repetition (if any).

As mentioned in section 1.1, paper can be considered as the oldest and cheapest support used for electrophoresis for conducting zone electrophoresis even though it was more well known for chromatography in the past [46]. Chromatography and electrophoresis are the most commonly used separation techniques since it may lead to the identification of one or more individual components within unknown mixtures by separating them from one another.

The origins of paper chromatography date back to the 1850s and it is still popular and well-known today [46, 48]. It started off with the German physicist, Friedlieb Ferdinand Runge, who observed circular colour-forming patterns on filter paper impregnated with metal solutions resulting from the difference in complexation with different dyes with the immobilised metals. Even though this initial observation was not used the way we know chromatography today, his work inspired many scientists to understand and subsequently exploit this behaviour and can be considered fundamental to paper chromatography. The inventor of paper chromatography as we know it, was Mikhail Semonovich Tswett who introduced fundamentals and principles of the technique through his experiments on plant pigments using filter paper as the replica to plant tissue in early 1900's [48-52].

Technically, paper chromatography can be considered as a variant of thin layer chromatography (TLC), and it was initially introduced in order to overcome the limitations of conventional substrates used at the time (i.e. silica gels). It suffered from complicated preparation of the support and difficulties in detection. By using filter paper, the preparations steps associated with silica gel were simply eliminated [53]. Paper chromatography is performed by placing a small sample spot near one end of the paper, followed by placing this end into a suitable solvent. The solvent, drawn through the paper by means of capillary action, carries the analytes across the paper, allowing for a separation based on the differences in retention between the components. Colorimetric detection is the most widely used method for visualisation, but fluorescence and UV imaging are also popular options. In early work, filter paper was attractive because it allowed

visualisation of the analytes directly on the substrate using a colorimetric spray, in contrast to silica gels where they needed to be transferred onto pre-treated paper [16]. The position of the spot – a measurement of the distance travelled – is indicative of the analytes' distribution between the mobile and the stationary phase and can be used for identification [46]. In the late 1940s, some researchers started to estimate the concentration of each component based on the intensity of the colour using optical scanners such as the transmission densitometer, the photoelectric densitometer and the X-ray viewer [46, 54-57]. Paper chromatography was initially developed for the separation of natural products, and later also applied to synthetic and inorganic compounds [46, 56, 58]. Because the separation of similar compounds was difficult to achieve using paper chromatography (selectivity could only be adjusted by varying the mobile phase), paper electrophoresis was proposed as an alternative, adding resolving power based on the differences in electrophoretic mobility.

Electrophoresis was initially thought to be superior to chromatography and to provide a micro-scale diagnosis capability, faster analysis time, and better resolved peaks. Because, electrophoresis requires an electric field to be imposed across the paper, more instrumentation is required than in the case of paper chromatography [46]. The popularity of paper as a substrate for electrophoresis started to decline after the 1950s with rapid developments in more sophisticated separation methods and principles (i.e. agarose and PAGE, ITP, 2-DE, and then CE/microchip electrophoresis), outperforming paper electrophoresis in terms of resolution and sensitivity [7, 59-61].

It was not until approximately 50 years later that paper was reintroduced in analytical research with the development of Microfluidic Paper-Based Analytical Devices (µPADs) for POC analysis (Figure 1.1). Since concept of POC mainly focuses on fast, user-friendly, and on-site detection, µPADs becomes one of the strong candidates because they are potentially cheap and environmentally friendly to produce, and easy to use. The rationale for this regained popularity has

been the low cost of paper as microfluidic substrate and the ability to move fluids by capillarity without the need for pumps [62]. Although most applications of µPADS are based on rather simple assays with relatively few applications incorporating an analytical separation, the interest in paper electrophoresis also revived [63]. This then leads to our interests in linking the past and the present efforts in this field. Firstly, in this section, historic perspectives on paper electrophoresis considering the hardware, conditions, potential uses in analysis, and the limitations leading to its dip in popularity are provided. Then, the section focuses on how this knowledge was used with the development of portable electrophoretic µPADs and how further improvements could lead towards easy to use, portable paper-based separation platforms.

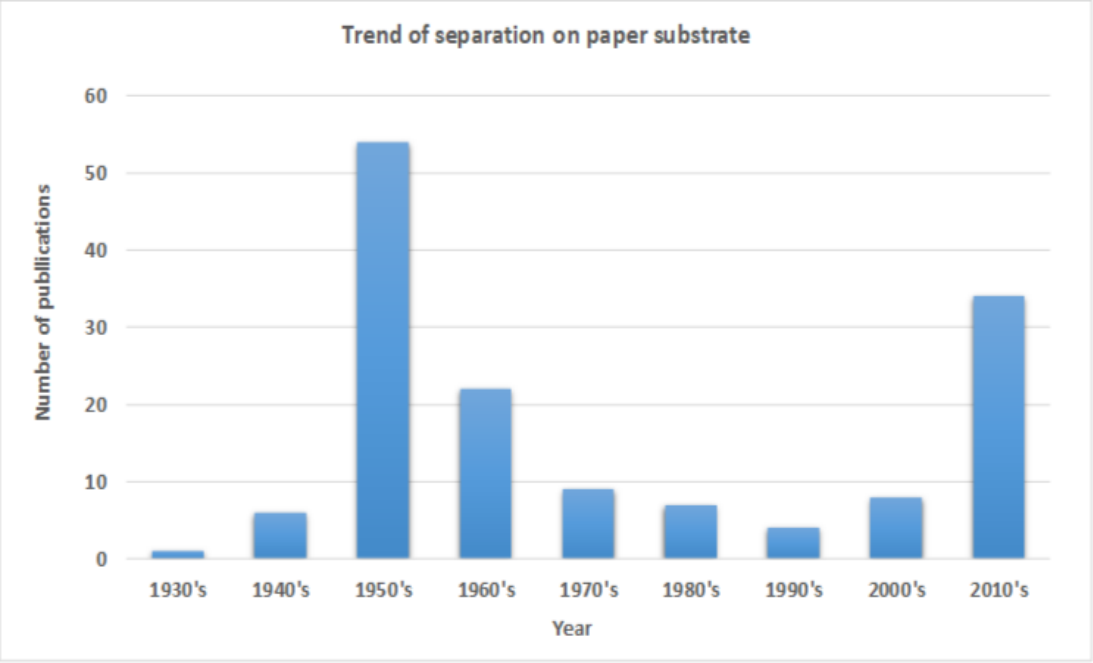

Figure 1.1. The trend of paper chromatography and paper electrophoresis (based on the selected journals cited in this chapter) from 1930 to present. *(*NOTE: publications and this statistic charts were obtained from Web of Science™, Google Scholar, and Scopus search engines under the following advanced search criteria. Keywords: paper chromatography, paper electrophoresis, AND paper-based microfluidic device. Years: all to present. Sort: by most cited publications.)*

1.2.1 History of electrophoresis on paper

Electrophoresis on paper was actually firstly reported in the late 1930s with the implementation of Tiselius' classical moving boundary method to separate amino acids [1]. Despite being over-shadowed in number by paper chromatography, comparisons between paper chromatography and paper electrophoresis all agreed on the higher resolution that could be obtained with paper electrophoresis [46, 60, 64-66].

It was the realisation that combining complementarity separations could achieve a higher resolution that led to the first two-dimensional separations on paper, combining chromatography and electrophoresis. Haugaard and Kroner introduced this combination and achieved the separation of 10 amino acids, which was considered difficult during that time [67]. This approach was then used for the identification, also referred to as the "fingerprinting" of peptides, where the electrophoretic dimension separated the peptides based on charge while the chromatographic dimension separated them based on hydrophobicity [7, 68]. While revolutionary, this approach was quickly superseded by 2-DE, where up to 5000 proteins could be resolved in a single experiment using IEF followed by PAGE. The smaller pore sizes in the gels minimised diffusion of the proteins during analysis leading to superior resolution [61, 69, 70].

The process of paper electrophoresis in the presence of a magnetic field was also investigated by Mukherjee and Majumdar in order to separate binary inorganic complex based on the electrophoretic mobility and on the magnetic properties [71]. The group claimed that by imposing a magnetic field in addition to the electric field, the mobility of the inorganic ions could be altered, facilitating more efficient separations for binary complexes. The same group subsequently used this method in order to separate the lanthanide ions [72]. During this time, there were very few research studies on the separation of lanthanides due to very high reactivity and similar mobility, complicating their separation [73-75]. Compared to previous reports on the electrophoretic separation of rare earths, the group revealed that the analysis time in the magnet-

assisting system was reduced from days and hours to minutes. The electrophoresis set-up was similar to those mentioned in section 2.1.1 with the addition of a magnetic field located in the proximity of the glass plates. While the addition of the magnetic field provided an improvement, it was still not possible to resolve all lanthanides [76].

1.2.1.1 Technology

During the 1930s, the U-tube apparatus designed by Tiselius for moving boundary electrophoresis of colloidal mixtures was the first pragmatic instrumental system and became a prototype for later models. Apart from the convection problems, the instrumentation was expensive, complicated, bulky and required large volumes [1], and hence far from ideal. Technical improvements started by connecting two glass vessels with a strip of paper in order to make a salt bridge [77]. Rapid evaporation led to the consumption of large volumes of the electrolyte and was a source of irreproducibility. Subsequent designs aimed to maintain consistent current and liquid flow and to ensure stable and repeatable separation conditions and introduced new ways to load the sample without disturbing the system [46, 78].

The first improved design was the so-called *inverted V* type apparatus. Developed by Durrum, paper was draped over a L-shaped rod to form a vertical apex with the buffer vessels as a support underneath [79]. The evaporation was minimised with a glass tumbler covering the inverted V section while the paper was flooded with buffer from the two ends dipping in the buffer vessels to maintain a stable saturation before separation. With this apparatus, the apex height (indicated in Figure 1.2A) was the most important factor influencing experimental reproducibility since the electrolytes can create an uneven fluidic movement when climbing towards the apex, leading to changes in the hydrodynamic and electrophoretic equilibrium within the paper. The uneven fluid movement could also lead to a drier apex, and consequently to the burning of the paper due to Joule heating. Owing to its simple and cheap set-up, the speed of operation system,

and its portability, this design was widely used in the medical field and a commercial version of this apparatus was also commercialised by the Spinco Division of Beckman Instruments in 1950 [80].

The second design was a *vertical* orientation and was predominantly used for preparative purposes (Figure 1.2B) where the buffer and sample solution were carried down a large sheet of paper (or paper curtain). Drip point tabs were positioned at the end and evenly drained by gravity, with the voltage applied perpendicularly to the flow direction (i.e. horizontal). The neutral species flowed vertically with gravity, while the charged species migrated horizontally with or against the electric field. This design was inspired by partition chromatography and was modified for continuous flow electrophoresis on paper by Grassman and Hannig in 1950 [67, 81]. The larger separation space allowed for a greater resolution in the case of large-scale electrophoresis. However, due to the bulky set-up, precautions were taken in order to ensure a constant field strength and flow rate of the electrolytes, as well as the evaporation and temperature control so as to maintain the sharpness of the separation bands [15, 82-89].

The so-called *Horizontal* type apparatus (Figure 1.2C), was developed by Cremer and Tiselius and later by Kunkel in 1951 [90, 91]. As the name suggests, the paper was positioned horizontally in order to eliminate the uneven buffer uptake, and to minimise the evaporation by sandwiching the buffer-saturated paper strips between glass plates. Cremer and Tiselius used the non-polar immiscible solvent, chlorobenzene, as a seal, but this was found to interfere with the analysis. Kunkel proposed greasing the edges of the glass plates using silicone the use of metal clamps not only to prevent evaporation and improve the dissipation of heat, but also to apply even pressure and keep the paper in place [91]. For more effective cooling, the set-up was placed in a cold room or between heavy metal plates cooled with a circulating coolant. This apparatus was claimed to be one of the simplest set-ups for paper electrophoresis and provided comparable results to the apex designs. The careful and rapid removal of the paper following the separation remained one of the experimental challenges [88].

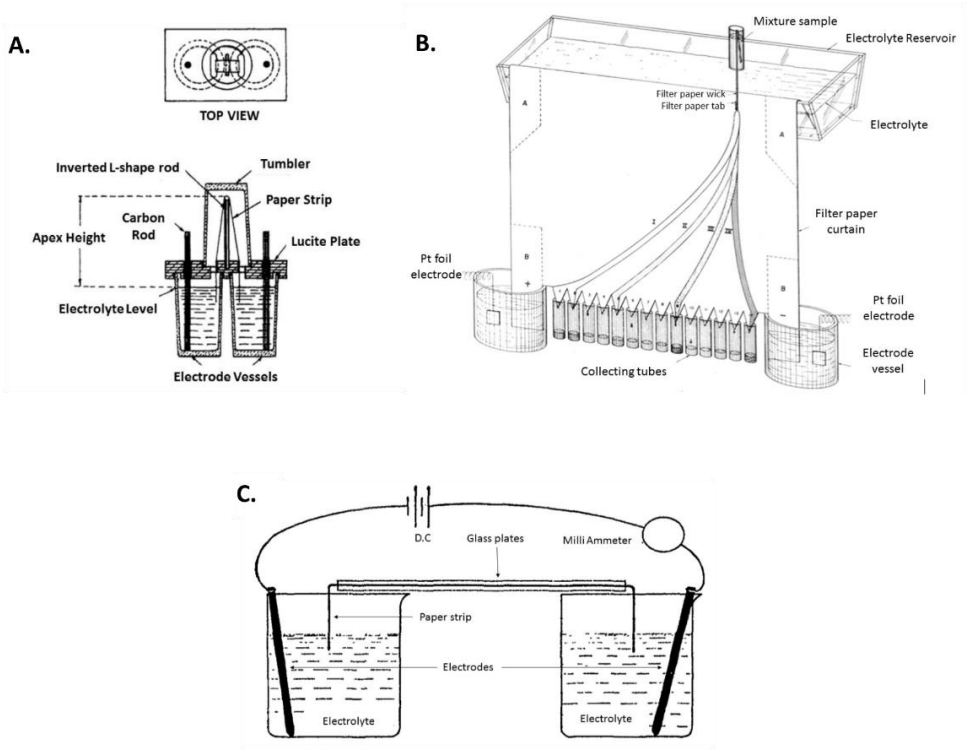

Figure 1.2. A. Inverted V-shaped apparatus designed by Durrum E.L. in 1950. Adapted with permission from ref. [79]. Copyright 1950 American Chemistry Society. B. The apparatus for vertical type or continuous-flow electrophoresis designed by Durrum E.L in 1951. Adapted with permission from ref. [83]. Copyright 1951 American Chemical Society. C. Horizontal-type apparatus used by Lederer and Ward in 1952. Adapted with permission from ref. [92] . Copyright 1952 Elsevier.

1.2.1.2 Understanding opportunities and limitations

Parameters including temperature, paper wetness, choice of electrolyte and paper, surface coating can significantly affect the efficiency, mobility, and reproducibility of the paper electrophoresis [88].

McDonald realised that evaporation is caused by the increase of temperature due to the current flow, which in turn resulted in the drying of the paper substrate. It was demonstrated that when this happened, the velocity and the distance of the analyte were not linear [77]. Holliger et al. concluded that velocity increased with temperature, as a higher temperature increased the electrolyte flow [93]. By maintaining a suitable temperature across the chamber, the paper wetness could be maintained, and the sample loading could be performed throughout the duration

of the experiment. Similar experiments were also conducted by Hackman and Goldberg for protein separations, where improved resolution and reproducibility were obtained on a wetter paper strip, observing denaturation on dryer paper [94]. Careful monitoring of temperature during paper electrophoresis with and without cooling was investigated by Kawerau [95]. When coolant circulation was provided, the stabilising time, electrical potential, and evaporation rate were reduced.

Because ionization can change based on the pH, it is important to carefully select the appropriate range of pH for their separation. Woods et al. suggested selecting a buffer pH with a higher value than the pI of the protein in order to avoid the electrostatic interaction between the positive charge of the protein and the negative charge of the paper [96]. Blank et al. agreed that an alkaline electrolyte increased the rate of mobility of steroids, and that buffering was essential to avoid pH changes and maintain a stable ionic strength during the experiment [97]. Gross confirmed that the alkaline pH was useful for inorganic ions [98]. Geller et al. however, demonstrated the separation of some amino acids below their pI with reduced absorption [99]. The strength of the electrolyte was investigated by Martin and Frenglen, concluding that as the ionic strength of the electrolyte increased, the resolution of the separated bands improved due to reduced diffusion, better pH control, and a higher current [100]. However, an excessively high ionic strength promoted the precipitation and denaturation of proteins and limited the mobility as well as increased the amount of heat generated.

Kabara et al. investigated the buffer equilibration process, identifying that direct pouring provided a greater and faster equilibrium while dipping required a longer time to stabilise and caused band distortion, presumably from an uneven saturation resulting in an unstable field strength [101].

The type of paper can exert a significant impact on the separation efficiency. It was believed to be a result from purity, in terms of the cellulose content, with each paper type causing

different levels of protein absorption, surface and wetting capability [102]. Martin and Flenglen concluded that Whatman No. 1, 4, 3MM and Munktell 20 were among the best and most used grades by most researchers [100, 103]. Varieties of Whatman filter paper with different thickness values were tested in order to study the separation power by Kawerau where the superior efficiency was associated with higher thickness due to the less compact cellulose structure [95]. Holdsworth also compared seven grades of Whatman paper and characterised them according to their suitability for different applications [87]. For example, a thin Whatman No.1 grade was found more suitable for a small amount of a high molecular weight sample while the thicker Whatman No. 31 grade is advantageous for small inorganic ions that have a high mobility. For protein separations, some researchers preferred the thicker filter paper since it was found to reduce the EOF and thinner paper was prone to evaporation [91, 104]. Thicker paper can carry a higher current and sustain a higher temperature which increases effective electrophoretic velocity [105]. Shiroma et al. reported the comparison of Whatman No.1 and Whatman P81, only resolving the paracetamol components using Whatman P81 due to the stronger cationic exchange on the P81 paper [106].

The mobility of the analyte on the paper is the mobility of the analyte in free solution combined with a contribution factor from the paper [107]. This factor is specifically referred to as the tortuosity factor, which Kawerau and Gross explored in relation to the direction in which the paper strips were cut [95, 98]. Their results demonstrated that those strips which had been cut along the direction of the main cellulose fibre had a higher current density, and a greater migration distance than those where the paper was cut across the fibre direction. The bands migrating across, not along, the fibres tapered and the analytes with similar mobility could not be resolved. This tapering effect is more pronounced in paper chromatography than in electrophoresis.

In order to enhance the fluorescence detection for the polycyclic aromatic compounds Cheng and Vo-Dinh investigated the effect of the coating on the paper surface prior to the

separation using amorphous fumed silica [108]. While the migration distance of the analytes was unaffected, a 1.5-fold increase in the fluorescence intensity was found on the coated paper without a significant increase in background interferences.

1.2.1.3 Applications

Paper electrophoresis was traditionally implemented for the analysis of clinical samples containing hemoglobin, proteins, amino acids, sugar derivatives, lipids, carbohydrates, and enzymes, with only a limited number of reports focusing on separating inorganic anions and cations. In terms of the detection and quantification of the separated bands, staining with colorimetric reagents constituted the easiest, cheapest, and most reliable method. An overview of these selected applications together with the experimental conditions and detection methods between 1930 and 2006 is provided in Table 1.2, providing an overview before the evolution to μPADs.

Despite paper electrophoresis losing its popularity in the mid-1970s due to the rise of polymeric gels and capillaries as more convenient and powerful platforms, paper continued to constitute an attractive approach for the multidimensional separation of complex samples. Asenstorfer et al. coupled the paper substrate with high performance liquid chromatography (HPLC) for the isolation, purification, and identification of anthocyanin from two cultural crops in Australia [109]. The anthocyanin was firstly isolated from the plant extract on Whatman No. 3 paper strips before fuming the spots with hydrochloric acid (HCl) and further eluting the paper with methanol. The eluents in methanol were then concentrated in a solid phase extraction cartridge prior to separation with HPLC-MS. There have also been a few reports on using ITP on paper. ITP is a non-linear electrophoretic separation technique employing two electrolytes: the leading electrolyte (LE) and the terminating electrolyte (TE) and has mainly been used for concentrating and focusing sample components into very sharp and intense bands [110]. ITP on paper dates back to 1973, when Taglia and Lederer separated anionic thiocyanate and bromate using chloride as the

LE and acetate as the TE [111]. The detection of thiocyanate and bromate was also achieved by complexing with ferric cation and potassium iodide, respectively. In the same work, chromate and molybdate were also separated using thiosulfate as the LE and oxalate as the TE, while sulphate was used as a spacer between the two in order to obtain physically separated analyte zones. A mixture of other various anions including chromate, molybdate, tungstate, and ammonium perrhenate was also separated. Subsequently, Taglia also used ITP in order to separate cationic thallium, silver, lead, and mercury using nitric acid as the LE and lithium nitrate as the TE [112].

1.2.2 µPADs: revisiting paper electrophoresis and chromatography

In 2007, paper was used to create a µPAD by Whiteside et al [113, 114] which has revitalised the interest in using paper as a substrate for all forms of analytical chemistry. The attraction is the simplicity of fluid movement by capillary action, making it similar to a traditional lateral flow assay (LFA) which are commonly used for diabetes, pregnancy, Human Immunodeficiency Virus (HIV) and influenza [115, 116]. µPADs started off with the pursuit of biochemical assays in the early days, but with the microfluidic control providing increased performance, µPAD applications include environmental monitoring and detection (organic, inorganic, and metal ions species), nutrition, and forensic investigations. While trying to maintain equivalent capabilities in terms of analysis principles with that of the previous technologies, ultimate goal in developing µPADs is to execute such systems into the portable scale where fabrications, chemicals, instrumentation and cost can be minimized together with comparatively fast and credible diagnosis [117-124]. For most assays on µPADs, the selectivity is provided through the selection of the appropriate regents and wetting of the paper provides the fluidic transport. For a more comprehensive overview of µPADs, readers are directed to some excellent reviews [125-133]. The focus of this section is on those µPADs incorporating a chemical separation to provide selectivity by resolving different analytes. An overview of µPADs incorporating an analytical separation is provided in Table 1.3**.**

Table 1.2. Selected applications of paper electrophoresis during 1900's until 2006

Applications of paper electrophoresis								
Year	**Author(s)**	**Separation**	**Experimental conditions**				**Detection**	**Ref.**
			Paper Type	**Buffer(s)**	**Potential gradient (V/cm)**	**Time (hr)**		
1948	Haugaard et al.	Amino acids	Whatman #1 (sheet)	Phosphate buffer	8.3-8.75	16-18	Ninhydrin reagent	[67]
1950	Durrum, E.L.	Amino acids and radioactive components	Whatman #2	Potassium hydrogen phthalate-Sodium hydroxide, acetic acid, phosphate, and barbital buffer	6-18	2-93	Ninhydrin reagent and autoradiography	[79]
1951	Strain, H.H. and Sullivan, J.C.	Metal ions	Commercial filter paper (Filpaco #046 and Eaton-Dikeman grade 320)	Ammonium hydroxide, ammonium acetate, and nitric acid	2.6-6.6	0.3-0.6	Colorimetric reagents	[82]
1952	Lederer, M. and Ward, F.L.	Cations and anions in metal complexes	Standard chromatography paper	Hydrochloric acid, potassium chloride, and potassium thiocyanate	1.3-4	0.25-3.5	Ammonia and hydrogen sulphide	[92]
1952	Consden, R. and Stanier, W.M.	Sugars	Whatman #1	Borate buffer	10.3	2	Aniline hydrogen phthalate reagent	[134]
1952	Kunkel, H.G. and Slater, R.J.	Lipoproteins of serum	Whatman 3MM	Barbital buffer	2.8-14.3	1	Bromophenol blue and alcohol ether	[91]
1953	Woods, E.F. and Gillespie, J.M.	Mixture of enzymes from protein	Whatman 3MM	Barbital buffer	9.5-19.5	5-6	Bromophenol blue	[96]

Year	Author(s)	Separation	Experimental conditions				Detection	Ref.
			Paper Type	Buffer(s)	Potential gradient (V/cm)	Time (hr)		
1953	Frenglen, G.T.	Insulin and parathyroid fractions in serum, spun milk, and urine	Whatman #1 and #4	Barbital buffer	3.4-4.2	12-16	Ammonia fume	[135]
1953	Spaet, T.H.	Animal proteins	Whatman 3MM	Barbital buffer	810-1200V*	2-24	Bromophenol blue	[136]
1953	Kinersly, T.	Organic components in saliva	Whatman #1 and Munktell 20	Acetate, citrate, phosphate and barbital buffer	150-300V*	5-24	Amido Black, Acid-Schiff staining, starch-iodine solution, and starch-sodium chloride solution	[137]
1954	Mackay et al.	Serum proteins	Whatman #1	Barbital buffer	8.3 5	6-7 14	Amido black and immersing in mineral oil	[138]
1955	Langen et al.	Alpha and beta lipoprotein cholesterol	Whatman 3MM	Barbital buffer	7.3	2	Sudan black	[139]
1955	Zentner, H.	Proteins fraction from wheat gluten	Whatman 3MM	Citrate-phosphate buffer	9	24	N/A	[140]
1955	Jencks et al.	Serum proteins	Whatman 3MM	Barbital buffer	3-3.5	16	Bromophenol blue-acetic acid-zinc sulphate	[141]
1955	Langen et al.	Cholesterol lipoproteins	Whatman 3MM	Barbital buffer	7.3	2	Sudan black and Ferric chloride-sulfuric acid cholesterol reagent	[139]
1955	Brown, C. and Kirk, P.L.	Identification of writing inks	Whatman #1	Acetate and barbital buffer	7.8	0.08	Colorimetric reagents spray	[64]

Year	Author(s)	Separation	Experimental conditions				Detection	Ref.
			Paper Type	Buffer(s)	Potential gradient (V/cm)	Time (hr)		
1956	Gross, D.	Non-volatile organic acids and amino acids	Whatman 3MM	Formic acid-acetic acid	160-240	0.2-0.5	Ninhydrin and bromophenol blue	[142]
1957	Lederer, M.	Inorganic anions	Arches No. 302	Ammonium carbonate	150 V*	1	Acid spray	[143]
1957	Gross, D.	Inorganic cations: Alkali, Alkaline-earth and others	Whatman 3MM	Ammonium carbonate	100	0.28-0.33	Bromothymol Blue spray	[144]
1957	Theander, O.	Aldehyde and ketone components from glucoside monosaccharide sugar	Whatman 3MM	Hydrogen sulphide	12-18.5	3-5	UV light, dinitrophenylhydrazine, silver-nitrate-sodium ethoxide or anisidine hydrochloride	[145]
1957	Leviton, A.	Amino acids of whey proteins in dairy products	Whatman 3MM	Barbital buffer	5-20	2	Bromophenol Blue	[146]
1958	Jach et al.	Radioactive by-products from Szilard-Chalmers reaction	Whatman 3MM	Sodium hydroxide	10-16	2-5	Radioactive scintillation counter and rate of decay calculation	[147]
1958	Macrae, H.F. and Baker, B.E.	Alpha, beta, and gamma Casein from milk sample	Whatman 3MM	Barbital buffer	5	16	Azocarmine B, naphthalene black and direct photometry	[148]
1959	Grassini, G. and Lederer, M.	Inorganic anions	Arches No. 302	Sodium hydroxide	240 V*	1	N/A	[149]

Year	Author(s)	Separation	Experimental conditions				Detection	Ref.
			Paper Type	Buffer(s)	Potential gradient (V/cm)	Time (hr)		
1959	Katz et al.	Peptides from controlled proteolytic digests	Whatman 3MM	Pyridine-acetic acid-water	35	16	Peptide and amino acids reagents	[150]
1960	Markakis, P.	Anthocyanins from berries and plants	Whatman (Spinco model R apparatus)	Phosphoric acid, acetic acid, and formic acid	7-15	2-10	Hydrochloric fume or alcohol elution	[151]
1960	Belling, G.B. and Underdown, R.E.	Inorganic anions	Whatman 3MM	Sodium carbonate	300 V*	1	Chromogenic reagent spray	[152]
1960	Geller et al.	α-casein complex and components	S&S 2043A	Lactic acid-propionic acid	8.2	5	Bromophenol blue	[99]
1961	Atfield, G.N. and Morris, C.J.O.R.	Amino acids in protein hydrolysates: mobility and recovery	Whatman 3MM	Pyridine-acetate, formic acid-acetic acid, and cadmium acetate	75-100	3-4.5	Cadmium-Ninhydrin, methanol distillation, and direct absorption photometry	[153]
1962	Bannard, R.A.B. and Casselman, A.A.	Clam poison in shellfish	Whatman 3MM	Formic acid, acetic acid, sodium acetate-acetic acid, phosphate and borate buffer	45	1.75	UV light, ninhydrin, and weber chromogenic agent	[154]
1963	Gross, D.	Inorganic cations: migration conditions and rates	Whatman 3MM	Formic acid	100	0.33	Ammonium sulphide, 8-hydroxyquinoline, ammonia fume, bromophenol blue, and ammonium ninhydrin	[98]

Year	Author(s)	Separation	Experimental conditions				Detection	Ref.
			Paper Type	Buffer(s)	Potential gradient (V/cm)	Time (hr)		
1963	Shukla et al.	Chemical effects beta-decay from ^{132}Te to ^{132}I production	Arches No. 302	Sodium hydroxide and sodium chloride	1.3-4 and 50-100	0.25-3.5 and 1	Scanning with Frieseke-Hoepfner FH 452 automatic scanner for radioelectropherogram	[155]
1964	Blank et al.	C-16, C-17-dioxygenated and some other polyhydroxylated steroids	Whatman 3MM	Borate buffer	10.9	5	UV light	[97]
1967	Jokl et al.	Inorganic ions: Mobility data	Whatman #1	N-(2-Hydroxyehtyl) iminodiacetic acid	15	1-3	Hydrochloric acid spray and specific metal complexing agents	[156]
1967	Horobin, R.W. and Murgatroyd, L.B.	Histological dyes	Whatman #4	Phosphate buffer	2.6	10	Azur A and methylene blue	[66]
1968	Adams, W.S. and Nakatani, M.	Purines and Pyrimidines: Mobility	Schleicher and Schuell 2043-A	Borate buffer	9.8	4	UV light	[157]
1970	Selegny et al.	Amino acids	Strong base ion exchange; SB-2 (Amberlite IRA-400), Strong acid ion exchange; SA-2 (Amberlite IR-120), Weak acid ion exchange; WA-2 (carboxylic IRD-50)	Phosphate and citrate buffer	14-28.5	1-6	N/A	[158]

Year	Author(s)	Separation	Experimental conditions				Detection	Ref.
			Paper Type	Buffer(s)	Potential gradient (V/cm)	Time (hr)		
1973	Mosini, V. and Lederer, M.	Investigation of metal and inorganic anions complexation	Whatman #1	Hydrochloric acid	3.5	1	N/A	[159]
1973	Taglia, V. and Lederer, M.	Inorganic anions (ITP)	Whatman #1	Chloride (LE) and acetate (TE)	7	3	Metal complexation and potassium iodide (KI-HCl)	[111]
1973	Taglia, V.	Metal cations (ITP)	Whatman #1	Nitric acid (LE) and Lithium nitrate (TE)	7	2	Potassium chromate	[112]
1974	Cvjeticanin, N.M. and Jovanovic-Kovacevic, O.	Divalent metal cations in inorganic and organic acids	Whatman 3MM	Ethylenediaminetetraacetic acid (EDTA)	60	0.75-1.5	Dithizone in acetone solution	[160]
1974	Mukherjee, H.G. and Majumdar, D.	Metal cations (with Magnetic field)	Whatman #1	Potassium chloride	5.5	0.25	Colour developing agent	[71]
1976	Jerzykowski et al.	Glyoxalase I and II from ox liver, red blood, and yeasts	Whatman #1	Barbital buffer	220V*	5.5	Bromophenol blue	[161]
1978	Corradini, C. and Lederer, M.	Optical isomers of metal complexes	Whatman 3MM	Aluminium chloride-ammonium tartrate	7.35	2-3	N/A	[162]
1979	Lederer, M.	Relevant factors relating to high-voltage electrophoresis on paper	Whatman 3MM	Hydrochloric acid, ammonium sulphate, and perchloric acid	25-57	0.08	N/A	[104]

Year	Author(s)	Separation	Experimental conditions				Detection	Ref.
			Paper Type	Buffer(s)	Potential gradient (V/cm)	Time (hr)		
1983	Mukherjee, H.G. and Datta, S.K.	Metal lanthanons (with magnetic field)	Whatman #1	Potassium chloride, hydrochloric acid, and potassium cyanide	6.3	0.4	Colour developing agent	[72]
1984	Fanali, S. and Ossicini, L.	Parameters influencing the electrophoretic separation	Whatman #1 and Whatman 3MM	Sodium sulphate and hydrochloric acid	25-100	0.05-0.16	N/A	[105]
1986	Hayman, A.R. and Gray, D.O.	Dansyl derivatives of amino acids and amines	Whatman #1	Formic acid, acetate, and phosphate buffer	16	0.5-2	UV light, potassium permanganate-sodium carbonate, and in-house chromogenic reagents	[163]
1988	Nagasaki et al.	Inorganic Neptunium in groundwater	TOYO No. 51A	Potassium chloride-boric acid-sodium hydroxide and Tris buffer	10 or 100 (with cooling system)	4 or 0.25 (with cooling system)	Gas-flow counter for ^{237}Np activities	[164]
1990	Cheng, Y.F. and Dinh, T.V.	Polycyclic carcinogenic compounds	S&S 591-C	Tris buffer	100	1.5	Fluorescence analysis	[108]
1994	Kobayashi et al.	Dihydroxyborylphynylalanine (BPA) compounds in dicarboxylic acid and tricarboxylic acid	Toyoroshi No. 51A	Tricarboxylic acids	33	0.5	Infrared spectrometry (IR), ninhydrin, boric acid-alcoholic curcumin solution	[165]

Year	Author(s)	Separation	Experimental conditions				Detection	Ref.
			Paper Type	Buffer(s)	Potential gradient (V/cm)	Time (hr)		
2001	Sharma et al.	Ion-pairs in inorganic anions complex	Whatman #1 (plain and coated with Titanium (IV) tungstate)	Nitrate buffer (sodium, magnesium, aluminium, chromium, and cobalt)	2.1	3	Silver nitrate, ferric chloride, diphenyl amine, zirconium tetrachloride, alizarin, phenolphthalein, potassium permanganate, and sodium nitro pruside	[166]
2003	Asenstorfer et al.	Anthocyanins from floricultural crops	Whatman #3	Bisulphite buffer	1400V*	1	Hydrochloric fume, alcohol elution, and Coupled with HPLC-MS	[109]
2006	Sato et al.	Histamine in fish and seafood	Special type equipped with JBB Histamine checker (Japan)	Pyridine-acetic acid-water	26	0.16	Chromogenic diazotized sulfanilic acid reagent and digital imaging software	[167]

**Applied voltage. Field strength could not be determined because of missing information.*

Table 1.3. Selected applications on separation using µPADs

Applications on Paper-based Analytical Devices (µPADs)								
Year	**Author(s)**	**Application**	**Experimental conditions**				**Detection**	**Ref.**
			Paper Type/Fabrication	**Reagents/buffers**	**Electrical parameter**	**Fabrication time/Analysis time**		
2010	Carvalhal et al.	Separation and quantification of ascorbic and uric acid	Whatman #1/Photolithography with S1811 Electrodes: Electron beam evaporation or sputtering of titanium and gold	Electroactive species of both acids/Acetate buffer	0.4 V vs Au (scanning)	Approx. 20.5 min/16 min	Electrochemical assay	[168]
2012	Ge et al.	Separation of blood plasma	Whatman chromatography paper/Wax printing (3D)	IgM antibodies for antigens D (anti-D)/Phosphate buffer and Tween-20	N/A	Approx. 3 min/ 16 min	Chemiluminescence assay (Luminuol-H_2O_2 and Ag nanoparticles)	[169]
2012	Tao et al.	Electrophoresis of gizzerosine in meals containing fish products	Commercial paper electrophoresis apparatus and paper disc (QS-Solution, Japan)	Pauly's reagent/Pyridine: acetic acid: water	800 V	18 min	Colorimetric assay	[170]

Year	Author(s)	Application	Experimental conditions				Detection	Ref.
			Paper Type/Fabrication	Reagents/buffers	Electrical parameter	Fabrication time/Analysis time		
2012	Songjaroen et al.	Separation of blood plasma from whole blood	Whatman #1 and blood separation paper (LF1, MF1, VF1, and VF2)/Wax dipping	Bromocresol green/K_3EDTA reagent	N/A	Approx. 1 s /2 min	Colorimetric assay	[171]
2012	Yang et al.	Separation of blood plasma from whole blood	Whatman #1/Wax printing	Anti-A,B antibodies for blood separation and potassium iodide for glucose oxidative species/Phosphate buffer	N/A	Approx. 3 min/5 min	Colorimetric assay	[172]
2012	Vella et al.	Detection of multi-components from single drop of blood for liver-related diseases	Whatman #1 (in assembly with separation membrane for vertical-flow chip)/Wax printing	Colorimetric reagents for Aspartate aminotransferase (AST), Alkaline phosphatase (ALP) and Proteins/Tris and citrate buffer	N/A	Approx. 3 min/20-45 min	Colorimetric assay	[173]
2012	Shiroma et al.	Separation of paracetamol and 4-aminophenol	Whatman #1 and P81 (cation exchanger paper)/Wax printing Electrode: Thin film sputtering of gold	Eater-linked orthophosphoric acid (with Na^+ counterion)/Acetate and phosphate buffer	0.4 V vs pseudo Au	Approx. 12 min/25 min	Electrochemical assay	[106]

Year	Author(s)	Application	Experimental conditions				Detection	Ref.
			Paper Type/Fabrication	Reagents/buffers	Electrical parameter	Fabrication time/Analysis time		
2013	Noiphung et al.	Detection of glucose from whole blood	Whatman #1 and blood separation membrane (VF1 and VF2)/Wax dipping Electrode: Screen printing Prussian blue/carbon electrodes (PB/SPCE) and silver chloride ink	Oxidative species for glucose/Phosphate buffer	0.0V to -0.2V vs. Ag/AgCl	Approx. 20 s /4 min	Electrochemical assay	[174]
2013	Abbas et al.	Separation and pre-concentration of fluorescent dyes	Whatman #1/Cutting	Rhodamine 6G and Fluorescein isothiocyanate/Poly(allylamine hydrochloride) and poly(sodium 4-styrenesulfonate)	N/A	N/A	Surface-enhanced Raman scattering (SERS)	[175]
2013	Dossi et al.	Separation of ascorbic acid and sunset yellow	Whatman #1/Wax printing Electrode: Hand-drawn with graphite pencils	Sodium acetate and potassium chloride buffer	0.9V vs. pseudo C	Approx. 10 min/6 min	Electrochemical assay	[176]
2014	Rosenfeld, T. and Bercovici, M.	Pre-concentration of fluorescein and DyLight 650 with isotachophoresis (ITP)	Whatman #595/Wax printing and lamination	BisTris-PVP and HCl-BisTris (LE) and Tricine-BisTris-PVP (TE)	200 V	6 min	Colorimetric assay (fluorescence)	[177]

Year	Author(s)	Application	Experimental conditions				Detection	Ref.
			Paper Type/Fabrication	Reagents/buffers	Electrical parameter	Fabrication time/Analysis time		
2014	Ouyang et al.	Separation of multi-metal complexes by moving chelation boundary (MCB)	Whatman #1/Photolithography with SU-8 2150 Electrode: N/A	EDTA disodium salt subspecies	N/A	Approx. 5-10 min/15 min	Colorimetric assay	[178]
2014	Moghadam et al.	Isotachophoresis of Alexa Flour 488 (AF488) succinimidyl ester	Nitrocellulose/CO2 laser cutting Electrode: Platinum wires	Tris-HCl-PVP (LE) and HEPES (TE)	250-600V	Approx. 20min/4 min	Colorimetric assay (fluorescence)	[179]
2014	Lou et al.	Separation of proteins and fluorescent molecules	Whatman #1/Wax printing (3D-origami) Electrode: Silver wires	Tris-HCl buffer for fluorescent molecules and phosphate buffer for proteins	10V	Approx. 45 s /5 min	Colorimetric assay (fluorescence)	[180]
2014	Chen et al.	Separation of coloured dye using paper-based fluidic batteries	Advantec #1/Wax printing Electrodes: Aluminium foil and Copper foil	Methylene blue/deionized water	30 to 40 V/cm	Approx. 1.5 min/2 min	Colorimetric assay	[181]
2014	Gong et al.	Concentration and transport of proteins and coloured dyes by ion concentration polarization (ICP)	Whatman #1 and nitrocellulose membrane/CO_2 laser cutting and wax printing	Fluorescein, bromocresol green, and fluorescein isothiocyanate conjugate bovine serum albumin/Tris-acetate-EDTA buffer	50 V	Approx. 32 min/3 to 10 min	Colorimetric assay (fluorescence)	[182]

Year	Author(s)	Application	Experimental conditions				Detection	Ref.
			Paper Type/Fabrication	Reagents/buffers	Electrical parameter	Fabrication time/Analysis time		
2015	Li et al.	Focusing of DNA	Whatman #1/Wax printing (3D-origami) Electrode: Platinum wires	Tris-taurine (LE) and Tris-HCl (TE)	18V	Approx. 45 s /4-10 min	Colorimetric assay (fluorescence)	[183]
2015	Ryan et al.	Separation of explosive compound in soil	Whatman 3MM/Cutting Electrode: Graphite and silver/silver chloride ink	Colorimetric reagents for each explosive components/Deionized water and mixture of acetone and water	0 V to -1 V vs. Ag/AgCl	8 min	Electrochemical assay	[184]
2015	Yang et al.	Pre-concentration of dilute sample solutions using ion concentration polarization (ICP)	Whatman #1 and nitrocellulose/ Wax printing	Fluorescein/Tris buffer	50 V	Approx. 7.5 min/2 to 3 min	Colorimetric assay (fluorescence)	[185]
2015	Gong et al.	Pre-concentration and separation of infectious disease DNA target by ion concentration polarization (ICP)	Nitrocellulose/Wax printing	Fluorescent tracers for biological samples /Deionized water	150 V/cm	Approx. 35 min/15 min	Colorimetric assay (fluorescence)	[186]
2015	Zhong et al.	Size-based separation and extraction of mixed proteins and free dyes	Whatman #3, #5, and Nitrocellulose/CO_2 Laser cutting	Naphthol blue black bovine serum (Blue-BSA) and Tartrazine/Phosphate buffer and deionized water	N/A	Approx. 5 min	Spectrophotometer	[187]

Year	Author(s)	Application	Experimental conditions				Detection	Ref.
			Paper Type/Fabrication	Reagents/buffers	Electrical parameter	Fabrication time/Analysis time		
2015	Moghadam et al.	Isotachophoresis of goat anti-rabbit IgG labelled with Alexa Fluor 488 fluorescent dye	Nitrocellulose/CO_2 laser cutting	Tris-HCl-PVP (LE) and glycine-Bis-Tris (TE)	500 µA (current)	1.5 to 60 min	Colorimetric assay (fluorescence)	[188]
2016	Hong et al.	Pre-concentration and separation of fluorescent dye using field-flow separator	Whatman #1/Wax printing Electrode: Silver/Silver chloride	Tris(bipyridine)ruthenium(II) chloride, Alexa Fluor 488 and Alexa Fluor 488-conjugated bovine serum albumin/Sodium chloride buffer	100 V	Approx. 1 min/10 min	Colorimetric assay (fluorescence)	[189]
2016	Chagas et al.	Paper-based microchip electrophoresis (pME) for separation of bovine serum albumin and creatinine	Whatman #1/Cutting and lamination Electrode: Hand-drawn with graphite pencils	2-(N-morpholino)ethane sulfonic acid (MES) and Histamine buffer	0.6 to 30 kV	2-6 min	Capacitively coupled contactless conductivity detection (C^4D)	[190]
2016	Xu et al.	Injection and electrophoretic separation of components in beverage sample	Filter paper/Cutting and lamination	Carmine and sunset yellow solution/Deionized water and phosphate-borate buffer	250 V to 300 V	10 min	Colorimetric assay	[191]
2016	Zhao et al.	Separation of amino acid and drug-doped samples	Whatman #2/Wax printing	Fuchsin basic and sulfo-cyanine 5/Acetate and bicarbonate buffer	10 V	Approx. 45 s /5 min	Colorimetric assay and mass spectrometry (MS)	[192]

Year	Author(s)	Application	Experimental conditions				Detection	Ref.
			Paper Type/Fabrication	Reagents/buffers	Electrical parameter	Fabrication time/Analysis time		
2016	Berry et al.	Measurement of hematocrit from red blood cells	Ahlstrom Chromatography paper #6130 and Whatman #4/Wax printing and lamination	Phenol red/Sodium chloride and EDTA	N/A	Approx. 30 s /30 min	Colorimetric assay (fluorescence)	[193]
2016	Phansi et al.	Separation of gaseous species (sulphide ion, ammonium ion, and ethanol) from wastewater sample	Whatman #4/Screen printing hydrophobic fabric ink	"Nessler" and 3-nitrophenol (NTP) and sodium hydroxide (for gas generation)	N/A	2-6 min	Colorimetric assay	[194]
2016	Hung et al.	Development of portable sample concentrator using fluorescent dyes	Whatman #1/Wax printing	Fluorescein/Tris buffer	0 to 196 V	Approx. 1.5 min/16 min	Colorimetric assay (fluorescence)	[195]
2016	Han et al.	Pre-concentration of fluorescent dye and protein using ion concentrator polarization (ICP)	Whatman #1/Wax printing and lamination Electrode: Silver/Silver chloride	Fluorescein and fluorescein isothiocyanate-conjugated albumin (FITC-albumin)/Sodium chloride buffer	100 to 200 V	Approx. 1.2 min/10 min	Colorimetric assay	[196]
2016	Yeh et al.	Pre-concentration of fluorescent dye and protein using ion concentrator polarization (ICP) at specific location	Nitrocellulose/Wax printing and lamination	Fluorescein and fluorescein isothiocyanate-conjugated albumin (FITC-albumin)/Tris buffer	0 to 210 V	Approx. 1.5 min/28 min	Colorimetric assay (fluorescence)	[197]

Year	Author(s)	Application	Experimental conditions				Detection	Ref.
			Paper Type/Fabrication	Reagents/buffers	Electrical parameter	Fabrication time/Analysis time		
2016	Ma et al.	Pre-concentration of fluorescein probe and double-stranded DNA by electrokinetic stacking	Glass fibre paper/Cutting Electrode: Platinum wires	Fluorescein and SYBR Green I/Tris-HCl buffer	300 V	5 min	Colorimetric assay (fluorescence)	[198]
2016	Ueland et al.	Screening of explosive residues in soil	Whatman #5/Wax printing	Agilent DNA 1000 dye®/Borate-SDS buffer	1400 V	Approx. 30 s /40 s	Agilent 2100 Bioanalyzer (fluorescence quenching)	[199]
2016	Phan et al.	Concentration enhancement of fluorescent dyes using ion concentration polarization (ICP)	Whatman #1/Cutting	Fluorescein/Tris buffer	50 V	Approx. 20 min/3 min	Colorimetric assay (fluorescence)	[200]

1.2.2.1 Current analytical separations on µPADs

Just like in the early days, it was chromatography on the µPAD that preceded electrophoresis. In 2010, Kubota et al. combined a chromatographic separation with electrochemical detection for the analysis of the ascorbic and uric acid [168, 201]. The paper-based device was fabricated using photolithography and combined with a glass substrate containing gold electrodes (Figure 1.3). The separation procedure was as simple as spotting the sample mixture on the paper and dipping the near end into the eluent with 0.4 V applied to the working electrode for detection purposes. The analytes are separated based on their retention differences on the paper, with the least retained passing the detector first. The run time in the µPAD (16 min) was longer than in a HPLC column (5 min); however, the µPAD was simpler and future developments in design may reduce the analysis time.

One of the challenges of chromatography on the µPAD remains the inhomogeneity of the liquid flow, leading to a loss in the separation efficiency. With the historic knowledge that higher separation efficiencies can be realised with electrophoretic paper-based separations, Ge and co-workers introduced electrophoretic µPADs for the separation of amino acids [202], employing the pencil-drawn electrodes previously introduced for electrokinetic fluid control [203]. The wax-printed µPAD was coupled with circuit boards for the on-column electrochemiluminescence detection. Prior to the assembly, different pieces of paper-based circuit boards with reservoirs and sample zones and separation strips were designed, as shown in Figure 1.4. The system performance was promising resolution in separation and repeatability of the runs and a linear relationship was found between the signal intensity and the analyte concentration.

Following the origami-inspired 3D µPAD by Crooks et al., a 3D device was created by folding in order to increase the number of fluidic layers without mechanical assistance [204]. Lou et al. incorporated the electrophoretic functionality into a 3D microfluidic µPAD for the analysis of the fluorescent molecules including proteins. The electric field strengths were approximately 24-

50 V/cm, which is lower than those reported by Ge (110-330 V/cm) [180]. Thin Whatman No. 1 was wax-printed, sandwiched with Ag/AgCl electrodes, and folded into a 3D device (Figure 1.5A). The multi-layer structure allowed for the separation to be completed within a period of 5 min. Proteins spots could then be visualised with a fluro-profile quantification kit, revealing the fluorescence spots from the analytes when unfolding the paper (Figure 1.5B). The digital images were processed using Image J software by means of hue conversion for quantitation.

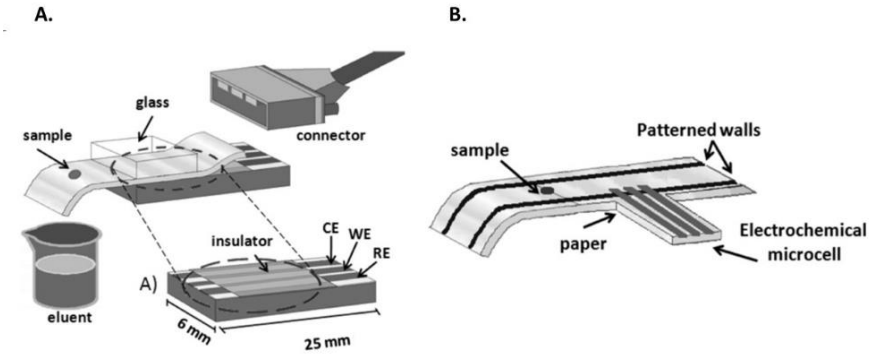

Figure 1.3. Paper-based separation devices with electrochemical detection. (A). Paper was pressed down in contact with the gold electrodes for electrochemical detection and (B). where the gold electrodes were screen-printed onto the paper device. Adapted with permission from ref. [168]. Copyright 2010 American Chemical Society.

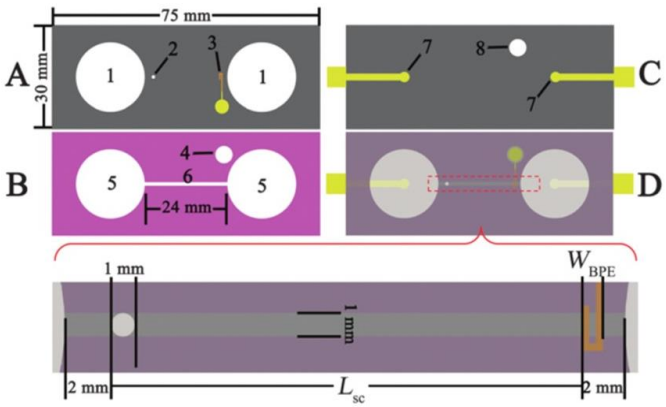

Figure 1.4. Circuit boards and paper-based electrophoretic device coupled with on-column wireless electro-generated chemiluminescence detection before (A-C) and after (D) assembly. (1) pierced zones for paper reservoirs, (2) sample zone, (3) bipolar electrodes, (4) electro-generated chemiluminescence reporting zones, (5) paper reservoirs, (6) paper channel, (7) gold electrodes, (8) pierced hole for bipolar electrodes. Reprinted with permission from ref. [202]. Copyright 2014 Royal Society of Chemistry.

Rosenfeld and Bercovici introduced ITP on a µPAD on Whatman paper, demonstrating a 1000-fold concentration of DyLight 650 in 10 min [177]. The wax-printed device was printed on both sides of the paper prior to heating in order to create shallower channels, limiting the current and hence, the Joule heating. The LE was a mixture of HCl and BisTris, while two different sets of TE, namely HEPES-BisTris and Tricine-BisTris, were used. A quantity of 1% of polyvinylpyrrolidone (PVP) was added to both the LE and the TE in order to suppress the EOF. The device comprised of 4 reservoirs with interconnecting channels and the detection was based on the fluorescence interface visualisation (Figure 1.6). The key advantage of the ITP over the conventional lateral flow assays is the improvement in speed and sensitivity, providing up to 3 orders of magnitude improvements in sensitivity. A 400-fold improvement in the detection limit was reported by this group in 2015, also demonstrating a 100-fold enhancement in sensitivity in 4 min for the detection of the DNA ladder previously demonstrated by Crooks 3D µPAD [183, 188].

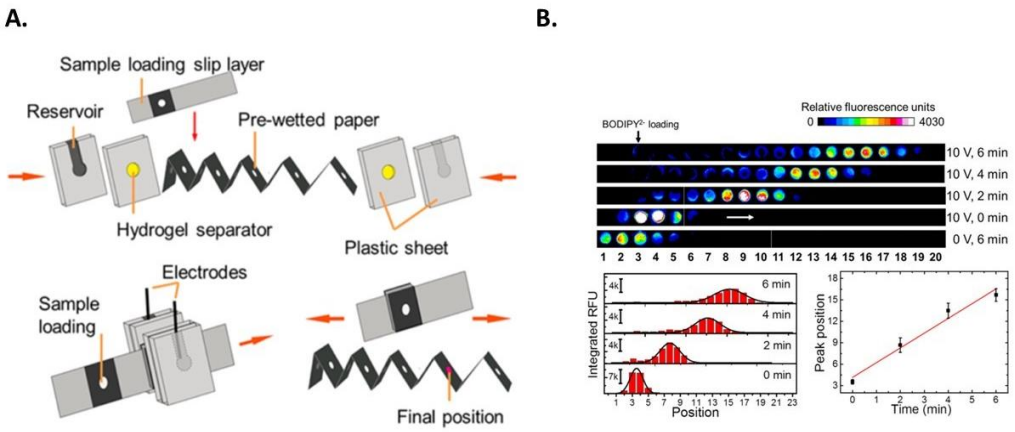

Figure 1.5. Fluorescence relative distribution (a) and micrograph of unfolded paper (b) of mixed fluorescence MPTS3^{-} and $[Ru(bpy)_3]^{2+}$ dyes at different running times. Conditions: voltage at 10 V, running time at 0, 1, 3, and 5 min, and sample loading was at layer 11 for a and b while the loading was at layer 3 for c and d. The arrows indicated the direction of the movements of each of the fluorescence dyes. Adapted with permission from ref. [180]. Copyright 2014 American Chemical Society.

Moghadam et al. carried out the ITP on a µPAD for the pre-concentration of dyes of up to 900-fold using a field strength of 11 V/cm within 4 min [179]. In this case, the LE was Tris-HCl and the TE was HEPES. Nitrocellulose was designed in strip- and cross-shapes using a CO_2 laser cutter before placing these on an acrylic holder (Figure 1.7A). Alexa Fluor 488 succinamidyl ester was added to the TE and 3% PVP was added to the LE. Images were collected using a fluorescence microscope to quantitate the sharp and intense band from 5-140 s (Figure 1.7B). Incorporation of a battery completed the integrated system for the portable diagnostics.

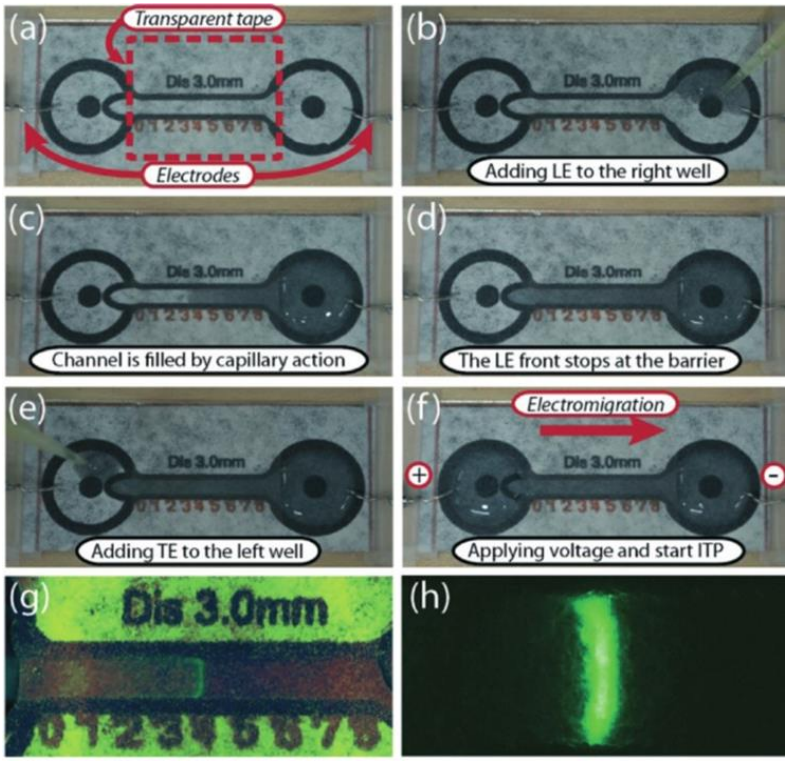

Figure 1.6. ITP protocol on the designed device starting from (a) placing the electrodes into the reservoirs with the channel covered with laminating tape as indicated with the dashed lines, (b) LE was added to the right reservoir and the chamber and channel were filled by capillary action on the paper (c and d). A mixture of the sample and the TE was added into the left reservoir (e.) before the voltage was applied for the ITP (f). Photograph of the fluorescence taken using a commercial camera (g) and a fluorescence microscope (h). Reprinted with permission from ref. [177]. Copyright 2014 Royal Society of Chemistry.

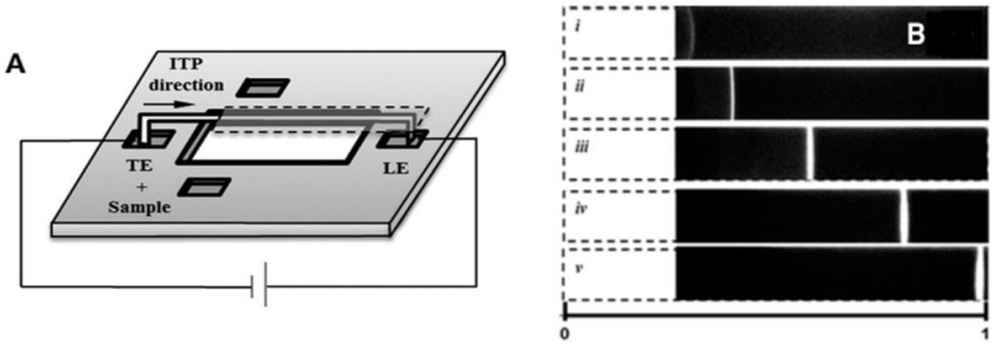

Figure 1.7. (A) Device design with the TE mixed with sample on the left and the PVP mixed with the LE on the right. The arrow indicated the flow direction of the ITP. (B) The ITP interface at (i) 5 s, (ii) 30 s, (iii) 60 s, (iv) 90 s, and (v) 140 s after the electric field was supplied. Adapted with permission from ref. [179]. Copyright 2014 American Chemical Society.

OuYang et al. claimed electrochromatographic separations using µPADs, combining the electrophoresis with the ion exchange chromatography for the separation of metal complexes on Whatman No. 1 [178]. The device was fabricated by means of photolithography using a SU-8 2150 negative photoresist. Paper strips were dipped into the buffer vessels containing the analytes and ethylenediaminetetraacetic acid (EDTA), respectively, while the electrodes were taped in place. Complexing agent, EDTA, was placed in the left cathodic vessel, while a mixed solution of metal ions (Co^{2+}, Cu^{2+} and Fe^{3+}) was placed in the right anodic vessel. When the potential was applied, EDTA and the ions moved towards one and another to meet at the chelation boundary, where the meeting of the two boundaries was marked by an increase in current. In the field, the chelation band separated into the three zones corresponding to the complexes, suggesting the separation may be more electrophoretic than chromatographic (Figure 1.8). Later in 2016, the author reported the modification of another moving chelation boundary (MCB) system to a paper-based chip in order to address the issue of poor detection limits for the separation of the trace metal ions found in the previous work [205]. Field-amplified sample stacking (FASS) was used to move the ions through the boundary between the low concentration and the high concentration background electrolyte, where the loss in velocity at the boundary resulted in concentration.

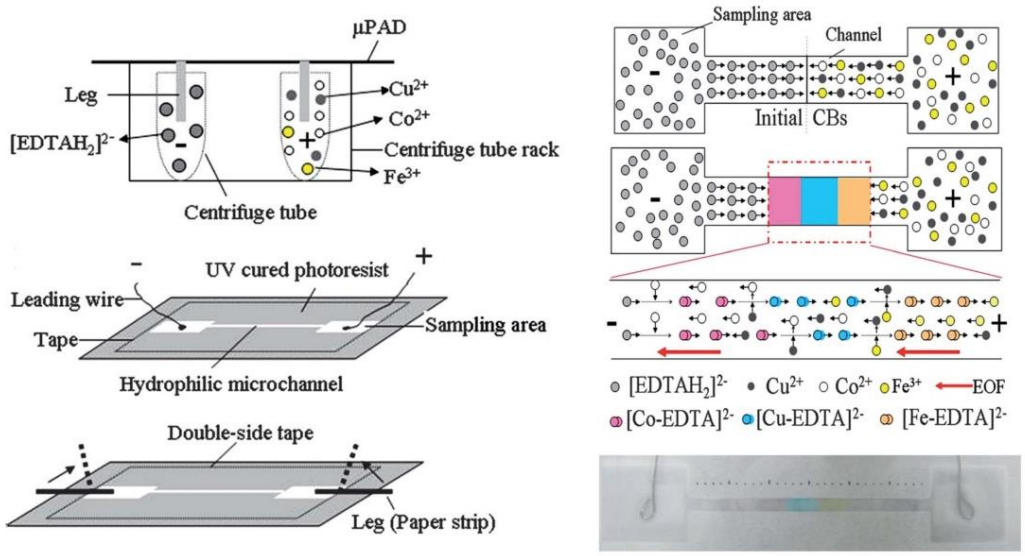

Figure 1.8. Schematic illustration of the electrochromatographic μPAD (left) and mechanism (right) on the paper device where the boundaries of the EDTA and metal ions migrate across in opposite directions and form coloured zones in the middle indicating the chelation boundaries (CBs). Adapted with permission from ref. [178]. Copyright 2014 Royal Society of Chemistry.

A fully disposable electrophoresis μPAD incorporating pencil-drawn electrodes for capacitively coupled contactless conductivity detection (C^4D) was developed [190]. The device was used for the analysis of biomarkers, including bovine serum albumin (BSA) and creatinine, in only 150 s. The microfluidic design included a cross shape, cut by a CO_2 laser engraver, in a foldable thin sheet of lamination film, serving as an insulator for the electrodes; the reservoirs were cut out of the film and attached to reservoirs made from pipette tips (Figure 1.9). The results from the μPAD were compared with a conventional glass microchip (i.e. free solution electrophoresis) where no separation of these compounds could be observed, probably because of non-specific binding of the BSA, demonstrating a benefit of this approach.

While not directly simple to use and portable, mass spectroscopy (MS) was considered in combination with μPADs due to its specificity and enhanced sensitivity compared with visual detection [206, 207]. The modification of the nanospray by using a paper substrate with a sharp

tip, led to the so-called paper spray ionisation (PSI) [208, 209]. Samples were separated using paper-chromatography with a compatible solvent prior to cutting the paper containing the analyte zones into sharp triangle shapes (or tips). These were wetted with more solvent, horizontally facing towards the inlet to the MS and the PSI started as soon as a voltage was applied using the metal crocodile clips. The Verpoorte group performed online chromatography of three dyes using modified PSI by combining it with a 3D printed polylactic-acid (PLA) cartridge containing solvent reservoirs for integrated control fluidic control [210].

Rapid in-situ ion-transmission MS for paper electrophoresis was developed by Zhang et al. [192]. A low-temperature plasma probe was used in order to directly ionise the sample from the µPADs, eliminating the need to cut the paper into sharp tips. A mixture of amino acids and a mixture of drugs in blood were electrophoretically separated on a 3D µPAD before being unfolded, subjecting each layer to the plasma probe for the MS detection without further treatment.

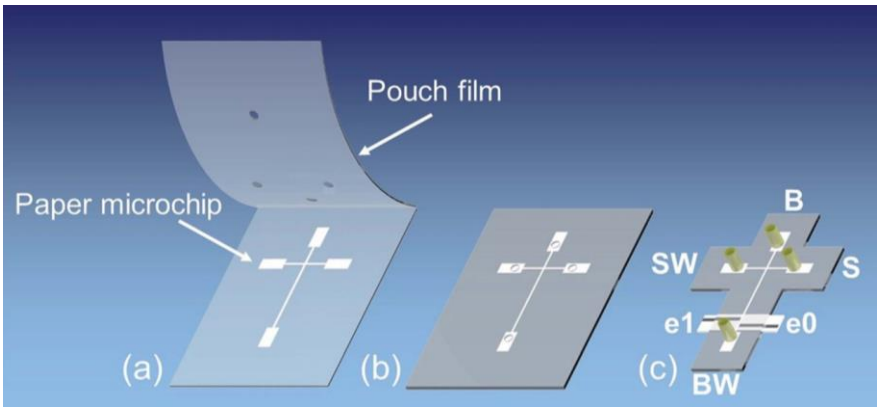

Figure 1.9. Fabrication of the fully disposable paper-based electrophoresis microchip. The laser-cut paper was placed between the laminating films with pre-pierced holes for detection zones (a-b). The electrodes for C^4D (e1 and e0) were pencil-drawn and attached to the pME with tape before lamination while the base of the pipette tips was used as a reservoir for buffer (B), sample waste (SW), sample (S), and buffer waste (BW). Reproduced with permission from ref. [190]. Copyright 2016 Royal Society of Chemistry.

1.2.3. Challenges of electrophoresis on paper-based substrates

Despite the fact that electrophoretic μPADs benefit from the advantages of miniaturisation, and have been demonstrated to be capable of rapid, simple, and portable assays in a low-cost and environmentally friendly manner, the resolution that has been achieved so far is lower than the column chromatography and CE/microchip electrophoresis. Progress has been made since the introduction of the μPAD, but some technical challenges still remain.

First, more rapid separations require higher electric fields, and higher current values lead to the generation of more heat [177, 179]. As known from the large-scale paper electrophoresis, the subsequent evaporation can compromise the wetting and even cause burning of the paper. Clamping of the paper between glass plates used in the past has been replaced by tape or laminating foils for sealing the device. Additionally, different fabrication approaches were successfully applied in order to reduce the cross-sectional area. These solutions add steps to the fabrication process and require accurate alignment [179, 211].

Second issue to address is the non-specific adsorption of proteins and bio-molecules. Compared with conventional microfluidic substrates, the surface area available for adsorption and immobilisation is significantly larger on the fibrous structure of the paper [132, 212, 213]. Surface treatment with specific enzymes or appropriate blocking agents prior to the separation was demonstrated to reduce this phenomenon.

Third, a better understanding of the effect of the type of paper for specific analyte groups is required, as it affects both resolution and detection. For example, charge density is important for electrochromatographic separations exploiting ion exchange interactions but may hinder the purer electrophoretic separations. Therefore, the selection and modification of the paper substrate with active functional groups is needed in order to enhance the efficiency in separation to different target compounds [214-216]. A potential information resource on

functionalised paper and paper-like substrates may be in the development of 'polymer paper' for bank notes.

Finally, similar to all electrophoretic separations, optimising the buffer and other conditions requires a delicate balance between speed and resolution [217]. Considering the relative youth of electrophoretic μPADs, fundamental studies in this area are yet to be conducted. With an increasing necessity to develop μPADs with electrophoretic functionality, these studies will be conducted for different analyte classes, contributing to a greater insight and faster optimisation strategies.

1.2.4. Conclusion and Future Direction

Paper electrophoresis was introduced almost 80 years ago, and despite the wealth of applications, it was surpassed by the electrophoresis in gels and capillaries based on the superior performance thereof in the 1970. The introduction of the μPAD in 1996 has provided a renaissance of paper-based assays and provides new opportunities for paper electrophoresis. This time, the scientific community is armed with a more developed understanding of the electrophoretic phenomena as well as the surface chemistry to help develop paper electrophoresis further. The microfluidic features in μPADs are relatively large, leading to Joule heating when using the high fields required for zone electrophoresis. Using the self-focusing effect of the ITP as a separation technique or concentration mechanism provides a means to address the sensitivity issues in the μPAD assays without the need for high field strengths, with up to 400-fold enhancement in the sensitivity reported. In addition to separations, an electric field can be used for the electrokinetic fluid control in order to mobilise and transport reagents, opening interesting opportunities when using zone passing techniques to gain control of the more complex and/or multistep reactions on the μPADs. While in today's form, μPADs may not be ideally suitable for high resolution electrophoretic separations, there are many uses for low resolution separations on μPADs for the purpose of performing sample preparation and/or concentration, or as orthogonal contributor to

a multidimensional separation system. It is therefore expected that the number of μPADs incorporating electrophoretic phenomena will increase in the future, particularly for those applications where sensitivity and specificity are required.

While electrophoresis on μPADs is still undergoing advancements, there has been existing technologies utilizing in commercialized POC platforms involving paper in their platforms. With general concepts of POC and μTAS being similar in several aspects in terms of miniaturization for rapid analysis, cost and resource reduction, and ease of operation, understanding the principles and limitations of these technologies might be essentially helpful as guidelines for future developments in this research. Hence, next section discussed around the special features and drawbacks of commercially available paper-based POC devices.

1.3 Point-of-care (POC) concept for clinal diagnostics

In the present day, modern instrumentation, infrastructure, techniques and innovations in medicine contribute to clinical diagnostics to identify pathogens and disease markers, boosting the capability of global health care system, and therapeutic drug monitoring (TDM) for personalized therapy of each individual [218]. However, this sophisticated improvement of the diagnostics is useful in developed countries where the clinical facilities, trained personnel, and resources are financially achievable. On the other hand, in developing countries where those conditions cannot be met, the utility of modern diagnostics has not been fully exploited [219]. POC is very demanding due to the limitations of lack of resources and affordability as well as diagnosis turn-around time [220]. Current innovations have developed POC to be suitable for routine indicative tests employed in physician's office and centralized laboratories, and potential improvement for remote areas or at home with extremely low budgets and resources are significantly growing.

1.3.1 Attractions of POC

POC is considered as a “near patient” laboratory diagnostic as the principles of traditional analysis are employed but scaled down onto a smaller platform, such as chip-based or stick-like devices, that can be operated without trained personnel or specific procedures together with immediate qualitative information without compromising the accuracy and sensitivity of the traditional laboratory test [221, 222]. Ideal features of POC were described by World Health Organization (WHO) and Food and Drugs Administration (FDA). WHO defined POC with an abbreviation “ASSURED” indicating that POC should be: affordable, sensitive, specific, user-friendly, rapid and robust, equipment-free, and deliverable to those who need it [223]. Similarly, FDA outlined POC must be automated, compatible with unprocessed samples, chemical handling-free, maintenance-free, and giving clear to read result [219].

The key characteristic of POC is the miniaturization of diagnostics from benchtop instrument to portable or handheld-sized analytical devices with a purpose of the system being used outside of centralized hospital or laboratories. The required volume of samples and reagents for the system, operational procedures, and analysis time are also reduced. And subsequently, an overall diagnostic cost could also be lowered; making it more affordable and practical for remote area use [221, 224].

1.3.1.1 Reduction of samples and reagents

Since samples used in clinical diagnostics are mostly body fluids such as whole blood, plasma, serum, saliva, urine, or sputum, the “less volume” feature of POCs not only assists for easier sample collection but also provides benefit to the users in terms of physical comfort, especially blood sampling [224, 225]. Typical blood collection usually involves phlebotomy, collecting mL of volume, and it poses risk of possible blood loss and anaemia which could be critical especially in infants. By using POC where only tens to hundreds of microliters of sample is needed, the potential health hazard is greatly reduced [222, 226]. Similarly, less volume of reagents

required reduces handling of unstable or sensitive chemical by users. In many POC devices, dried reagents are deposited on the platform, completely removing the process of reagent handling for the users [227]. Additionally, less volume and less frequency of reagent use contribute to reduction in diagnostic cost since reagent can be one of the most expensive components [228]. Also, lower consumption of chemicals consecutively lowers the chemical waste generation and disposal [229].

1.3.1.2 Rapid analysis and turn-around therapeutic time

Miniaturization combined with microfluidics makes portable handheld devices robust when some, if not all, of the procedures are either eliminated or integrated onto the platform [219]. Microfluidic integration assists with automatic control of the assay on a lab-on-a-chip approach where all the essential steps of diagnostics tests including sample loading, sample preparation (if any), chemical interactions (i.e. separation, mixing, centrifugation), and detection are combined into a single continuous process [221]. Complex operations on microfluidic POC can be manipulated by designing microchannel dimensions influencing robust and tunable fluid flows without the need of additional instrumentations such as pump or power supply. Diagnostic platform of smaller scale with on-device detection zones allow faster indicative “yes/no” response within minutes or hours and not days or weeks [230]. Faster turn-around information of POC profits both patients/users and physicians as this facilitate for faster therapeutic design and treatments which could be critical life and death decision in some case.

1.3.1.3 Improvement users’ satisfaction

The availability of the POC technology may also result in improved patient satisfaction in personal health in terms of personal time and financial management [222]. In a regular centralized laboratory setting, diagnostics are acquired through two scenarios [231]. In the first case, a patient needs to attend a laboratory prior to physician visit for sample collection and the test results are presented in person at the physician’s office at the appointment. In the second case, patient visits the office first, then attends a laboratory for sample collection and test results

are reviewed and delivered via post or phone. In both cases, a second trip to the physician/laboratory is sometimes unavoidable causing inconvenience both physically and financially. In developed countries, the use of POC introduces another option for patient where immediate indicative analysis could be performed and the test result can be discussed during a single visit at the office indicating re-visit/follow-up appointments, phone calls and letters could be greatly reduced or even eliminated unless absolutely necessary [220]. This availability also generates an opportunity for developing world for better access and affordability to the latest diagnostic technology. Some POCs are even self-operated with very simple result display (i.e. line or colour) making it easier for patient to perform and understand the assay while only report to the physicians should unusual results are shown [221].

1.3.1.4 Lower medical cost

Regarding cost effectiveness, POC tests compared to traditional centralized laboratory tests are generally more expensive as most of individual parts are consumables and made for single use purpose [221, 222]. This implies that each unit of POC requires its own stable reagents (sometimes more expensive than those in the centralized laboratory), assemblies, packaging, labour, transportation, quality assurance, and maintenance [232]. Even though each complete unit composed of inexpensive chemicals and materials allowing multiple-unit mass production, but hidden costs in the processes in-between, such as polymer moulding, deposition of reagents, or electrode integrations are often not considered. However, cost-effectiveness as one of the characteristics of POC always refers to the overall medical cost per one user/patient. As mentioned previously, all aspects of POC support affordability in which users from remote areas could have access to diagnostic simply by a device being deliverable or can be purchased off from the shelf at low cost. Subsequently, further cost reduction would derive from eliminating the necessity of patients travelling to the hospital or laboratory [220]. In some cases, similar symptoms could lead to confusion and misinterpretation of one illness with another, multiple tests are usually assigned by the physicians for confirmation; hence, there may be additional expense. Instant affirmative

test information may greatly facilitate earlier triage, strategy and treatment toward specific illness, significantly avoiding the amount likely to be spent for unnecessary tests, hospital fees (admission) and prescriptions caused by uncertainty of diagnosis and mistreatments [221, 233].

1.3.2 Types of POC

For a POC unit to be affordable, a significant contribution is the cost of the substrate itself [234]. One of the most common substrates used in POC assay is paper owing to its low cost, wicking capability, abundancy, biodegradability, versatility in functionalization and many more advantages expressed in section 1.2. Therefore, almost all developed POCs have paper, sometimes combining with membranes, as one of the materials for the bioassays. And with paper as a part of the substrate, its capillary feature provides the fundamental capability for LFA in forms of dry specific immuno-reagent strip and 3D-network μPADs for multiple analytes become the popular formats for developing POC for developing areas [235].

1.3.2.1 Pregnancy test

One of the classic commercial POCs available on market is the home pregnancy test strips. The basic principle behind pregnancy test is the lateral flow assay-based test or LFA using urine as sample and the assay will detect target hormone, human chorionic gonadotropin (hCG), presented only during pregnancy [236]. The diagnostic assay relies on the chromatographic effect from one end to another while the fluid wicks along the strip by capillary forces. The strip is composed of several pads connecting to each other as substrates with specific functionalities. These are usually made from different materials including porous membrane and cellulose with some of them having pre-stored reagents. The outputs are mostly presented simply by colour visualization as line observable on-device with naked eyes. The latest advance in home pregnancy test today is made to be able to the determine concentration of hCG detected allowing the assay to approximately estimate the period of pregnancy with digital word display shown in Figure 1.10e [237].

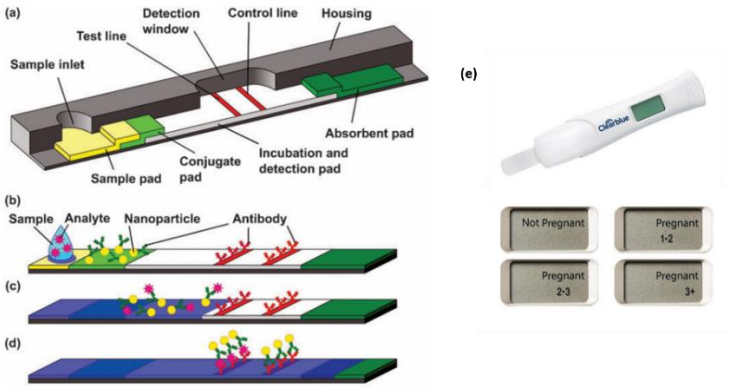

Figure 1.10. Scheme showing multiple components, chemicals and their functions (a and b) and concept of LFA strip test with fluid flowing in direction from left to right via capillary action of the substrates (b to d). Reproduced with permission from ref. [238]. Copyright 2010 Royal Society of Chemistry. The latest advance in commercial home pregnancy with digital result and week estimation of pregnancy using Smart Dual Sensor™ (e). Image downloaded from ref. [239] in December 2018.

Major internal parts of typical LFA devices are normally composed of sample pad, conjugate pad, incubation pad, detection pad, and absorbent pad where only sample and detection zones are visible externally after assembling in enclosed plastic housing (figure 1.10) [115]. The sample pad is normally made of cellulose or cross-linked silica and used for filtration of the target and interference particles. Located next to the sample pad is the conjugate pad, typically cellulose, cross-linked silica, or polyesters, consisting of conjugated-antibodies specific to hCG. The conjugating particles used are signal generating species such as nanoparticles or fluorescent tag molecules. As liquid flows, hCG from the urine is bound to conjugated-antibodies and they migrated together to the incubation and detection pad, made of nitrocellulose membrane due to its adequate physical support and excellent biorecognition molecule binding affinity. Located in this pad are another two types of antibodies: one to capture antibody-bound hCG resulting in a positive test and another as a negative control which is specific to the unbound-hCG complex [240]. Control line always appears to validate the performance of the detection of the assay while test line will display only when analytes were present in the sample [238]. The absorbent pad at the

strip will wick the fluid flow to the waste reservoir. This pad also allows for more volume of sample if needed or it could prevent the sample from flowing back in the opposite direction [241].

1.3.2.2 Blood glucose meter

Another well-known commercial POC is a self-operated blood glucose meter mainly used in diabetes patients in hospitals, medical centres and at home to monitor the blood sugar level such that the daily diet can be controlled, and the medication can be appropriately administered [242]. Glucose monitoring assay is mostly based on the electrochemical current displayed using the pocket-sized digital readers. The signal is generated from the redox reaction (oxidation) of glucose with specific enzymes such as glucose oxidase or glucose dehydrogenase (GDH) [221]. With this principle, the higher the concentration of glucose presented in the blood sample, the higher current from oxidation reaction was generated corresponding to the number displayed on the reader as concentration of glucose translated by the integrated transducer [243]. Blood glucose POCs are normally available for purchase over the counter (OTC) in package or kit comprised of the digital reader, lancing device, single-use lancets, control solution and single-use test strips (Figure 1.11) [244]. A small volume of blood is collected by finger prick using the lancet and lancing device before being drawn into the test strips pre-inserted into the reader and the result displayed within approximately from 5 to 30s [245]. Since there are many commercially available glucose meters in the market, each brand may have different technology and design so that it fits into the reader from that specific brand; however, the fundamental concept of components in the test strips are almost identical [243].

The main parts of the strip are several stacked polymer membranes and cellulose layers of adhesive, liquid wicking pad, and circuit board shown in Figure 1.11 [246]. The uppermost layer (Figure 1.11a) is the coating adhesive or plastic materials to protect the components and circuit within the strip, in some cases, the brand logo is also screened here on this layer. Within the sample chambers, there are typically alternate layers of capillary liquid pad (Figure 1.11b) to attract and

soak the blood drop drawn from finger prick, adhesive layers (Figure 1.11c and 1.11e) and layer of spacer (Figure 1.11d). The spacer serves as another protective layer segregating the circuit from touching other components and potentially filter and direct the wicking direction towards the reagent pad (Figure 1.11f). Reagent pad is also referred as reaction center where the glucose conversion enzymes and chemical mediator are pre-deposited, and the oxidation process occurs. The current generated is then carried by the gold and palladium coated electrodes (working electrode, counter electrodes and reference electrodes) on the circuit board sitting underneath delivering signal to the reader. Some further advances made to glucose strip was fabrication on a single layer of paper in the form of a µPAD in which the electrodes can be screen-printed directly on the substrate and different zones can be partitioned using wax-printing barriers making it simpler than multiple layers stacking [45, 247, 248]. The µPAD strip was also tested to be compatible with commercial digital reader and the performance was almost comparable to that of commercial strip presenting a potential of µPADs being commercialized in the future [45]. A glucose diagnostic test was also designed on origami 3D µPADs, based on colorimetric assay, similar concept as mention above in section 1.2 to detect and quantify the concentration of glucose using the colour intensity without using the digital reader [249].

Figure 1.11. A complete kit of commercial OTC blood glucose meter consisting all essential tools for in-home diagnostic (left) and cross-section image showing major components of glucose test strips and their functions (right). Images downloaded from ref. [244] (left) and ref. [246] (right) in December 2018.

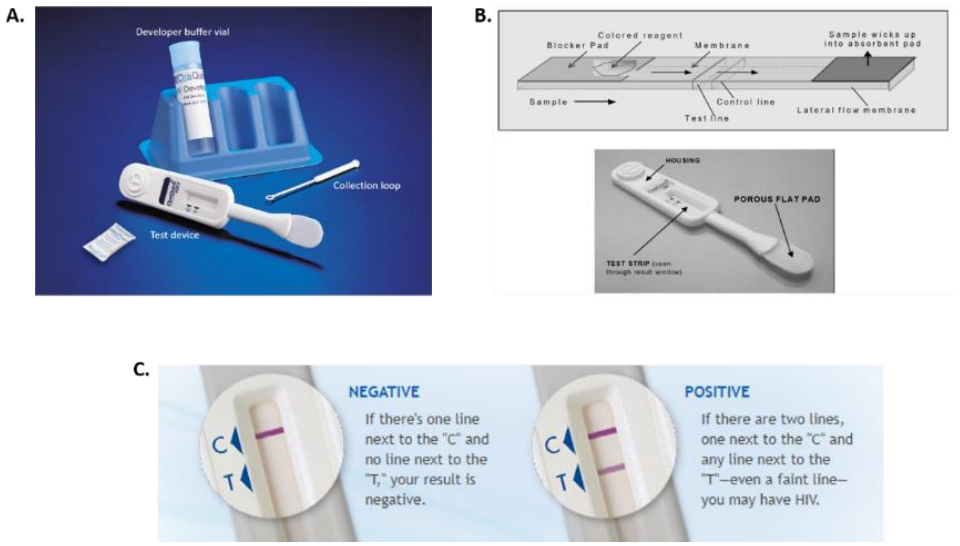

Figure 1.12. (A.) Commercial OTC OraQuick® in-home HIV Test kit (image downloaded from ref. [250] in December 2018) and (B.) components of testing device based on lateral flow assay format (image downloaded from ref. [251] in December 2018). (C.) The test displays result with purple colour lines visible from the detection window (image downloaded from ref. [252] in December 2018.

1.3.2.3 HIV/AIDS CD4 test

Human Immunodeficiency Virus (HIV) and Acquired Immune Deficiency syndrome (AIDS) are a global concern and it mostly resides in the undeveloped countries such as Africa or those in southeast Asia [253]. The diagnostic is performed by determining the HIV antibodies and viral nucleic acid from fluid samples to indicate the potential of infection followed by monitoring of the number of T-helper cells suggesting the commencement of treatment. In these locations, the gold standards for HIV/AIDS diagnostics such as HIV viral load testing (VL), Enzyme Linked Immunosorbent Assay (ELISA) and western blot for p24 antigen and flow cytometry for CD4 cell count are either inaccessible or difficult to perform without being trained meaning that patients need to travel or samples need to be sent to the medical center where test are to be taken and results are presented on the next visit which could take several days to weeks [254, 255]. In some cases, the patients are too sick to return while waiting for the diagnostic result. Faster decision then needs to be made for HIV-infected patients, so they can undergo the process of antiretroviral treatment (ART) as soon as possible from the acute stage.

One example of OTC LFA-based HIV diagnostics is OraQuick® in-home HIV test which is quite comparable to conventional ELISA [252, 256]. The assay relies on the detection of antibody against the HIV with oral fluids as preferred sample even though whole blood collected through finger prick and plasma specimen can also be used [257]. The package comes with the test device (Figure 1.12) and a separate sealed vial of buffer reagent for operation. For oral fluid, collection is done by direct swabbing using the flat collecting pad on the device and the device inserted into the buffer vial. Alternatively, blood is collected through the collection loop and mixed into the buffer vial before the device is inserted. Capillary action then draws the sample towards the absorbent pad. The base materials for the test strips are identical to those in the pregnancy test with conjugated antibodies and antigens preloaded on the conjugate, incubation and detection zones. A purple line will appear in the T-zone with presence of HIV captured by the antibodies. Colour intensity does not relay any quantitative information; however, faint colour must not be neglected as it could hint that patient might be infected with HIV and further appropriate testing is required for confirmation. Again, regardless of negative or positive result, there is also a separate place where the purple colour will appear to validate the assay. The complete assay finishes in approximately 20-60 min.

Currently, many companies are developing handheld LFA for CD4 cell count and strip/device. Blood is used as specimen and available for both Viral load (VL) and CD4 cell count. POCs today are mainly portable single-used cartridge and compact benchtop analyser equipped with fluorescent imaging detection [225]. Lymphocyte CD4 cell count serves as immune system marker assisting physicians to start ART treatment and also its follow-up response to the treatment in case of treatment failure due to various conditions such as drug resistance [258]. Principle of LFA is also applied where the antibodies are conjugated with fluorescent tags, dried and deposited onto the anticoagulant coated substrate within the cartridge to eliminate the need for refrigerated storage of the reagent. Specifically, the CD4 T-lymphocytes from blood interact with presented antihuman monoclonal antibodies then the cartridge is inserted into the analyser generating

fluorescent images for cell counts captured by the analyser software [259]. VL is a quantitative diagnostic method based on amplification techniques to investigate patients' response to the treatment while undergoing ART by quantifying viral RNA and enzymes [255]. Until now, there has been no commercial in-home assay that can be performed by the patients since the method relies on the specific procedures including polymerase chain reaction (PCR) or branched DNA (bDNA) requiring specially trained personnel to both operate the device and evaluate the results.

1.3.3 Challenges in current paper-based POCs

At the moment, commercialized POCs are designed to specifically detect one target analyte at a time implying that fresh sample is required each time for different assays [235]. This is inconvenient for patients in terms of sample collection especially blood, even when only a small volume is collected via finger pricking, as repeated puncture can also result in significant amount of discomfort. Despite the fact that improved µPADs are designed to address this limitation by allowing multiple assays to be performed in a single platform, mobility of samples on µPAD depend on capillary action of the paper combining with nature of different samples in terms of viscosity or surface tension which put the limit on the mobility control (i.e. mobility and speed could not be modified) and analysis time would likely to depend on the sample's nature such as viscosity [115]. The specificity in ELISA LFA-based POCs solely depends on antibodies being very sensitive and accurate in capturing and forming complex with an analyte not only meaning some of them are very expensive but also implying that small transformation of antibody structures could lead to impaired coupling ability and cross-reactivity especially with unfiltered sample resulting in sensitivity loss and inaccurate outcome [260].

In some assays, by using a smaller volume of sample, liquid solvents or buffers are required to drive the sample towards detection zones to retain continuous capillary flow. Some other complications with enzyme-specific POCs may also occur during manufacturing from potential non-uniform distribution and drying rate of the reagents onto porous substrate during

deposition of enzymes or reactive reagents; for example, insufficient hydration would result in dysfunction of the reactive enzymes while overhydration would then cause them to denature resulting in faulty assay [246]. On the contrary, small volume could also considered to be large and become insufficient when the actual sample is not in abundancy such as ocular fluid [260].

Since the largest area of POCs application is clinical diagnostics, the major type of sample remains blood in the form of serum or plasma. Not all assays can be used with whole blood directly, and sample preparation (i.e. plasma extraction) is still required [115, 261].Conventionally, sample pre-treatment steps are often referred to protein precipitation, solid-phase, liquid-liquid extraction and/or additional separation processes including chromatography and electrophoresis where they are considered the rate-limiting step in clinical diagnostics with large consumption of additional solvents or sorbents to ensure maximum removal of interferences, and recovery and purity of the target species as possible [262, 263]. The ultimate goal for developing POCs is to have an assay without sample preparation, with current µPADs being developed to either completely eliminate or integrate the step such as mixing, separating, extraction, or pumping onto the directly on a single platform; however, not many have been fully developed. As shown above, typical commercialized POCs are designed with combination of different pads with specific features connected to each other or by stacking them together and sometimes they require external instrument to complete the assay (i.e. glucose meter device). The disadvantage from having many materials is the possible heterogeneity of the flow and sensitivity of the assay due to different complexity of each material as well as a concern over how they are aligned and connected with each other [115]. Another persistent flaw found in paper and nitrocellulose used in LFA is the non-specific absorption of interference biomolecules, mostly proteins, that might be present in the sample. This adsorption can disrupt the flow and cause errors in detection due to imprecise amount of analyte to be detected [264-266]. Additional step of washing/blocking or surface pre-treatment of the substrate is almost mandatory. Even though µPADs with electrochemical detection have been presented in a single paper-based material with conductive ink printing method, this can be

very complicated and sensitive step as the paste mixture need to be printed very precisely, not only to prevent defect in electrical transfer signal but also to ensure the reproducibility of each strip [246]. Instrument-wise, some simple error such as user's action could also induce false positive result; for example, in commercial glucose reader, false positive could have been resulted simply from the test strip was not inserted properly; hence, connection between one assembly to another is very crucial [246].

1.3.4 Paper-based home collection device

Currently, well-developed POCs are commercially available and being used extensively for common infectious diseases including HIV, syphilis, and malaria; however, there are still many other endemic infectious diseases such as bloodborne infections, tuberculosis, trypanosomiasis and black fever as well as those where the disease-relating information can only be obtained through blood in which rapid POCs tests have not been made practical [233, 267]. In general scenarios, patients are being treated based on the evident symptoms and the standard guidelines of diagnostics for feasible diseases and this could lead to mistreatment due to non-specific examination. With diagnostic POCs not yet available in some areas, routine cycle of hospital and laboratory visits becomes inevitable and not many patients, especially in the rural area, can manage to do so. In attempt to prevent healthcare failure, an alternative option is to collect the sample at home by the patients themselves or at the site by clinicians or personnel at the local health facilities, and then send it to a central laboratory to be analysed using modern technology. In this area, sample collection POCs are available in form of filter paper card such as well-known newborn blood screening Guthrie card, pioneered by Dr. Robert Guthrie, mainly for potential genetic disorders [268].

The Guthrie card has long been used to collect blood from heel prick in almost every new born infant during their very first days of life at the hospital to scan for risk of fatal diseases [269]. A single card is designed with allocated circles in which blood will be soaked (approximate

volume from 5-50 µL per each circle) together with demographic data which is written with a pen before being placed in a sealed plastic bag and sent to the laboratory [270-272]. Guthrie card, made from filter paper is cheap, easy to use and safe in term of biological hazard as the blood collected on the card is air-dried and stored in the form of a dried blood spot (DBS) making it possible to be transported with only desiccant while fluid samples must be treated as infective and contagious; hence, have much more strict handling procedures [271, 273]. Despite all the advantages, the steps of sample preparation after the collection is still a major concern as mentioned previously [274].

In Guthrie card, standard DBS extraction involves the following steps: physical punching of the circles from the card, incubating overnight in suitable buffers strong enough to elute blood off the paper resulting in liquid-containing-blood solution followed by agitation (i.e. centrifugation, sonication, vortex, or shaking) with reactive reagents extracting target analytes and sometimes optional dilution for particular assay before being injected into analytical instruments [272, 275]. Another minor issue is the long drying time of DBS on the card before shipment, preferably between 3 hours up to overnight, as complete drying of fluid blood is critical to prevent possibility of bacterial growth during transportation [274]. Insufficient amount of analyte after DBS processing is also possible when compared to pure serum or plasma samples due to strong absorption of the molecules within the DBS onto the paper and enrichment of the sample may be needed [273, 275]. Manual cutting or punching of the specified areas from the card could also affect the quantitative results and reproducibility as certain areas might contain different amount of analytes [273].

1.4 Polymer Inclusion Membranes (PIMs)

Attempting to address issues found previously on paper-based POCs, attention has turned towards functionalized membranes as a platform for portable POC devices. Polymeric membranes have been introduced and utilized extensively in heavy metal industries as non-porous ion-selective electrodes (ISEs) and optodes for potentiometric sensors for decades and recently

have been further employed in sample treatment for biological, chemical, environmental, and clinical monitoring as they are considered greener alternative for conventional solvent extraction [276, 277].

1.4.1 Characteristics of PIMs

PIMs are examples of novel polymeric membranes where viscous and water-immiscible components (i.e. plasticizers and/or carriers) homogeneously integrated within the polymer matrix such as Polyvinyl Chloride (PVC) or cellulose triacetate (CTA) allowing specific ion exchange/extraction and providing better stability compared to conventional liquid membranes (LMs). Conventional LMs, where carrier was in a form of emulsion or impregnated with porous support, are prone to membrane breakdown causing leaching of chemical during operations [278], a problem not observed in PIMs. In many cases, thin film PIMs typically contain compatible hydrophobic plasticizer, so called membrane solvent, to create a gel-like environment preventing chemical leakage and supporting the flexibility of the film and mobility of ions at the same time [279]. Some degree of selectivity can also be achieved by the plasticizers based on their lipophilic partitioning property, even though plasticizers are more recognized in enhancing the ion extracting and binding performance of the carrier with the target ions [276]. There are also some PIMs those are plasticizer-free and consist of polymer base and carrier, as some carriers also have some extent plasticizing effect [277]. The carrier in the PIM is mainly responsible for specific binding with the target analyte in the sample, transport across the PIM via facilitated transport mechanism, before the analytes are released into the receiving solution [277].

PIMs are thin and transparent, constructed by homogeneously dissolving the three main components with suitable organic solvents (i.e. dichloromethane, chloroform, or tetrahydrofuran), then cast on the onto the flat surfaces [277]. The three constituents are bound to each other via physical forces without having strong permanent chemical bonding (i.e. hydrogen bonding or ionic bonding), and the chemical properties of each chemical is not altered after

combination [280]. Therefore, these compositions can be easily formulated as required for specific applications.

1.4.1.1 Polymer

The main responsibility of the polymer is to provide mechanical support and formation of the film with the two most popular polymers used in PIMs being CTA and PVC. These are very simple to prepare, have high solubility in volatile organic solvents and give mechanically stable films [281]. CTA membranes are reported to be more crystalline with their acetyl and hydroxyl functional group enabling them to form strong hydrogen bonds while PVC possesses a more amorphous phase held by dispersion force from the chloride groups making CTA stronger than PVC and could be reused several times. However, the polymer bases are also chosen based on their chemical resistance against various solution environment (i.e. extremely acidic or basic source solution) in which PVC shows better performance as CTA is prone to degrade from hydrolysis [282, 283]. The thickness of the PIM can also be controlled by optimizing the concentration of polymer bases, however too high a concentration of polymer provides a thick PIM with diminished diffusive flux [284, 285]. Therefore, most PIMs are cast as thin as possible to reduce the distance through which molecules are transported [286].

1.4.1.2 Plasticizer

As the polymer used to form PIMs are thermoplastic, having both crystalline and amorphous phases, a high degree of crystallinity from high polar intermolecular force could become be problematic as PIMs that are too rigid restrict the extraction and diffusive flux of molecules [287]. Plasticizers plays an important role in in loosening the intermolecular forces between the polymer chains making them less packed and the PIMs become softer and more flexible with more pathways for molecules to diffuse [288, 289]. With these abilities, plasticizers are regularly added into PIMs, making up highest proportion of all three components [290]. Plasticizers suitable for PIMs should have a certain level of lipophilicity that does not induce more

crystallization within the PIM as well as being able to dissolve (and be dissolved with) the substrates and additives [291, 292]. Optimal concentration of the plasticizer is crucial to the PIM for its physical morphology and the extraction efficiency. Too low concentration is insufficient to soften the film and may in fact become more rigid due to small available space from plasticizer allowing polymer chains to re-arrange themselves into a more tightly packed configuration, so-called anti-plasticizing effect [293]. Conversely, a high concentration of plasticizer reduces the mechanical strength of the PIM and there is the possibility of plasticizer leakage forming unfavourable gel-like hydrophobic barrier at the PIM surface restricting flux [281, 290]. In some cases, a high concentration of plasticizer increases the viscosity of the PIM leading to thicker membrane due to their high dielectric constant [293]. Examples of common plasticizers used in PIM are 2-nitrophenyl octyl ether (2-NPOE), dibutyl phthalate (DBP), tris(2-ethylhexyl) phosphate (TEHP) and dioctyl phthalate (DOP) [294].

1.4.1.3 Carrier

Also called ionophores, extracting agents or extractants, the carrier is a complexing agent that binds and exchanges with ions to achieve selective extraction into the PIM and influences diffusive flux [281]. Most research conducted on PIMs involves commercially available carriers, typically common solvent extraction reagents or macrocyclic compounds, while only a few have been custom synthesized [295-297]. Room temperature ionic liquid (RTILs) are another class of chemicals often employed in membrane technology as carriers. ILs are attractive because of their low vapor pressure, low flammability, large electrochemical window, and high ionic and electronic conductivity [298]. ILs are molten salts containing large variety of interchangeably cation and anion combinations exhibiting tunable properties (i.e. solubility, melting points, viscosity, and selectivity). Again, careful optimization of carrier concentration is important. Increasing the concentration of carrier may assist extraction due to increasing the number of possible complexes formed between carrier and analytes; however, the viscosity of the PIM also increases, or carrier molecules may cause precipitation, which restricts the diffusive flux of analytes within the PIM. On

the other hand, too low concentration inhibits the formation of the complex resulting in poor performance of specific binding; hence, unproductive extraction [280, 308, 322].

1.4.2. Basic set-up and application of PIMs

The basic set-up of PIM-based extraction cells is shown in Figure 1.13a. PIMs are sandwiched between two continuously-stirred compartments containing sample solution and receiving solution. In most settings, PIMs are designed and positioned for use against flat smooth surfaces with solutions on both sides; however, there are also some other configurations adapted for different platforms. One example was where a PIM was cast around glass capillary tubing giving them a hollow structure where they could also be used as a compartment containing receiving solution after one end was sealed (Figure 1.13b) [318]. PIMs are also very flexible and can be designed to fit a customized space like pipette tip where it was used as online microextraction device directly coupled to automated CE injection system (Figure 1.13c) [316]. Kinetically, the rate of extraction into a PIMs can be improved by incorporating into a system with electric field, namely electro-membrane extraction (EME) or electro-driven extraction (Figure 1.13d) [304]. This advancement enhances the enrichment factor of the sample (i.e. preconcentration) as well as the speed of analysis by active transport of molecules in the sample phase to the surface of the membrane where they are extracted and diffuse across the PIM. Further upgrade with EME was later introduced as sequential injection unit directly attached to the liquid chromatography-electrospray mass spectrometry (LC-MS) making the analysis system fully automated [305].

Many recent researches and industries reported using PIMs for recovery and/or removal of small organic molecules and heavy metals to either purify and preconcentrate the target ions or separating the interfering ions [281, 307, 314, 319, 323-325]. Examples of reported applications and their components including polymer bases, plasticizers, carriers are listed in Table 1.4. PIMs are valued for this purpose due to their ease of construction and modification, cost, and they are user- and environmental-friendly. As stated in section 3.3, traditional extraction methods

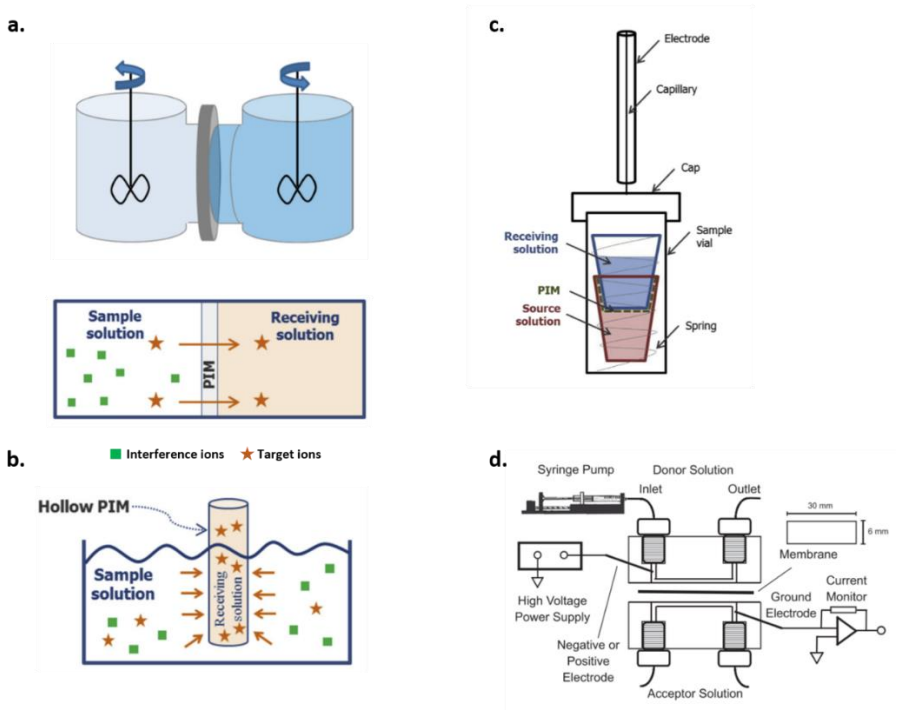

Figure 1.13. PIM-based set-up and concepts for sample preparation in (a) vertical two compartments configuration (reproduced with permission from ref. [277] Copyright 2017 Royal Society of Chemistry and ref. [321] Copyright 2018 Royal Society of Chemistry), (b) cylindrical hollow-PIM configuration (reproduced with permission from ref. [277] Copyright 2017 Royal Society of Chemistry), (c) shape-fitted microextraction configuration (reproduced with permission from ref. [277] Copyright 2017 Royal Society of Chemistry), and electric field assisted flow through extraction cells (reproduced with permission from ref. [326] Copyright 2014 Elsevier)

are considered hazardous and laborious mainly from amount of solvent consumption and vulnerability to leakage. With the "solvent" embedded within the PIMs matrix, this eliminates this risk making it practically solvent-less and further leads to higher stability, convenience and cost reduction.

1.5 Aim of the research

With all the limitations described on clinical diagnostics, current POC technology, together with electrophoresis being one of the simplest and easiest separation methods to make amendable to POC technology, the main goal was to address these restrictions using the newly

Table 1.4. Examples of PIM-based applications in extraction, transportation and pre-concentration and their compositions

Year	Authors	Applications/Sample sources	Target analytes	PIM components			Ref.
				Polymer	Plasticizers	Carriers	
2006	Fontàs et al.	Electroplating wastewater	Chromium (VI)	PVC	2-NPOE	Aliquat®336	[299]
2008	Pont et al.	Seawater and a Ni–Cd battery leaching solution	Cadmium (II)	CTA	2-NPOE	Aliquat®336	[300]
2009	Kalyan et al.	Tap water and groundwater	Mercury (II)	CTA	TEHP	Aliquat®336	[301]
2009	Kalyan et al.	Groundwater	Uranium (VI)	CTA	TEHP	HQ	[302]
2011	Zhang et al.	Pharmaceutical tablets and galvanizing industry solutions	Zinc (II)	PVC	DOP	D2EHPA	[303]
2011	See, H.H. and Hauser, P.C. *	River water	Herbicides and by-products	CTA	2-NPOE	Aliquat®336	[304, 305]
2011	Güell et al.	Environmental and industrial waters	Inorganic Arsenic species	CTA	N/A	Aliquat®336	[306]
2012	Salima et al.	Textile dye solution	Methylene blue	CTA	2-NPOE	D2EHPA	[307]
2012	Pérez-Silva et al.	Synthetic Wastewater	Phenol	CTA	*o*-NPPE and 2-NPOE	Cyanex 923	[308]
2012	Gajda, B. and Bogacki, M.B.	Polymetallic solution	Zinc (II)	CA	2-NPOE	1-decylimidazole	[309]
2012	Pérez-Silva et al.	Milk samples	Oxytetracycline	CA	2-NPOE	Cyanex 923	[310]

Year	Authors	Applications/Sample sources	Target analytes	PIM components			Ref.
				Polymer	Plasticizers	Carriers	
2013	Nagul et al.	Natural water sample	Orthophosphate	PVC	N/A	Aliquat®336	[311]
2013	Jayawardane et al.	Hot tap water and mine tailings water	Copper (II)	PVC	DOP	D2EHPA	[312]
2013	Onac et al.	Wastewater	Chromium (VI)	CTA	2-NPOE	5,11,17,23-Tetrakis[4-carboethoxy-N-piperidino] -25, 26,27,28-tetrahydroxy calix[4]arene	[285]
2013	Zawierucha et al.	Landfill leachate	Lead (II), Cadmium (II), and Zinc (II)	CTA	*o*-NPPE	Alkyl(aliphatic) resorcinarene derivatives	[313]
2014	Senhadji-Kebiche et al.	Wastewater	Zinc (II), Copper (II) and Iron (II)	CTA	2-NPOE	Cyanex 302	[314]
2015	Suah et al.	Lake and river water	Aluminium (III)	PVC	DOP	Triton X-100	[315]
2015	Pantůčková et al.	Human serum and blood samples	Formate	CTA	N/A	Aliquat®336	[316]
2015	Garcia-Rodríguez et al.	Environmental water	Antibiotics	CTA and PVC	2-NPOE**	Aliquat®336	[317]
2015	Mamat, N.A. and See, H.H. *	Plasma samples	Basic drugs	CTA	TEHP	D2EHPA	[318]
2016	Casadellà et al.	Urine	Potassium	CTA	2-NPOE	Dicyclohexan-18-crown-6 (DCH18C6)	[319]
2016	Chaudhury et al.	Nuclear wastewater	Cesium	CTA	2-NPOE	Chlorinated cobalt dicarbollide (HCCD)	[320]
2018	Sharaf et al.	Rare earth metals solution	Scandium (III)	CTA	DOP	Mixture of PC-88A and Versatic 10	[321]

**Electric-field assisted*

***Also investigated without plasticizer*

emerged PIMs as a platform for electrophoresis integration. In contrast to all other uses of PIMs for separation, the aim was to transport molecules along the PIM, rather than through the PIM.

In chapter 2, the investigation the capability of PIM for electrophoresis was explored. The PIM was made up of CTA as base polymer, 2-NPOE as plasticizer, and ionic liquid [EMIM][NTf2], as carrier. It was used laterally as a standalone electrokinetic platform in a dipstick/strip manner by using fluorescent dyes as model analytes to perform electromigration without using liquid electrolytes. Optimization of PIM constituents, PIMs selectivity towards different charges of dyes including neutral coumarin 334, cationic rhodamine 6G (R6G), and anionic fluorescein, and electrophoretic conditions are studied. Physical characterization of the PIM is also provided. A mixture of several cationic dyes was used to demonstrated electrophoresis on the PIM as well as their diffusion coefficients and electrophoretic mobilities.

In chapter 3, optimized PIM and electrophoretic conditions are further explored by applying the concept with small cationic pharmaceutical molecules, berberine chloride (BC), followed by the feasibility of the analytes presented in a real biological sample, a drop of whole blood deposited and dried on the PIM to form a dried drop of blood. The platform was then pursued towards implementation for pocket-sized, portable point-of-care sampling device for the extraction of BC from the drop of dried blood while the package transported thorough ground mail to the laboratory. This was to test the potential of perform sample preparation during transportation. Without further sample processing, extracted BC was quantified with a photon multiplier tube-fluorescence microscope. The workflow was also preliminarily emphasized by combining the PIM with imaging instrumentation, matrix assisted laser desorption /ionization-time of flight mass spectrometry (MALDI-TOF), inspecting the possibility in detection of non-coloured charged molecules, reported in chapter 5.

In chapter 4, another ionic liquid, Aliquat®336, was used in PIMs to investigate the selectivity towards anionic molecules using negatively charged fluorescent dyes. Again,

optimization of PIM constituent and electrophoretic migration was studied. Several surfactants with a similar structure to Aliquat®336 were also examined in the same manner to determine the how their structures influence the fundamentals of PIMs extraction and electromigration of charged molecules.

1.6 References

[1] A. Tiselius, A new apparatus for electrophoretic analysis of colloidal mixtures, T. Faraday Soc., 33 (1937) 524.

[2] S. Hjerten, The history of the development of electrophoresis in Uppsala, Electrophoresis, 9 (1988) 3-15.

[3] L.E. Kay, Laboratory technology and biological knowledge: the Tiselius electrophoresis apparatus, 1930-1945, History and philosophy of the life sciences, (1988) 51-72.

[4] O. Vesterberg, History of electrophoretic methods, J. Chromatogr, 480 (1989) 3-19.

[5] O. Vesterberg, A short history of electrophoretic methods, Electrophoresis, 14 (1993) 1243-1249.

[6] S.C. Plate, D. Perrett, An Outline of the Historical Background to Electrophoretic Separations, (2000).

[7] P.G. Righetti, Electrophoresis: The march of pennies, the march of dimes, J. Chromatogr. A, 1079 (2005) 24-40.

[8] A. Bathinapatla, S. Kanchi, M. Sabela, K. Bisetty, Chapter 7 Theoretical Principles and Applications of High Performance Capillary Electrophoresis, 2015.

[9] L. Rosenfeld, A golden age of clinical chemistry: 1948-1960, Clin. Chem., 46 (2000) 1705-1714.

[10] A. Tiselius, Experimental techniques. Zone electrophoresis in filter paper and other media, Discussions of the Faraday Society, 13 (1953) 29-33.

[11] A. Gordon, Electrophoresis and chromatography of amino acids and proteins, Annals of the New York Academy of Sciences, 325 (1979) 95-106.

[12] H. McDonald, Development of paper electrophoresis, Clin. Chem., 27 (1981) 781-782.

[13] D. Perrett, From 'protein' to the beginnings of clinical proteomics, Proteomics Clin. Appl., 1 (2007) 720-738.

[14] D. Perrett, 200 years of Electrophoresis, Chromatog. Today December, (2010) 4-7.

[15] H. Svensson, I. Brattsten, An apparatus for continuous electrophoretic separation in flowing liquids, Arkiv for Kemi, 1 (1950) 401-411.

[16] R. Consden, A.H. Gordon, A.J.P. Martin, Ionophoresis in silica jelly: A method for the separation of animo-acids and peptides, Biochem. J., 40 (1946) 33-41.

[17] S. Hjertén, Agarose as an anticonvection agent in zone electrophoresis, Biochim. Biophys. Acta, 53 (1961) 514-517.

[18] S. Hjertén, A new method for preparation of agarose for gel electrophoresis, Biochim. Biophys. Acta, 62 (1962) 445-449.

[19] O. Smithies, Zone electrophoresis in starch gels: group variations in the serum proteins of normal human adults, Biochem. J., 61 (1955) 629-641.

[20] S. Raymond, L. Weintraub, Acrylamide Gel as a Supporting Medium for Zone Electrophoresis, Science, 130 (1959) 711-711.

[21] S. Hjertén, “Molecular-sieve” electrophoresis in cross-linked polyacrylamide gels, J. Chromatogr. A, 11 (1963) 66-70.

[22] E. McDaniel, D. Martin, W. Barnes, Drift tube-mass spectrometer for studies of low-energy ion-molecule reactions, Review of Scientific Instruments, 33 (1962) 2-7.

[23] L. Ornstein, Disc electrophoresis-i background and theory, Annals of the New York Academy of Sciences, 121 (1964) 321-349.

[24] B.J. Davis, Disc electrophoresis–II method and application to human serum proteins, Annals of the New York academy of sciences, 121 (1964) 404-427.

[25] A.L. Shapiro, E. Viñuela, J. V. Maizel, Molecular weight estimation of polypeptide chains by electrophoresis in SDS-polyacrylamide gels, Biochem. Biophys. Res. Commun., 28 (1967) 815-820.

[26] K. Weber, M. Osborn, The reliability of molecular weight determinations by dodecyl sulfate-polyacrylamide gel electrophoresis, J. Biol. Chem., 244 (1969) 4406-4412.

[27] P.H. O'Farrell, High Resolution Two-Dimensional Electrophoresis of Proteins, J. Biochem., 250 (1975) 4007-4021.

[28] F. Sanger, S. Nicklen, A.R. Coulson, DNA sequencing with chain-terminating inhibitors, Proc. Natl. Acad. Sci. U.S.A., 74 (1977) 5463-5467.

[29] S. Hjerten, Free zone electrophoresis, Chromatogr. Rev., 9 (1967) 122-219.

[30] R. Virtanen, Zone electrophoresis in a narrow-bore tube employing potentiometric detection-theoretical and experimental study, Acta Polytechnica Scandinavica-Chemical Technology Series, (1974) 1-67.

[31] J.W. Jorgenson, K.D. Lukacs, Zone electrophoresis in open-tubular glass capillaries, Anal. Chem., 53 (1981) 1298-1302.

[32] J.W. Jorgenson, K.D. Lukacs, High-resolution separations based on electrophoresis and electroosmosis, J. Chromatogr. A, 218 (1981) 209-216.

[33] J.W. Jorgenson, Zone electrophoresis in open-tubular capillaries, TrAC Trends in Analytical Chemistry, 3 (1984) 51-54.

[34] S. Hjerten, High-performance electrophoresis: the electrophoretic counterpart of high-performance liquid chromatography, J. Chromatogr. A, 270 (1983) 1-6.

[35] S. Terabe, K. Otsuka, K. Ichikawa, A. Tsuchiya, T. Ando, Electrokinetic separations with micellar solutions and open-tubular capillaries, Anal. Chem., 56 (1984) 111-113.

[36] J.A. Olivares, N.T. Nguyen, C.R. Yonker, R.D. Smith, On-line mass spectrometric detection for capillary zone electrophoresis, Anal. Chem., 59 (1987) 1230-1232.

[37] A. Manz, D.J. Harrison, E.M. Verpoorte, J.C. Fettinger, A. Paulus, H. Lüdi, H.M. Widmer, Planar chips technology for miniaturization and integration of separation techniques into monitoring systems: capillary electrophoresis on a chip, J. Chromatogr. A, 593 (1992) 253-258.

[38] D.J. Harrison, K. Fluri, K. Seiler, Z. Fan, C.S. Effenhauser, A. Manz, Micromachining a miniaturized capillary electrophoresis-based chemical analysis system on a chip, Science, 261 (1993) 895-897.

[39] S.C. Jacobson, A.W. Moore, J.M. Ramsey, Fused quartz substrates for microchip electrophoresis, Anal. Chem., 67 (1995) 2059-2063.

[40] C. Henry, S. Lunte, J. Santiago, Ceramic microchips for capillary electrophoresis–electrochemistry, Analytical Communications, 36 (1999) 305-307.

[41] C.S. Effenhauser, G.J.M. Bruin, A. Paulus, M. Ehrat, Integrated Capillary Electrophoresis on Flexible Silicone Microdevices: Analysis of DNA Restriction Fragments and Detection of Single DNA Molecules on Microchips, Anal. Chem., 69 (1997) 3451-3457.

[42] C. Heller, Separation of double-stranded and single-stranded DNA in polymer solutions: I. Mobility and separation mechanism, ELECTROPHORESIS: An International Journal, 20 (1999) 1962-1976.

[43] L. Ge, S. Wang, S. Ge, J. Yu, M. Yan, N. Li, J. Huang, Electrophoretic separation in a microfluidic paper-based analytical device with an on-column wireless electrogenerated chemiluminescence detector, Chem. Commun. (Camb.), 50 (2014) 5699-5702.

[44] K. Adamski, W. Kubicki, R. Walczak, 3D Printed electrophoretic lab-on-chip for DNA separation, Procedia Eng., 168 (2016) 1454-1457.

[45] Z. Nie, F. Deiss, X. Liu, O. Akbulut, G.M. Whitesides, Integration of paper-based microfluidic devices with commercial electrochemical readers, Lab Chip, 10 (2010) 3163-3169.

[46] R.J. Block, E.L. Durrum, G. Zweig, A manual of paper chromatography and paper electrophoresis, Academic Press, New York, 1964.

[47] P. Lisowski, P.K. Zarzycki, Microfluidic Paper-Based Analytical Devices (muPADs) and Micro Total Analysis Systems (muTAS): Development, Applications and Future Trends, Chromatographia, 76 (2013) 1201-1214.

[48] L.S. Ettre, The predawn of paper chromatography, Chromatographia, 54 (2001) 409.

[49] H. Weil, T.I. Williams, Early History of Chromatography, Nature, 167 (1951) 906-907.

[50] L. Zechmeister, Early History of Chromatography, Nature, 167 (1951) 405-406.

[51] H. Weil, T.I. Willams, History of Chromatography, Nature, 166 (1950) 1000-1001.

[52] K. Sakodynskii, K. Chmutov, M. S. Tswett and Chromatography, Chromatographia, 5 (1972) 471-476.

[53] R. Consden, A.H. Gordon, A.J.P. Martin, Qualitative analysis of proteins: a partition chromatographic method using paper, Biochem. J., 38 (1944) 224-232.

[54] H.B. Bull, J.W. Hahn, V.H. Baptist, Filter paper chromatography, J. Am. Chem. Soc., 71 (1949) 550-553.

[55] R.J. Block, Quantitative Estimation of Amino Acids on Paper Chromatograms, Science, 108 (1948) 608-609.

[56] A. Polson, V.M. Mosley, R.W. Wyckoff, The Quantitative Chromatography of Silk Hydrolysate, Science, 105 (1947) 603-604.

[57] L.B. Rockland, J.L. Blatt, M.S. Dunn, Small Scale Filter Paper Chromatography - Filter Papers and Solvents, Anal. Chem., 23 (1951) 1142-1146.

[58] J.M. Bremner, R.H. Kenten, Paper chromatography of amines, Biochem J, 49 (1951) 651-655.

[59] O. Smithies, Starch-gel electrophoresis, Metabolism, 13 (1964) 974-984.

[60] O. Vesterberg, History of electrophoretic methods, J. Chromatogr., 480 (1989) 3-19.

[61] D. Perrett, From 'protein' to the beginnings of clinical proteomics, Proteomics Clin. Appl., 1 (2007) 720-738.

[62] A.W. Martinez, S.T. Phillips, M.J. Butte, G.M. Whitesides, Patterned paper as a platform for inexpensive, low-volume, portable bioassays, Angew. Chem., Int. Ed., 46 (2007) 1318-1320.

[63] Y. Yang, E. Noviana, M.P. Nguyen, B.J. Geiss, D.S. Dandy, C.S. Henry, Paper-Based Microfluidic Devices: Emerging Themes and Applications, Anal. Chem., 89 (2016) 71-91.

[64] C. Brown, P.L. Kirk, Paper Electrophoresis in the Identification of Writing Inks--Comparison with Horizontal Paper Chromatography, J. Crim. L. Criminology & Police Sci, 45 (1955) 473-480.

[65] T. Kaya, S. Osaki, T. Sato, Investigation of caeruloplasmin. III. Terminal amino acids and sugars of porcine caeruloplasmin, J. Biochem., 50 (1961) 24-28.

[66] R.W. Horobin, L.B. Murgatroyd, A comparison of rapid electrophoretic and chromatographic methods for the investigation of common histological dyes, Histochemie, 11 (1967) 141-151.

[67] G. Haugaard, T.D. Kroner, Partition Chromatography of Amino Acids with Applied Voltage, J. Am. Chem. Soc., 70 (1948) 2135-2137.

[68] V.M. Ingram, Abnormal human haemoglobins. I. The comparison of normal human and sickle-cell haemoglobins by fingerprinting, Biochim. Biophys. Acta, 28 (1958) 539-545.

[69] P.H. O'Farrell, High Resolution Two-Dimensional Electrophoresis of Proteins, The Journal of biological chemistry, 250 (1975) 4007-4021.

[70] S. Magdeldin, S. Enany, Y. Yoshida, B. Xu, Y. Zhang, Z. Zureena, I. Lokamani, E. Yaoita, T. Yamamoto, Basics and recent advances of two dimensional- polyacrylamide gel electrophoresis, Clin. Proteomics, 11 (2014) 16-16.

[71] H.G. Mukherjee, D. Majumdar, Magneto-electrophoretic separation of some inorganic ions, Fresenius J. Anal. Chem., 277 (1975) 205-205.

[72] H.G. Mukherjee, S.K. Datta, Magneto-Paper Electrophoresis in the Separation of Inorganic-Ions, Mikrochim. Acta., 1 (1983) 431-436.

[73] T.R. Sato, H. Diamond, W.P. Norris, H.H. Strain, Electrochromatographic separations of rare earths, J. Am. Chem. Soc., 74 (1952) 6154-6155.

[74] M. Lederer, The paper electrophoretic separation of rare earths using 1% citric acid as electrolyte, J. Chromatogr., 1 (1958) 86-89.

[75] W. Kraak, G. Wals, Electrophoretic separation of some actinide and lanthanide elements, J. Chromatogr. A, 20 (1965) 197-201.

[76] K. Robards, S. Clarke, E. Patsalides, Advances in the analytical chromatography of the lanthanides. A review, Analyst, 113 (1988) 1757-1779.

[77] H.J. McDonald, Ionography: A new frontier in electrophoresis, J. chem. Educ, 29 (1952) 428.

[78] G.T. Franglen, N.H. Martin, J.D. Treherne, An apparatus for paper electrophoresis, J. Clin. Pathol., 8 (1955) 144-149.

[79] E.L. Durrum, A Microelectrophoretic and Microionophoretic Technique, J. Am. Chem. Soc., 72 (1950) 2943-2948.

[80] L. Rosenfeld, A golden age of clinical chemistry: 1948-1960, Clin. Chem., 46 (2000) 1705-1714.

[81] W. Grassmann, K. Hannig, Ein einfaches Verfahren zur kontinuierlichen Trennung von Stoffgemischen auf Filterpapier durch Elektrophorese, Naturwissenschaften, 37 (1950) 397-397.

[82] H.H. Strain, J.C. Sullivan, Analysis by Electromigration plus Chromatography, Anal. Chem., 23 (1951) 816-823.

[83] E.L. Durrum, Continuous Electrophoresis and Ionophoresis on Filter Paper, J. Am. Chem. Soc., 73 (1951) 4875-4880.

[84] I. Brattsten, A. Nilsson, A study in continuous zone electrophoresis in filter paper, Arkiv for Kemi, 3 (1951) 337-345.

[85] I. Brattsten, Continuous zone electrophoresis by crossed velocity fields in a supporting medium-fractionation of protein mixtures and description of the cuvette, Arkiv for Kemi, 8 (1955) 227-244.

[86] T. Sato, W. Norris, H. Strain, Apparatus for continuous electrochromatography, Anal. Chem., 24 (1952) 776-778.

[87] E.S. Holdsworth, An apparatus for continuous electrophoresis on paper, Biochem. J., 59 (1955) 340-345.

[88] L.F.J. Parker, Zone electrophoresis on filter-paper. A review, Analyst, 80 (1955) 638-651.

[89] Z. Pučar, Continuous electrophoresis and two-dimensional electrochromatography, Chromatogr. Rev., 3 (1961) 38-91.

[90] H.D. Cremer, A. Tiselius, Electrophoresis of proteins on filter paper, Biochem Z, 320 (1950) 273-283.

[91] H.G. Kunkel, A. Tiselius, Electrophoresis of proteins on filter paper, J. Gen. Physiol., 35 (1951) 89-118.

[92] M. Lederer, F.L. Ward, Paper electro-chromatography of inorganic substance, Anal. Chim. Acta, 6 (1952) 355-362.

[93] N.F. Hollinger, R.K. Lansing, Paper electrophoresis: temperature, paper wetness and serum component mobility with the kunkel system, J. Chromatogr. A, 5 (1961) 38-45.

[94] R.H. Hackman, M. Goldberg, Some Factors Affecting Mobility Measurements in Paper Electrophoresis, Anal. Chem., 36 (1964) 1220-1222.

[95] E. Kawerau, Electrophoresis of serum and urine proteins on filter-paper strips and agar jelly with the bridge unit, Analyst, 79 (1954) 681-688.

[96] E.F. Woods, J.M. Gillespie, A critical study of the use of paper electrophoresis for separating proteins and measuring their isoelectric points, Aust. J. Biol. Sci., 6 (1953) 130-141.

[97] R.H. Blank, W.K. Hausmann, C.E. Holmlund, N. Bohonos, Paper Electrophoresis of Steroids in Borate Buffers, J. Chromatogr., 17 (1965) 528-531.

[98] D. Gross, High-voltage paper electrophoresis of inorganic cations. Conditions for cathodic migration and measurement of migration rates, J. Chromatogr., 10 (1963) 221-230.

[99] J.H. Geller, J.H. Custer, C.A. Zittle, Paper electrophoresis of proteins in acid buffer, J. Chromatogr., 3 (1960) 369-371.

[100] N.H. Martin, G.T. Franglen, The Use and Limitations of Filter-Paper Electrophoresis, J. Clin. Pathol., 7 (1954) 87-105.

[101] J.J. Kabara, D. Zyskowski, N. Spafford, Effect of Buffer Equilibration on Paper Electrophoresis, J. Chromatogr., 13 (1964) 556-557.

[102] P. Alexander, R. Block, The Composition, Structure and Reactivity of Proteins: A Laboratory Manual of Analytical Methods of Protein Chemistry (Including Polypeptides), Elsevier2014.

[103] R. Consden, W.M. Stanier, A simple paper electrophoresis apparatus, Nature, 170 (1952) 1069-1070.

[104] M. Lederer, High-Performance Paper-Electrophoresis, J. Chromatogr., 171 (1979) 403-406.

[105] S. Fanali, L. Ossicini, High-Performance Paper-Electrophoresis .3. Influence of Various Parameters on Electrophoretic Separations, J. Chromatogr, 287 (1984) 148-154.

[106] L.Y. Shiroma, M. Santhiago, A.L. Gobbi, L.T. Kubota, Separation and electrochemical detection of paracetamol and 4-aminophenol in a paper-based microfluidic device, Anal. Chim. Acta, 725 (2012) 44-50.

[107] J.T. Edward, A note on the obstructive or tortuosity factor in paper electrophoresis, J. Chromatogr., 1 (1958) 446-448.

[108] Y.F. Cheng, T. Vodinh, Paper-Electrophoresis with Surface-Enhanced Fluorimetric Detection, Anal. Chim. Acta., 229 (1990) 295-297.

[109] R.E. Asenstorfer, A.L. Morgan, Y. Hayasaka, M. Sedgley, G.P. Jones, Purification of anthocyanins from species of Banksia and Acacia using high-voltage paper electrophoresis, Phytochem. Anal., 14 (2003) 150-154.

[110] F.M. Everaerts, J.L. Beckers, T.P.E.M. Verheggen, Isotachophoresis : theory, instrumentation and applications, Elsevier Scientific Publishing Company, Amsterdam, 1976.

[111] V. Taglia, M. Lederer, Isotachophoresis on paper, J. Chromatogr. A, 77 (1973) 467-471.

[112] V. Taglia, Isotachophoresis on paper, J. Chromatogr. A, 79 (1973) 380-382.

[113] A.W. Martinez, S.T. Phillips, M.J. Butte, G.M. Whitesides, Patterned paper as a platform for inexpensive, low-volume, portable bioassays, Angew. Chem. Int. Ed. Engl., 46 (2007) 1318-1320.

[114] J. Hu, S. Wang, L. Wang, F. Li, B. Pingguan-Murphy, T.J. Lu, F. Xu, Advances in paper-based point-of-care diagnostics, Biosensors and Bioelectronics, 54 (2014) 585-597.

[115] M. Sajid, A.N. Kawde, M. Daud, Designs, formats and applications of lateral flow assay: A literature review, J. Saudi. Chem. Soc., 19 (2015) 689-705.

[116] C.D. Chin, V. Linder, S.K. Sia, Commercialization of microfluidic point-of-care diagnostic devices, Lab Chip, 12 (2012) 2118-2134.

[117] X. Li, D.R. Ballerini, W. Shen, A perspective on paper-based microfluidics: Current status and future trends, Biomicrofluidics, 6 (2012) 11301-1130113.

[118] D.M. Cate, J.A. Adkins, J. Mettakoonpitak, C.S. Henry, Recent developments in paper-based microfluidic devices, Anal. Chem., 87 (2015) 19-41.

[119] J.C. Jokerst, J.M. Emory, C.S. Henry, Advances in microfluidics for environmental analysis, Analyst, 137 (2012) 24-34.

[120] J. Adkins, K. Boehle, C. Henry, Electrochemical paper-based microfluidic devices, Electrophoresis, 36 (2015) 1811-1824.

[121] S.M. Hossain, R.E. Luckham, M.J. McFadden, J.D. Brennan, Reagentless bidirectional lateral flow bioactive paper sensors for detection of pesticides in beverage and food samples, Anal. Chem., 81 (2009) 9055-9064.

[122] A. Pesenti, R.V. Taudte, B. McCord, P. Doble, C. Roux, L. Blanes, Coupling paper-based microfluidics and lab on a chip technologies for confirmatory analysis of trinitro aromatic explosives, Anal. Chem., 86 (2014) 4707-4714.

[123] K.L. Peters, I. Corbin, L.M. Kaufman, K. Zreibe, L. Blanes, B.R. McCord, Simultaneous colorimetric detection of improvised explosive compounds using microfluidic paper-based analytical devices (µPADs), Anal. Methods, 7 (2015) 63-70.

[124] C. Rozand, Paper-based analytical devices for point-of-care infectious disease testing, Eur. J. Clin. Microbiol. Infect. Dis., 33 (2014) 147-156.

[125] W. Dungchai, O. Chailapakul, C.S. Henry, Electrochemical detection for paper-based microfluidics, Anal. Chem., 81 (2009) 5821-5826.

[126] X. Li, J. Tian, G. Garnier, W. Shen, Fabrication of paper-based microfluidic sensors by printing, Colloids Surf. B. Biointerfaces, 76 (2010) 564-570.

[127] Y. Lu, W. Shi, J. Qin, B. Lin, Fabrication and characterization of paper-based microfluidics prepared in nitrocellulose membrane by wax printing, Anal. Chem., 82 (2010) 329-335.

[128] Y. Sameenoi, P.N. Nongkai, S. Nouanthavong, C.S. Henry, D. Nacapricha, One-step polymer screen-printing for microfluidic paper-based analytical device (muPAD) fabrication, Analyst, 139 (2014) 6580-6588.

[129] X. Jiang, Z.H. Fan, Fabrication and Operation of Paper-Based Analytical Devices, Annual Review of Analytical Chemistry, (2016).

[130] J.C. Cunningham, P.R. DeGregory, R.M. Crooks, New Functionalities for Paper-Based Sensors Lead to Simplified User Operation, Lower Limits of Detection, and New Applications, Annual Review of Analytical Chemistry, (2016).

[131] M. Santhiago, E.W. Nery, G.P. Santos, L.T. Kubota, Microfluidic paper-based devices for bioanalytical applications, Bioanalysis, 6 (2014) 89-106.

[132] E.W. Nery, L.T. Kubota, Sensing approaches on paper-based devices: a review, Anal. Bioanal. Chem., 405 (2013) 7573-7595.

[133] N.A. Meredith, C. Quinn, D.M. Cate, T.H. Reilly, J. Volckens, C.S. Henry, Paper-based analytical devices for environmental analysis, Analyst, 141 (2016) 1874-1887.

[134] R. Consden, W.M. Stanier, Ionophoresis of sugars on paper and some applications to the analysis of protein polysaccharide complexes, Nature, 169 (1952) 783-785.

[135] G.T. Franglen, An improved apparatus for the filter paper electrophoresis of serum and other proteins, J. Clin. Pathol., 6 (1953) 183-186.

[136] T.H. Spaet, Practical applications of paper electrophoresis, Calif. Med., 79 (1953) 271-273.

[137] T. Kinersly, Paper Electrophoresis of Saliva, Yale J. Biol. Med., 26 (1953) 211.

[138] I.R. Mackay, W. Volwiler, P.D. Goldsworthy, Paper electrophoresis of serum proteins: photometric quantitation and comparison with free electrophoresis, J. Clin. Invest., 33 (1954) 855-866.

[139] T.A. Langan, E.L. Durrum, W.P. Jencks, Paper electrophoresis as a quantitative method: measurement of alpha and beta lipoprotein cholesterol, J. Clin. Invest., 34 (1955) 1427-1436.

[140] H. Zentner, A modified method of filter paper electrophoresis, Nature, 175 (1955) 953.

[141] W.P. Jencks, E.R.B. Smith, E.L. Durrum, Clinical Significance of the Analysis of Serum Protein Distribution by Filter Paper Electrophoresis, Am. J. Med., 21 (1956) 387-405.

[142] D. Gross, High-voltage paper electrophoresis of non-volatile organic acids and their mixtures with amino-acids, Nature, 178 (1956) 29-31.

[143] M. Lederer, A Note on the Paper Electrophoretic Separation of Inorganic Anions, Anal. Chim. Acta., 17 (1957) 606-607.

[144] D. Gross, High-Voltage Paper Electrophoresis of Inorganic Cations - Alkali, Alkaline-Earth and Other Metals, Nature, 180 (1957) 596-598.

[145] O. Theander, Paper Ionophoresis of Aldehydes and Ketones in the Presence of Hydrogen Sulphite, Acta. Chem. Scand., 11 (1957) 717-723.

[146] A. Leviton, Milk Proteins, Quantitative Ionophoretic Determination of Some Whey Proteins in Skim Milk, J. Agric. Food Chem., 5 (1957) 532-538.

[147] J. Jach, H. Kawahara, G. Harbottle, The Application of Paper Electrophoresis to the Separation of Radioactive Products Found in the Szilard-Chalmers Reaction, J. Chromatogr, 1 (1958) 501-507.

[148] H.F. Macrae, B.E. Baker, Application of Electrophoresis on Paper to the Estimation of Alpha-Casein, Beta-Casein, and Gamma-Casein, J. Dairy Sci., 41 (1958) 233-240.

[149] G. Grassini, M. Lederer, Paper Electrophoresis of Inorganic Anions in 0.1N NaOH Solution, J. Chromatogr, 2 (1959) 326-326.

[150] A.M. Katz, W.J. Dreyer, C.B. Anfinsen, Peptide separation by two-dimensional chromatography and electrophoresis, J. Biol. Chem., 234 (1959) 2897-2900.

[151] P. Markakis, Zone electrophoresis of anthocyanins, Nature, 187 (1960) 1092-1093.

[152] G.B. Belling, R.E. Underdown, Paper Electrophoresis of Inorganic Anions in Sodium Carbonate Solution, Anal. Chim. Acta., 22 (1960) 203-204.

[153] G.N. Atfield, C.J.O.R. Morris, Analytical Separations by High-Voltage Paper Electrophoresis - Amino Acids in Protein Hydrolysates, Biochem. J., 81 (1961) 606-&.

[154] R.A.B. Bannard, A.A. Casselman, Clam Poison: III. Paper Electrophoresis of Clam Poison, Can. J. Chem., 40 (1962) 1649-1655.

[155] S.K. Shukla, M. Bacher, J.P. Adloff, Paper electrophoresis in the study of the chemical effects produced during beta decay of 132-Te to 132-I, J. Chromatogr., 10 (1963) 93-97.

[156] V. Jokl, M. Undeutsch, J. Majer, Separations of inorganic ions by paper electrophoresis in solutions of N-(2-hydroxyethyl)iminodiacetic acid, J. Chromatogr., 26 (1967) 208-214.

[157] W.S. Adams, M. Nakatani, Filter paper electrophoresis of purines and pyrimidines: mobility data, J. Chromatogr., 37 (1968) 343-347.

[158] E. Selegny, J.C. Fenyo, G. Brown, F. Matray, C. De Bernardy, Rapid separation of some amino acids by ion-exchange paper electrophoresis, J. Chromatogr. A, 47 (1970) 552-554.

[159] V. Mosini, M. Lederer, Cross-Electrophoresis on Paper of Some Inorganic Systems, J. Chromatogr, 77 (1973) 464-466.

[160] Cvjetica.Nm, Jovanovi.O, High-Voltage Paper-Electrophoresis of Hg(Ii), Cd(Ii), Pb(Ii) and Cu(Ii) in Aqueous-Solution of Edta and Glycolic Acid, J. Chromatogr., 94 (1974) 349-352.

[161] T. Jerzykowski, D. Piskorska, M. Ostrowska, The separation of glyoxalase I and glyoxalase II by paper electrophoresis, J. Chromatogr., 116 (1976) 225-229.

[162] C. Corradini, M. Lederer, Separation of Optical Isomers of Metal-Complexes by Paper-Electrophoresis in Mixtures of Aluminum-Chloride and Tartrate, J. Chromatogr, 157 (1978) 455-457.

[163] A.R. Hayman, D.O. Gray, Paper-Electrophoresis of the Dansyl Derivatives of Amino-Acids and Amines, J. Chromatogr, 370 (1986) 194-202.

[164] S. Nagasaki, S. Tanaka, Y. Takahashi, Speciation and Solubility of Neptunium in Underground Environments by Paper-Electrophoresis, J. Radioan. Nucl. Ch. Ar., 124 (1988) 383-395.

[165] M. Kobayashi, Y. Kitaoka, Y. Tanaka, K. Kawamoto, Electrophoretic Behavior and Infrared-Spectra of Dihydroxyboryl Compounds in Aqueous Di-Carboxylic and Tricarboxylic Acids - Paper-Electrophoresis as a Tool for Determining the Chemical-States of a Substance in Solution, J. Chromatogr. A, 678 (1994) 351-358.

[166] S. Sharma, M. Bhalwar, R. Gupta, Low-voltage paper electrophoretic study of ion-pair formation and electrochromatography of inorganic anions on papers impregnated with titanium (IV) tungstate, J. Chromatogr. Sci., 39 (2001) 463-467.

[167] M. Sato, Z.H. Tao, K. Shiozaki, T. Nakano, T. Yamaguchi, T. Yokoyama, N. Kan-No, E. Nagahisa, A simple and rapid method for the analysis of fish histamine by paper electrophoresis, Fish Sci., 72 (2006) 889-892.

[168] R.F. Carvalhal, M. Simão Kfouri, M.H. de Oliveira Piazetta, A.L. Gobbi, L.T. Kubota, Electrochemical Detection in a Paper-Based Separation Device, Anal. Chem., 82 (2010) 1162-1165.

[169] L. Ge, S. Wang, X. Song, S. Ge, J. Yu, 3D origami-based multifunction-integrated immunodevice: low-cost and multiplexed sandwich chemiluminescence immunoassay on microfluidic paper-based analytical device, Lab Chip, 12 (2012) 3150-3158.

[170] Z.H. Tao, M. Sato, K.G. Wu, H. Kiyota, T. Yamaguchi, T. Nakano, A simple, rapid method for gizzerosine analysis in fish meal by paper electrophoresis, Fish Sci., 78 (2012) 923-926.

[171] T. Songjaroen, W. Dungchai, O. Chailapakul, C.S. Henry, W. Laiwattanapaisal, Blood separation on microfluidic paper-based analytical devices, Lab Chip, 12 (2012) 3392-3398.

[172] X. Yang, O. Forouzan, T.P. Brown, S.S. Shevkoplyas, Integrated separation of blood plasma from whole blood for microfluidic paper-based analytical devices, Lab Chip, 12 (2012) 274-280.

[173] S.J. Vella, P. Beattie, R. Cademartiri, A. Laromaine, A.W. Martinez, S.T. Phillips, K.A. Mirica, G.M. Whitesides, Measuring markers of liver function using a micropatterned paper device designed for blood from a fingerstick, Anal. Chem., 84 (2012) 2883-2891.

[174] J. Noiphung, T. Songjaroen, W. Dungchai, C.S. Henry, O. Chailapakul, W. Laiwattanapaisal, Electrochemical detection of glucose from whole blood using paper-based microfluidic devices, Anal. Chim. Acta, 788 (2013) 39-45.

[175] A. Abbas, A. Brimer, J.M. Slocik, L. Tian, R.R. Naik, S. Singamaneni, Multifunctional Analytical Platform on a Paper Strip: Separation, Preconcentration, and Subattomolar Detection, Anal. Chem., 85 (2013) 3977-3983.

[176] N. Dossi, R. Toniolo, A. Pizzariello, F. Impellizzieri, E. Piccin, G. Bontempelli, Pencil-drawn paper supported electrodes as simple electrochemical detectors for paper-based fluidic devices, Electrophoresis, 34 (2013) 2085-2091.

[177] T. Rosenfeld, M. Bercovici, 1000-fold sample focusing on paper-based microfluidic devices, Lab Chip, 14 (2014) 4465-4474.

[178] L.F. OuYang, C.H. Wang, F. Du, T.F. Zheng, H. Liang, Electrochromatographic separations of multi-component metal complexes on a microfluidic paper-based device with a simplified photolithography, Rsc Adv., 4 (2014) 1093-1101.

[179] B.Y. Moghadam, K.T. Connelly, J.D. Posner, Isotachophoretic preconcenetration on paper-based microfluidic devices, Anal. Chem., 86 (2014) 5829-5837.

[180] L. Luo, X. Li, R.M. Crooks, Low-voltage origami-paper-based electrophoretic device for rapid protein separation, Anal. Chem., 86 (2014) 12390-12397.

[181] S.S. Chen, C.W. Hu, I.F. Yu, Y.C. Liao, J.T. Yang, Origami paper-based fluidic batteries for portable electrophoretic devices, Lab Chip, 14 (2014) 2124-2130.

[182] M.M. Gong, P. Zhang, B.D. MacDonald, D. Sinton, Nanoporous membranes enable concentration and transport in fully wet paper-based assays, Anal. Chem., 86 (2014) 8090-8097.

[183] X. Li, L. Luo, R.M. Crooks, Low-Voltage Paper Isotachophoresis Device for DNA Focusing, Lab Chip, 15 (2015) 4090-4098.

[184] P. Ryan, D. Zabetakis, D.A. Stenger, S.A. Trammell, Integrating Paper Chromatography with Electrochemical Detection for the Trace Analysis of TNT in Soil, Sensors, 15 (2015) 17048-17056.

[185] R.-J. Yang, H.-H. Pu, H.-L. Wang, Ion concentration polarization on paper-based microfluidic devices and its application to preconcentrate dilute sample solutions, Biomicrofluidics, 9 (2015) 014122.

[186] M.M. Gong, R. Nosrati, M.C. San Gabriel, A. Zini, D. Sinton, Direct DNA analysis with paper-based ion concentration polarization, J. Am. Chem. Soc., 137 (2015) 13913-13919.

[187] Z. Zhong, R. Wu, Z. Wang, H. Tan, An investigation of paper based microfluidic devices for size based separation and extraction applications, J. Chromatogr. B, 1000 (2015) 41-48.

[188] B.Y. Moghadam, K.T. Connelly, J.D. Posner, Two Orders of Magnitude Improvement in Detection Limit of Lateral Flow Assays Using Isotachophoresis, Anal. Chem., 87 (2015) 1009-1017.

[189] S. Hong, R. Kwak, W. Kim, Paper-based flow fractionation system applicable to preconcentration and field-flow separation, Anal. Chem., 88 (2016) 1682-1687.

[190] C.L. Chagas, F.R. de Souza, T.M. Cardoso, R.C. Moreira, J.A. da Silva, D.P. de Jesus, W.K. Coltro, A fully disposable paper-based electrophoresis microchip with integrated pencil-drawn electrodes for contactless conductivity detection, Anal. Methods, 8 (2016) 6682-6686.

[191] C. Xu, M. Zhong, L. Cai, Q. Zheng, X. Zhang, Sample injection and electrophoretic separation on a simple laminated paper based analytical device, Electrophoresis, 37 (2016) 476-481.

[192] Y. Zhao, Z. Wei, H. Zhao, J. Jia, Z. Chen, S. Zhang, Z. Ouyang, X. Ma, X. Zhang, In Situ Ion-Transmission Mass Spectrometry for Paper-Based Analytical Devices, Anal. Chem., 88 (2016) 10805-10810.

[193] S.B. Berry, S.C. Fernandes, A. Rajaratnam, N.S. DeChiara, C.R. Mace, Measurement of the hematocrit using paper-based microfluidic devices, Lab Chip, 16 (2016) 3689-3694.

[194] P. Phansi, S. Sumantakul, T. Wongpakdee, N. Fukana, N. Ratanawimarnwong, J. Sitanurak, D. Nacapricha, Membraneless Gas-Separation Microfluidic Paper-Based Analytical Devices for Direct Quantitation of Volatile and Nonvolatile Compounds, Anal. Chem., 88 (2016) 8749-8756.

[195] L.-H. Hung, H.-L. Wang, R.-J. Yang, A portable sample concentrator on paper-based microfluidic devices, Microfluid Nanofluidics, 20 (2016) 1-9.

[196] S.I. Han, K.S. Hwang, R. Kwak, J.H. Lee, Microfluidic paper-based biomolecule preconcentrator based on ion concentration polarization, Lab Chip, 16 (2016) 2219-2227.

[197] S.-H. Yeh, K.-H. Chou, R.-J. Yang, Sample pre-concentration with high enrichment factors at a fixed location in paper-based microfluidic devices, Lab Chip, 16 (2016) 925-931.

[198] B. Ma, Y.-Z. Song, J.-C. Niu, Z.-Y. Wu, Highly efficient sample stacking by enhanced field amplification on a simple paper device, Lab Chip, 16 (2016) 3460-3465.

[199] M. Ueland, L. Blanes, R.V. Taudte, B.H. Stuart, N. Cole, P. Willis, C. Roux, P. Doble, Capillary-driven microfluidic paper-based analytical devices for lab on a chip screening of explosive residues in soil, J. Chromatogr. A, 1436 (2016) 28-33.

[200] D.-T. Phan, S.A.M. Shaegh, C. Yang, N.-T. Nguyen, Sample concentration in a microfluidic paper-based analytical device using ion concentration polarization, Sensors Actuators B: Chem., 222 (2016) 735-740.

[201] R.F. Carvalhal, E. Carrilho, L.T. Kubota, The potential and application of microfluidic paper-based separation devices, Bioanalysis, 2 (2010) 1663-1665.

[202] L. Ge, S. Wang, S. Ge, J. Yu, M. Yan, N. Li, J. Huang, Electrophoretic separation in a microfluidic paper-based analytical device with an on-column wireless electrogenerated chemiluminescence detector, Chem. Commun. (Camb.), 50 (2014) 5699-5702.

[203] P. Mandal, R. Dey, S. Chakraborty, Electrokinetics with “paper-and-pencil” devices, Lab Chip, 12 (2012) 4026-4028.

[204] H. Liu, R.M. Crooks, Three-dimensional paper microfluidic devices assembled using the principles of origami, J. Am. Chem. Soc., 133 (2011) 17564-17566.

[205] L. Ouyang, Q. Liu, H. Liang, Combining field-amplified sample stacking with moving reaction boundary electrophoresis on a paper chip for the preconcentration and separation of metal ions, J. Sep. Sci., (2016).

[206] S. Koster, E. Verpoorte, A decade of microfluidic analysis coupled with electrospray mass spectrometry: An overview, Lab Chip, 7 (2007) 1394-1412.

[207] M. Wilm, M. Mann, Analytical properties of the nanoelectrospray ion source, Anal. Chem., 68 (1996) 1-8.

[208] H. Wang, J. Liu, R.G. Cooks, Z. Ouyang, Paper spray for direct analysis of complex mixtures using mass spectrometry, Angew. Chem., 122 (2010) 889-892.

[209] J. Liu, H. Wang, N.E. Manicke, J.-M. Lin, R.G. Cooks, Z. Ouyang, Development, characterization, and application of paper spray ionization, Anal. Chem., 82 (2010) 2463-2471.

[210] G.I. Salentijn, H.P. Permentier, E. Verpoorte, 3D-printed paper spray ionization cartridge with fast wetting and continuous solvent supply features, Anal. Chem., 86 (2014) 11657-11665.

[211] C.L. Cassano, Z.H. Fan, Laminated paper-based analytical devices (LPAD): fabrication, characterization, and assays, Microfluid Nanofluidics, 15 (2013) 173-181.

[212] M.P. Sousa, J.o.F. Mano, Superhydrophobic paper in the development of disposable labware and lab-on-paper devices, ACS Appl. Mater. Interfaces, 5 (2013) 3731-3737.

[213] D.D. Liana, B. Raguse, J.J. Gooding, E. Chow, Recent advances in paper-based sensors, Sensors (Basel), 12 (2012) 11505-11526.

[214] H. Juvonen, A. Määttänen, P. Laurén, P. Ihalainen, A. Urtti, M. Yliperttula, J. Peltonen, Biocompatibility of printed paper-based arrays for 2-D cell cultures, Acta. Biomater., 9 (2013) 6704-6710.

[215] J. Wang, Printing and Characterization of Inks for Paper-Based Biosensors, Chemical Engineering, McMaster University, 2014, pp. 79.

[216] R. Pelton, Bioactive paper provides a low-cost platform for diagnostics, TrAC, Trends Anal. Chem., 28 (2009) 925-942.

[217] C. Laurell, S. Laurell, N. Skoog, Buffer composition in paper electrophoresis, Clin. Chem., 2 (1956) 99-111.

[218] K. Jain, Personalized medicine, Current opinion in molecular therapeutics, 4 (2002) 548-558.

[219] P. Yager, G.J. Domingo, J. Gerdes, Point-of-care diagnostics for global health, Annual review of biomedical engineering, 10 (2008).

[220] E.-L. Lewandrowski, S. Yeh, J. Baron, J.B. Crocker, K. Lewandrowski, Implementation of point-of-care testing in a general internal medicine practice: A confirmation study, Clinica Chimica Acta, 473 (2017) 71-74.

[221] V. Gubala, L.F. Harris, A.J. Ricco, M.X. Tan, D.E. Williams, Point of care diagnostics: status and future, Anal. Chem., 84 (2011) 487-515.

[222] P. St-Louis, Status of point-of-care testing: promise, realities, and possibilities, Clinical biochemistry, 33 (2000) 427-440.

[223] G. Wu, M.H. Zaman, Low-cost tools for diagnosing and monitoring HIV infection in low-resource settings, Bull. World. Health. Organ., 90 (2012) 914-920.

[224] P. Yager, T. Edwards, E. Fu, K. Helton, K. Nelson, M.R. Tam, B.H. Weigl, Microfluidic diagnostic technologies for global public health, Nature, 442 (2006) 412-418.

[225] C.D. Chin, V. Linder, S.K. Sia, Commercialization of microfluidic point-of-care diagnostic devices, Lab Chip, 12 (2012) 2118-2134.

[226] A.C. Salisbury, K.J. Reid, K.P. Alexander, F.A. Masoudi, S.-M. Lai, P.S. Chan, R.G. Bach, T.Y. Wang, J.A. Spertus, M. Kosiborod, Diagnostic blood loss from phlebotomy and hospital-acquired anemia during acute myocardial infarction, Archives of internal medicine, 171 (2011) 1646-1653.

[227] A.K. Yetisen, M.S. Akram, C.R. Lowe, Paper-based microfluidic point-of-care diagnostic devices, Lab Chip, 13 (2013) 2210-2251.

[228] A. St John, C.P. Price, Existing and emerging technologies for point-of-care testing, The Clinical Biochemist Reviews, 35 (2014) 155.

[229] P. Abgrall, A. Gue, Lab-on-chip technologies: making a microfluidic network and coupling it into a complete microsystem—a review, Journal of micromechanics and microengineering, 17 (2007) R15.

[230] E.B. Bahadır, M.K. Sezgintürk, Lateral flow assays: Principles, designs and labels, TrAC Trends in Analytical Chemistry, 82 (2016) 286-306.

[231] B. Crocker, E.-L. Lewandrowski, N. Lewandrowski, K. Gregory, K. Lewandrowski, Patient satisfaction with point-of-care laboratory testing: report of a quality improvement program in an ambulatory practice of an academic medical center, Clinica chimica acta, 424 (2013) 8-11.

[232] J.L. Shaw, Practical challenges related to point of care testing, Practical laboratory medicine, 4 (2016) 22-29.

[233] C.P. Price, Regular review: Point of care testing, BMJ: British Medical Journal, 322 (2001) 1285.

[234] H. Sharma, D. Nguyen, A. Chen, V. Lew, M. Khine, Unconventional low-cost fabrication and patterning techniques for point of care diagnostics, Ann. Biomed. Eng., 39 (2011) 1313-1327.

[235] B. Liu, D. Du, X. Hua, X.Y. Yu, Y. Lin, Paper-Based Electrochemical Biosensors: From Test Strips to Paper-Based Microfluidics, Electroanalysis, 26 (2014) 1214-1223.

[236] G. Grenache David, Variable accuracy of home pregnancy tests: truth in advertising?, Clinical Chemistry and Laboratory Medicine (CCLM), 2015, pp. 339.

[237] C. Gnoth, S. Johnson, Strips of Hope: Accuracy of Home Pregnancy Tests and New Developments, Geburtshilfe und Frauenheilkunde, 74 (2014) 661-669.

[238] D. Mark, S. Haeberle, G. Roth, F. Von Stetten, R. Zengerle, Microfluidic lab-on-a-chip platforms: requirements, characteristics and applications, Microfluidics Based Microsystems, Springer2010, pp. 305-376.

[239] SPD Swiss Precision Diagnostics GmbH, "Clearblue® Pregnancy Test with Weeks Indicator" (2018) [Online] Available at: https://uk.clearblue.com/pregnancy-tests/digital-with-weeks-indicator (Accessed December 25, 2018).

[240] We Have Kids, "The most accurate pregnancy tests" (2018) [Online] Available at: https://wehavekids.com/having-baby/The-Most-Accurate-Pregnancy-Tests (Accessed December 24, 2018).

[241] G.A. Posthuma-Trumpie, J. Korf, A. van Amerongen, Lateral flow (immuno)assay: its strengths, weaknesses, opportunities and threats. A literature survey, Anal. Bioanal. Chem., 393 (2009) 569-582.

[242] D.C. Klonoff, Point-of-care blood glucose meter accuracy in the hospital setting, Diabetes Spectrum, 27 (2014) 174-179.

[243] American Diabetes Association, "Anatomy of a Test Strip Each tiny bit of plastic contains big technology " (2012) [Online] Available at: http://www.diabetesforecast.org/2012/jul/anatomy-of-a-test-strip.html (Accessed December 26, 2018).

[244] Everyday Health, "The best blood sugar monitors to help you manage diabetes" (2018) [Online] Available at: https://www.everydayhealth.com/products/reviews/best-blood-sugar-monitors/ (Accessed December 26, 2018).

[245] Canadian Agency for Drugs Technologies in Health, Systematic review of use of blood glucose test strips for the management of diabetes mellitus, CADTH technology overviews, 1 (2010).

[246] The Diabetes Council, "Everything you need to know about diabetes test strips" (2016) [Online] Available at: https://www.thediabetescouncil.com/everything-you-need-to-know-about-diabetes-test-strips/ (Accessed December 27, 2018).

[247] S. Liu, W. Su, X. Ding, A review on microfluidic paper-based analytical devices for glucose detection, Sensors, 16 (2016) 2086.

[248] W. Dungchai, O. Chailapakul, C.S. Henry, Electrochemical detection for paper-based microfluidics, Anal. Chem., 81 (2009) 5821-5826.

[249] D. Sechi, B. Greer, J. Johnson, N. Hashemi, Three-dimensional paper-based microfluidic device for assays of protein and glucose in urine, Anal. Chem., 85 (2013) 10733-10737.

[250] Meridian Bioscience Inc., "OraQuick ADVANCE® HIV -1/2 Rapid Antibody Test Kit Controls" (2019) [Online] Available at: http://www.meridianbioscience.eu/oraquick-em-advance-em-reg-rapid-hiv-1-2-antibody-test-kit-controls.html (Accessed December 26, 2018).

[251] OraSure Technologies Inc., "OraQuick® ADVANCE Rapid HIV-1/2 Antibody Test" (2004) [Online] Available at: https://www.fda.gov/downloads/BiologicsBloodVaccines/BloodBloodProducts/ApprovedProducts/PremarketApprovalsPMAs/UCM091919.pdf (Accessed December 26, 2018).

[252] OraSure Technologies Inc., "OraQuick: In-Home HIV Test" (2016) [Online] Available at: http://www.oraquick.com/What-is-OraQuick/OraQuick-In-Home-HIV-Test (Accessed December 25, 2018).

[253] K. Pattanapanyasat, Immune status monitoring of HIV/AIDS patients in resource-limited settings: a review with an emphasis on CD4+ T-lymphocyte determination, Asian Pacific journal of allergy and immunology, 30 (2012) 11.

[254] R. Zachariah, S. Reid, P. Chaillet, M. Massaquoi, E. Schouten, A. Harries, Why do we need a point-of-care CD4 test for low-income countries?, Tropical Medicine & International Health, 16 (2011) 37-41.

[255] S. Manoto, M. Lugongolo, U. Govender, P. Mthunzi-Kufa, Point of care diagnostics for HIV in resource limited settings: an overview, Medicina, 54 (2018) 3.

[256] D. Arora, M. Maheshwari, B. Arora, Rapid point-of-care testing for detection of HIV and clinical monitoring, ISRN AIDS, 2013 (2013).

[257] U.S. Food & Drug Administration, "OraQuick ADVANCE Rapid HIV-1/2 Antibody Test" (2004) [Online] Available at: https://www.fda.gov/biologicsbloodvaccines/bloodbloodproducts/approvedproducts/premarketapprovalspmas/ucm091491.htm (Accessed December 25, 2018).

[258] D.M. Moore, A. Awor, R. Downing, J. Kaplan, J.S. Montaner, J. Hancock, W. Were, J. Mermin, CD4+ T-cell count monitoring does not accurately identify HIV-infected adults with virologic failure receiving antiretroviral therapy, JAIDS Journal of Acquired Immune Deficiency Syndromes, 49 (2008) 477-484.

[259] K. Sukapirom, N. Onlamoon, C. Thepthai, K. Polsrila, B. Tassaneetrithep, K. Pattanapanyasat, Performance evaluation of the Alere PIMA CD4 test for monitoring HIV-infected individuals in resource-constrained settings, JAIDS Journal of Acquired Immune Deficiency Syndromes, 58 (2011) 141-147.

[260] T.G. Cross, M.P. Hornshaw, Can LC and LC-MS ever replace immunoassays?, Journal of Applied Bioanalysis, 2 (2016) 936.

[261] N. Grüner, O. Stambouli, R.S. Ross, Dried blood spots-preparing and processing for use in immunoassays and in molecular techniques, Journal of visualized experiments: JoVE, (2015).

[262] J.H. Oh, Y.J. Lee, Sample preparation for liquid chromatographic analysis of phytochemicals in biological fluids, Phytochemical analysis, 25 (2014) 314-330.

[263] J.E. Adaway, B.G. Keevil, Therapeutic drug monitoring and LC–MS/MS, J. Chromatogr. B, 883-884 (2012) 33-49.

[264] F. Kong, Y.F. Hu, Biomolecule immobilization techniques for bioactive paper fabrication, Anal. Bioanal. Chem., 403 (2012) 7-13.

[265] S. Ma, Y. Tang, J. Liu, J. Wu, Visible paper chip immunoassay for rapid determination of bacteria in water distribution system, Talanta, 120 (2014) 135-140.

[266] M.L. Sin, K.E. Mach, P.K. Wong, J.C. Liao, Advances and challenges in biosensor-based diagnosis of infectious diseases, Expert review of molecular diagnostics, 14 (2014) 225-244.

[267] R. Peeling, D. Mabey, Point-of-care tests for diagnosing infections in the developing world, Clinical microbiology and infection, 16 (2010) 1062-1069.

[268] D.M. Bowman, D.M. Studdert, Newborn screening cards: a legal quagmire, Med J Aust, 194 (2011) 319-322.

[269] Public Health England, "Guidelines for newborn blood spot sampling" (2016) [Online] Available at: www.gov.uk/topic/population-screening-programmes (Accessed January 8, 2019).

[270] P.D. Usha, R.D. Bibhu, Newborn screening—From 'Guthrie age to Genomic age', The Journal of Obstetrics and Gynecology of India, 60 (2010) 210-214.

[271] R.J. Biggar, W. Miley, P. Miotti, T.E. Taha, A. Butcher, J. Spadoro, D. Waters, Blood collection on filter paper: a practical approach to sample collection for studies of perinatal HIV transmission, JAIDS Journal of Acquired Immune Deficiency Syndromes, 14 (1997) 368-373.

[272] S. Parker, W. Cubitt, The use of the dried blood spot sample in epidemiological studies, J. Clin. Pathol., 52 (1999) 633.

[273] A. Sharma, S. Jaiswal, M. Shukla, J. Lal, Dried blood spots: concepts, present status, and future perspectives in bioanalysis, Drug testing and analysis, 6 (2014) 399-414.

[274] T.W. McDade, S. Williams, J.J. Snodgrass, What a drop can do: dried blood spots as a minimally invasive method for integrating biomarkers into population-based research, Demography, 44 (2007) 899-925.

[275] W. Li, F.L.S. Tse, Dried blood spot sampling in combination with LC-MS/MS for quantitative analysis of small molecules, Biomedical Chromatography, 24 (2010) 49-65.

[276] E. Bakker, P. Bühlmann, E. Pretsch, Carrier-based ion-selective electrodes and bulk optodes. 1. General characteristics, Chem. Rev., 97 (1997) 3083-3132.

[277] M.I.G.S. Almeida, R.W. Cattrall, S.D. Kolev, Polymer inclusion membranes (PIMs) in chemical analysis-A review, Anal. Chim. Acta., 987 (2017) 1-14.

[278] J.A. Riggs, B.D. Smith, Facilitated transport of small carbohydrates through plasticized cellulose triacetate membranes. Evidence for fixed-site jumping transport mechanism, J. Am. Chem. Soc., 119 (1997) 2765-2766.

[279] F. Pena-Pereira, M. Tobiszewski, The Application of Green Solvents in Separation Processes, Elsevier2017.

[280] A. Casadellà, O. Schaetzle, K. Loos, Ammonium across a Selective Polymer Inclusion Membrane: Characterization, Transport, and Selectivity, Macromolecular rapid communications, 37 (2016) 858-864.

[281] L.D. Nghiem, P. Mornane, I.D. Potter, J.M. Perera, R.W. Cattrall, S.D. Kolev, Extraction and transport of metal ions and small organic compounds using polymer inclusion membranes (PIMs), J. Memb. Sci., 281 (2006) 7-41.

[282] M. O'Rourke, R.W. Cattrall, S.D. Kolev, I.D. Potter, The extraction and transport of organic molecules using polymer inclusion membranes, Solvent Extr. Res. Dev. Jpn, 16 (2009) 1-12.

[283] C.-V. Gherasim, M. Cristea, C.-V. Grigoras, G. Bourceanu, NEW POLYMER INCLUSION MEMBRANE. PREPARATION AND CHARACTERIZATION, Dig. J. Nanomater. Biostruct., 6 (2011) 1499-1508.

[284] J. Schmidt-Marzinkowski, H.H. See, P.C. Hauser, Electric field driven extraction of inorganic anions across a polymer inclusion membrane, Electroanalysis, 25 (2013) 1879-1886.

[285] C. Onac, H.K. Alpoguz, E. Akceylan, M. Yilmaz, Facilitated Transport of Cr(VI) through Polymer Inclusion Membrane System Containing Calix[4]arene Derivative as Carrier Agent, J. Macromol .Sci. A, 50 (2013) 1013-1021.

[286] M. Baczynska, M. Regel-Rosocka, M. Nowicki, M. Wisniewski, Effect of the structure of polymer inclusion membranes on zn(II) transport from chloride aqueous solutions, J. Appl. Polym. Sci., 132 (2015) 1-11.

[287] P.J. Flory, Principles of polymer chemistry, Cornell University Press1953.

[288] C.E. Wilkes, J. Summers, C. Daniels, PVC Handbook 2005, Google Scholar, (2005).

[289] Y. Yıldız, A. Manzak, B. Aydin, O. Tutkun, Preparation and application of polymer inclusion membranes (PIMs) including Alamine 336 for the extraction of metals from an aqueous solution, 2014.

[290] G. Wypych, Handbook of Plasticizers, ChemTec Publishing2004.

[291] M.a. de los A. Arada Pérez, L.P. Marín, J.C. Quintana, M. Yazdani-Pedram, Influence of different plasticizers on the response of chemical sensors based on polymeric membranes for nitrate ion determination, Sens. Actuators B Chem., 89 (2003) 262-268.

[292] R. Eugster, T. Rosatzin, B. Rusterholz, B. Aebersold, U. Pedrazza, D. Rüegg, A. Schmid, U.E. Spichiger, W. Simon, Plasticizers for liquid polymeric membranes of ion-selective chemical sensors, Anal. Chim. Acta., 289 (1994) 1-13.

[293] E.R. de San Miguel, J.C. Aguilar, J. de Gyves, Structural effects on metal ion migration across polymer inclusion membranes: Dependence of transport profiles on nature of active plasticizer, J. Memb. Sci., 307 (2008) 105-116.

[294] C. Mihali, N. Vaum, Use of plasticizers for electrochemical sensors, Recent Advances in Plasticizers, InTech2012.

[295] M. Cox, Solvent extraction in hydrometallurgy, Solvent Extraction Principles and Practice, Revised and Expanded, CRC Press2004, pp. 466-515.

[296] G.W. Stevens, J.M. Perera, F. Grieser, Interfacial aspects of metal ion extraction in liquid-liquid systems, Reviews in Chemical Engineering, 17 (2001) 87-110.

[297] W. Walkowiak, M. Ulewicz, C. Kozłowski, Application of macrocycle compounds for metal ions separation and removal-a review, Ars Separatoria Acta, (2002) 87-98.

[298] T.D. Ho, C. Zhang, L.W. Hantao, J.L. Anderson, Ionic liquids in analytical chemistry: fundamentals, advances, and perspectives, Anal. Chem., 86 (2013) 262-285.

[299] C. Fontàs, I. Queralt, M. Hidalgo, Novel and selective procedure for Cr (VI) determination by X-ray fluorescence analysis after membrane concentration, Spectrochimica Acta Part B: Atomic Spectroscopy, 61 (2006) 407-413.

[300] N. Pont, V. Salvadó, C. Fontàs, Selective transport and removal of Cd from chloride solutions by polymer inclusion membranes, J. Memb. Sci., 318 (2008) 340-345.

[301] Y. Kalyan, A. Pandey, P. Bhagat, R. Acharya, V. Natarajan, G. Naidu, A. Reddy, Membrane optode for mercury (II) determination in aqueous samples, Journal of hazardous materials, 166 (2009) 377-382.

[302] Y. Kalyan, A. Pandey, G. Naidu, A. Reddy, Membrane optode for uranium (VI) ions preconcentration and quantification based on a synergistic combination of 4-(2-thiazolylazo)-resorcinol with 8-hydroxyquinaldine, Spectrochimica Acta Part A: Molecular and Biomolecular Spectroscopy, 74 (2009) 1235-1241.

[303] L.L. Zhang, R.W. Cattrall, S.D. Kolev, The use of a polymer inclusion membrane in flow injection analysis for the on-line separation and determination of zinc, Talanta, 84 (2011) 1278-1283.

[304] H.H. See, P.C. Hauser, Electric field-driven extraction of lipophilic anions across a carrier-mediated polymer inclusion membrane, Anal. Chem., 83 (2011) 7507-7513.

[305] H.H. See, P.C. Hauser, Automated electric-field-driven membrane extraction system coupled to liquid chromatography–mass spectrometry, Anal. Chem., 86 (2014) 8665-8670.

[306] R. Güell, E. Anticó, S.D. Kolev, J. Benavente, V. Salvadó, C. Fontàs, Development and characterization of polymer inclusion membranes for the separation and speciation of inorganic As species, J. Memb. Sci., 383 (2011) 88-95.

[307] A. Salima, K.S. Ounissa, M. Lynda, B. Mohamed, Cationic dye (MB) removal using polymer inclusion membrane (PIMs), Procedia Eng., 33 (2012) 38-46.

[308] I. Perez-Silva, C.A. Galan-Vidal, M.T. Ramirez-Silva, J.A. Rodriguez, G.A. Alvarez-Romero, M.E. Paez-Hernandez, Phenol Removal Process Development from Synthetic Wastewater Solutions Using a Polymer Inclusion Membrane, Ind. Eng. Chem. Res., 52 (2013) 4919-4923.

[309] B. Gajda, M. Bogacki, The application of polymer inclusive membranes for removal of heavy metal ions from waste solutions, J. Achiev. Mater. Manuf. Eng., 55 (2012) 673--678.

[310] I. Pérez-Silva, J.A. Rodríguez, M.T. Ramírez-Silva, M.E. Páez-Hernández, Determination of oxytetracycline in milk samples by polymer inclusion membrane separation coupled to high performance liquid chromatography, Anal. Chim. Acta., 718 (2012) 42-46.

[311] E.A. Nagul, C. Fontàs, I.D. McKelvie, R.W. Cattrall, S.D. Kolev, The use of a polymer inclusion membrane for separation and preconcentration of orthophosphate in flow analysis, Anal. Chim. Acta., 803 (2013) 82-90.

[312] B.M. Jayawardane, R.W. Cattrall, S.D. Kolev, The use of a polymer inclusion membrane in a paper-based sensor for the selective determination of Cu (II), Anal. Chim. Acta., 803 (2013) 106-112.

[313] I. Zawierucha, C. Kozlowski, G. Malina, Removal of toxic metal ions from landfill leachate by complementary sorption and transport across polymer inclusion membranes, Waste Manag., 33 (2013) 2129-2136.

[314] O. Senhadji-Kebiche, T. Belaid, M. Benamor, Polymer Inclusion Membrane (PIM) as Competitive Material for Applications in SPE for Water Treatment Process, Open Access Library Journal, 1 (2014) 1.

[315] F.B.M. Suah, M. Ahmad, L.Y. Heng, A novel polymer inclusion membranes based optode for sensitive determination of Al3+ ions, Spectrochimica Acta Part A: Molecular and Biomolecular Spectroscopy, 144 (2015) 81-87.

[316] P. Pantůčková, P. Kubáň, P. Boček, In-line coupling of microextractions across polymer inclusion membranes to capillary zone electrophoresis for rapid determination of formate in blood samples, Anal. Chim. Acta., 887 (2015) 111-117.

[317] A. Garcia-Rodríguez, V. Matamoros, S.D. Kolev, C. Fontàs, Development of a polymer inclusion membrane (PIM) for the preconcentration of antibiotics in environmental water samples, J. Memb. Sci., 492 (2015) 32-39.

[318] N.A. Mamat, H.H. See, Development and evaluation of electromembrane extraction across a hollow polymer inclusion membrane, J. Chromatogr. A, 1406 (2015) 34-39.

[319] A. Casadellà, O. Schaetzle, K. Nijmeijer, K. Loos, Polymer Inclusion Membranes (PIM) for the Recovery of Potassium in the Presence of Competitive Cations, Polymers (Basel), 8 (2016) 76.

[320] S. Chaudhury, A. Bhattacharyya, A. Goswami, Electrodriven Transport of Cs+ through Polymer Inclusion Membrane as “Solvent Separated Ions”, Ind. Eng. Chem. Res., 55 (2016) 3120-3124.

[321] M. Sharaf, W. Yoshida, F. Kubota, S.D. Kolev, M. Goto, A polymer inclusion membrane composed of the binary carrier PC-88A and Versatic 10 for the selective separation and recovery of Sc, Rsc Adv., 8 (2018) 8631-8637.

[322] A. Kaya, H.K. Alpoguz, A. Yilmaz, Application of Cr (VI) transport through the polymer inclusion membrane with a new synthesized calix [4] arene derivative, Ind. Eng. Chem. Res., 52 (2013) 5428-5436.

[323] M. O’Rourke, R.W. Cattrall, S.D. Kolev, I.D. Potter, The extraction and transport of organic molecules using polymer inclusion membranes, Solvent Extr. Res. Dev. Jpn., 16 (2009) 1-12.

[324] A.M.S. Silva, M.F. Pimentel, I.M. Raimundo, Y.M.B. Almeida, Effect of plasticizers on a PVC sensing phase for evaluation of water contamination by aromatic hydrocarbons and fuels using infrared spectroscopy, Sens. Actuators B Chem., 139 (2009) 222-230.

[325] N.N. Maximous, G.F. Nakhla, W.K. Wan, Removal of Heavy Metals from Wastewater by Adsorption and Membrane Processes: a Comparative Study, International Journal of Environmental, Chemical, Ecological, Geological and Geophysical Engineering, 4 (2010) 124-130.

[326] H.H. See, P.C. Hauser, Electro-driven extraction of low levels of lipophilic organic anions and cations across plasticized cellulose triacetate membranes: Effect of the membrane composition, J. Memb. Sci., 450 (2014) 147-152.

Chapter 2

Polymer Inclusion Membrane (PIM) as a solvent-less platform for electrophoresis

2.1 Introduction and objectives

Until now, there are many reports of successful transportation, removal, recovery and separation of small metal and charged organic ions from sample mixtures using PIMs as described in *chapter 1* with examples shown in table 1.4; however, they have not been examined for electrophoretic separation even though there has been incorporated with electric field [1-3]. Furthermore, the basic configuration of PIM use reported in all research currently involves using the horizontal surface of PIMs between two containers of different solution for transportation and extraction through the thickness of the PIMs. There has never been a report deploying PIM sideway (i.e. laterally) using its length as path for transportation or extraction or PIM being operated solvent-free.

This chapter is the very first investigation into whether electromigration of charged molecules can be observed on a PIM using neutral, positively charged, and negatively charged fluorescent dyes. Then, the optimization of PIM by varying the constituents and electrophoretic conditions were studied alongside with conventional membrane extraction to help understand the fundamental principles of transport and establish suitable experimental settings for electromigration of charged dyes. A mixture of selected charged dyes was used to further verify the electrophoretic separation capability as well as to calculate diffusion coefficients and electrophoretic mobilities of each dye. The physiology of prepared PIMs was characterized by Fourier-transform infrared spectroscopy (FT-IR), Scanning electron microscopy (SEM), Thermogravimetric analysis (TGA), and N_2 adsorption.

Based on the literature in *chapter 1*, CTA and 2-NPOE have been frequently employed as base polymer and plasticizer and were selected as the initial composition of the PIM. While a large number of carriers have been explored for a variety of applications, ionic liquids are a popular

choice due to several advantages including their chromatographic properties [4, 5]. In this research, 1-ethyl-3-methylimidazolium bis(trifluoromethylsulfonyl) imide ([EMIM][NTf_2]) was selected as the carrier not only because it was it is readily available in the laboratory but combination of imidazolium cation and bis(trifluoromethylsulfonyl) imide anion has been used for both extraction and chromatography [6-8].

2.2 Electromigration and selectivity study on PIM

2.2.1 Chemicals and equipment

Chemicals for PIM creation and all fluorescent dyes used are listed in Table 2.1. Dichloromethane (DCM) (AR, stabilised with amylene) was purchased from Chem-supply (Gillman, SA). Deionized water (DI) was obtained from Direct-Q 3 UV with Pump (Millipore, 24.3°C, 18.2 MΩ.cm). A glass circular petri dishes for membrane casting (80 o.d. x 60 i.d. x 15H mm, Anumbra) was purchased from Livingstone Laboratory Supplies (Rosebery, NSW). Flat Styrofoam was used as a platform or station upon which the membrane was fixed. Power supply used in electrophoresis was LabSmith High Voltage Sequencer (HVS448LC 6000D). Disposable FINE-JECT needles (HSW FINE-JECT®, 27Gx3/4", 0.4x20mm) was used as electrodes connecting up to LabSmith power supply. Dino-Lite Edge (AM4115T-GFBW, 20-220x, green fluorescence) and Dino-Lite Premier (AM4113T-FV2W, 20-50x, UV/white light) digital microscopes were used as fluorescence and white light monitoring detectors respectively through DinoCapture 2.0 software.

2.2.2 PIM preparation

A schematic drawing of the PIM casting process is shown in Figure 2.1A. The PIM was made by weighing 0.075 g of CTA, 0.10 g of 2-NPOE, and 0.05 g of [EMIM][NTf_2] into a vial, dissolved in 8 mL of DCM, yielding a clear solution after stirring until homogeneous. The polymer solution (2.5 mL) was cast onto a glass petri dish and left to dry under ambient conditions overnight to evaporate the DCM yielding a transparent thin film approximately 15-20 µm thick (figure 2.1B and C). A small amount of DI was added onto the glass petri dish and swirled around the surface before

using sharp-tipped tweezers to gently peel the PIM from the edge inwards to prevent rupture. Excess DI was left to evaporate, and the PIM was wrapped in a lint-free Kimwipe before packing in a zip-lock bag in which their stability can be maintained up to 4 weeks. PIMs used for all experiment in this thesis were stored in zip-lock bags. Before use, the thickness of each PIM was measured using a commercial digital micrometer (Mitutoyo, 293 MDC-MX). The thickness was confirmed by an optical profiler (Wyko NT 1100, Veeco Instrument Inc.) at 5X magnification for the first few batches of films (Figure 2.1D).

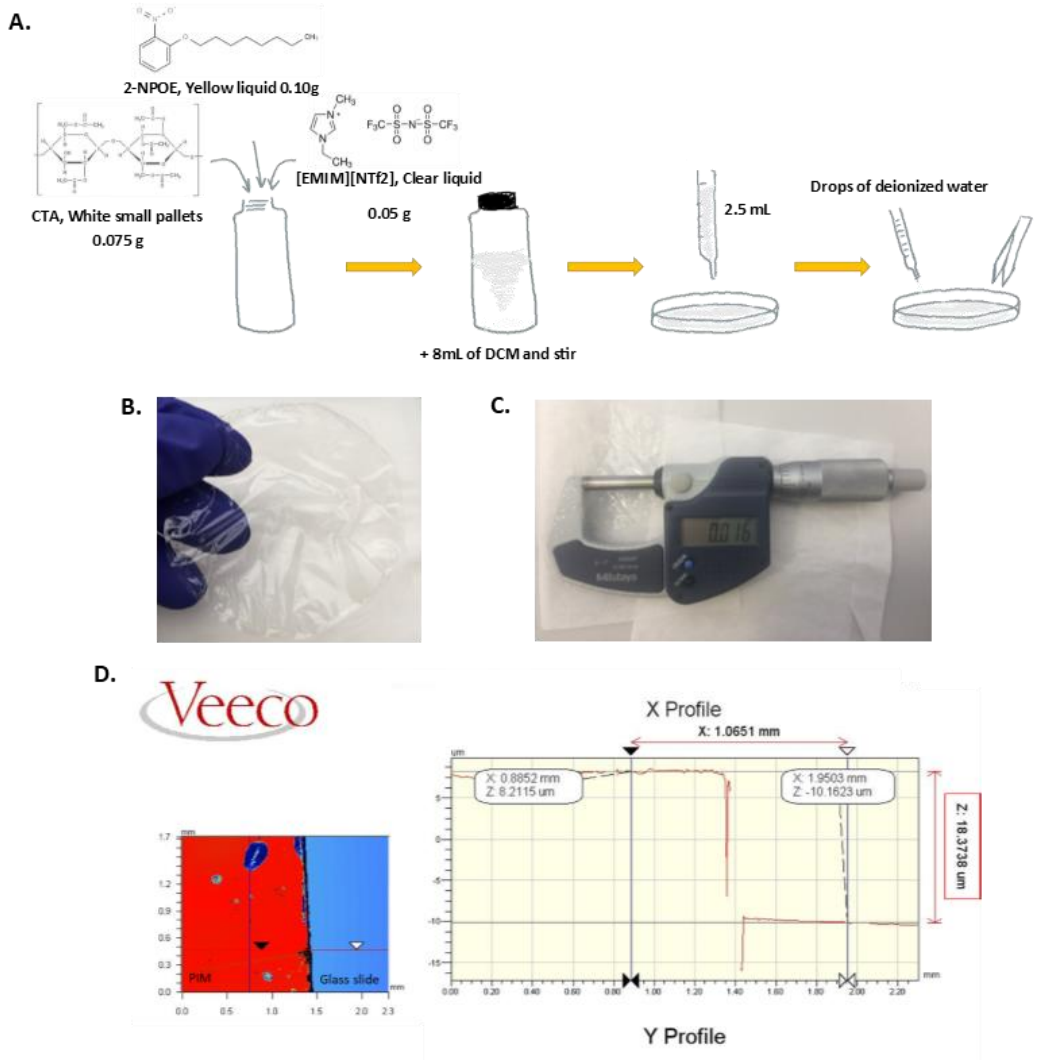

Figure 2.1. PIM appearance and thickness measurement. (A) Scheme showing process of casting PIM (B) cast PIM after being peeled off from the petri dish and dried. (C) Film thickness measured using a commercial digital micrometer. (D) Film thickness measured with an optical profiler. PIM (red zone) was pressed gently on the glass slide (blue zone) to create flat surface for uniform depth measurement, displayed in red box, of multiple spots on the PIM.

2.2.3 Components and set-up of electrophoresis platform

The electrokinetic separation platform is illustrated in Figure 2.2. A PIM was cut with scissors into a strip with dimension of 0.25 cm x 5.0 cm for all experiments described. The Styrofoam support was attached to the base of the microscope stand (Dino-lite, MS-08B Rack) using adhesive tape. Two disposable, stainless steel needles were inserted through the PIM into the Styrofoam approximately 0.5 cm from each end of the PIM strip to hold it in place resulting in a distance between the electrodes of 4 cm. These needles were also used as electrodes connected to the power supply with crocodile clips. A paper ruler was placed above the strip for measurement of the migration distance. Handheld blue-light and white-light digital microscopes were used to visualize the separations along the PIM, with images and video recorded using DinoCapture 2.0 software and a laptop computer. Migration distance was measured using the ruler and ImageJ graphic software at the left side of the spot before and after electrophoresis. Image processing was conducted using Image J graphic software.

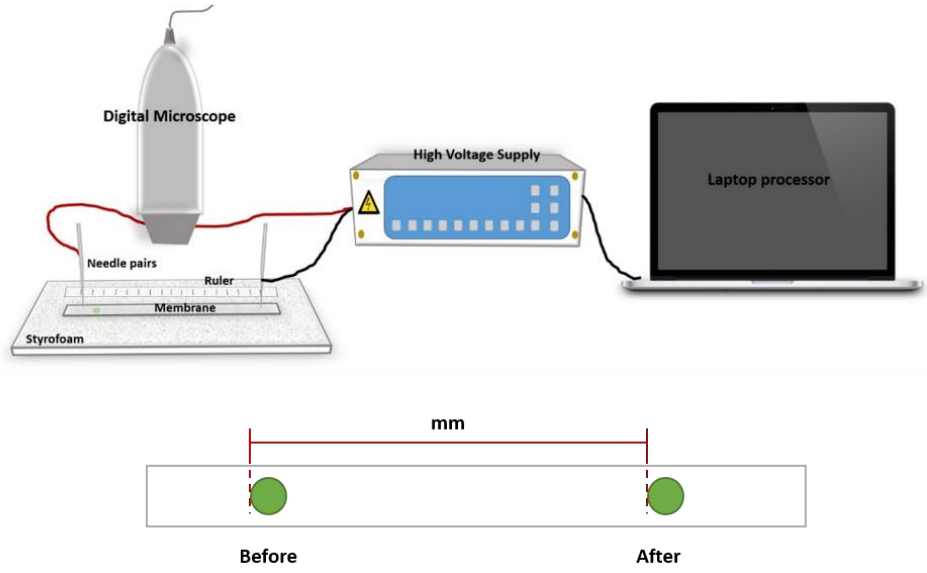

Figure 2.2. Scheme demonstrating the electrokinetic set-up for thin film electrophoresis platform and migration distance measurement process.

Table 2.1. List of PIM constituents and dyes used in chapter 2

Chemicals/Dyes	CAS #	Formula	Structure	MW (g/mol)	Grade/Purity	Supplier
[EMIM][NTf_2]	174899-82-2	$C_8H_{11}F_6N_3O_4S_2$	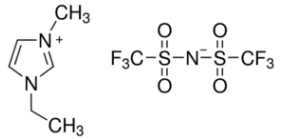	391.31	≥97% (NMR)	Sigma-Aldrich (St. Louis, MO)
2-NPOE	37682-29-4	$O_2NC_6H_4O(CH_2)_7CH_3$	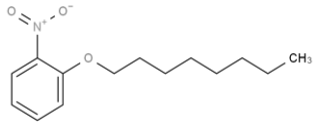	251.32	Selectophore ™, ≥99%	Sigma-Aldrich (Castle Hills, NSW)
Astrazon Blue BG 200% (Basic Blue 3)	4444-00-3	$C_{20}H_{26}ClN_3O$	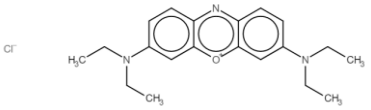	359.89	Textile dyes	Dyechem Industries Ltd.
Astrazon Blue FGRL (200%) *	105953-73-9	$C_{16}H_{24}N_6S$	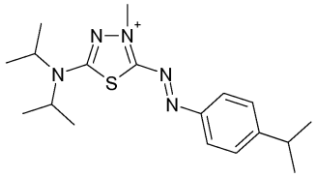	332.261	Commercial textile dyes	Dyechem Industries Ltd.
	33203-80-6	$C_{20}H_{26}ClN_3O$	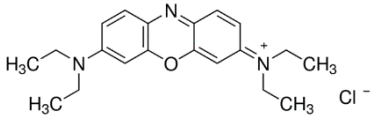	359.89		

Chemicals/Dyes	CAS #	Formula	Structure	MW (g/mol)	Grade/Purity	Supplier
Astrazon Dark Blue 2RN **	569-64-2	$C_{23}H_{25}ClN_2$	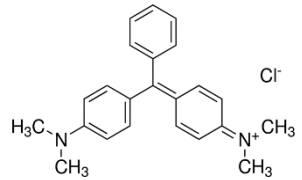	364.911	Commercial textile dyes	Dyechem Industries Ltd.
	12217-48-0	$C_{23}H_{26}ClN_3$	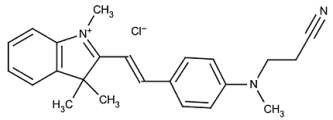	379.93		
Astrazon Golden Yellow A-GL (Basic Yellow 28)	54060-92-3	$C_{21}H_{27}N_3O_5S$	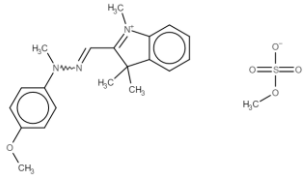	433.52	Commercial textile dyes	Dyechem Industries Ltd.
Astrazon Red A-FBL (Basic Red 46)	12221-69-1	$C_{18}H_{21}BrN_6$	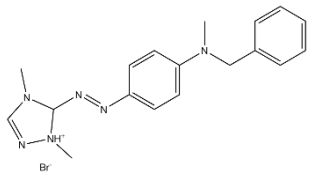	403.328	Commercial textile dyes	Dyechem Industries Ltd.
Astrazon Yellow 8GL 200 (Basic Yellow 13)	12217-50-4	$C_{20}H_{23}ClN_2O$	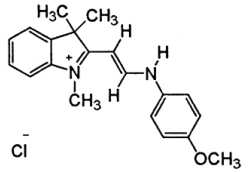	342.86	Commercial textile dyes	Dyechem Industries Ltd.

Chemicals/Dyes	CAS #	Formula	Structure	MW (g/mol)	Grade/Purity	Supplier
Astrazon Yellow GRL (Basic Yellow 29)	39279-59-9	$C_{20}H_{24}ClN_3$	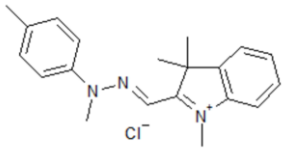	341.88	Commercial textile dyes	Dyechem Industries Ltd.
Bismarck Brown Y (G) (Basic Brown 1)	10114-58-6	$C_{18}H_{20}Cl_2N_8$	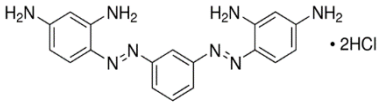	419.311	50%	Fluka
Brilliant Cresyl Blue	81029-05-2	$C_{17}H_{23}ClN_4O$	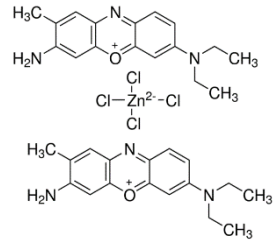	385.96	≥60%	Harwood
CTA	9012-09-3	N/A	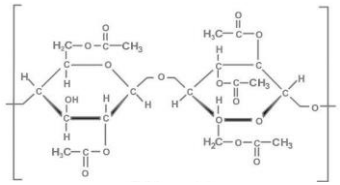	N/A	Selectophore ™	Sigma-Aldrich (St. Louis, MO)
Coumarin 334	55804-67-6	$C_{17}H_{17}NO_3$	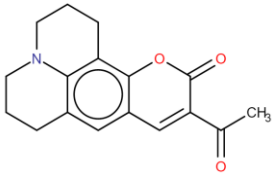	283.32	99%	Sigma-Aldrich (St. Louis, MO)

Chemicals/Dyes	CAS #	Formula	Structure	MW (g/mol)	Grade/Purity	Supplier
Crystal Violet (Basic Violet 3)	548-62-9	$C_{25}H_{30}ClN_3$	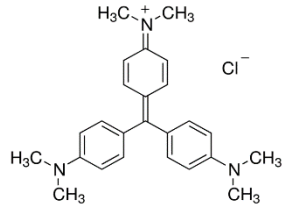	407.979	≥90%	Sigma-Aldrich (Castle Hills, NSW)
Fluorescein sodium salt	518-47-8	$C_{20}H_{10}O_5Na_2$	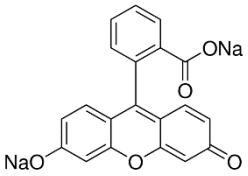	376.275	fluorescent tracer	Sigma-Aldrich (Castle Hills, NSW)
Malachite Green chloride (Basic Green 4)	569-64-2	$C_{23}H_{25}ClN_2$	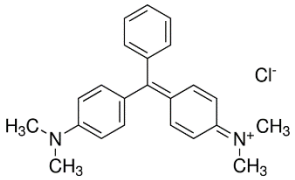	364.911	≥96% (HPLC)	Sigma-Aldrich (Castle Hills, NSW)
Methylene Blue	122965-43-9	$C_{16}H18ClN_3S$	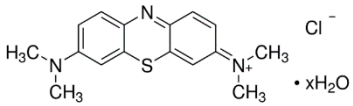	319.85	≥82%	British Drug House (BDH)
Nile Blue A perchlorate	3625-57-8	$C_{20}H_{20}ClN_3O_5$	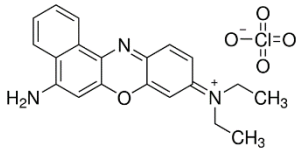	417.84	95%	Sigma-Aldrich (Castle Hills, NSW)

Chemicals/Dyes	CAS #	Formula	Structure	MW (g/mol)	Grade/Purity	Supplier
Rhodamine 123 (R123)	62669-70-9	$C_{21}H_{17}ClN_2O_3$	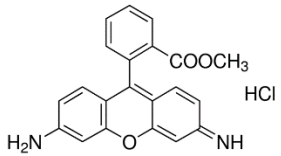	380.821	mitochondrial specific fluorescent dye	Sigma-Aldrich (Castle Hills, NSW)
Rhodamine 6G (R6G)	989-38-8	$C_{28}H_{31}ClN_2O_3$	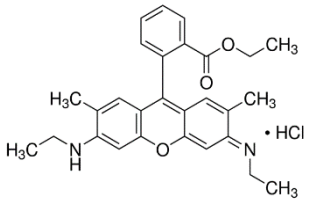	479.01	approx. 95%	Sigma-Aldrich (Castle Hills, NSW)
Rhodamine B (RB)	81-88-9	$C_{28}H_{31}ClN_2O_3$	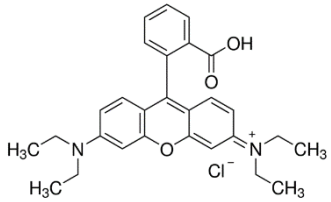	479.01	≥95%	British Drug House (BDH)
Victoria Blue BO (Basic Blue 7)	2390-60-5	$C_{33}H_{40}ClN_3$	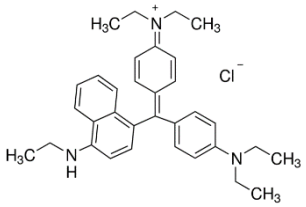	514.144	90%	Sigma-Aldrich (St. Louis, MO)

** Mixture of basic blue 159 and 3 **Mixture of malachite green and basic red 14*

2.2.4 Electrophoresis procedures

All laboratory-based electrophoresis experiments were performed according to the following procedures unless stated otherwise. Coumarin 334, Fluorescein sodium salt, and R6G were used as neutral, anionic, and cationic species, respectively, to determine the electrokinetic transport of different charged molecules in the PIM. Stock solutions of each dye at 1000 ppm were prepared in DI and were further diluted as stated in each experiment with DI. Sample solution was spotted using an auto-pipette (0.5 µL) or syringe (0.1 µL, Hamilton, 7000 Series Modified Microliter™) close to the anode (left side of the strip) and left to dry for approximately 5-10 min. Only after the spot was completely dried, the electrodes were connected, and voltage was applied. At least three or more replicates on separate strips were conducted in parallel for each experiment. The potential difference was maintained for 60 min with 2000 V applied (500 V/cm).

2.3 Electromigration study of different charged dyes

As the potential of the PIM to carry charge was unknown, trial experiments were performed with fluorescent dyes to allow easy visualisation of the molecules and their feasibility for electromigration in the PIM. Neutral Coumarin 334 (10 ppm), anionic Fluorescein (10 ppm) and cationic R6G (10 ppm) were selected as they are similarly sized molecules with different charge state. Based on this investigation, two observations were concluded as shown in Figure 2.3.

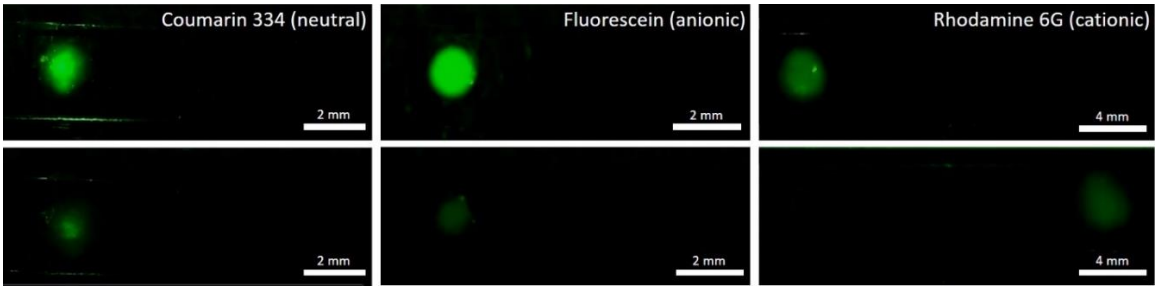

Figure 2.3. Images of migration of different charge fluorescent dyes before applying voltage (top row) and after 60 min application of 2000 V (bottom row). Conditions: PIM dimensions: 0.25 cm x 5 cm; length between electrodes: 4 cm. Voltage: 2000 V. Duration: 60 min. Sample(s): 10 ppm of each dye in water. Sample volume (spot size): 0.5 µL. Drying time (before electrophoresis): 5-10 min.

First, electrophoretic migration of small organic molecules can be performed using prepared PIM in a lateral strip configuration and simple set-up where both sample and platform were in dry state without being submerged in solution tanks or involved with liquid reagents. The experiment procedure was also initially performed with R6G where voltage was applied immediately after the sample was spotted without drying. However, the electromigration of R6G can only be partially observed with severe distortion of R6G band along the length of PIM suggesting the possibility of incomplete extraction of dye and that electromigration on PIM is not a surface phenomenon. Hence, drying step prior to voltage application is essential in assuring complete extraction of analytes. This observation could also indicate that electromigration on PIM in this study involves two important steps where sample was firstly extracted vertically into the PIM followed by lateral migration under applied electric field.

Second, the electromigration was only observed with cationic R6G, while neutral Coumarin and anionic Fluorescein did not show any migration, only loss of dye intensity presumably due to photobleaching. This suggested the PIM is cation-selective. At this point, the initial hypothesis of this selectivity was based on the that proposed by Gadjourova et al. reporting preferential transport of cations dominated by crystalline phase in solid polymer electrolytes (SPEs) [9]. SPEs are another type of polymer-based thin film which have been known for more than 3 decades for their ability to conduct electricity by the movement of ions – typically small inorganic cations such as lithium, sodium, and potassium. Lithium has been the focus of much research because of its high reduction potential, and consequent use in electrolytic cells in solid-state batteries which is the most commonly used batteries around the world due to high power density that can be obtained [10-13]. It was illustrated that the polymer chains form tunnel structures together with coordination with cations, in this case lithium, inside the hollow space which was sufficient for them to migrate through while the anions remained outside of these tunnels and did not facilitate in migration and ionic conductivity. This might be applicable to CTA-based PIMs as CTA is dominant with crystalline phase as described earlier *chapter 1*. However, SPEs do not involve

the use of carrier while PIM contain both plasticizer and carrier. Therefore, more extensive investigations are still needed to explain the selectivity and transport efficiency relationship of both plasticizer and carrier towards the target ions, various transport mechanisms between them has been proposed for different target analytes [14-19].

2.4 Optimization of PIM composition

After the conclusion of PIM being cation-selective, the influence of PIM composition was studied by varying composition of CTA, 2-NPOE, and [EMIM][NTf_2] in 8 mL of DCM as indicated in Table 2.2 with R6G chosen as model analyte. For each component, four different weights were tested leaving the amount weighed of the other components unchanged.

The PIM performance was evaluated based on the migration distance, spot size and spot shape of R6G, as illustrated in table 2.2 A-L. An amount of CTA lower than 0.05 g could not be assessed as the PIM did not form with adequate physical strength and was prone to tear. At 0.05 g of CTA (33 wt%), migration of R6G was observed to be partially streaking (table 2.2 A). Even though the PIM at this concentration was strong enough to be cast into physically stable film, it was relatively soft and needed to be handled with care to prevent tearing. It was also possible that the matrix environment within the PIM was still more liquid or gel-like because of the higher relative proportion of plasticizer. Increasing the amount of CTA decreased the migration of R6G as the thickness of the film increased and became more rigid (table 2.2 B-D). The effect of PIM thickness has been previously reported to cause restriction of ion diffusive motion [20-23].

When varying the content of the plasticizer, no migration was observed in the absence of 2-NPOE reflecting tightly packed CTA polymer chains may be blocking the pathway where the ion can be transported (table 2.2 E). Increasing the amount of 2-NPOE showed improvement on migration distance of R6G presumably because of more space between the polymer chains and the flexibility within PIM (table 2.2 F-H) [24, 25]. Even though 0.15 g (54.5 wt%) showed greater migration distance of R6G; however, there were traces of liquid droplets on the surface of PIMs overnight

that may be from the plasticizers leaking out of the PIM (table 2.2 H) [26]. Therefore, 0.10 g (44.4 wt%) of 2-NPOE was chosen as an efficient amount to support the migration of R6G in this case.

Table 2.2. Variation of PIM components for the platform optimization. For each component, four different weights were tested leaving the amount weighed of the other components unchanged. The Migration of R6G for each composition ratio of PIM component after 60 min of electrophoresis is shown in the last column (A-L). Dashed circle indicates the starting position of the dye spot at 0 min. Conditions: PIM dimensions: 0.25 cm x 5 cm; length between electrodes: 4 cm. Voltage: 2000 V. Duration: 60 min. Sample(s): 10 ppm of R6G in water. Sample volume (spot size): 0.5 µL. Drying time (before electrophoresis): 5-10 min.

	CTA (g)	2-NPOE (g)	[EMIM][NTf_2] (g)	Mass ratio (weight%) *(CTA : 2-NPOE : [EMIM][NTf2])*	Recorded images after 60 min of electrophoresis
Variation of CTA	0.05	0.05	0.05	33.3 : 33.3 : 33.3	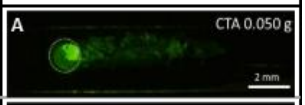
	0.075			42.9 : 28.6 : 28.6	
	0.1			50 : 25 : 25	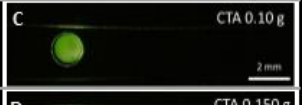
	0.15			60 : 20 : 20	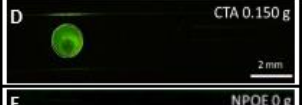
Variation of 2-NPOE	0.075	0	0.05	60 : 0 : 40	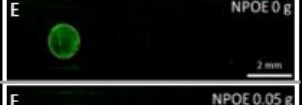
		0.05		42.9 : 28.6 : 28.6	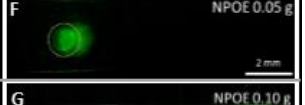
		0.1		33.3 : 44.4 : 22.2	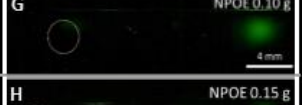
		0.15		27.3 : 54.5 : 18.2	
Variation of [EMIM][NTf2]	0.075	0.1	0	42.9 : 57.1 : 0	
			0.03	36.6 : 48.8 : 14.6	
			0.05	33.3 : 44.4 : 22.2	
			0.1	27.3 : 36.4 : 36.4	

Finally, in the absence of carrier, [EMIM][NTf_2], migration was observed but with a severely distorted spot indicating the migration was permitted due to presence of plasticizer, 2-NPOE (table 2.2 I). Increasing the amount of [EMIM][NTf_2] improved the spot shape implying possibility of better specific binding with R6G exhibiting more systematic migration (table 2.2 J and K). However, higher amount of [EMIM][NTf_2] was found to not only limit the migration of R6G but also made the PIM softer with more visible wrinkles. Leftover traces of liquid droplets on the surface on the PIM were also observed which could be again the leakage of plasticizers [26], of carrier itself [14] or both. As shown in table 2.2 L, the highest amount of [EMIM][NTf_2] resulted in shorter distance and non-smooth migration of R6G in which could have been a result from precipitation of excess carrier within the PIM [27]. Therefore, the optimal PIM composition was finalized with 33.3% CTA : 44.4% 2-NPOE : 22.2% [EMIM][NTf_2].

2.5 Migration studies of different cationic dyes

To determine the selectivity of PIM towards cations, several cationic dyes were separated in the PIM. All non-fluorescent and fluorescent dyes available in the laboratory were chosen for the investigation. Textile dyes listed in Table 2.2 with Astrazon tradename were kindly supplied for research purpose from Dyechem Industries Ltd. The concentration used was 10 ppm for R6G and Rhodamine B (RB) while 1 ppm was used for Rhodamine 123 (R123). For all visible textile dyes, a concentration of 1000 ppm was used.

Electromigration of some selected cationic dyes is shown in figure 2.4 and the result showed the potential selectivity of PIM towards cationic dyes as electromigration of all positively charged dyes was observed with different migration distance for each dye. With each dye showing different migration distances, the estimation of electrophoretic mobility of each dye used in the experiment was calculated using equation (2.1) with values displayed in table 2.3. Comparing with available data on electrophoretic mobility of R6G in aqueous system performed in capillary electrophoresis (CE), the mobility of R6G on PIM was found to be approximately 160 times lower

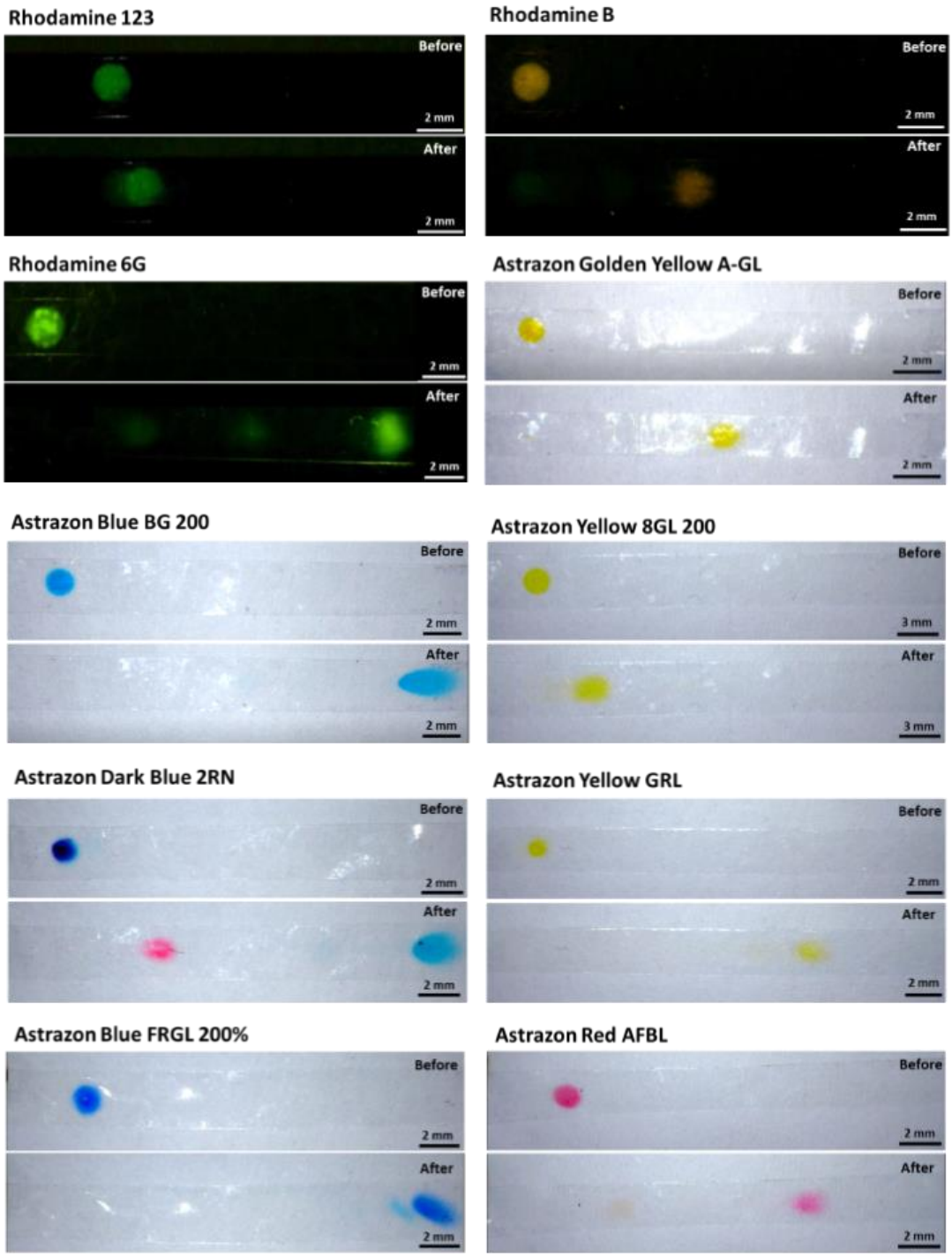

Figure 2.4. Electromigration of selected cationic fluorescent dyes (black background) and visible textile dyes (white background) before and after electrophoresis on optimal PIM platform. Conditions: PIM dimensions: 0.25 cm x 5 cm; length between electrodes: 4 cm. Voltage: 2000 V. Duration: 60 min. Sample(s): 10 ppm of fluorescent dyes in water and 1000 ppm of visible textile dyes in water. Sample volume (spot size): 0.5 µL (fluorescent dyes) and 0.1 µL (visible textile dyes). Drying time (before electrophoresis): 5-10 min. White trace observed along the PIM was the result of reflection from the white light camera and was found irrelevant to electromigration result.

than that reported in CE [28]. Literature for other dyes were not found and were assumed to be a similar order of magnitude.

$$Electrophoretic\ mobility\ (\mu) = \frac{(Migration\ distance)\ x\ (Effective\ length\ of\ PIM)}{(Voltage)\ x\ (Time)} \qquad (2.1)$$

Table 2.3 Estimation of electrophoretic mobility of cationic dyes on PIM. Calculation parameters: PIM effective length: 40 mm (0.04 m), voltage: 2000V, and time: 60 min (3600 s).

Dyes	Alternative name	Migration distance (mm ± mm)	Electrophoretic migration rate ($x10^{-11}$ m^2/Vs)
Brilliant Cresyl Blue	Brilliant Blue C	3.9 ± 0.1	2.2 ± 0.1
Crystal Violet	Basic Violet 3	16.1 ± 0.7	8.9 ± 0.4
		20.6 ± 1.6	11.4 ± 0.9
Malachite Green Chloride	Basic Green 4	18.8 ± 1.2	10.4 ± 0.7
Methylene Blue	Basic Blue 9	16.0 ± 1.2	8.9 ± 0.7
Nile Blue A perchlorate	N/A	3.5 ± 0.4	1.9 ± 0.2
R123	N/A	1.4 ± 0.2	0.8 ± 0.1
R6G	Basic Red 1	3.3 ± 0.3	1.8 ± 0.2
		8.8 ± 0.5	4.9 ± 0.3
		15.6 ± 0.8	8.7 ± 0.5
RB	Basic Violet 10	8.1 ± 0.9	4.5 ± 0.5
Victoria Blue BO	Basic Blue 7	10.4 ± 1.2	5.8 ± 0.7
Astrazon Blue FGRL 200	Basic Blue 159	15.2 ± 0.5	8.4 ± 0.3
	Basic Blue 3	17.2 ± 0.5	9.6 ± 0.3
Astrazon Yellow GRL	Basic Yellow 29	11.1 ± 1	6.2 ± 0.5
Astrazon Yellow 8GL 200	Basic Yellow 13	3.3 ± 0.9	1.9 ± 0.5
Astrazon Dark Blue 2RN	Basic Red 14	4.4 ± 0.4	2.5 ± 0.2
	Basic Green 4	17.1 ± 0.7	9.5 ± 0.4
Astrazon Red A-FBL	Basic Red 46	2.3 ± 0.5	1.3 ± 0.3
		11.6 ± 0.7	6.5 ± 0.4
Astrazon Golden Yellow A-GL	Basic Yellow 28	8.7 ± 0.7	4.9 ± 0.4
Astrazon Blue BG 200	Basic Blue 3	18.4 ± 0.4	10.3 ± 0.3

Additionally, and more importantly, we can also observe multiple spots in some of the dyes including R6G. These arise from the impurities that might be present. Similarly, some textile dyes are simply a mixture of two basic dyes as described in remark for table 2.1. This finding revealed that optimal concentration of prepared PIM and experimental conditions are potentially suitable as solvent-less electrophoresis platform.

2.6 Electrophoresis of mixture of cationic dyes

2.6.1 Electrophoresis of dyes on PIM

To further explore the hypothesis of PIM of being solvent-platform for separation, electrophoresis was performed using a mixture of cationic dyes from the previous section. A mixture of fluorescent dyes at a final concentration of 10 ppm for R6G and RB and 1 ppm for R123, was prepared in water. For visible dyes, all Astrazon textile dyes were mixed with another commercial cationic visible dye, Crystal violet, and neutral Bismarck brown as initial spot marker at a concentration of 500 ppm in DI. The spot size for fluorescent dyes was reduced from 0.5 µL to 0.1 µL in order to reduce spot elongation which might lead to overlapping bands and incomplete separation due to similar mobilities of several dyes. The resulting separation is shown in figure 2.5A and B for fluorescent dyes and visible dyes, respectively. The migration order of the dyes is as follows:

Fluorescent dyes : Rhodamine 123 < Rhodamine B < Rhodamine 6G

Visible dyes : Bismarck brown < Astrazon Yellow 8GL 200 < Basic Red 14 from Astrazon Dark Blue 2RN < Astrazon Golden Yellow A-GL < Astrazon Red A-FBL < Astrazon Yellow GRL < trace of Crystal violet < Basic Green 4 from Astrazon Dark Blue 2RN < overlapping spots of Basic Blue 3 from Astrazon Blue FGRL 200, Astrazon Blue BG 200 and Crystal violet

As there were only three fluorescent dyes in the mixture together with a large difference in electromigration rate of each dye, distinct separation was achieved including traces

of R6G (following R123 in spot #1 and overlapping with RB in spot #2). The order of migration clearly correlates with the values presented in table 2.3. In Figure 2.5B, the 9 visible dyes showed a few inseparable spots due to very close migration distance as well as spot elongation, presumably due to diffusion while migrating or possible interaction between dyes themselves; hence, complete separation of 9 dyes was not be obtained. However, the migration distance of each dye matched well with the distance measured when separated individually. Some faint colour spots (i.e. trace of Astrazon Red AFBL and basic blue 3 from Astrazon Blue FGRL 200) were not be detected due to limited resolution and lighting of the camera setting.

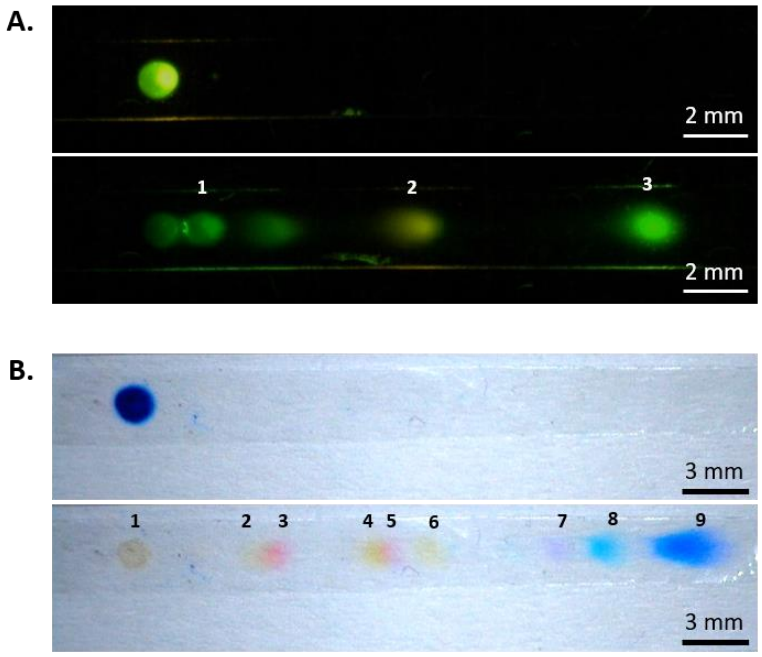

Figure 2.5. Electrophoretic separation of a mixture of cationic (A) fluorescent dyes with (1) R123, (2) RB and (3) R6G and (B) visible dyes with (1) Bismarck brown, (2) Astrazon 8GL 200, (3) Basic red 14 from Astrazon Dark Blue 2RN, (4) Astrazon Golden Yellow A-GL, (5) Astrazon Red A-FBL, (6) Astrazon Yellow GRL, (7) trace from Crystal violet, (8) Basic green 4 from Astrazon Dark Blue 2RN and (9) inseparable Basic blue 3 from Astrazon Blue FGRL 200, Astrazon Blue BG 200 and Crystal violet. Top and bottom images are before and after application of 2000 V for 60 min respectively. Conditions: PIM dimensions: 0.25 cm x 5 cm; length between electrodes: 4 cm. Sample(s): Fluorescent : 10 ppm of RB and R6G, 1 ppm of R123 in mixture, Visible: 500 ppm of commercial textile and visible dyes in mixture. Sample volume (spot size): 0.1 µL. Drying time (before electrophoresis): 5-10 min.

To understand the elongation and enlargement of dye spots during migration, experiments were conducted by spotting the dye (100-1000 ppm) onto the PIM with and without applying the voltage (2000V) in which the width of the spot before and after 60 min was measured using ImageJ graphic program. The differences in width of the spot before and after 60 min allowed for calculation of diffusion coefficients using equation 2.2 where σ is the increase of spot width (in mm) from 0 to 60 min and the values are shown in table 2.4.

$$\sigma = \sqrt{2Dt} \qquad (2.2)$$

Table 2.4. Calculated diffusion coefficient of selected dyes in PIM measured from dye spot broadening with and without applying voltage.

Dye	$\sigma_{\text{without voltage}}$ (mm)	$D_{\text{without voltage}}$ (x10^{-10} m^2/s)	$\sigma_{\text{with voltage}}$ (mm)	$D_{\text{with voltage}}$ (x10^{-10} m^2/s)
Bismarck Brown	0.039	0.0021	0.111	0.0171
Brilliant Cresyl Blue	0.308	0.1318	0.375	0.1953
Brilliant Yellow	0.049	0.0033	0.032	0.0014
Crystal Violet	0.059	0.0048	0.242	0.1220
Fluorescein sodium salt	0.062	0.0053	0.128	0.0228
Malachite Green	0.332	0.1531	0.546	0.6211
Methylene Blue	0.132	0.0242	0.553	0.5097
Nile Blue	0.171	0.0406	0.575	0.4592
Orange G	0.052	0.0038	0.115	0.0184
R123	0.144	0.0288	0.474	0.3121
R6G	0.257	0.0917	0.882	1.0805
RB	0.26	0.0939	0.33	0.1513

2.6.2 Capillary electrophoresis of dyes

Identical groups of dye were also separated using CE to investigate the possible mechanism of electromigration of dyes in the PIM. As the dyes are cationic, an acidic background electrolyte was used in CE to ensure the dyes were protonated and positively charged.

Electrophoresis was performed using an Agilent 7100 capillary electrophoresis system equipped with a UV-Visible diode-array detector (190-600 nm) (Agilent Technologies, Santa Clara, CA, USA). Fused silica capillaries of 50 µm i.d. with 60 cm total length (51 cm effective length) were used (Polymicro Technologies, Phoenix, AZ, USA). Capillary temperature was maintained at 25°C throughout the experiment. New capillary was preconditioned by flushing 1 M of Sodium hydroxide (NaOH) for 20 min, followed by DI for 10 min, then 100 mM formic acid for 1 min, and background electrolyte for 5 min. Background electrolytes were 100 mM of ammonium formate with pH 2.7 (in DI) for fluorescent dyes and pH 3 (in DI) for visible dyes. Mixtures of three fluorescent dyes (R6G, RB, and R123) with final concentration for each dye at 100 ppm and 7 textile dyes (all Astrazon label dyes) with final concentration for each dye at 1000 ppm were dissolved in DI and injected into CE system by hydrodynamic pressure at 50 mbar for 2 s. The separation voltage was at 19 kV and 30 kV for fluorescent dyes and visible dyes, respectively. Detection wavelengths of 254 nm with 20 nm bandwidth was chosen for both fluorescent dyes and 200 nm with 20 nm bandwidth for visible dyes. Electropherograms were processed through equipped Agilent ChemStation software. As shown in figure 2.6, the order of migration in the CE experiments for both fluorescent and visible dyes are:

Fluorescent dyes : RB < R6G < R123

Visible dyes : Astrazon Blue FGRL 200 < Astrazon Dark Blue 2RN (not specified) < Astrazon Yellow GRL < Astrazon Golden Yellow A-GL < Astrazon Yellow 8GL = Astrazon Blue BG 200 < Astrazon Red FBL < Astrazon Dark Blue 2RN (not specified)

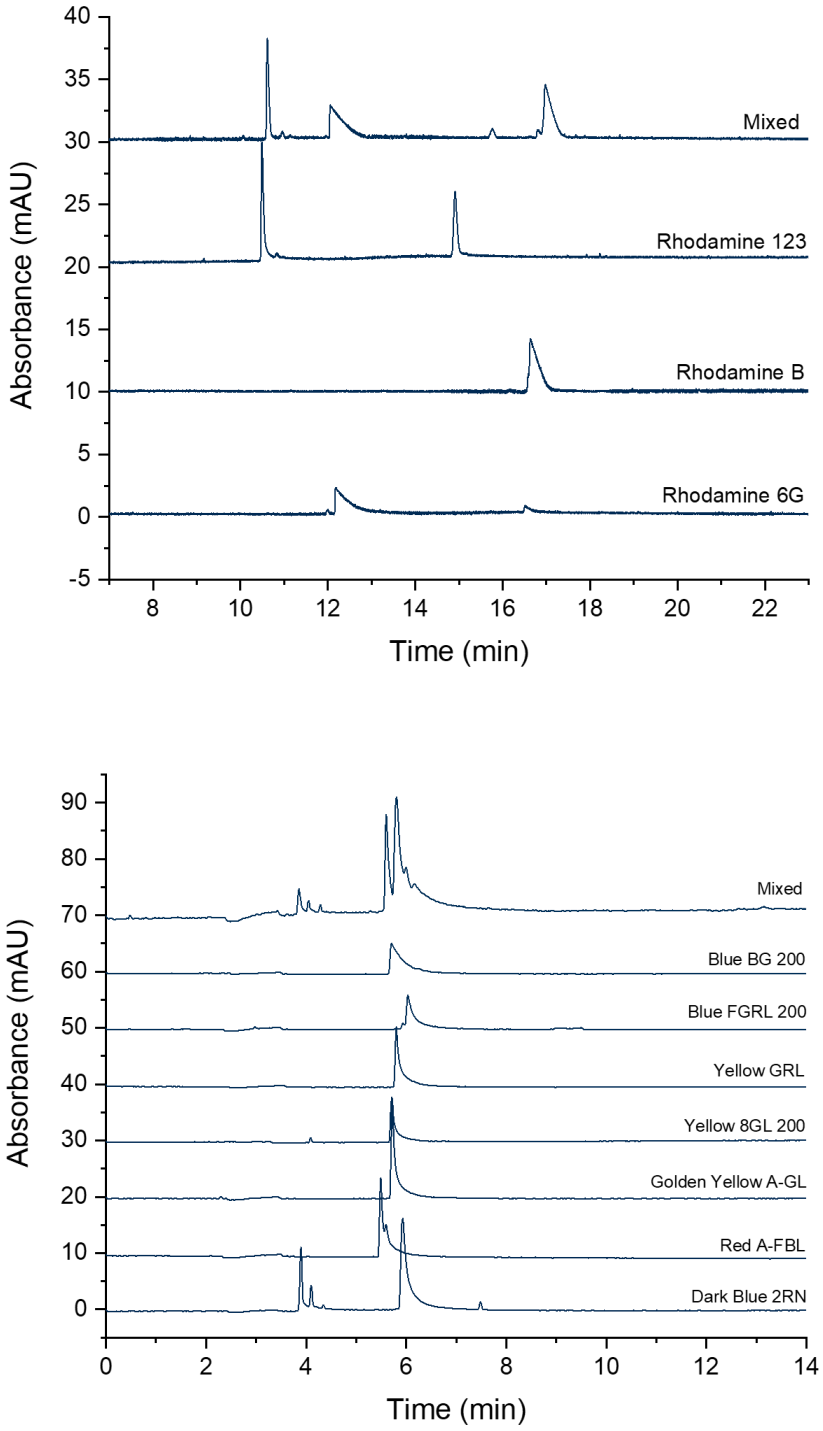

Figure 2.6. Electropherograms of three fluorescent dyes (100 ppm in water) and seven visible dyes (1000 ppm in water). CE conditions: fused silica capillary, 60 cm x 50 µm id; BGE: fluorescent dyes: 100 mM Ammonium Formate pH 2.7, visible dyes: 100 mM Ammonium Formate pH 3 in water; Injection: 50 mbar, 2 s; separation voltage: fluorescent dyes: 19 kV, visible dyes: 30 kV.

These migration orders are different to that obtained in the PIM. In aqueous CE, R123 showed multiple peaks which cannot be detected on PIM presumably due to it having the lowest mobility in the PIM preventing the separation. While there are no reports on separation of these three dyes with CE/microchip electrophoresis, some literature involving Rhodamine dyes (R6G and RB or RB and R123) and the order of migration – based on size, charge, and pKa of dyes –agreed with what that observed here [35, 36]. For visible dyes, the migration time of all dyes were quite close to each other indicating they exhibit a similar charge and shape/size; hence, the mixture of these dyes could not be completely resolved as many of them were overlapping. Since the order of migration was a key factor in this experiment, further optimization of CE conditions was not performed. Greater selectivity in PIM towards the cationic dyes, more obviously in textile dyes, and different order of migration suggested that electromigration within the PIM was not solely influenced by size and charged as typically proposed in CE.

2.7 Membrane extraction of dyes with variation of PIM components

* *Experiments were conducted with identical casting process, platform set-up and electrophoretic procedures explained in section 2.2.2 to 2.2.4*

Alongside investigation of cation electromigration through the PIM, conventional membrane extraction was also performed by simple immersion of the PIM into a solution of individual dyes to understand their significance and contribution to the selectivity of cationic dyes. Four different PIMs cast in 8 mL DCM were examined: CTA only (100 wt%), CTA+2-NPOE (42.9 wt%+57.1 wt%), CTA+[EMIM][NTf_2] (60 wt%+40 wt%) and CTA+2-NPOE+[EMIM][NTf_2] (33.3 wt%+44.4 wt%+ 22.2 wt%) with each PIM was used for extraction with Coumarin 334, Fluorescein sodium salt, and R6G. The membrane extraction was performed using a beaker filled with 50 mL of 5 ppm of Coumarin 334, Fluorescein sodium salt, and 2 ppm R6G in water. The beaker was constantly stirred throughout the experiment. Each PIM was immersed into the stirred solution and 1.5 mL of solution was withdrawn at 0, 1, 5, 10, 20, and 30 min then every hour up to 4 hr.

After withdrawal, the same volume of fresh dye was added to the solution to replace the taken portions to maintain constant concentration. The absorbance of the dye solution at these times was measured using a quartz cuvette (1 cm pathlength) in a UV-Vis spectrophotometer (Metertech, SP8001, Glen Osmond Australia) with Metertech UVmate software. The absorbance was measured at 459.5 nm for Coumarin 334, 490.4 nm for Fluorescein sodium salt, and 525.5 nm for R6G and the absorbance was plotted using Microsoft Excel or Origin.

The results from these extractions are shown in figure 2.7. The PIM containing only CTA (figure 2.7A) did not show significant decrease in the absorbance for Fluorescein sodium salt and R6G suggesting CTA does not have any capability to extract charged dyes. A gradual decline of absorbance and slight colour change on PIM (from transparent) was observed for neutral Coumarin 334 indicating that it was partially extracted. The explanation of this phenomena is still unsure as there has been no report employing PIM with only polymer base for extraction. However, CTA-based membrane without additives was reported to be highly porous and these pores were then fully impregnated with PIM additives [14, 37, 38]. Therefore, the potential extraction observed in this experiment (figure 2.7A) could be that neutral Coumarin 334 diffusively penetrated and resided within the pores of polymer. The extraction of neutral Coumarin 334 continued to be observed in all variants of PIM with the greatest decrease in absorbance observed in the CTA+2-NPOE system (figure 2.7B). It is believed that further extent of extraction over adsorption on CTA could possibly be due to the lipophilicity of Coumarin 334 (logP = 2.78-2.90 [39, 40]) partitioning into the hydrophobic 2-NPOE (logP = 4.86-5.8 [40-42]) phase. This partitioning effect could also be responsible for the moderate decrease of neutral Coumarin 334 observed in PIM made from CTA+[EMIM][NTf_2] where it partially distributed into water-immiscible [EMIM][NTf_2] (logP = 0.06-0.44 [43, 44]) phase (figure 2.7C). Similarly, a very small decrease in absorbance was noticed on both Fluorescein sodium salt and R6G, in the PIM made from CTA+2-NPOE (figure 2.7B) and this could be an influence from their distribution coefficients (logD). In acidic pH, Fluorescein sodium

salt and R6G have a logD (pH 1.7) of 3.01 and 0.07 respectively [40] suggesting that small degree of extraction of these two species into the organic phase might be allowed.

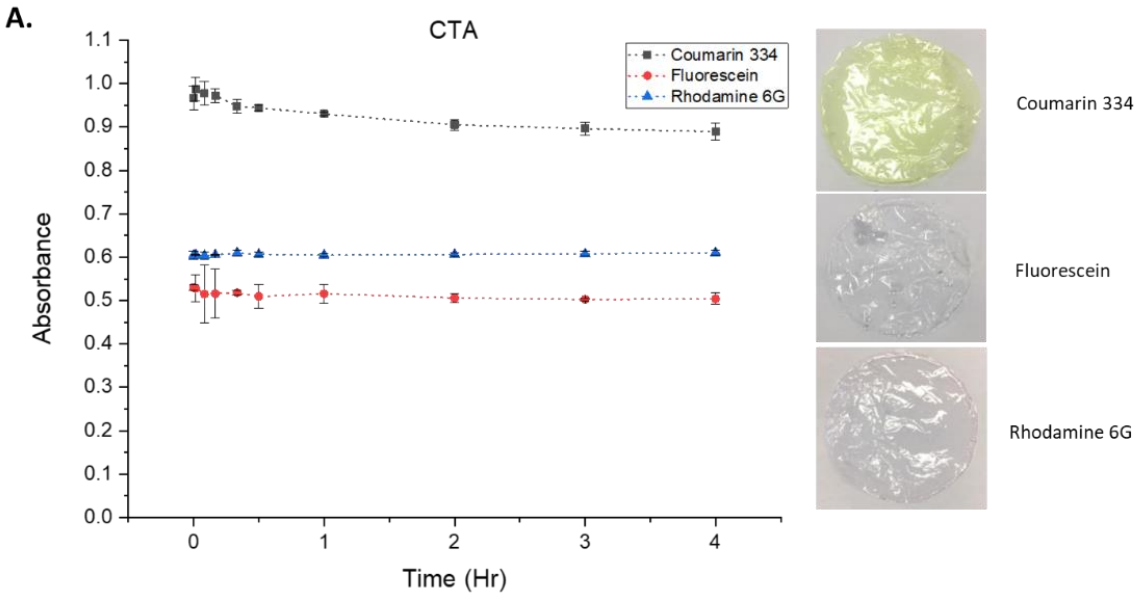

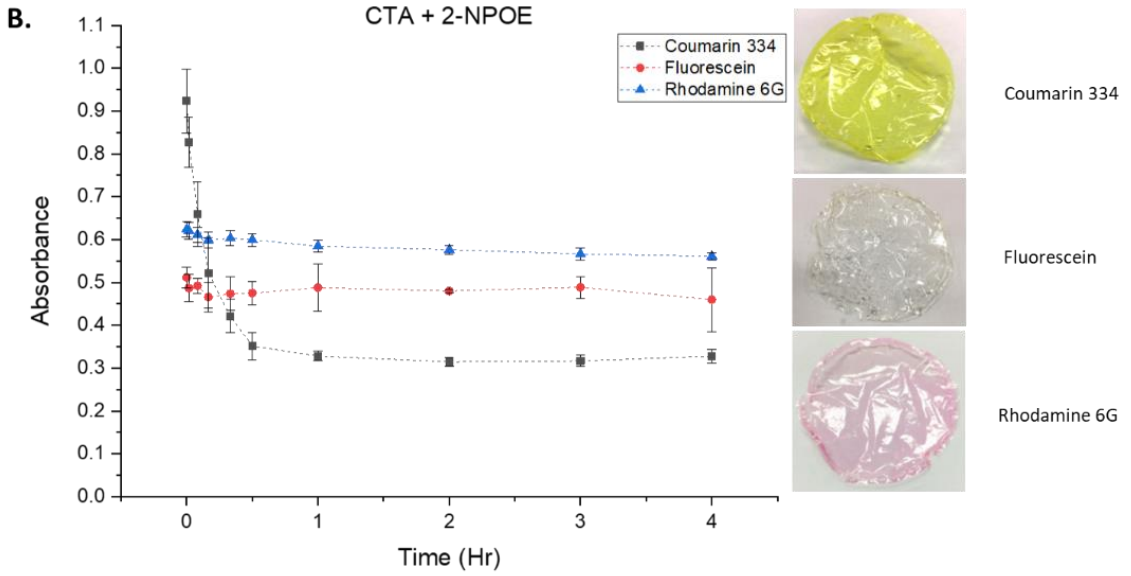

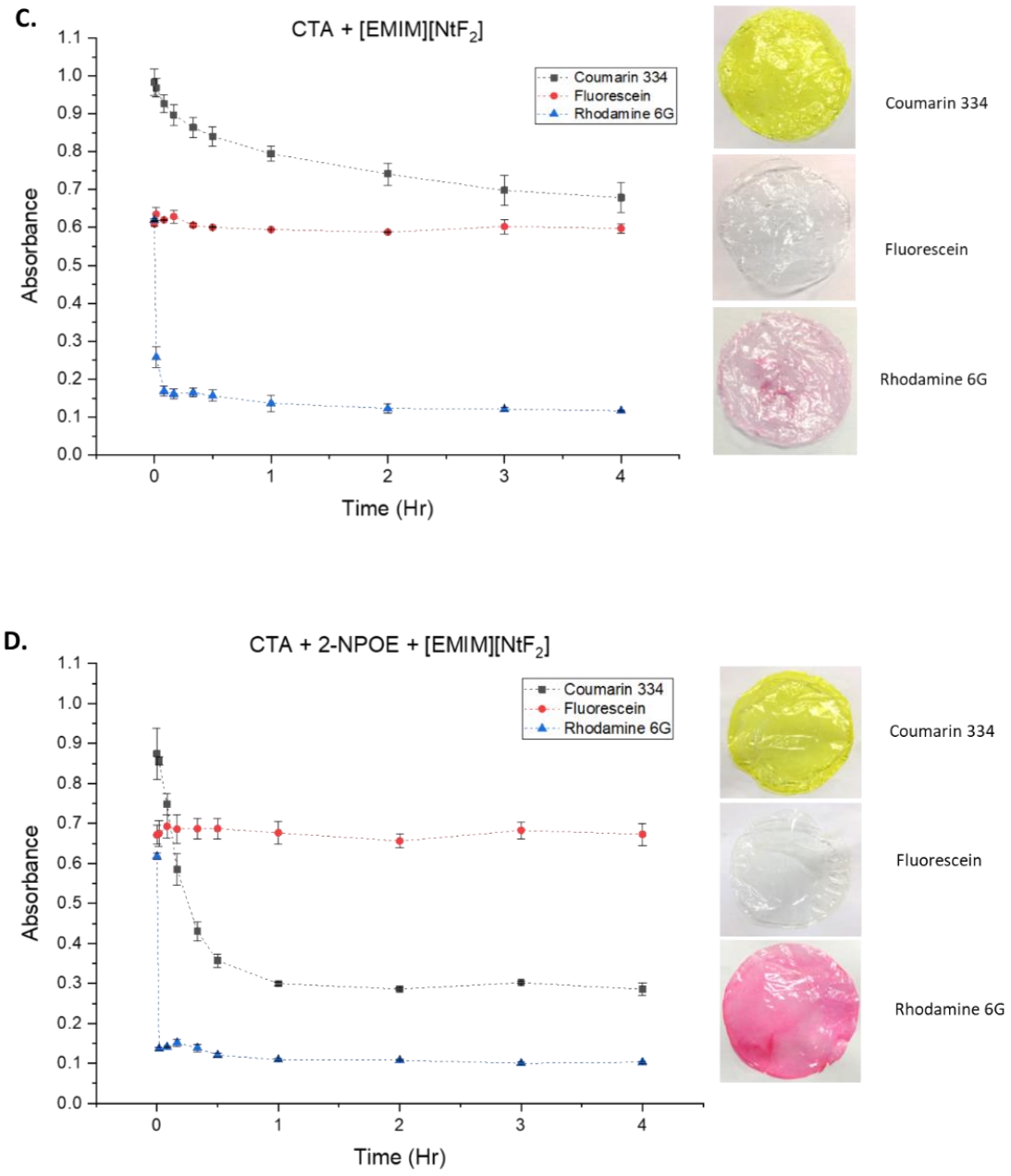

Figure 2.7. UV-Vis absorbance spectra of Coumarin 334 (square), Fluorescein sodium salt (circle) and R6G (triangle) after 4 hr of membrane extraction using PIMs composing of (A) CTA only, (B) CTA+2-NPOE, (C) CTA+[EMIM][NTf_2], and (D) CTA+2-NPOE+[EMIM][NTf_2]. Each symbol represents individual collected aliquot. Blank (DI) absorbance was 0.126±0.007 (Coumarin 334), 0.079±0.005 (Fluorescein sodium salt) and 0.092±0.01 (R6G). Actual photographs of PIM in each variation of components and dyes after 4 hr of extraction were shown next to each plot. *(*note: phots were manually taken using mobile phones, direct comparison might be inaccurate due to lighting conditions*).

With the PIM made from CTA+[EMIM][NTf_2] (figure 2.7C), a steep drop in absorbance was observed for R6G indicating a rapid extraction into the ionic liquid phase suggesting that extraction of cationic species into the PIM might not be an effect of lipophilicity and partition actions even though there was a report of [EMIM][NTf_2] having high partitioning constants towards cations [7]. Combined with cationic selectivity reported on optimal PIM from section 2.3 and 2.4, it is believed that extraction in this case occurs from ionic interactions between R6G and [EMIM][NTf_2] by ion-complexing, ionic exchange, or solvation affinity towards cations. Absorbance plot of R6G shown for PIM made with all three components (figure 2.7D) displays exactly the same trend as that of CTA+[EMIM][NTf_2] (figure 2.7C) suggesting that extraction of R6G was largely dependent on carrier, [EMIM][NTf_2]. Meanwhile, obvious enhancement of dye colour on PIM was shown in figure 2.7D in presence of 2-NPOE, especially with R6G, and this was suspected that 2-NPOE, as an organic solvent in PIM, provide a more mobile environment within the PIM where R6G molecules were allowed to move freely and evenly distributed throughout the PIM.

The membrane extraction experiment does not explain the order of migration of cationic dyes, but possible implications can be made regarding the fundamental properties of the PIM. Only neutral (Coumarin 334) and cationic (R6G) species can be extracted into the PIM phase via partitioning and ionic interaction while anionic species (Fluorescein sodium salt) were not. This means that they possibly remain dried on the surface of PIM. If this is the case, it could explain the lack of migration of Fluorescein observed above implying that electromigration occurs only within the internal PIM matrix and is not a surface phenomenon.

2.8 PIM Characterization

2.8.1 Scanning electron microscopy (SEM)

PIM morphology was characterized using Scanning Electron Microscopy (SEM). SEM images were collected using Hitachi SU-70 field emission analytical scanning electron microscope

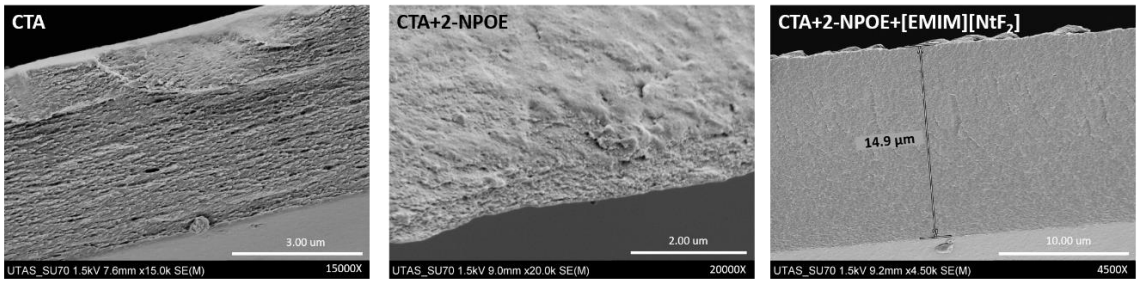

Figure 2.8. SEM images of cross-sections of PIMs containing only CTA (left), CTA+2-NPOE (middle) and 2-CTA+2-NPOE+[EMIM][NTf_2] (right). **Note: Cross-sections of PIM with CTA only and CTA+2-NPOE were obtained via cutting with scissors.*

(Hitachi-Hitech, Tokyo, Japan). The cross-section of PIMs made with CTA+2-NPOE and CTA+2-NPOE+[EMIM][NTf_2] were obtained by immersing PIMs in liquid Nitrogen for 15 s and fractured using forceps. Pieces of PIMs were then fixed onto aluminium stubs with carbon tape and sputtered with platinum for 15 s. The acceleration voltage used was 1.5 kV and the thickness were also measured with measuring feature in SEM software.

As shown in figure 2.8, PIM containing CTA was observed to be noticeably porous while there was a tendency in reduction of porosity with PIM containing CTA+2-NPOE and likely became dense with no obvious pores in addition of [EMIM][NTf_2]. This was resulting from 2-NPOE and [EMIM][NTf_2] filling the pores of CTA [14]. The rough surfaces were also observed after the addition of plasticizer correlates with literature reports and could be due to their structural arrangements. A smoother surface was observed when [EMIM][NTf_2] was added with some detectable debris resulted from the PIM surface being exposing to the atmosphere and the opposite side was facing the glass petri dish [14]. The measurement of optimal PIM thickness was measured to be at 14.9 µm showing acceptable thickness relatively close to measurements from optical profiler and micrometre.

2.8.2 Fourier transform infrared spectroscopy (FT-IR)

FT-IR equipped with diamond Attenuated total reflectance (ATR) (Bruker Vector 22, Bruker SA, Wissembourg, France) was used to characterize chemical compositions of optimal PIM

and possible chemical bonding between each other. Pure components of PIM : CTA, 2-NPOE and [EMIM][NTf_2] were used as standard references. The optimal PIM was scanned in the range of 4000-600 cm^{-1} (absorbance mode) and FT-IR spectrum of optimal standard references and PIMs are shown in figure 2.9 and their main peak assignments in table 2.5. In FT-IR spectrum of the optimal PIM, the characteristic peaks of three main constituents can still be observed without any detectable additional peaks; however, the difference can be noted from the signal intensity. Most of the intensity signals from 2-NPOE and [EMIM][NTf_2] in the optimal PIM spectra were found to decrease slightly compared to those in the standards while the intensity signals from CTA increased which could possibly be referred to 2-NPOE or [EMIM][NTf_2] successfully attaching or filling the pores of CTA. Results from FT-IR indicated that there was no permanent chemical alteration after the membrane was cast since the number and positions of the peaks correlates to those in the standard samples. It was reported that interaction between three constituents took place with weak temporary intermolecular forces (hydrogen, van der Waal, or dipole) [23, 45, 46].

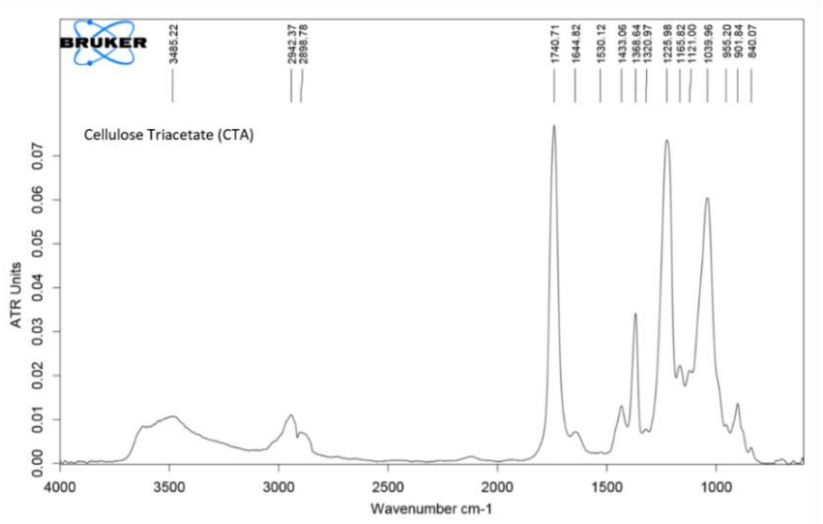

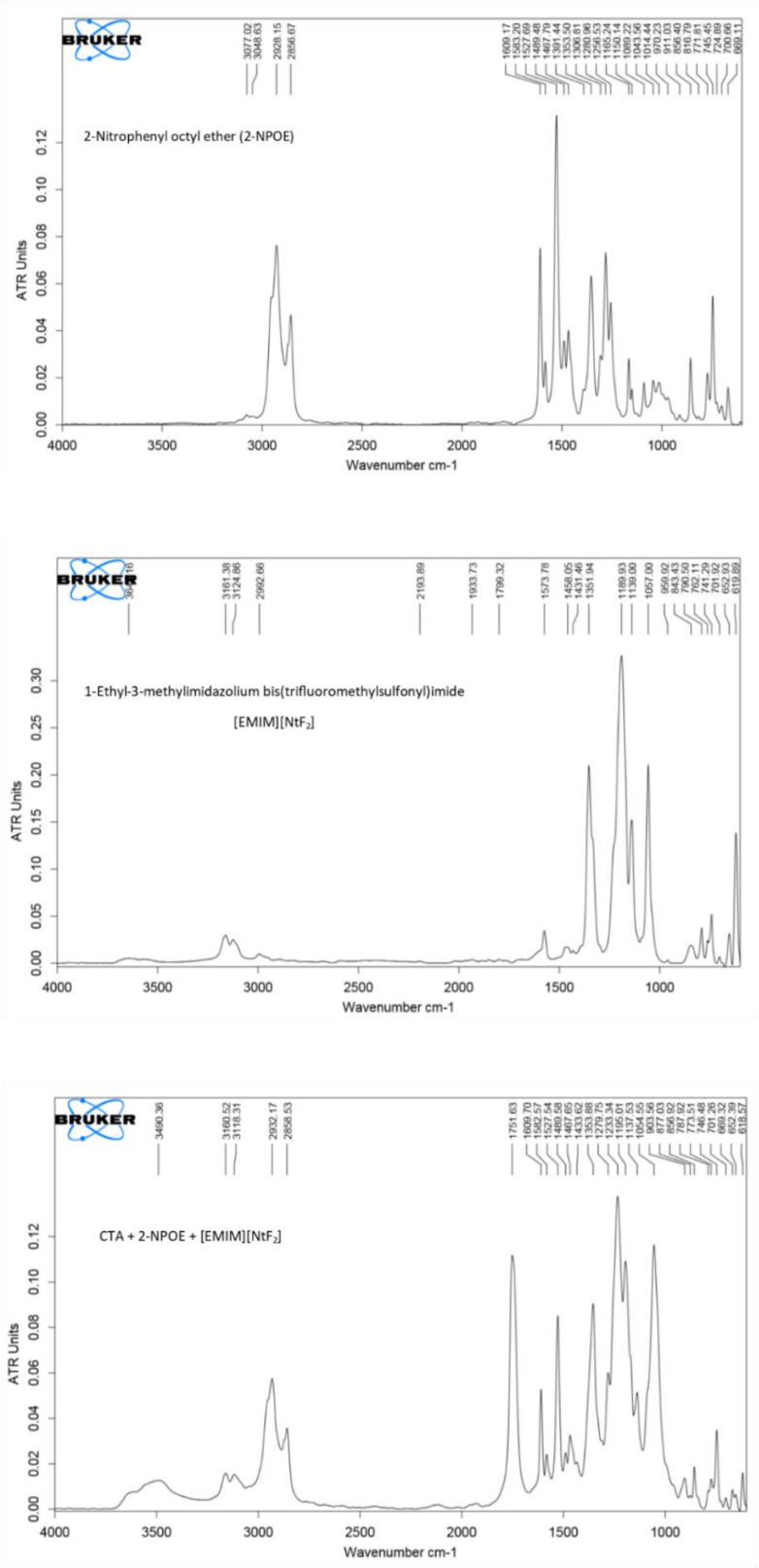

Figure 2.9. FT-IR spectrum of standards (pure CTA, 2-NPOE, and [EMIM][NTf_2]) and PIM (composing of all three components with optimal concentration from section 2.4).

Table 2.5. FT-IR peak values and assignments of PIM components and final PIM.

Compound	Peak value (cm^{-1})	Assignment	Ref(s)
CTA	3485	O–H	[37, 45-48]
	2942	C–H	
	1740	C=O (acetate)	
	1368	C–H (deformation of CH_3)	
	1225	C–O–C (asymmetric)	
	1039	C–O–C (symmetric)	
2-NPOE	2928-2856	$–CH_2–$	[37, 45, 46, 48, 49]
	1609-1583	C=C (aromatic ring)	
	1527	N=O (NO_2)	
	1467	$–CH_3$ (octyl)	
	1353	C–N	
	1256	R–O–CH_2	
	856	C–N	
	724	$–CH_2$	
[EMIM][NTf_2]	3161-2992	C–H (from $[EMIM]^+$)	[50-52]
	1573	N–C–H (from $[EMIM]^+$)	
	1351	$–CH_2$ (from $[EMIM]^+$)	
	1189	CF_3 (from $[NTf_2]^-$)	
	1139	O=S=O (symmetric, from $[NTf_2]^-$)	
	1057	S–N–S (asymmetric, from $[NTf_2]^-$)	
		Ring (asymmetric, from $[EMIM]^+$)	
		C–C (from $[EMIM]^+$)	
		$N–CH_3$ (from $[EMIM]^+$)	
	741	CF_3 (symmetric, from $[NTf_2]^-$)	
	652	S–N–S (symmetric, from $[NTf_2]^-$)	
	619	O=S=O (asymmetric, from $[NTf_2]^-$)	

2.8.3 Thermogravimetric Analysis (TGA)

One of the early hypotheses made regarding the possible migration of dye inside PIM was that there was a sufficient amount of water (moisture) present. TGA analysis was performed to monitor the water content with Labsys Evo instrument (Setaram, Caluire, France). The optimal PIM was chopped into small pieces, weighed (at least 20 mg) and placed in an alumina crucible. The instrument was run with flowing N_2 at 150 kPa with a heating rate at 5°C/min from 25°C to 140°C and another repeated experiment was run up to 120°C and held at this temperature for 6 hours to ensure noticeable weight loss from water evaporation, if any. Pure CTA pallets, 2-NPOE plasticizer, and [EMIM][NTf_2] ionic liquid was also run in TGA to confirm their thermal properties under the same instrument setting but with temperature up to 550°C for CTA, 350°C for 2-NPOE and 600°C for [EMIM][NTf_2]. The data was collected using system software and the plot was constructed using origin.

TGA profile of optimized PIM showed no sign of weight loss within temperature range from 25°C-140°C which was well above the boiling point of water implying that there was no significance loss of water or moisture from the PIM (figure 2.10). This result does not mean that there was no water, but the amount was well below the sensitivity of TGA at 0.0009% (calculated from TGA resolution from LABSYS evo spec sheet). We believe that this amount of water or moisture is negligible and shows no consequential impact on PIM performance. In figure 2.10, TGA results of raw components of PIM used in the experiments correlated well with those reported TGA on PIM components from literatures where the vaporization, degradation, and decomposition of substances occur above 200°C [38, 53-56].

2.8.4 Nitrogen (N_2) adsorption

PIM porosity and surface area were estimated using N_2 adsorption/desorption technique with surface area analyser (TriStar II 3020, Micromeritics Gemini, Georgia, USA). The optimized PIM was cut into small pieces before being weighed in a test tube. The sample was left

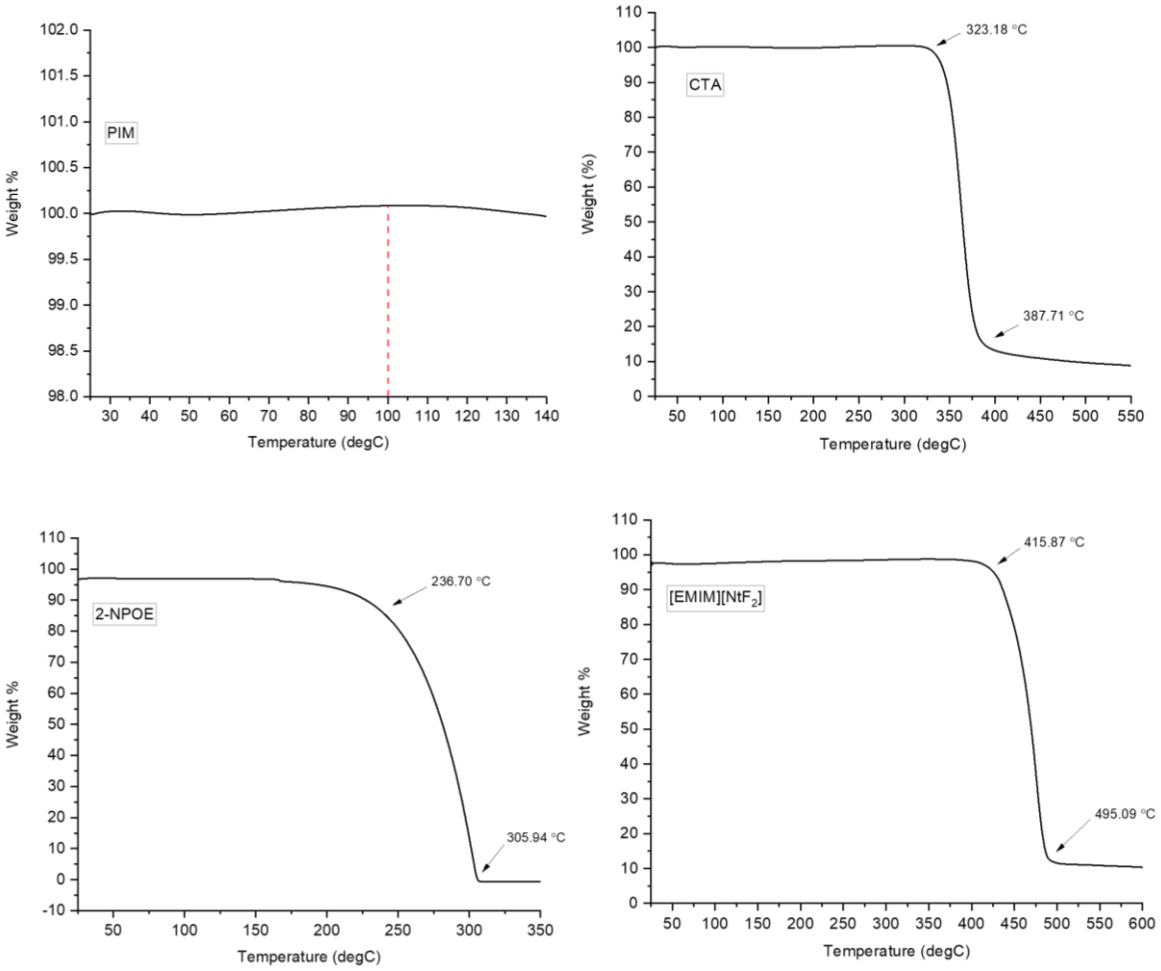

Figure 2.10. Zoomed-in TGA profile of optimized PIM where red dashed line represent water boiling points at 100°C and full-scale profiles of individual PIM components.

to degas in vacuum for 24 hr at room temperature. The surface area (S_{BET}), total pore volume (V_p), and pore diameter of the PIM were reported to be 1.58±0.435 m^2/g, 0.0162±0.002 cm^3/g and 42.9±11.09 nm respectively. The adsorption curve of (figure 2.11) shows no obvious hysteresis loop in which corresponds to type II isotherms typically found for non-porous materials with weak adsorption [57, 58]. This result also correlates well with dense bulk of PIM observed with SEM previously indicating PIM being potentially non-porous. The surface area reported here was found to be very low with pore size in nanometre range; therefore, expected to have no contributions to electromigration in PIM in this case.

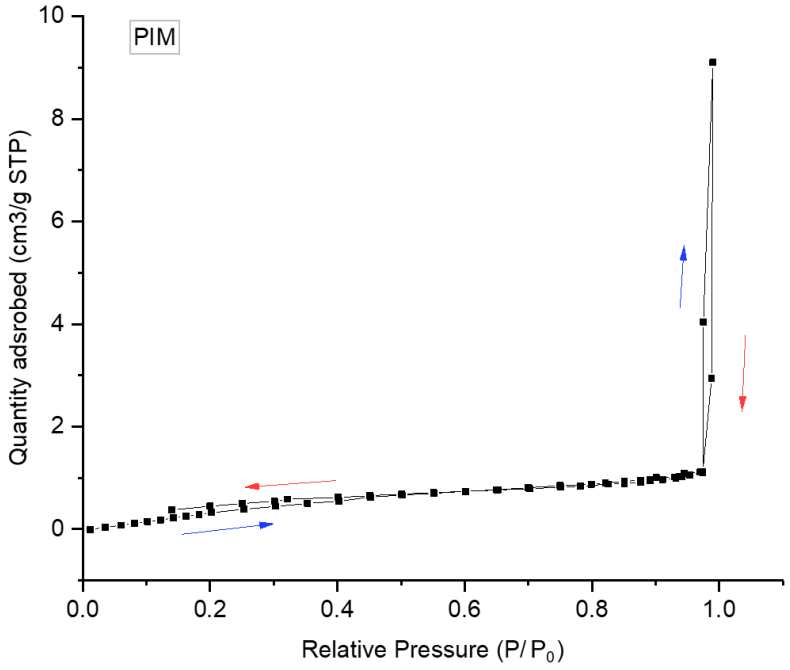

Figure 2.11. N_2 adsorption/desorption BET curve of optimized PIM. Blue and red arrows represent adsorption and desorption respectively.

2.9 Principles of migration in PIM

Based on the fundamental experiments conducted and the literature reports of PIMs mentioned throughout the chapter, the most probable principle for migration is based on those proposed by Religa et al. [59]. It is illustrated in figure 2.12 using R6G as a model cation.

By having only CTA, the polymer chain is tightly packed prohibiting R6G from being efficiently extracted into the PIM, hence no changes in the absorbance of the solution as well as no electromigration of R6G was observed on the PIM strip. Addition of plasticizers (figure 2.12 top right) provide extra space between the chains through weak physical bonding with CTA frameworks allowing R6G to be extracted into the PIM phase and directionally migrate under electric field; hence appearing as streaks and a distorted spot . A slow and gradual decrease in R6G absorbance observed in CTA+2-NPOE indicates that R6G was partially extracted into the PIM phase. This suggests that 2-NPOE behaves similarly to organic phase within CTA matrix improving affinity for extraction of organic R6G. This finding also supports electromigration observed for R6G on PIM

strip in an absence of carrier shown in table 2.2 I. With CTA+[EMIM][NTf_2], extraction of R6G into the PIM improved, but the absence of plasticizer meant that the space between the polymer chains may be reduced. The lack of electromigration then could be explained by [EMIM][NTf_2] plating themselves onto CTA chains similar to 2-NPOE but without flexible movement. As for the optimized system when PIM are composed of three components, it could be possible that 2-NPOE and [EMIM][NTf_2] weakly interact into a unit then being attached onto the CTA chains as proposed by Religa et al. [59] in which has been adapted in a figure below for our research. This postulation strongly supported the well-structured electromigration in the PIM where [EMIM][NTf_2] could be semi-mobile to the extent of 2-NPOE branches providing the migration of dye spot in a controlled manner.

This theory accounts for the PIM specific features observed in the current experiments. However, no solid confirmation was drawn as the focus was primarily on the use of the PIM as a lateral solvent-less platform for electrophoresis of positively-charged organic. Therefore, more in-depth investigation of PIM fundamentals will have to be further explored.

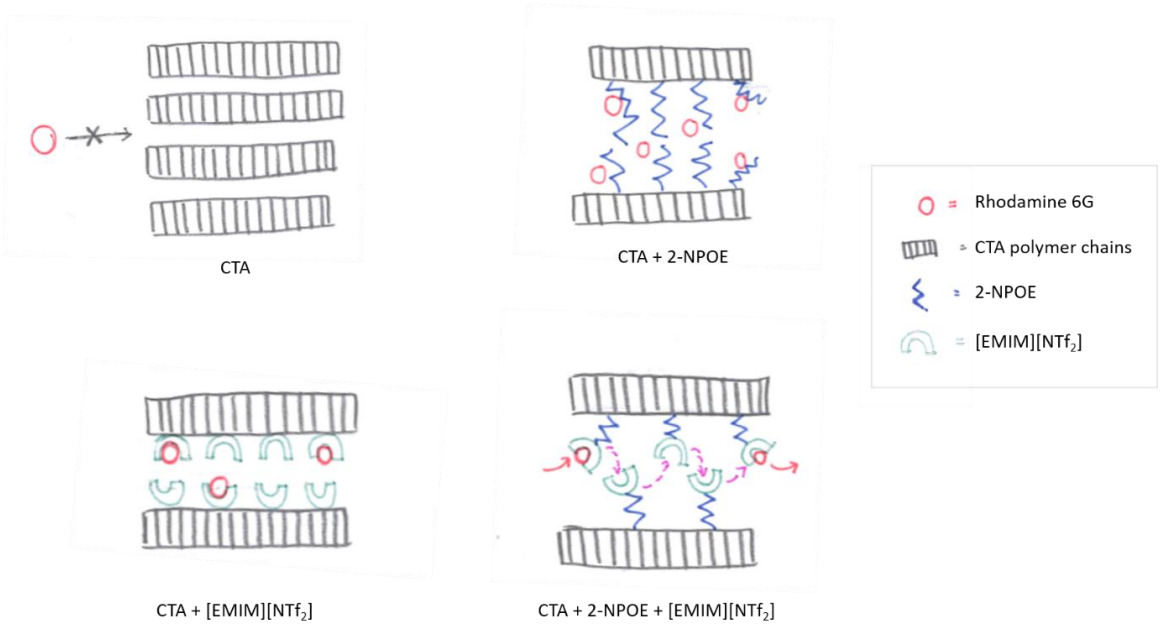

Figure 2.12. Illustration of possible mechanism for selective electrophoretic migration (transport) in PIM formulated in this research. The drawing was modified based on original scheme by ref. [59].

2.10 Conclusion

In summary, a PIM-based thin film constructed as a strip was successfully utilized for electrophoretic separation of cationic dyes in absence of liquid solvents. The PIM consists of three components CTA, 2-NPOE, and [EMIM][NTf_2] in which each component specifically contributed to physical strength, flexibility, and selectivity of the PIM. Electrophoretic migration and separation were performed under the potential of 500 V/ cm and monitored using portable fluorescent microscope. Electrophoretic migration was observed only with cationic dyes while no migration was observed with anionic and neutral dyes indicating the PIM was selective towards cations. With each cationic dye exhibiting different electrophoretic mobilities, separation of several cationic dyes was also successfully performed. The investigations showed that electrophoretic separation on PIM may occur through combined mechanisms even though further confirmation is still required. However, PIM capability for cationic dye electrophoresis together with low diffusion/dispersion coefficients displayed strong possibility for electrophoretic migration and separation to be operated at lower voltage leading for PIM to be employed in prospective applications concerning rapid analysis and portable platform or devices.

2.11 References

[1] H.H. See, P.C. Hauser, Electric field-driven extraction of lipophilic anions across a carrier-mediated polymer inclusion membrane, Anal. Chem., 83 (2011) 7507-7513.

[2] H.H. See, P.C. Hauser, Automated electric-field-driven membrane extraction system coupled to liquid chromatography–mass spectrometry, Anal. Chem., 86 (2014) 8665-8670.

[3] M.I.G.S. Almeida, R.W. Cattrall, S.D. Kolev, Polymer inclusion membranes (PIMs) in chemical analysis-A review, Anal. Chim. Acta., 987 (2017) 1-14.

[4] A. Berthod, M. Ruiz-Ángel, S. Carda-Broch, Recent advances on ionic liquid uses in separation techniques, J. Chromatogr. A, 1559 (2018) 2-16.

[5] M.D. Joshi, J.L. Anderson, Recent advances of ionic liquids in separation science and mass spectrometry, Rsc Adv., 2 (2012) 5470-5484.

[6] T.D. Ho, C. Zhang, L.W. Hantao, J.L. Anderson, Ionic liquids in analytical chemistry: fundamentals, advances, and perspectives, Anal. Chem., 86 (2013) 262-285.

[7] M.C. Breadmore, Ionic liquid-based liquid phase microextraction with direct injection for capillary electrophoresis, J. Chromatogr. A, 1218 (2011) 1347-1352.

[8] B. Dilasari, Y. Jung, G. Kim, K. Kwon, Effect of Cation Structure on Electrochemical Behavior of Lithium in [NTf2]-based Ionic Liquids, ACS Sustainable Chemistry & Engineering, 4 (2015) 491-496.

[9] Z. Gadjourova, Y.G. Andreev, D.P. Tunstall, P.G. Bruce, Ionic conductivity in crystalline polymer electrolytes, Nature, 412 (2001) 520-523.

[10] M.A. Ratner, D.F. Shriver, Ion transport in solvent-free polymers, Chem. Rev., 88 (1988) 109-124.

[11] F. Croce, G.B. Appetecchi, L. Persi, B. Scrosati, Nanocomposite polymer electrolytes for lithium batteries, Nature, 394 (1998) 456-458.

[12] H.C. Ferraz, L.T. Duarte, M. Di Luccio, T.L.M. Alves, A.C. Habert, C.P. Borges, Recent achievements in facilitated transport membranes for separation processes, Brazilian Journal of Chemical Engineering, 24 (2007) 101-118.

[13] R.C. Agrawal, G.P. Pandey, Solid polymer electrolytes: materials designing and all-solid-state battery applications: an overview, J. Phys. D Appl. Phys., 41 (2008) 223001.

[14] L.D. Nghiem, P. Mornane, I.D. Potter, J.M. Perera, R.W. Cattrall, S.D. Kolev, Extraction and transport of metal ions and small organic compounds using polymer inclusion membranes (PIMs), J. Memb. Sci., 281 (2006) 7-41.

[15] K.M. White, B.D. Smith, P.J. Duggan, S.L. Sheahan, E.M. Tyndall, Mechanism of facilitated saccharide transport through plasticized cellulose triacetate membranes, J. Memb. Sci., 194 (2001) 165-175.

[16] T. A. Munro, B. D. Smith, Facilitated transport of amino acids by fixed-site jumping, Chem. Commun., (1997) 2167-2168.

[17] J.A. Riggs, B.D. Smith, Facilitated transport of small carbohydrates through plasticized cellulose triacetate membranes. Evidence for fixed-site jumping transport mechanism, J. Am. Chem. Soc., 119 (1997) 2765-2766.

[18] M.I.G. Almeida, R.W. Cattrall, S.D. Kolev, Polymer inclusion membranes (PIMs) in chemical analysis-A review, Anal. Chim. Acta, 987 (2017) 1-14.

[19] T. A. Munro, B. D. Smith, Facilitated transport of amino acids by fixed-site jumping, Chem. Commun. (Camb.), (1997) 2167-2168.

[20] E.A. Nagul, C. Fontàs, I.D. McKelvie, R.W. Cattrall, S.D. Kolev, The use of a polymer inclusion membrane for separation and preconcentration of orthophosphate in flow analysis, Anal. Chim. Acta., 803 (2013) 82-90.

[21] M. Baczynska, M. Regel-Rosocka, M. Nowicki, M. Wisniewski, Effect of the structure of polymer inclusion membranes on zn(II) transport from chloride aqueous solutions, J. Appl. Polym. Sci., 132 (2015) 1-11.

[22] M. Matsumoto, Y. Murakami, Y. Minamidate, K. Kondo, Separation of lactic acid through polymer inclusion membranes containing ionic liquids, Sep. Sci. Technol., 47 (2012) 354-359.

[23] A. Manzak, Y. Yildiz, O. Tutkun, Characterization of polymer inclusion membrane containing Aliquat 336 as a carrier, The 2014 World CongressBusan, Korea, 2014.

[24] Y. Yıldız, A. Manzak, B. Aydin, O. Tutkun, Preparation and application of polymer inclusion membranes (PIMs) including Alamine 336 for the extraction of metals from an aqueous solution, 2014.

[25] C.E. Wilkes, J. Summers, C. Daniels, PVC Handbook 2005, Google Scholar, (2005).

[26] G. Wypych, Handbook of Plasticizers, ChemTec Publishing2004.

[27] A. Casadellà, O. Schaetzle, K. Loos, Ammonium across a Selective Polymer Inclusion Membrane: Characterization, Transport, and Selectivity, Macromolecular rapid communications, 37 (2016) 858-864.

[28] D. Milanova, R.D. Chambers, S.S. Bahga, J.G. Santiago, Electrophoretic mobility measurements of fluorescent dyes using on-chip capillary electrophoresis, Electrophoresis, 32 (2011) 3286-3294.

[29] D.G. Leaist, The effects of aggregation, counterion binding, and added NaCl on diffusion of aqueous methylene blue, Can. J. Chem., 66 (1988) 2452-2457.

[30] P.-O. Gendron, F. Avaltroni, K. Wilkinson, Diffusion coefficients of several rhodamine derivatives as determined by pulsed field gradient–nuclear magnetic resonance and fluorescence correlation spectroscopy, J. Fluoresc., 18 (2008) 1093.

[31] A. Masuda, K. Ushida, T. Okamoto, New fluorescence correlation spectroscopy enabling direct observation of spatiotemporal dependence of diffusion constants as an evidence of anomalous transport in extracellular matrices, Biophys. J., 88 (2005) 3584-3591.

[32] W.M. Saltzman, M.L. Radomsky, K.J. Whaley, R.A. Cone, Antibody diffusion in human cervical mucus, Biophys. J., 66 (1994) 508.

[33] S.A. Rani, B. Pitts, P.S. Stewart, Rapid diffusion of fluorescent tracers into Staphylococcus epidermidis biofilms visualized by time lapse microscopy, Antimicrobial agents and chemotherapy, 49 (2005) 728-732.

[34] C.T. Culbertson, S.C. Jacobson, J.M. Ramsey, Diffusion coefficient measurements in microfluidic devices, Talanta, 56 (2002) 365-373.

[35] X. Wei, P. Sun, S. Yang, L. Zhao, J. Wu, F. Li, Q. Pu, Microchip electrophoresis with background electrolyte containing polyacrylic acid and high content organic solvent in cyclic olefin copolymer microchips for easily adsorbed dyes, J. Chromatogr. A, 1457 (2016) 144-150.

[36] X. Yang, H. Gao, F. Qian, C. Zhao, X. Liao, Internal standard method for the measurement of doxorubicin and daunorubicin by capillary electrophoresis with in-column double optical-fiber LED-induced fluorescence detection, J. Pharm. Biomed. Anal., 117 (2016) 118-124.

[37] O. Arous, F.S. Saoud, H. Kerdjoudj, Cellulose triacetate properties and their effect on the thin films morphology and performance, IOP Conference Series: Materials Science and Engineering, IOP Publishing, 2010, pp. 012001.

[38] F.B.M. Suah, M. Ahmad, Preparation and characterization of polymer inclusion membrane based optode for determination of Al3+ ion, Anal. Chim. Acta., 951 (2017) 133-139.

[39] V.A. Lapina, T.A. Pavich, P.P. Pershukevich, A.V. Trofimov, N.N. Trofimova, Y.B. Tsaplev, P.P. Zak, Exploring the utility of coumarins-based luminescent spectra converters, Journal of Physical Organic Chemistry, 30 (2017) e3731.

[40] ChemAxon Ltd., https://chemicalize.com/#/.

[41] W. Zhang, L. Jenny, U.E. Spichiger, A comparison of neutral Mg2+-selective ionophores in solvent polymeric membranes: complex stoichiometry and lipophilicity, Anal. Sci., 16 (2000) 11-18.

[42] H.H. See, P.C. Hauser, Electro-driven extraction of low levels of lipophilic organic anions and cations across plasticized cellulose triacetate membranes: Effect of the membrane composition, J. Memb. Sci., 450 (2014) 147-152.

[43] M. Montalbán, M. Collado-González, R. Trigo, F. Díaz Baños, G. Víllora, Experimental measurements of octanol-water partition coefficients of ionic liquids, J. Adv. Chem. Eng, 5 (2015) 1000133.

[44] L. Ropel, L.S. Belvèze, S.N. Aki, M.A. Stadtherr, J.F. Brennecke, Octanol–water partition coefficients of imidazolium-based ionic liquids, Green Chemistry, 7 (2005) 83-90.

[45] A. Salima, K.S. Ounissa, M. Lynda, B. Mohamed, Cationic dye (MB) removal using polymer inclusion membrane (PIMs), Procedia Eng., 33 (2012) 38-46.

[46] L.S. Mansouri, A. Kachbi, O. Kebiche-Senhadji, M. Benamor, Characterization and Stability Of CTA-Based Polymer Inclusion Membranes Using 2-NPOE as Plasticizer and BMIMPF6 as Ionic Liquid, CMA4CH 2012, Mediterraneum MeetingRome, Italy, Europe, 2012.

[47] O. Arous, F.S. Saoud, M. Amara, H. Kerdjoudj, Efficient facilitated transport of lead and cadmium across a plasticized triacetate membrane mediated by D2EHPA and TOPO, Materials Sciences and Applications, 2 (2011) 615.

[48] O. Kebiche-Senhadji, L.S. Mansouri, M. Benamor, Consideration of Polymer Inclusion Membranes Containing D2EHPA for Toxic Metallic Ion (Pb2+) Extraction Recovery, 2015 5th International Conference on Environment Science and Engineering, 2015.

[49] O. Arous, M. Amara, H. Kerdjoudj, Selective transport of metal ions using polymer inclusion membranes containing crown ethers and cryptands, Arabian Journal for Science and Engineering, 35 (2010) 79.

[50] J. Kiefer, J. Fries, A. Leipertz, Experimental vibrational study of imidazolium-based ionic liquids: Raman and infrared spectra of 1-ethyl-3-methylimidazolium bis (trifluoromethylsulfonyl) imide and 1-ethyl-3-methylimidazolium ethylsulfate, Applied spectroscopy, 61 (2007) 1306-1311.

[51] S. Vyas, C. Dreyer, J. Slingsby, D. Bicknase, J.M. Porter, C.M. Maupin, Electronic structure and spectroscopic analysis of 1-ethyl-3-methylimidazolium bis (trifluoromethylsulfonyl) imide ion pair, The Journal of Physical Chemistry A, 118 (2014) 6873-6882.

[52] N.R. Dhumal, K. Noack, J. Kiefer, H.J. Kim, Molecular structure and interactions in the ionic liquid 1-ethyl-3-methylimidazolium bis (trifluoromethylsulfonyl) imide, The Journal of Physical Chemistry A, 118 (2014) 2547-2557.

[53] J.M. Lee, D.Q. Nguyen, S.B. Lee, H. Kim, B.S. Ahn, H. Lee, H.S. Kim, Cellulose triacetate-based polymer gel electrolytes, J. Appl. Polym. Sci., 115 (2010) 32-36.

[54] Z. Xue, L. Qin, J. Jiang, T. Mu, G. Gao, Thermal, electrochemical and radiolytic stabilities of ionic liquids, Physical Chemistry Chemical Physics, 20 (2018) 8382-8402.

[55] C. Schmidt, M. Beck, M. Ahrenberg, C. Schick, O. Keßler, U. Kragl, Room temperature ionic liquids in a heat treatment process for metals, Rsc Adv., 4 (2014) 55077-55081.

[56] O. Kebiche-Senhadji, L. Mansouri, S. Tingry, P. Seta, M. Benamor, Facilitated Cd (II) transport across CTA polymer inclusion membrane using anion (Aliquat 336) and cation (D2EHPA) metal carriers, J. Memb. Sci., 310 (2008) 438-445.

[57] L.M. Anovitz, D.R. Cole, Characterization and analysis of porosity and pore structures, Reviews in Mineralogy and geochemistry, 80 (2015) 61-164.

[58] P. Klobes, R.G. Munro, Porosity and specific surface area measurements for solid materials, 2006.

[59] P. Religa, J. Rajewski, P. Gierycz, Advantages and Disadvantages of SLM and PIM Systems Used for Chromium (III) Separation from Aqueous Solutions, Polish Journal of Environmental Studies, 24 (2015).

Chapter 3

In-Transit electroextraction of small molecule pharmaceuticals from blood

Declaration: Main context and supporting information in this chapter has been published as an original paper in Angewandte Chemie International Edition [1] with the contribution for the published works listed in the statement of co-authorship. Changes including paragraph layouts, figure/table arrangements, numbering, and fonts are modified from original published paper to fit the format of this thesis and to minimize repetition (if any).

In *chapter 2*, a PIM composed of CTA, 2-NPOE and [EMIM][NTf_2] was prepared, optimized, and successfully employed as a "dry" electrophoretic platform for several cationic molecules. To exploit the capability of PIM for personalized medicine and point-of-care diagnostics as expressed in *Chapter 1*, a portable device featuring the PIM and commercial batteries was designed and used to demonstrate the separation of the plant-derived alkaloid, Berberine Chloride (BC), from a drop of blood dried on the PIM while it was being transported in the mail. BC is used in traditional Chinese herbal medicine and as a dietary supplement [2, 3]. It has reported therapeutic use in the treatment of cancer [4, 5], inflammation [6, 7], diabetic [8, 9], Alzheimer's disease [10, 11] and cardiovascular disorders [12, 13]. BC was selected here as a model compound for small molecule pharmaceuticals also due to its native fluorescence eliminating any derivatization step to make it fluorescent.

3.1 Abstract

An electrokinetic platform was developed for extracting small molecule pharmaceuticals from a dried drop of blood. Through the exclusion of liquid reagents and use of low field strength (6 V/cm), the electroextraction of a drug from a dried drop of blood, deposited on a PIM, could be realised while in transit in the mail. *In transit* sample preparation provides a potential solution to *in-situ* sample degradation and may accelerate the workflow upon arrival of a patient sample at the analytical facility. The electroextraction method was enabled through our discovery of the use of 15-20 µm thin PIMs as electrophoretic separation medium in absence of liquid reagents. Here, a PIM consisting of CTA as polymer base, 2-NPOE as plasticizer and

[EMIM][NTf_2] as carrier was used. The PIM was packaged with two 12 V batteries to supply the separation voltage. A blood spot containing BC was deposited and dried before applying the separation potential, allowing for the electroextraction while the packaged device was sent through the mail. Upon arrival in the laboratory, the PIM was scanned using a fluorescence microscope with a photon multiplier tube, quantifying the BC extracted away from the sample matrix. This platform represents a new opportunity for processing clinical samples during transport to the laboratory, saving time and manual handling to accelerate the time to result.

3.2 In-Transit electroextraction of small molecule pharmaceuticals from blood

Personalised medicine, which aims to treat every patient as an individual has been shown to be highly effective with diabetes but expanding the analytical target range is one of the most important challenges of the forthcoming century [14-21]. A holistic approach to personalised medicine requires the ability to detect and quantify a significant and diverse range of pharmaceuticals and their metabolites. The gold standard for point-of-collection testing is the use of immunoassays, however, these frequently suffer from high cross-reactivity given the structural similarity of many pharmaceuticals and their metabolites, hence few have been accepted for drug monitoring [22-24]. Despite recent achievements in Lab on a Chip devices for Point of Care diagnostics [25, 26], significant advances in chemical resolution and sensitivity are required before their widespread use for routine monitoring of pharmaceuticals and their metabolites. As such, the capability to detect and quantify a significant and diverse range of pharmaceuticals and their metabolites can be anticipated to remain with centralised laboratories and the use of high-resolution analytical instrumentation [27] and this requires the blood and/or urine sample to be sent off for analysis. Upon arrival at the laboratory, the sample is processed by wet-chemistry techniques - manual or with automated instrumentation - and analysed by any number of instruments, with the sample preparation typically the most time- and labour-intensive process. The data is then sent back to the managing clinician and/or the patient [28-30]. To mitigate sample

transport risk and hence cost, blood samples can be sent as dried spots, which are considered to be of low biological risk and exempt from classification as UN3373 Biological Substance Category B [31-34], but there are additional complications with quantitative measurement of pharmaceuticals in DBS.

Here, we demonstrate a novel electrophoresis concept, where small molecule pharmaceuticals can be separated away from a dried drop of blood in an environment free of liquid reagents. Owing to the low diffusion in the solid substrate, this electroextraction can be realised at a field strength of only 6 V/cm, supplied by two A23 12V batteries. The set-up, packaged in a box to provide ruggedness during transport, was used for *in-transit* extraction from a complex biological matrix and is illustrated in Figure 3.1.

Liquid samples and reagents are challenging elements of portable analytical instrumentation and point of care diagnostics for reasons including their stability, safety and handling [35-39] and their exclusion would significantly simplify the development of field-deployable instrumentation. The demonstrated transport of lithium ions in solid polymer electrolytes used in rechargeable lithium ion batteries [40, 41] inspired a quest for transport of larger ions in solid materials for analytical purposes. PIMs were selected to study their potential as a dry medium for electrokinetic ion transport. PIMs are non-porous membranes used for extraction, separation, and pre-concentration, and have been used for the removal and analysis of metals and contaminants from environmental sources such as wastewater [42-44].

The PIM used here was cast from an optimized concentration of CTA, 2-NPOE, and [EMIM][NTf_2] as finalised in section 2.4 (*chapter 2*). PIM casting process, PIM dimension and electrophoresis set-up were identical to those described in section 2.2.3 (*chapter 2*). As reported in *chapter 2*, field-induced migration was observed for cationic dyes together with their differences in migration rates allowing separation of cationic dyes and estimation of their diffusion (and dispersion) rates and electrophoretic mobilities in the PIM.

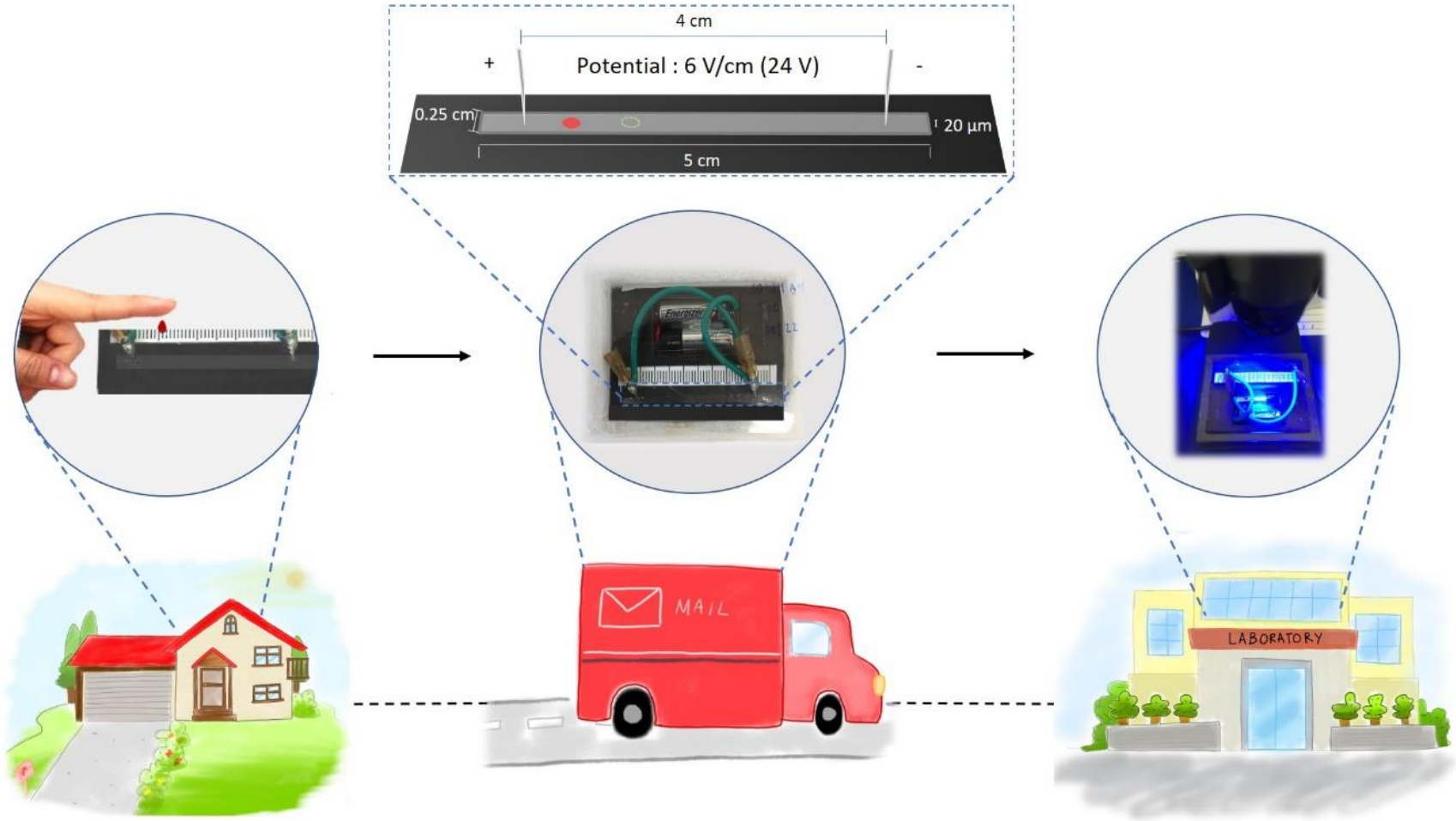

Figure 3.1. Schematic illustration of thin film electrophoresis for in-transit analyte extraction. A blood spot is deposited and dried onto the membrane in a POC setting and connected to two 12 V batteries before being mailed. In transit, the analytes are electrokinetically extracted from matrix components, and can be quantified upon arrival in the laboratory with no additional sample processing.

The importance of extracting small molecule pharmaceuticals from the matrix can be gauged by a recent review of 208 liquid chromatography – mass spectrometry (LC-MS) methods for the analysis of pharmaceuticals in clinical samples. Every method in the review required either solid phase or liquid-liquid extraction before analysis by LC-MS, sample processing that imposes a significant cost in both time and money [45]. To demonstrate the electrokinetic extraction of the BC from a dried drop of blood, fresh blood from a healthy volunteer was spiked with 50 ppm of BC, and 0.1 μL was spotted onto the PIM; drying yielded a spot size of approximately 1.2 mm. A voltage of 2000 V (500 V/cm) was then applied across the PIM containing the dried drop of blood for 60 min. As illustrated in figure 3.2A, white light images demonstrate that the red components of blood matrix remained stationary, whereas the fluorescent images show the electrokinetic transport of BC. Inspection by SEM confirmed the cells from the blood remained located where the blood was deposited on top of the PIM (figure 3.3), while confocal imaging suggested impregnation of the BC into the membrane (figure 3.4). It must also be noted that there were several times the dried drop of blood fell off the PIM strips after 5-10 min of drying, during transport, and while being detached from the platform. However, all strips were subjected to fluorescent detection and included in the dataset reported in this thesis with no significant deviation. This finding confirmed that dried drop of blood was completely dried after 10 min and relatively comparable concentration of free analyte was extracted on each PIM without impacting fluorescence signal.

Experiments with fluorescently derivatised proteins indicate that these also penetrate the PIM. Upon application of the electric field, BC migrated along the PIM while no electromigration of proteins was observed as shown in figure 3.2. This demonstrates the ability to electrokinetically extract BC from matrix components from a dried drop of blood on a PIM. Considering this electroextraction takes place in absence of liquid reagents, this technique provides a promising alternative to solid and liquid based extraction techniques currently essential for nearly every laboratory-based analysis of small molecule metabolites and pharmaceuticals from whole blood.

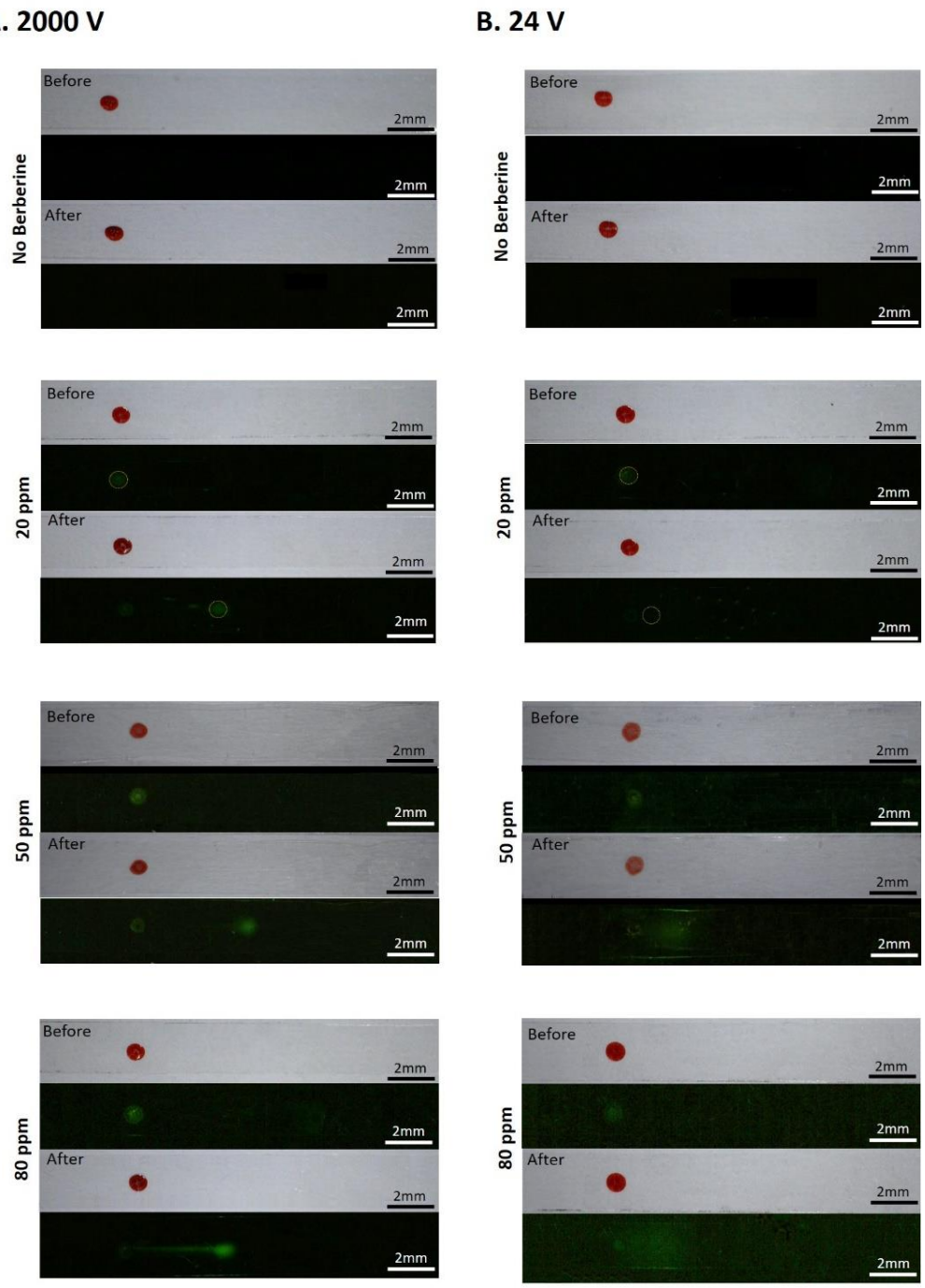

Figure 3.2. PIM electrophoresis for analysis of 0, 20, 50, and 80 ppm of BC from dried drop of blood with A) 2000 V and B) 24 V was applied across the membrane. Images recorded using white light (top) show the position of the dried drop of blood whereas images recorded using blue LED induced fluorescence (bottom) show the position of BC. *Note: dashed yellow circle is used to mark the BC where the fluorescence intensity is very low and cannot be clearly visualized in the image. Conditions: Membrane 0.25 cm x 5 cm; length between electrodes 4 cm. Voltage: (A) 2000 V and (B) 24V. Duration: (A) 60 min and (B) 24 hr. Sample(s): 0, 20, 50, and 80 ppm of BC in whole blood. Sample volume (spot size): 0.1 µL. Drying time (before electrophoresis): 5-10 min.

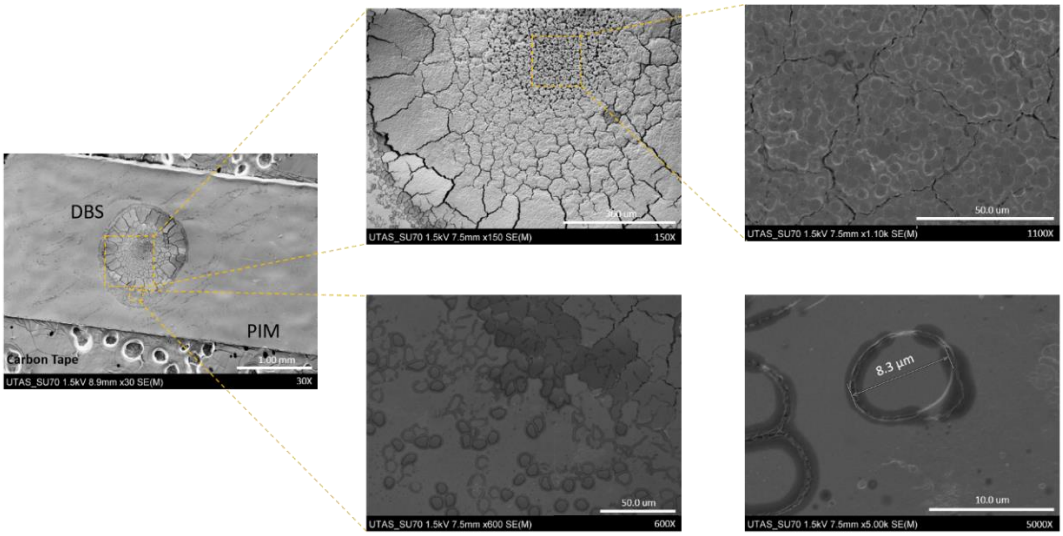

Figure 3.3. SEM image of a dried drop of blood on the PIM after electrophoresis. Each zoomed in image shows blood cells and the bottom right image shows a size blood cell on the PIM surface.

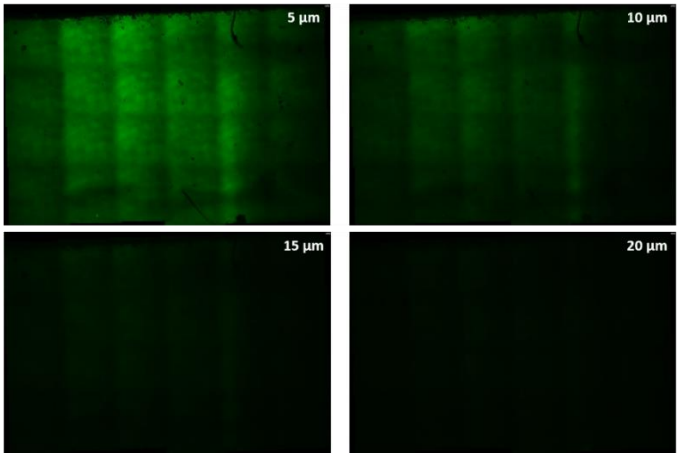

Figure 3.4. Confocal spinning disk images of R6G where each image represents the depth (Z-plane) of the PIM at 5, 10, 15 and 20 µm from the top surface.

The PIM-based electrokinetic platform has eliminated the need for liquid reagents, thereby simplifying the analytical process, but the use of 2000 V to drive the electrophoretic separations, however, limits the safety and hence usability of the instrumentation. Since both diffusion and electrokinetic transport in the PIM are 100 times lower than in aqueous media, the separation force can theoretically be decreased by the same order of magnitude. Using diffusion constants, dispersion estimates and mobilities obtained at 2000 V, the position and theoretical spot size was estimated for voltages ranging from 9-24 V applied across the 4 cm PIM. Figure 3.5

shows that a voltage above 18 V would be required to extract BC from the matrix spot within 24 hr. Experimental data using a potential difference of 24 V supplied using two 12 V batteries (A23) confirmed 6 V/cm was indeed sufficient to separate BC away from the matrix, as illustrated in Figure 3.2B. This represents the lowest electric field strength reported for electrophoretic separations in the published literature –lower than the field strength of 43 V/cm achieved using a 9 V battery over 2 mm for the polyacrylamide gel electrophoresis separations of proteins [46].

The battery-powered set-up shown in Figure 3.1 was used for extraction in the mail. A 0.1 µL drop of freshly drawn whole blood spiked with 60 ppm BC was deposited onto the PIM and allowed to dry for 5 min. Dried blood spots are known for their ease in handing and transportation because the components remain stable and the infectious risks are low [31, 32]. The PIM was pinned in place using syringe needles and connected to the batteries before placing the packaged device in an envelope. Recognising international restrictions on mailing dry cell batteries (IATA, Special Provision A123), the universities internal mail was used to send the PIM-based electrokinetic platform to another campus and back. In the laboratory, standards containing 0-100 ppm BC were separated as control, also using two batteries to supply 24 V. Based on the low current during separation, the two 12 V batteries are calculated to last for approximately 633 years of continuous use, not affecting the device's usable lifetime. The mailed device returned to the laboratory 34 hrs later and after unpackaging, fluorescence intensity of the spots (Figure 3.2) was determined using a confocal fluorescent microscope equipped with a PMT (Figure 3.6A). The mailed and control membranes were analysed three times by manually passing them through the focused light source on a confocal microscope, recording the fluorescence intensity with a PMT. Data from three passes through the membrane approximately 0.1 mm apart were averaged to reduce the impact of wrinkles, dust and small debris. Using the calibration curve constructed using standards (figure 3.6B), the concentration of BC in the blood spot was calculated to be 57.8 ± 4.5 ppm, which is well within acceptable measurement error and confirms quantitative extraction of BC from the blood spot. The migration distance and spot dispersion also found to be within the

range predicted in figure 3.5 at 34 hr suggesting good correlation between experimental result and theoretical calculation.

Considering the reported values of BC in blood and plasma are typically 10,000 times lower than the limit of detection (LOD) of 10 ppm, the presented set-up using fluorescence detection does not provide the sensitivity required for clinical analysis. It does, however, demonstrate a novel approach to sample treatment for the extraction of small molecules from biological fluids. The simple set-up combined with low safety risks using dried drops of blood and low voltage allow for the extraction of the target analytes in the mail, effectively using the transit time required to send a remotely collected sample to a central laboratory thereby reducing manual processing upon receipt. Delays in transportation to the laboratory would not compromise the resolution of the separation but would influence the sensitivity given the additional dispersion that would occur while the molecules are being separated.

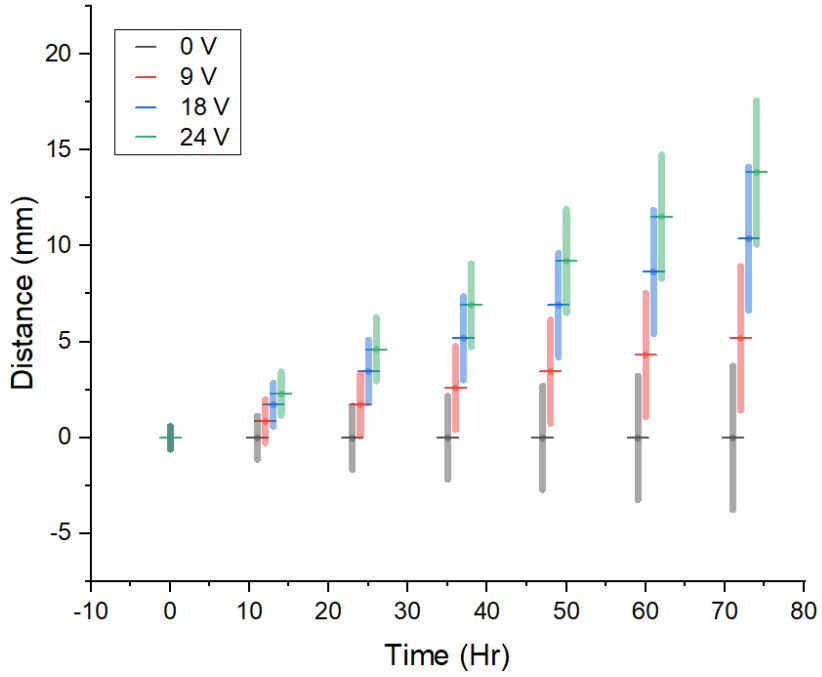

Figure 3.5. Migrated distance (horizontal marker) and dispersion (bar) of BC in the PIM at 0, 9, 18 and 24 V. The distance BC electromigrated was calculated from its electrophoretic mobility and the electric field strength, while the width of the spot was estimated from the diffusion constant in the PIM, the time, and then multiplied by 1.15 to account for dispersion through the PIM.

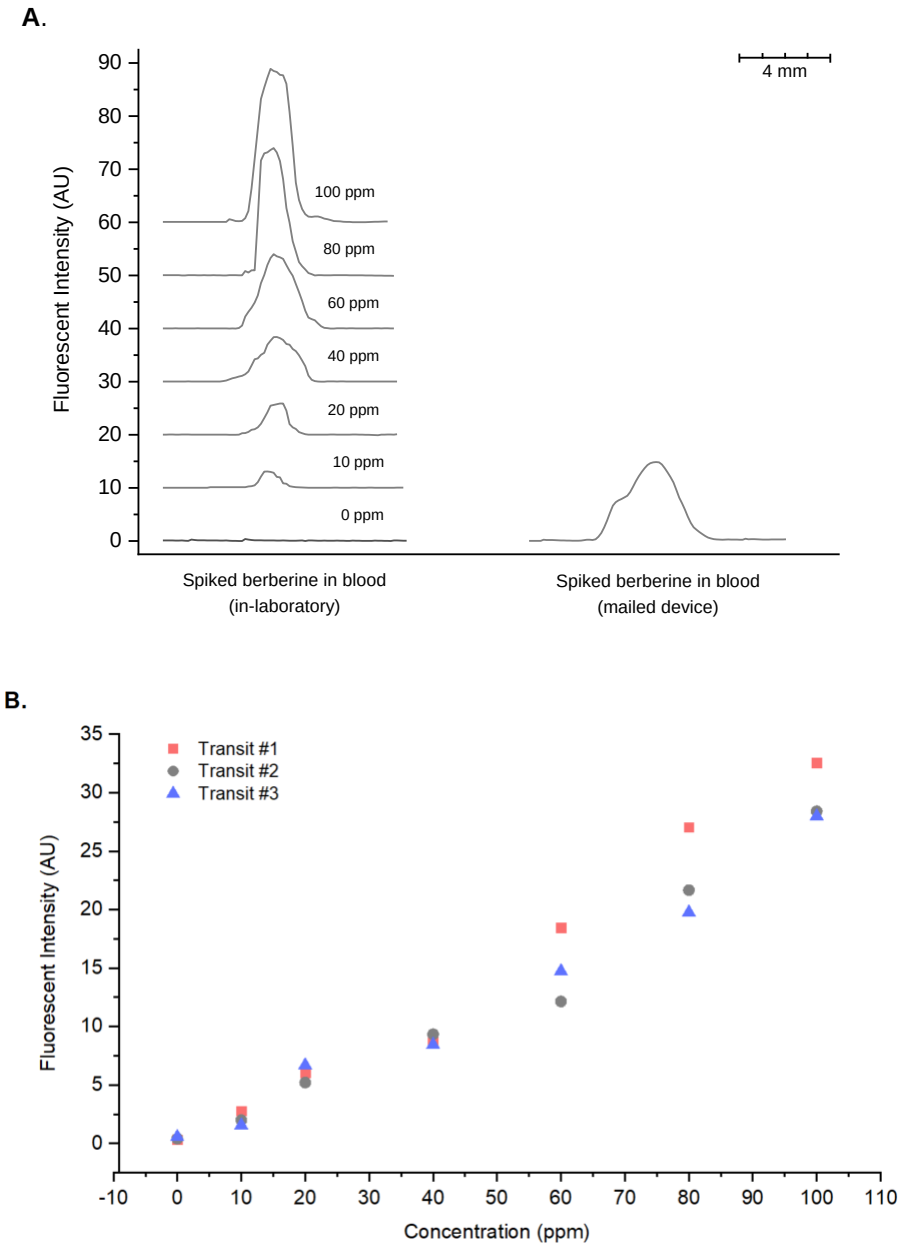

Figure 3.6. Fluorescent signal of BC in standards and dried drop of blood. A) Fluorescence intensity along the PIM following a 34-hr electrophoretic separation of spiked BC from a dried drop of blood. The dried drop of blood for the mailed sample (right column) contained 60 ppm BC while that on the left column were separated at 24 V in the laboratory containing 10, 20, 40, 60, 80 and 100 ppm BC. This trace was constructed by moving the PIM through a confocal microscope system equipped with a PMT to obtain quantitative fluorescent data. B) Calibration curve constructed using the fluorescence intensity from each scan. Conditions: Membrane 0.25 cm x 5 cm; length between electrodes 4 cm. Voltage: 24 V (Batteries). Duration: 34 hr. Sample(s): (A) 60 ppm of BC in blood and (B) 0-100 ppm BC standards in blood. Sample volume (spot size): 0.1 uL. Drying time (before electrophoresis): 5-10 min. Repetition: (A) 4, and (B) 3.

In summary, a new electrokinetic platform has been developed for the extraction of small molecules from matrix components in a dried drop of blood while in transit. The electrokinetic extraction is conducted in a thin membrane in absence of liquid reagents, with low diffusion rates allowing the separation to be powered by two A23 12 V batteries. Combined with the established safety of transporting dried drop of blood, this unique and novel approach is anticipated to improve efficiency in clinical analysis, using the time required to transport clinical samples from the point of collection to a centralised laboratory for extracting the target analytes from matrix interferences in a simple low-cost manner. With PIM platform being non-porous media restricting dried drop of blood absorption, our approach differs from that of typical DBS collection card where the sample extraction was performed during the transit and ready for detection upon arrival; hence, completely eliminate time-consuming sample preparation steps involved.

In a practical point of view, more than three strips might be required as a calibration within a device to improve liability of the quantitative test readouts. Furthermore, the longest transit time predicted for portable electrokinetic platform in this thesis corresponding analyte migration distance and dispersion was at 72 hr as shown in figure 3.5. However, actual transit time may delay from days to weeks and electromigration of analyte could exceed that predicted. To prevent this issue, improvement of the portable platform could include incorporation of single use, short-life battery or pre-set timer so that the voltage could be deactivated and stop the migration of the analyte. Another issue the system could encounter from this integration would then be the significance of dispersion impacting the sensitivity in detection as mentioned previously. Hence, future combination with advanced chemical imaging instrumentation, such as MALDI imaging MS, may create a simple and powerful workflow for the analysis of clinical samples, freeing up capacity to realise the throughput required to realise a more personalised approach in medicine. A more advanced alternative could also include the step of simultaneous pre-concentration of analyte after electrophoresis, i.e. ITP, and this could allow a lower LOD resulting for portable PIM resulting in a closer step towards practical clinical analysis.

3.3 Experimental materials and methods and supporting information

3.3.1 PIM preparation

PIM preparation process for this chapter is illustrated in figure 2.1 and is identical to that described in section 2.2.2 (*chapter 2*).

3.3.2 Components and set-up of electrophoresis platform

The electrokinetic separation platform is illustrated in figure 2.2 (*chapter 2*). Electrophoretic procedures for this chapter are identical to those described in section 2.2.4 (*chapter 2*).

3.3.3 Electrophoresis procedures and chemicals

All laboratory-based electrophoresis experiments were performed according to the following procedures. Sample solution in DI (0.5 µL for all fluorescent dyes and 0.1 µL for BC and blood samples) was spotted using an auto-pipette (0.5 µL) or syringe (0.1µL) close to the anode (left side of the strip in this case) and left to dry for approximately 5-10 min. Only after the spot was completely dried, the electrodes were connected, and voltage was applied. At least three replicates on separate strips were conducted in parallel for each experiment. The potential difference was maintained for 60 min when 2000 V was applied (500 V/cm) and for at least 24 hr when 24 V (6 V/cm) was applied. Chemicals used in each experiment are listed below.

3.3.3.1 Migration studies of different charge dyes.

Coumarin 334 (Sigma-Aldrich, 99%, 283.32 g/mol), Fluorescein sodium salt (Sigma-Aldrich, fluorescent tracer, 376.27 g/mol), and R6G (Sigma-Aldrich, 95%, 479.01 g/mol) were used as neutral, anionic, and cationic species respectively, to determine the electrokinetic transport of different charged molecules on PIM. Stock solutions of each dye at 1000 ppm in DI were diluted to 10 ppm with DI for all experiments.

3.3.3.2 Electrophoretic separation of three cationic dyes.

Stock solutions 1000 ppm of R6G and RB (BDH, 479.02 g/mol) in DI, and R123 in ethanol (Sigma-Aldrich, mitochondrial specific fluorescent dye, 380.82 g/mol) were diluted to 10 ppm for R6G and RB and 1 ppm for R123, all with DI. These were prepared as individual samples as well as a mixture of the three fluorescent dyes.

3.3.3.3 Migration of BC and its separation from blood matrix.

Three stock solutions of BC (Sigma-Aldrich, 371.81 g/mol) were made in DI; a 1000 ppm stock solution was made for the pure drug experiment, a 6000 ppm stock solution was made to spike the blood sample and a 10000 ppm stock solution was made to construct the calibration curves for BC in blood. Stock solution of 1000 ppm was diluted to 50 ppm before performing electrophoresis. 1% of 6000 ppm stock was added and mixed into fresh blood, yielding a final concentration of 60 ppm of BC in blood. For calibration of BC from blood, 10000 ppm stock solution was further diluted to 8000, 6000, 4000, 2000, and 1000 ppm with DI and 1% of each concentration was added into fresh blood yielding final concentrations of 100, 80, 60, 40, 20, and 10 ppm of BC in blood.

3.3.4 Optimization of PIM composition

R6G was chosen as model analyte to investigate the PIM optimization. Migration was studied using PIMs using varying composition of CTA, 2-NPOE, and [EMIM][NTf_2] as indicated in Table 2.2 (*chapter 2*) under applied electric field. The optimum performance was assessed based on migration distance, spot size and spot shape, with the optimal PIM made with 0.075 g CTA, 0.1 g 2-NPOE and 0.05 g [EMIM][NTf_2]. No migration was observed in absence of the plasticizer 2-NPOE, and in absence of [EMIM][NTf_2] migration was observed but with severely distorted the spot. Increasing the amount of CTA deteriorated the migration of R6G assuming the thickness of the film increased and became very stiff. Increasing the amount of [EMIM][NTf_2] also limited the migration of R6G but made the PIM softer with more visible wrinkles and leftover traces of liquid

droplets on the surface on the PIM after overnight casting. Increasing the amount of 2-NPOE showed improvement on migration of R6G; however, 0.10 g was chosen as an efficient amount to support the migration of R6G.

3.3.5 Migration of different charge fluorescent dyes and separation of cationic fluorescent dyes

Fluorescein, Coumarin 334, and R6G, were used as anionic, neutral, and cationic analytes to determine PIM selectivity. Figure 2.3 (*chapter 2*) shows only electrophoretic transport of the cationic R6G and no migration of anionic Fluorescein and neutral Coumarin 334 suggesting the PIM being specific to cations. Additional cationic fluorescent dyes including R6G, RB, and R123 were investigated, with Figure 2.5A (*chapter 2*), showing differential migration of these dyes allowing successful separation on PIM.

3.3.6 Blood sample handing

Research using blood was performed under the ethic approval (H0016575) approved by The Tasmanian Health and Medical Human Research Ethics Committee. All blood samples were handled under Biosafety Level-2 hood in PC-2 facility until the blood spot was completely dry before being taken out of the facility. Blood was taken from a healthy volunteer using a single-use lancet from commercial lancing device (Accu-Chek® FastClix). Excess blood after depositing the sample on the PIM, contaminated tubes, pipette tips, and all materials in contact with blood was immediately disinfected using 10% bleach solution overnight and discarded in biohazard bin.

3.3.7 Portable platform: electrokinetic procedures, and detection

The portable device to send the PIM through the mail was designed using DraftSight™ Professional software made by laser cutting the several PMMA plastic pieces using Laser Engraver (Hobby laser engraver, MLE-40) and assembled using glue and tape (Figure 3.7). A soldered wire connected the batteries (A23) with the needles, which were used to pin the PIM in a block of Styrofoam covered with black paper to facilitate detection. The batteries and ruler were fitted into

the allocated spaces. The mail package included two portable devices, “device 1” containing the single concentration of spiked BC (60 ppm) in blood sample and “device 2” containing replicates of the same concentration of BC in blood for control. The devices were placed in bubble wrap-padded postal envelope and was sent through internal university mail. A benchtop control was also conducted in parallel, using an identical set-up on the bench, started and stopped at the same times as the mailed devices. The duration of the electrophoretic separation was determined by the mail schedule on each transit and as such not controlled. Upon arrival of the package by return mail, the strips were detached from their separation platform and placed on a glass slide, attached with tape at both ends of the strips before fluorescence detection using a fluorescence microscope (Nikon Eclipse Ti) with photomultiplier tube (PMT, Hamamatsu Photonics KK, Hamamatsu, Japan). A mercury light source and blue light filter ($\lambda_{Ex/Em}$ 488/525 nm) were used for excitation/emission, and the microscopes stage was operated manually to scan all the strips at the magnification power of 10X. Each strip was scanned three times along the migration direction. Data acquisition was performed using an Agilent interface (35900E) and the calibration curve was plotted from the average values of maximum height of the peaks.

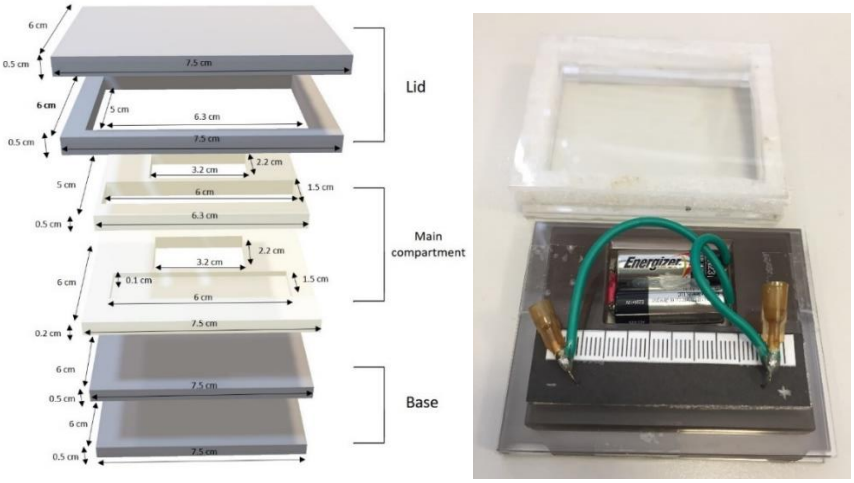

Figure 3.7. 3D design and dimensions of the through-mail portable device. The 3D layers were designed to fit actual batteries and true-to-size Styrofoam base for PIM pinning (left). Identical size of soft foam was attached to the lid in actual device to allow more space for the wire cords from the battery and expect to help reduce the collision during transportation.

3.3.8 Scanning Electron Microscope (SEM) characterization of blood spot on PIM

SEM images of blood spot on PIM were performed with a Hitachi SU-70 field emission analytical scanning electron microscope (FESEM) instrument with 1.5 kV operating voltage. The dried drop of blood on PIM section was sputtered with Platinum prior to imaging. As shown in figure 3.2, electrophoretic migration of dried drop of blood was not observed. This was assumed to be due to the large size of blood cells restricting their extraction into the PIM. The images in Figure 3.3 of a dried drop (0.1 µL) of blood on the PIM confirm the accumulation of cells on the surface of the PIM, suggesting that only small molecules like BC can be extracted into PIM matrix before migration. The measured cell size of 8.3 µm correlates well with average size of human red blood cells [47-49].

3.3.9 Spinning disk confocal microscope for depth analysis of PIM

The Z-plane images of R6G after electrophoretic migration (2000 V, 60 min) on PIM strip were captured using an UltraVIEW Vox upright spinning disk confocal microscope equipped with running Velocity Software (PerkinElmer Australia Pty Ltd, VIC Australia) and a Plan Apo 20×/0.345 air objective (Nikon, New York USA). Four slices of image of R6G spot after field-induced separation at 2000 V for 60 min were collected corresponding to 5, 10, 15, and 20 µm from the top of PIM (figure 3.4). Intensity of R6G can be observed intensely at the depth of 5 and 10 µm suggesting that the dye penetrated into the PIM.

3.3.10 Electrophoretic mobility and diffusion coefficient of cationic dyes

As shown in Figure 2.5A (*chapter 2*), three cationic dyes could be separated and the apparent electrophoretic mobility for R6G, RB, and R123 in the PIM were calculated to be 8.9 $x10^{-11}$, 4.4 $x10^{-11}$ and 0.56 $x10^{-11}$ m^2/Vs, respectively with an applied voltage of 2000 V. The mobility of fastest analyte, of R6G was approximately 160 times lower in the PIM than then value reported in aqueous media (14.0 $x10^{-9}$ m^2/Vs) [50].

Based on the reduced electrophoretic mobility, the diffusion rates were calculated the diffusion rates of R6G, RB, and R123 are calculated to be 9.17 $x10^{-12}$ m^2/s, 9.39 $x10^{-12}$ m^2/s and 2.88 $x10^{-12}$ m^2/s respectively. The diffusion rate of BC was found to be 3.47 $x10^{-11}$ m^2/s. The electrophoretic mobility of BC in the PIM was calculated to be 3.88 x 10^{-11} m^2/Vs from the distance the spot moved in 60 min with an applied voltage of 2000 V. Electrophoresis of BC was also investigated in laboratory at 9, 18, and 24 V up to 24 hr. Migration distance and width of the spot at these voltages were collected. The diffusion constant and electrophoretic mobility were then calculated and used to predict the position and width of the spot for longer transit time from 12-72 hr at voltages from 9 – 24 V. Figure 3.5 shows that a voltage higher than 18 V would be needed to resolve the BC spot from the blood matrix spot. A voltage of 24 V was used experimentally by coupling two 12 V batteries.

3.4 References

[1] P. Nanthasurasak, H.H. See, M. Zhang, R.M. Guijt, M.C. Breadmore, In-Transit Electroextraction of Small-Molecule Pharmaceuticals from Blood, Angewandte Chemie International Edition, 58 (2019) 3790-3794.

[2] Y. Jin, D.B. Khadka, W.-J. Cho, Pharmacological effects of berberine and its derivatives: a patent update, Expert Opin. Ther. Pat., 26 (2016) 229-243.

[3] F. Gao, Y. Hu, G. Fang, G. Yang, Z. Xu, L. Dou, Z. Chen, G. Fan, Recent developments in the field of the determination of constituents of TCMs in body fluids of animals and human, J. Pharm. Biomed. Anal., 87 (2014) 241-260.

[4] P.-L. Peng, Y.-S. Hsieh, C.-J. Wang, J.-L. Hsu, F.-P. Chou, Inhibitory effect of berberine on the invasion of human lung cancer cells via decreased productions of urokinase-plasminogen activator and matrix metalloproteinase-2, Toxicol. Appl. Pharmacol., 214 (2006) 8-15.

[5] W. Tan, Y. Li, M. Chen, Y. Wang, Berberine hydrochloride: anticancer activity and nanoparticulate delivery system, Int. J. Nanomedicine, 6 (2011) 1773-1777.

[6] K. Lin, S. Liu, Y. Shen, Q. Li, Berberine Attenuates Cigarette Smoke-Induced Acute Lung Inflammation, Inflammation, 36 (2013) 1079-1086.

[7] P.N. Brown, M.C. Roman, Determination of hydrastine and berberine in goldenseal raw materials, extracts, and dietary supplements by high-performance liquid chromatography with UV: Collaborative study, J. AOAC. Int., 91 (2008) 694-701.

[8] J. Yin, J. Ye, W. Jia, Effects and mechanisms of berberine in diabetes treatment, Acta. Pharmacol. Sin. B, 2 (2012) 327-334.

[9] W. Xie, Y. Zhao, Y. Zhang, Traditional chinese medicines in treatment of patients with type 2 diabetes mellitus, Evid. Based Complement. Alternat. Med., 2011 (2011).

[10] M. Asai, N. Iwata, A. Yoshikawa, Y. Aizaki, S. Ishiura, T.C. Saido, K. Maruyama, Berberine alters the processing of Alzheimer's amyloid precursor protein to decrease Aβ secretion, Biochem. Biophys. Res. Commun., 352 (2007) 498-502.

[11] H.-F. Ji, L. Shen, Berberine: A Potential Multipotent Natural Product to Combat Alzheimer's Disease, Molecules, 16 (2011) 6732.

[12] F. Affuso, V. Mercurio, V. Fazio, S. Fazio, Cardiovascular and metabolic effects of Berberine, World J. Cardiol., 2 (2010) 71.

[13] X. Zeng, X. Zeng, Relationship between the clinical effects of berberine on severe congestive heart failure and its concentration in plasma studied by HPLC, Biomedical Chromatography, 13 (1999) 442-444.

[14] N. Malandrino, R.J. Smith, Personalized Medicine in Diabetes, Clin. Chem., 57 (2011) 231.

[15] N.J. Schork, Personalized medicine: time for one-person trials, Nature, 520 (2015) 609-611.

[16] K. Susztak, E.P. Böttinger, Diabetic nephropathy: a frontier for personalized medicine, J. Am. Soc. Nephrol., 17 (2006) 361-367.

[17] I.S. Chan, G.S. Ginsburg, Personalized medicine: progress and promise, Annual Review of Genomics and Human Genetics, 12 (2011) 217-244.

[18] D.C. Klonoff, Personalized medicine for diabetes, J. Diabetes Sci.Technol., 2 (2008) 335-341.

[19] M. Swan, Emerging patient-driven health care models: an examination of health social networks, consumer personalized medicine and quantified self-tracking, Int. J. Environ. Res. Public Health, 6 (2009) 492-525.

[20] P.C. Ng, S.S. Murray, S. Levy, J.C. Venter, An agenda for personalized medicine, Nature, 461 (2009) 724-726.

[21] J.K. Nicholson, Global systems biology, personalized medicine and molecular epidemiology, Mol. Syst. Biol., 2 (2006) 52.

[22] D. Żochowska, I. Bartłomiejczyk, A. Kamińska, G. Senatorski, L. Pączek, High-performance liquid chromatography versus immunoassay for the measurement of sirolimus: comparison of two methods, Transplantation proceedings, Elsevier, 2006, pp. 78-80.

[23] I. Gomila, L. Quesada, V. López-Corominas, J. Fernández, M.Á. Servera, L. Sahuquillo, M. Dastis, A. Torrents, B. Barceló, Cross-Reactivity of Chloroquine and Hydroxychloroquine With DRI Amphetamine Immunoassay, Therapeutic drug monitoring, 39 (2017) 192-196.

[24] A. Saitman, H.-D. Park, R.L. Fitzgerald, False-positive interferences of common urine drug screen immunoassays: a review, Journal of analytical toxicology, 38 (2014) 387-396.

[25] M. Zarei, Portable biosensing devices for point-of-care diagnostics: Recent developments and applications, TrAC Trends Anal. Chem., 91 (2017) 26-41.

[26] S. Nayak, N.R. Blumenfeld, T. Laksanasopin, S.K. Sia, Point-of-Care Diagnostics: Recent Developments in a Connected Age, Anal. Chem., 89 (2017) 102-123.

[27] T.G. Cross, M.P. Hornshaw, Can LC and LC-MS ever replace immunoassays?, Journal of Applied Bioanalysis, 2 (2016) 936.

[28] L.J. Stoot, N.A. Cairns, F. Cull, J.J. Taylor, J.D. Jeffrey, F. Morin, J.W. Mandelman, T.D. Clark, S.J. Cooke, Use of portable blood physiology point-of-care devices for basic and applied research on vertebrates: a review, Conserv. Physiol., 2 (2014) 1-21.

[29] W. Li, F.L. Tse, Dried blood spot sampling in combination with LC-MS/MS for quantitative analysis of small molecules, Biomedical Chromatography, 24 (2010) 49-65.

[30] P. St-Louis, Status of point-of-care testing: promise, realities, and possibilities, Clinical biochemistry, 33 (2000) 427-440.

[31] T.W. McDade, S. Williams, J.J. Snodgrass, What a drop can do: dried blood spots as a minimally invasive method for integrating biomarkers into population-based research, Demography, 44 (2007) 899-925.

[32] P.A. Demirev, Dried blood spots: analysis and applications, Anal. Chem., 85 (2012) 779-789.

[33] W. Li, F.L.S. Tse, Dried blood spot sampling in combination with LC-MS/MS for quantitative analysis of small molecules, Biomedical Chromatography, 24 (2010) 49-65.

[34] A. Sharma, S. Jaiswal, M. Shukla, J. Lal, Dried blood spots: concepts, present status, and future perspectives in bioanalysis, Drug testing and analysis, 6 (2014) 399-414.

[35] R.J. Biggar, W. Miley, P. Miotti, T.E. Taha, A. Butcher, J. Spadoro, D. Waters, Blood Collection on Filter Paper: A Practical Approach to Sample Collection for Studies of Perinatal HIV Transmission, JAIDS Journal of Acquired Immune Deficiency Syndromes, 14 (1997) 368-373.

[36] A.J. Tüdős, G.A. Besselink, R.B. Schasfoort, Trends in miniaturized total analysis systems for point-of-care testing in clinical chemistry, Lab Chip, 1 (2001) 83-95.

[37] R. Sista, Z. Hua, P. Thwar, A. Sudarsan, V. Srinivasan, A. Eckhardt, M. Pollack, V. Pamula, Development of a digital microfluidic platform for point of care testing, Lab Chip, 8 (2008) 2091-2104.

[38] G.J. Kost, S.S. Ehrmeyer, B. Chernow, J.W. Winkelman, G.P. Zaloga, R.P. Dellinger, T. Shirey, The Laboratory-Clinical Interface, CHEST, 115 (1999) 1140-1154.

[39] P. Yager, G.J. Domingo, J. Gerdes, Point-of-care diagnostics for global health, Annual review of biomedical engineering, 10 (2008).

[40] J.B. Goodenough, K.S. Park, The Li-ion rechargeable battery: A perspective, J. Am. Chem. Soc., 135 (2013) 1167-1176.

[41] W.H. Meyer, Polymer electrolytes for lithium-ion batteries, Adv. Mater., 10 (1998) 439-448.

[42] M.I.G.S. Almeida, R.W. Cattrall, S.D. Kolev, Polymer inclusion membranes (PIMs) in chemical analysis-A review, Anal. Chim. Acta., 987 (2017) 1-14.

[43] A. Garcia-Rodríguez, V. Matamoros, S.D. Kolev, C. Fontàs, Development of a polymer inclusion membrane (PIM) for the preconcentration of antibiotics in environmental water samples, J. Memb. Sci., 492 (2015) 32-39.

[44] H.H. See, P.C. Hauser, Electric field-driven extraction of lipophilic anions across a carrier-mediated polymer inclusion membrane, Anal. Chem., 83 (2011) 7507-7513.

[45] J.E. Adaway, B.G. Keevil, Therapeutic drug monitoring and LC–MS/MS, J. Chromatogr. B, 883-884 (2012) 33-49.

[46] T.A. Duncombe, A.E. Herr, Use of Polyacrylamide Gel Moving Boundary Electrophoresis to Enable Low-Power Protein Analysis in a Compact Microdevice, Anal. Chem., 84 (2012) 8740-8747.

[47] G. Benga, D. Porutiu, I. Ghiran, P. Kuchel, C. Gallagher, G. Cox, Scanning electron microscopy of red blood cells from eleven species of marsupial, Comp. Haematol. Int., 2 (1992) 227-230.

[48] A. Hyono, T. Yonezawa, K. Kawai, S. Abe, M. Fujihara, H. Azuma, S. Wakamoto, SEM observation of the live morphology of human red blood cells under high vacuum conditions using a novel RTIL, Surf. Interface Anal., 46 (2014) 425-428.

[49] P. Canham, A.C. Burton, Distribution of size and shape in populations of normal human red cells, Circ. Res., 22 (1968) 405-422.

[50] D. Milanova, R.D. Chambers, S.S. Bahga, J.G. Santiago, Electrophoretic mobility measurements of fluorescent dyes using on-chip capillary electrophoresis, Electrophoresis, 32 (2011) 3286-3294.

Chapter 4

Aliquat®336 and common surfactants as selective carriers in Polymer Inclusion Membrane (PIM) for anionic analytes

4.1 Introduction and objectives

As selectivity of the PIM is mainly influenced and tuned by the nature of the carrier (also called extractants and ionophores), a large variety of carriers and ionic liquids have been studied and employed by many researchers specific for particular applications [1-9]. The prepared PIM used in *chapter 2 and 3* involved the use of ionic liquid ([EMIM][NTf_2]) as the carrier which was found to be cation-selective and the extraction of anions was not observed. Based on the published literatures investigated for extraction of anions, Aliquat®336 (trioctylmethyl ammonium chloride) was among the most popular ionic liquids used as anion exchangers [10-22], was selected to be investigated to see whether it could be used to create a solvent-less PIM for anions. As the structure of Aliquat®336 -polar core with long chain non-polar branches (figure 4.1) – is similar to typical surfactants, these were also investigated. Another ionic liquid usually employed in extraction of heavy metals is a commercially available phosphonium-based CYPHOS® IL [16, 23-26], and was also investigated.

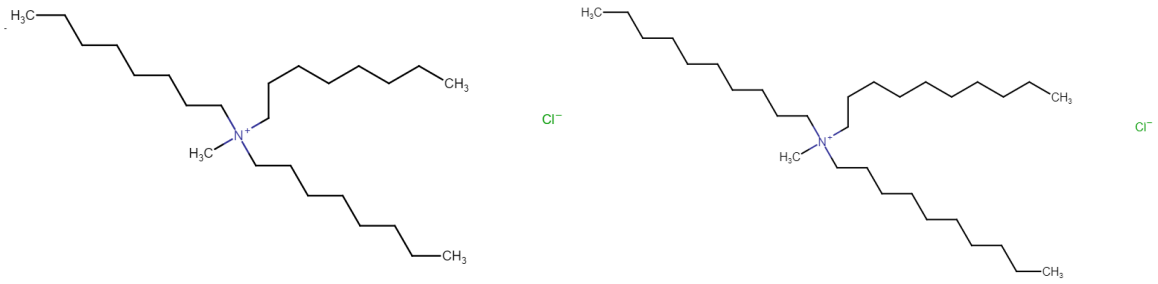

Figure 4.1. Structure of Aliquat®336 commonly consisting of mixture between trioctylmethyl ammonium chloride (C_8, left) and tridecylmethyl ammonium chloride (C_{10}, right) in the ratio of 2:1 [27].

4.2 Experimental chemicals, equipment, and methods

4.2.1 Chemicals and equipment

The ionic liquids, surfactants, and dyes introduced in this chapter are presented in table 4.1 while chemicals for PIM is listed in table 2.1 (*chapter 2*). Equipment for electrophoresis experiment was described in section 2.2.1 (*chapter 2*).

4.2.2 PIM preparation

PIM preparation and casting process is identical to that described in section 2.2.2 (*chapter 2)* with few modifications where PIM was made by weighing 0.075 g of CTA, 0.10 g of 2-NPOE, and 0.05g or 0.10 g of carrier or surfactant into a vial and dissolved in 8 mL of DCM.

4.2.3 Set-up of electrophoresis platform and electrophoresis procedure

The electrokinetic separation platform is illustrated in figure 2.2 (*chapter 2*). Electrophoretic procedures for this chapter are identical to those described in section 2.2.4 (*chapter 2*).

4.3 Electromigration study of different charged dyes with PIM containing Aliquat®336 as a carrier

Similar to *chapter 2*, initial investigation was to determine whether the electromigration of specific charged dyes can be observed on the prepared PIM. Coumarin 334 (500 ppm), Fluorescein sodium salt (1000 ppm), and R6G (10 ppm) were used as neutral, negatively charged and positively charged dyes, respectively, and the result of these dyes on the PIM strips (thickness approximately 24-29 µm) containing 0.10 g of Aliquat®336 is shown in figure 4.2. As anticipated, electromigration of Fluorescein was observed while R6G showed no migration. Migration of Coumarin 334, together with a loss of intensity, was also observed, possibly due to Coumarin 334 forming a conjugate with chloride (Cl^-) counter-anion of Aliquat®336 resulting in Coumarin bearing a potential negative charge.

Table 4.1. List of PIM constituents, dyes, and surfactants used in chapter 4

Chemicals/Dyes	CAS#	Formula	Structure	MW (g/mol)	Grade/Purity	Supplier
5(6)-Carboxynaphthofluorescein (CNF)	128724-35-6	C29H16O7	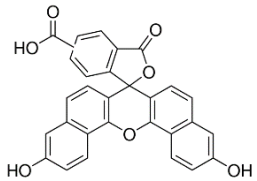	476.43	≥90% (HPLC)	Sigma-Aldrich
Aliquat®336 (Trioctyl methyl ammonium chloride)	63393-96-4	C25H54ClN	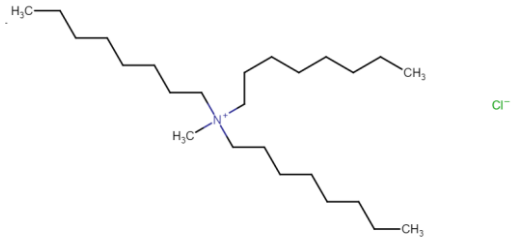	404.16	88.2-93%	Sigma-Aldrich
Bisoctyl Dimethyl Ammonium Chloride (BDAC)	5538-94-3	$C_{18}H_{40}ClN$	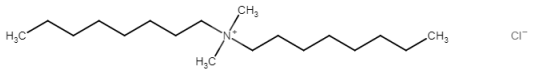	305.97	80-82%	Toronto Research Chemicals
Butyl trimethyl ammonium bromide (BTAB)	2650-51-3	C7H18BrN	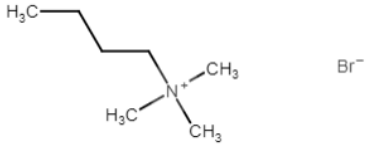	196.13	>97%	TCI Chemicals

Chemicals/Dyes	CAS#	Formula	Structure	MW (g/mol)	Grade/Purity	Supplier
Butyl trimethyl ammonium chloride (BTAC)	14251-72-0	$C_7H_{18}ClN$	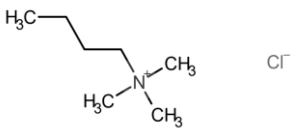	151.68	98%	Combi Blocks (Aksci)
Cetyltrimethylammonium bromide (CTAB)	57-09-0	C19H42BrN	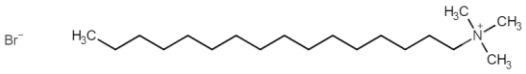	364.45	≥99%	Sigma-Aldrich
Coumarin 334	55804-67-6	C17H17NO3	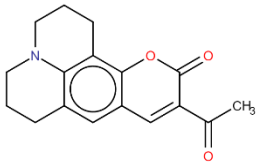	283.32	99%	Sigma-Aldrich
CYPHOS® IL 104 (Trihexyl(tetradecyl)phosphonium bis(2,4,4-trimethylpentyl)phosphinate)	465527-59-7	C48H102O2P2	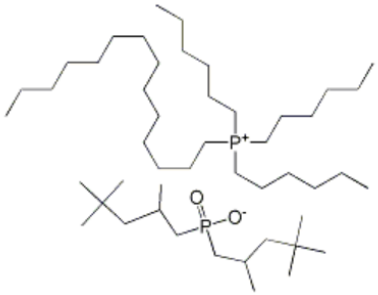	773.27	93%	Strem Chemicals

Chemicals/Dyes	CAS#	Formula	Structure	MW (g/mol)	Grade/Purity	Supplier
Decyl trimethyl ammonium bromide (DTAB)	2082-84-0	C13H30BrN	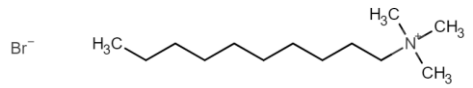	280.29	≥98%	Sigma-Aldrich
Decyl trimethyl ammonium chloride (DTAC)	10108-87-9	C13H30ClN	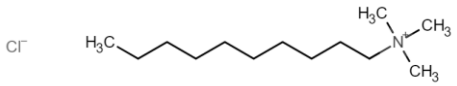	235.84	>98%	TCI Chemicals
Didecyl dimethyl ammonium chloride (DDAC)	7173-51-5	C22H48ClN	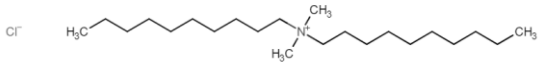	362.08	analytical standard	Sigma-Aldrich
Dodecyltrimethylammonium Chloride (DoTAC)	112-00-5	C15H34ClN	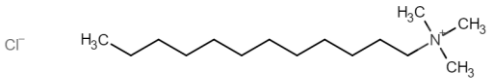	263.89	>97%	TCI Chemicals
Fluorescein Isothiocyanate (FITC)	3326-32-7	C21H11NO5S	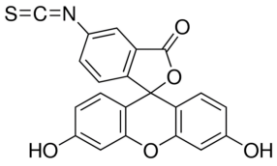	389.38	≥90%	Sigma-Aldrich

Chemicals/Dyes	CAS#	Formula	Structure	MW (g/mol)	Grade/Purity	Supplier
Fluorescein Sodium Salt	518-47-8	C20H10O5Na2	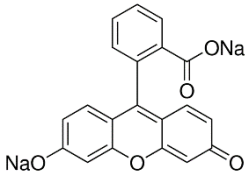	376.275	fluorescent tracer	Sigma-Aldrich
Octyl trimethyl ammonium bromide (OTAB)	2083-68-3	C11H26BrN	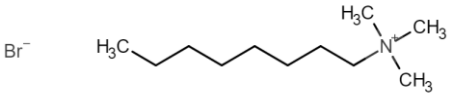	252.23	≥98%	Sigma-Aldrich
Octyl trimethyl ammonium chloride (OTAC)	10108-86-8	C11H26ClN	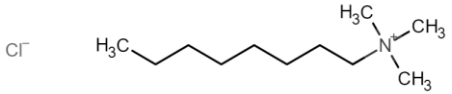	207.78	≥97%	Sigma-Aldrich
Oregon green 488	195136-52-8	C20H10F2O5	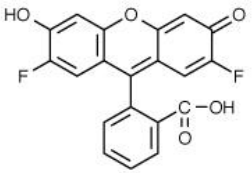	368.29	≥98% (HPLC)	Invitrogen
Rhodamine 6G (R6G)	989-38-8	C28H31ClN2O3	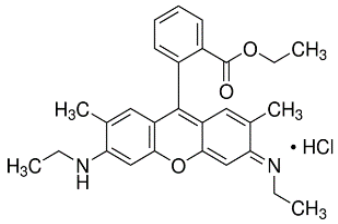	479.01	approx. 95%	Sigma-Aldrich

Chemicals/Dyes	CAS#	Formula	Structure	MW (g/mol)	Grade/Purity	Supplier
Sodium decyl sulfate (SDCS)	142-87-0	C10H21NaO4S	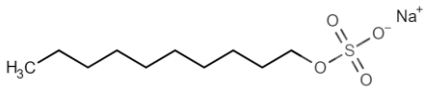	260.324	≥99%	Sigma-Aldrich
Sodium decyl sulfonate (SDCSF)	13419-61-9	C10H21NaO3S	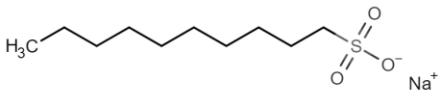	244.32	>98%	TCI Chemicals
Sodium dodecyl sulfate (SDS)	151-21-3	C12H25SO4Na	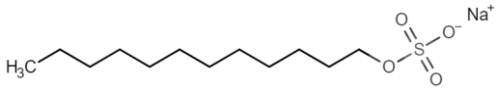	288.38	≥98.5%	Sigma-Aldrich
Sodium Laurate (SLC)	629-25-4	C12H23NaO2	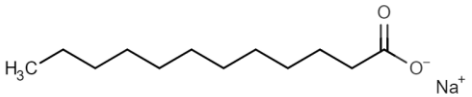	222.3	>97%	TCI Chemicals
Sodium Nonanoate (SN)	14047-60-0	C9H17NaO2	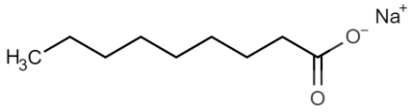	180.22	>98%	TCI Chemicals

Chemicals/Dyes	CAS#	Formula	Structure	MW (g/mol)	Grade/Purity	Supplier
Sodium octyl sulfate (SOS)	142-31-4	C8H17O4SNa	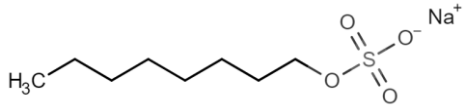	232.27	≥99%	Chem-Impex
Triton™ X-100	9002-93-1	C16H26O2	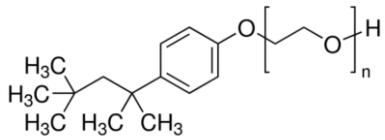	~625	Laboratory grade	Sigma-Aldrich
Tween® 20	9005-64-5	C26H50O10	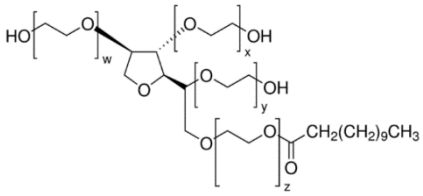	~1228	Molecular biology	Sigma-Aldrich

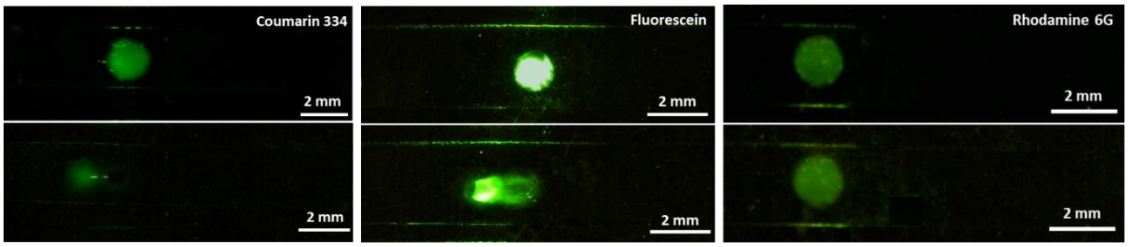

Figure 4.2. Images of migration of different charge fluorescent dyes before applying voltage (top row) and after 60 min application of 2000 V (bottom row). Conditions: PIM dimensions: 0.25 cm x 5 cm; length between electrodes: 4 cm. Voltage: 2000 V. Duration: 60 min. Sample(s): 500 ppm of Coumarin 334, 1000 ppm of Fluorescein sodium salt and 10 ppm of R6G in DI. Sample volume (spot size): 0.5 µL. Drying time (before electrophoresis): 5-10 min.

This movement of neutral species has also been reported in several investigations of PIM extraction involving Aliquat®336 as a carrier. Kolev's group employed Aliquat®336 PIM for extraction of Gold (III) from acidic solutions with thiourea added to enhance the speed and transport efficiency [28-30]. However, the gold was not effectively transported into the receiving phase, but thiourea was found to be competitively transported back into the feed phase and complexed with gold (III) inhibiting further transportation. The explanation to this extraction was the hydrogen bonding between thiourea and the Cl^- anion of Aliquat®336 forming heteroconjugate anion capable of complexing with gold (III). Riggs and Smith also reported using Aliquat®336, referred to as TOMA-Cl in their works, directly for extraction and transportation of neutral saccharides based on their hydrogen bonding and heteroconjugation of sugar hydroxyl groups with Cl^- anions [31]. The migration of Coumarin 334 which is also susceptible to form hydrogen bonding, may be explained from this theory.

4.4 Effect of PIM composition

Since Aliquat®336 was also reported to exhibit degree of plasticizing effect and some of the PIM was utilized for extraction without the addition of plasticizer [13, 14, 32-34], a PIM containing Aliquat®336 without adding plasticizers was also investigated (figure 4.3). No migration was observed for any charged dyes and this could be related to the mechanism proposed in *chapter 2* suggesting the presence of plasticizer, 2-NPOE, is essential for transportation in the solvent-less

PIM. This was confirmed by further optimization shown in figure 4.4B where increasing amount of 2-NPOE allowed better migration of Fluorescein. Even though the amount of 2-NPOE at 0.15 g (54.5 wt%) showed a better migration distance, the PIM at this ratio was found to have noticeable liquid stain on Kimwipe while being stored assuming from the leakage of 2-NPOE; hence, 0.10 g was chosen optimum.

Further investigation of electromigration was undertaken using the negatively charged Fluorescein sodium salt. Variation and mass ratio of 2-NPOE and Aliquat®336 is listed in table 4.2 with the result shown in figure 4.3. The amount of CTA was not varied and kept constant at 0.075 g based on optimization in *chapter 2* where the PIM at this concentration of CTA provided adequate thickness and was able to prevent leakage of the other components. Increasing the amount of Aliquat®336 improved the electromigration of Fluorescein showing a similar trend to that observed with R6G and [EMIM][NTf_2] in *chapter 2* suggesting the possibility of similar interaction between the dye and carrier in both cases.

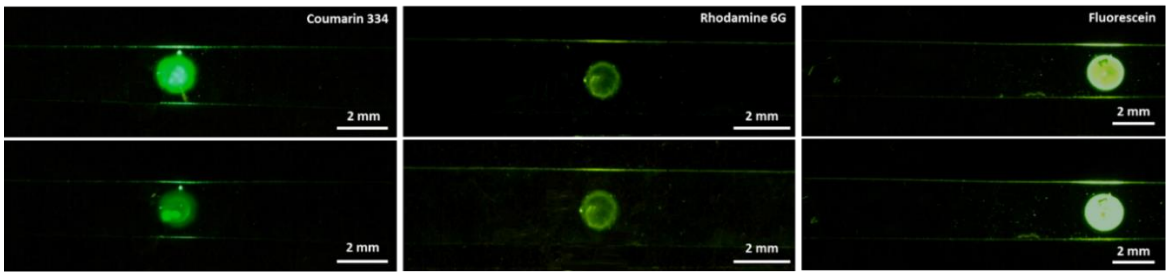

Figure 4.3. Images of migration of different charge fluorescent dyes before applying voltage (top row) and after 60 min application of 2000 V (bottom row) on PIM without 2-NPOE (plasticizer). Conditions: PIM dimensions: 0.25 cm x 5 cm; length between electrodes: 4 cm. Voltage: 2000 V. Duration: 60 min. Sample(s): 500 ppm of Coumarin 334, 1000 ppm of Fluorescein sodium salt and 10 ppm of R6G in DI. Sample volume (spot size): 0.5 µL. Drying time (before electrophoresis): 5-10 min.

However, without Aliquat®336 (figure 4.4B), Fluorescein did not move while streaking of R6G was observed previously with this composition. This could be supporting evidence for fluorescein not being extracted into the PIM with 2-NPOE, as presented in the membrane extraction experiment presented in *chapter 2* (figure 2.9). It is then expected that both extraction and electromigration of Fluorescein occurs based on the its ionic interaction with Aliquat®336 while 2-NPOE creates a mobile environment. In this case, the final concentration of PIM components based on the electromigration of Fluorescein sodium salt was chosen at 27.3% CTA : 36.4% 2-NPOE : 36.4% Aliquat®336.

Table 4.2. Variation of PIM components for the platform optimization tested with four different weights leaving the amount weighed of the other components unchanged. Amount of CTA in this investigation was kept constant at 0.075 g based on the physical observation and its variation was not studied.

	CTA (g)	**2-NPOE (g)**	**Aliquat®336 (g)**	**Mass ratio (weight%)** *(CTA : 2-NPOE : Aliquat®336)*
Variation of 2-NPOE	0.075	0	0.05	60 : 0 : 40
		0.05		42.9 : 28.6 : 28.6
		0.1		33.3 : 44.4 : 22.2
		0.15		27.3 : 54.5 : 18.2
Variation of Aliquat®336	0.075	0.1	0	42.9 : 57.1 : 0
			0.05	33.3 : 44.4 : 22.2
			0.075	30 : 40 : 30
			0.1	27.3 : 36.4 : 36.4

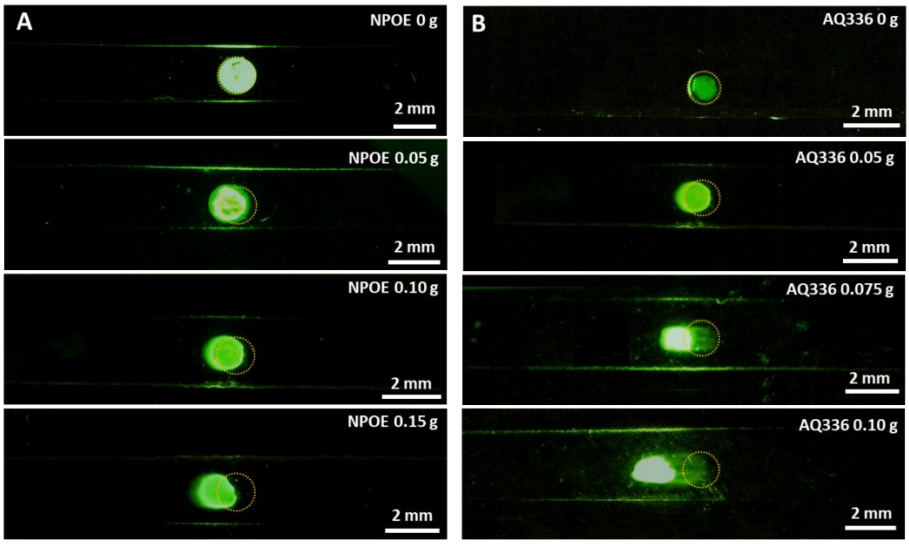

Figure 4.4. Migration of Fluorescein sodium salt with various composition ratio of PIM components. PIM compositions as displayed in Table 4.2 with migration of Fluorescein after 60 min of electrophoresis at 2000 V with 0.075 g of CTA, variation of 2-NPOE in column A and variation of Aliquat®336 in column B. Dashed circle indicates the starting position of the dye spot at 0 min. Conditions: PIM dimensions: 0.25 cm x 5 cm; length between electrodes: 4 cm. Voltage: 2000 V. Duration: 60 min. Sample(s): 1000 ppm of Fluorescein sodium salt in DI. Sample volume (spot size): 0.5 µL. Drying time (before electrophoresis): 5-10 min.

4.5 Membrane extraction of dyes with variation of PIM components

Membrane extraction was performed using the experimental method mentioned in section 2.7 and the results for PIM containing CTA only and CTA+2-NPOE are reported in figure 2.7 (*chapter 2*). The anionic PIM cast in this investigation was based on the final concentration (27.3% CTA : 36.4% 2-NPOE : 36.4% Aliquat®336) and the results for PIM containing CTA+Aliquat®336 and CTA+2-NPOE+Aliquat®336 are presented in figure 4.5.

A sharp decrease of Fluorescein absorbance was observed with PIM containing only CTA+Aliquat®336 which is similar to that of R6G in CTA+[EMIM][NTf_2] suggesting a dominating ionic interaction leading to the extraction and selectivity of both systems. While the absorbance of Fluorescein was observed to be almost identical for both CTA+Aliquat®336 and CTA+2-NPOE+ Aliquat®336, the enhancement of fluorescein colour can also be noticed similar to that reported in

section 2.7 (*chapter 2*). Again, this was believed to be due to 2-NPOE allowing molecules to be more mobile and evenly distributed throughout the PIM.

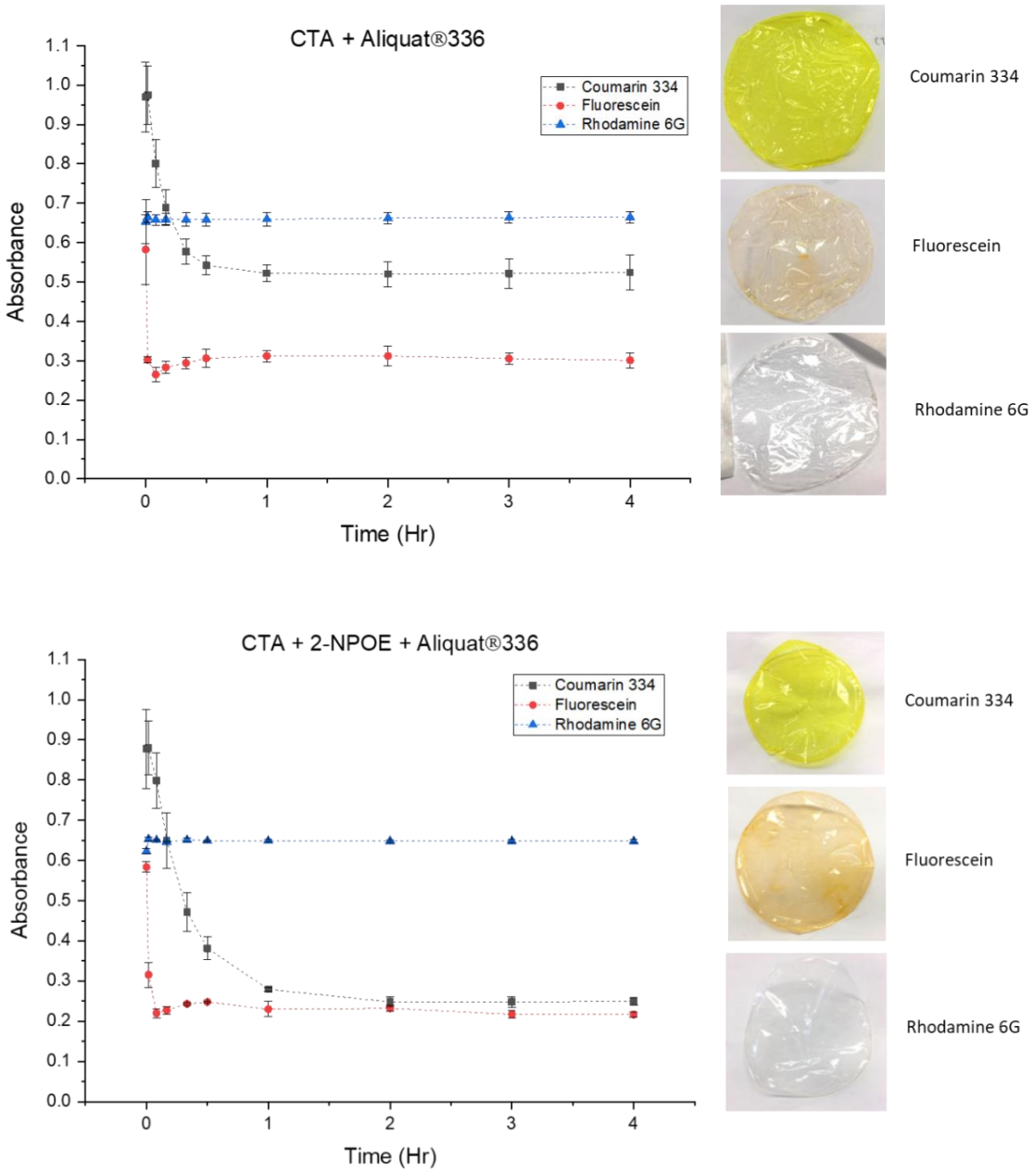

Figure 4.5. UV-Vis absorbance spectra of Coumarin 334 (square), Fluorescein sodium salt (circle) and R6G (triangle) after 4 hours of membrane extraction using PIMs with components variation. Each symbol represents individual collected aliquot. Blank (DI) absorbance was 0.126±0.007 (Coumarin 334), 0.079±0.005 (Fluorescein sodium salt) and 0.092±0.01 (R6G). Actual photographs of PIM in each variation of components and dyes after 4 hr of extraction were shown next to each plot. *(*note: photos were manually taken using mobile phones, direct comparison might be inaccurate due to lighting conditions*).

Extraction of Coumarin 334was also observed with CTA+Aliquat®336 and was more efficient compared to CTA+[EMIM][NTf_2] presumably due to partitioning or hydrogen bonding or the combination of both. Aliquat®336 is reported to have a log P of 5.33 [35] which is comparable with 2-NPOE; hence, there is a possibility of a partitioning effect. The confirmation of Coumarin 334 forming a heteroconjugate with anion of Aliquat®336 together with electromigration observed on our PIM (figure 4.2) leads to a hypothesis of this action cooperatively influencing extraction. The extraction of Coumarin 334 was further improved with PIM containing CTA+2-NPOE+Aliquat®336 implying that 2-NPOE enhanced the extraction of Coumarin 334 as a result of partitioning effect. Therefore, it could be possible that extraction of Coumarin 334 in CTA+Aliquat®336 (absence of 2-NPOE) was influenced by the heteroconjugation rather than partitioning. This heteroconjugation concept could perhaps indirectly refer to extraction of Coumarin 334 with CTA+[EMIM][NTf_2] (figure 2.7) being a result from physical bonding but with a lower bonding affinity of $[NTf_2]^-$ anion comparing to Cl^- anion. In case of R6G, the absorbance of the solution remained unchanged throughout the experiment with both systems denoting no extraction and agreeing with the observation of no electromigration in the PIM.

4.6 Electromigration of different anionic dyes

It could be seen that the Fluorescein did not migrate very far along the PIM in section 4.4 indicating that it might have a low mobility (0.469 x 10^{-11} m^2/Vs) similar to that of R123 in capillary electrophoresis of three Rhodamine dyes reported in *chapter 2* (figure 2.5A). Therefore, some anionic dyes available in the laboratory detectable with the fluorescence microscope were examined. These included 5(6)-Carboxynaphthofluorescein (CNF, 100 ppm), Fluorescein isothiocyanate (FITC, 100 ppm), and Oregon green (100 ppm). These three dyes were found to migrate a similar distance (with electrophoretic mobilities of 0.931, 0.661, and 1.27 x10^{-11} m^2/Vs for CNF, FITC and Oregon green respectively). Streaking of the spot and intensity loss of both CNF and FITC (figure 4.6) was also observed. Consequently, electrophoretic separation of these three

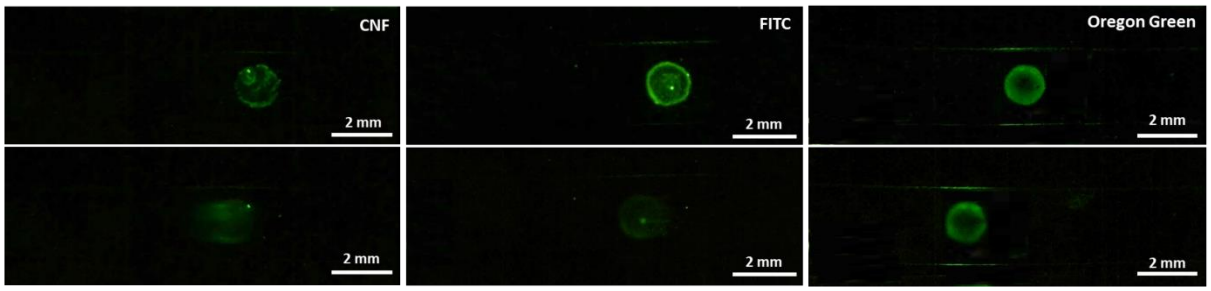

Figure 4.6. Migration of 5(6)-Carboxynaphthofluorescein (CNF), Fluorescein isothiocyanate (FITC) and Oregon green on optimized PIM-AQ after 60 min of electrophoresis at 2000 V. Conditions: PIM dimensions: 0.25 cm x 5 cm; length between electrodes: 4 cm. Voltage: 2000 V. Duration: 60 min. Sample(s): 100 ppm of FITC and Oregon green in DI and CNF (diluted from 1000 ppm stock in methanol). Sample volume (spot size): 0.5 µL. Drying time (before electrophoresis): 5-10 min.

dyes could not be achieved because of the overlapping spots and poor visualization. Moreover, streaking of the dye spots could be due to heterogeneity of PIM resulting from inadequate ratio of PIM components similar to distortion of R6G spot reported in *chapter 2* (section 2.4).

4.7 Investigation of using surfactants as carriers in PIM

In order to better understand the influence and behavior of Aliquat®336 towards the electromigration of Fluorescein in PIM, surfactants with similar chemical structures were considered to replace Aliquat®336 as the carrier. Surfactants with a different number of carbon units and carbon chains with two different counter anions were selected and are listed in table 4.1 and will be referred to in the section using their abbreviated names in the table. The composition for all PIM was used with 27.3% CTA : 36.4% 2-NPOE : 36.4% carrier/surfactant, except for DoTAC and SDS in which the composition used was 33.3% CTA : 44.4% 2-NPOE : 22.2% carrier/surfactant as this was the maximum concentration that produced a transparent PIM. The experiments were performed using Coumarin 334, Fluorescein sodium salt, and R6G as the selectivity of these surfactants are not initially known. Electromigration of these dyes were compared with PIM containing Aliquat®336 to determine the effect of chemical structure and perhaps elucidate the mechanisms of electromigration.

Electrophoretic mobilities of these dyes on PIM containing different surfactants were calculated using the equation 2.1 and listed in table 4.3 with bar graph representing the migration distance of all carriers in figure 4.7A, cationic surfactants in figure 4.7B and anionic and neutral surfactants in figure 4.7C. Negative values and positive values represent the migration of dyes towards the anode and cathode, respectively. Anionic surfactants including SOS, SDS, and SLC would not be dissolved with DCM; therefore, the solution of PIM containing these surfactants required up to 30% methanol or ethanol for complete dissolution of all components. PIM composing of SOC, SNC, and SDCSF did not form a stable PIM and could not be peeled off from the petri dish even with 0.05 g, or they required a large amount of methanol/ethanol leaving other PIM components undissolved; hence, no electromigration data was obtained.

From inspection of the mobilities in table 4.3 and figure 4.7, most of the carriers showed affinity towards the cationic dye, R6G, except for Aliquat®336. From the list of carriers, Aliquat®336 is the only carrier with three carbon chains which was the highest number of repeating aliphatic chains. As such there could be the steric hindrance when compared to the rest of the carriers. The possibility of the chains blocking the complexing active site and limiting the diffusive flux within the PIM with increasing amount of the Aliquat®336 was reported in the literature, providing one explanation why Aliquat®336 did not show movement of R6G in the PIM [36-41]. Electromigration of R6G was observed on the PIM containing Aliquat®336 only when less than or 0.05 g was used (figure 4.8); although it was not very noticeable after 60 min. The electromigration of R6G deteriorated with increasing chain lengths and increasing number of aliphatic chains for cationic surfactants and this, again, might be the result for steric hindrance. Surprisingly, electromigration of R6G was found to be slightly better with PIM containing CYPHOS®104 IL, which was expected to exert greater steric hindrance with four aliphatic chains, when comparing to Aliquat®336 indicating that steric hindrance might not be a factor for CYPHOS®104 IL.

A.

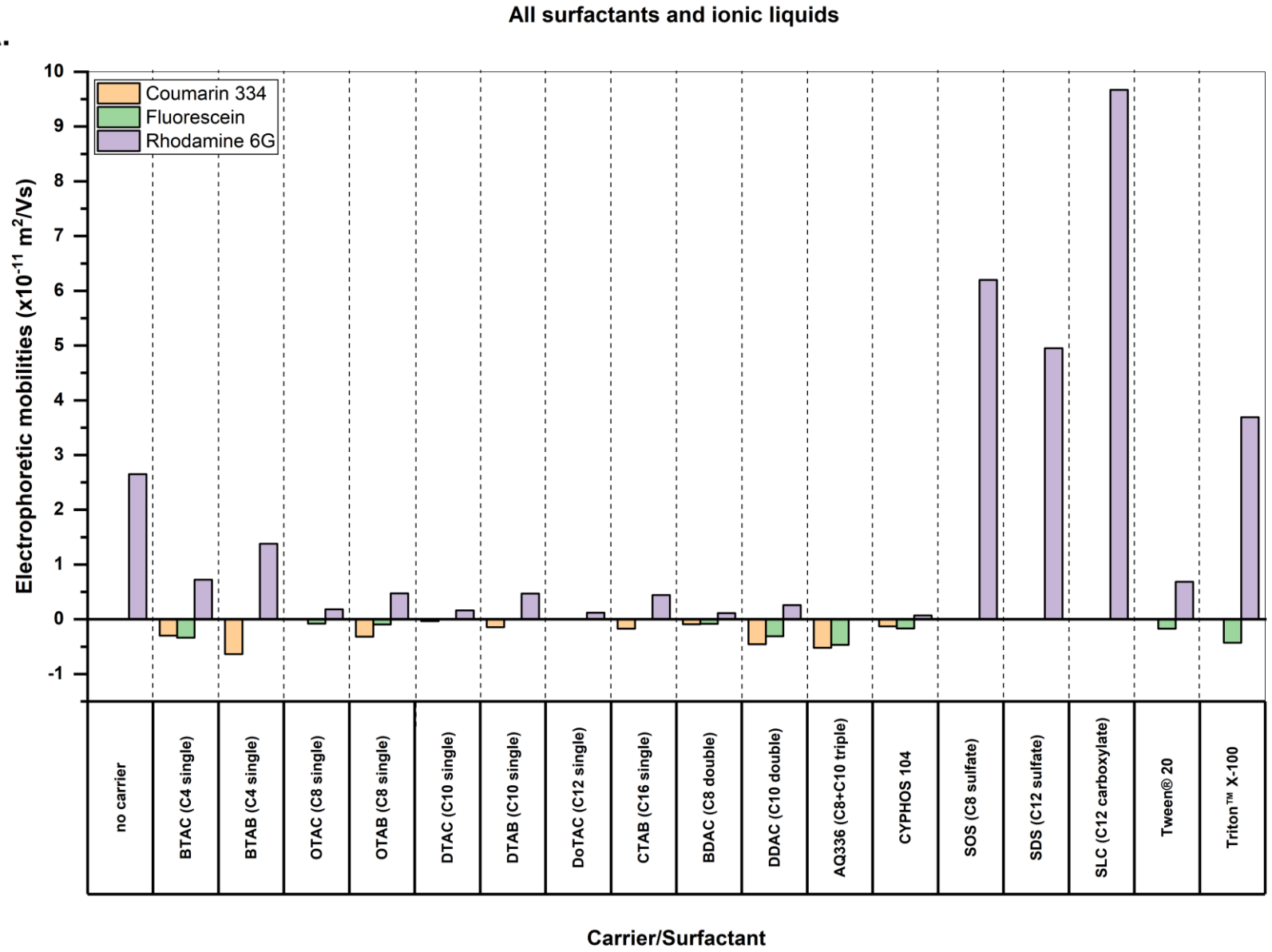
All surfactants and ionic liquids
Coumarin 334
Fluorescein
Rhodamine 6G
Electrophoretic mobilities (x10^{-11} m^2/Vs)
10
9
8
7
6
5
4
3
2
1
0
-1
no carrier
BTAC (C4 single)
BTAB (C4 single)
OTAC (C8 single)
OTAB (C8 single)
DTAC (C10 single)
DTAB (C10 single)
DoTAC (C12 single)
CTAB (C16 single)
BDAC (C8 double)
DDAC (C10 double)
AQ336 (C8+C10 triple)
CYPHOS 104
SOS (C8 sulfate)
SDS (C12 sulfate)
SLC (C12 carboxylate)
Tween® 20
Triton™ X-100
Carrier/Surfactant

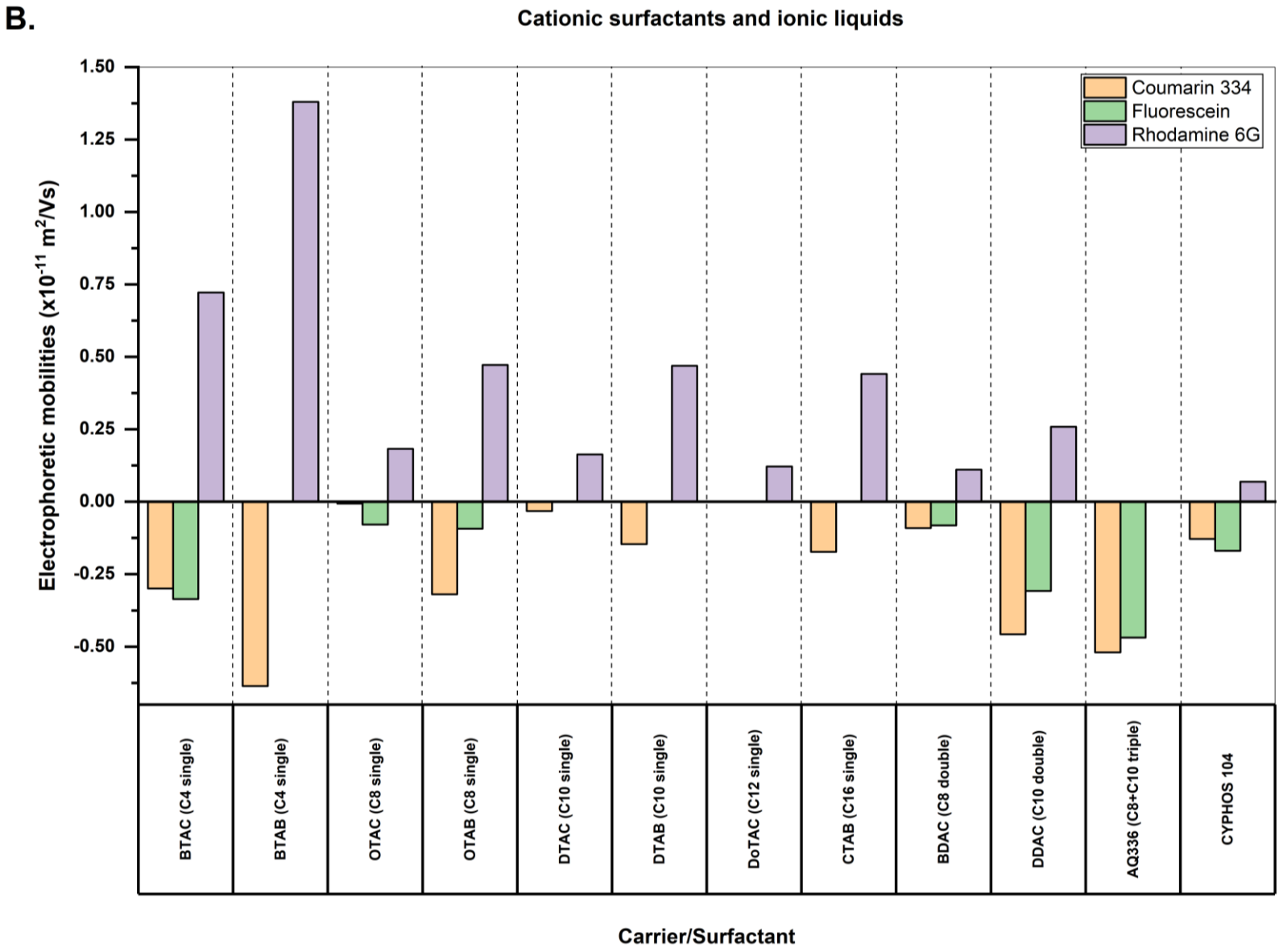
B.
Cationic surfactants and ionic liquids
Electrophoretic mobilities (x10^{-11} m^2/Vs)
1.50
1.25
1.00
0.75
0.50
0.25
0.00
-0.25
-0.50
Coumarin 334
Fluorescein
Rhodamine 6G
BTAC (C4 single)
BTAB (C4 single)
OTAC (C8 single)
OTAB (C8 single)
DTAC (C10 single)
DTAB (C10 single)
DoTAC (C12 single)
CTAB (C16 single)
BDAC (C8 double)
DDAC (C10 double)
AQ336 (C8+C10 triple)
CYPHOS 104
Carrier/Surfactant

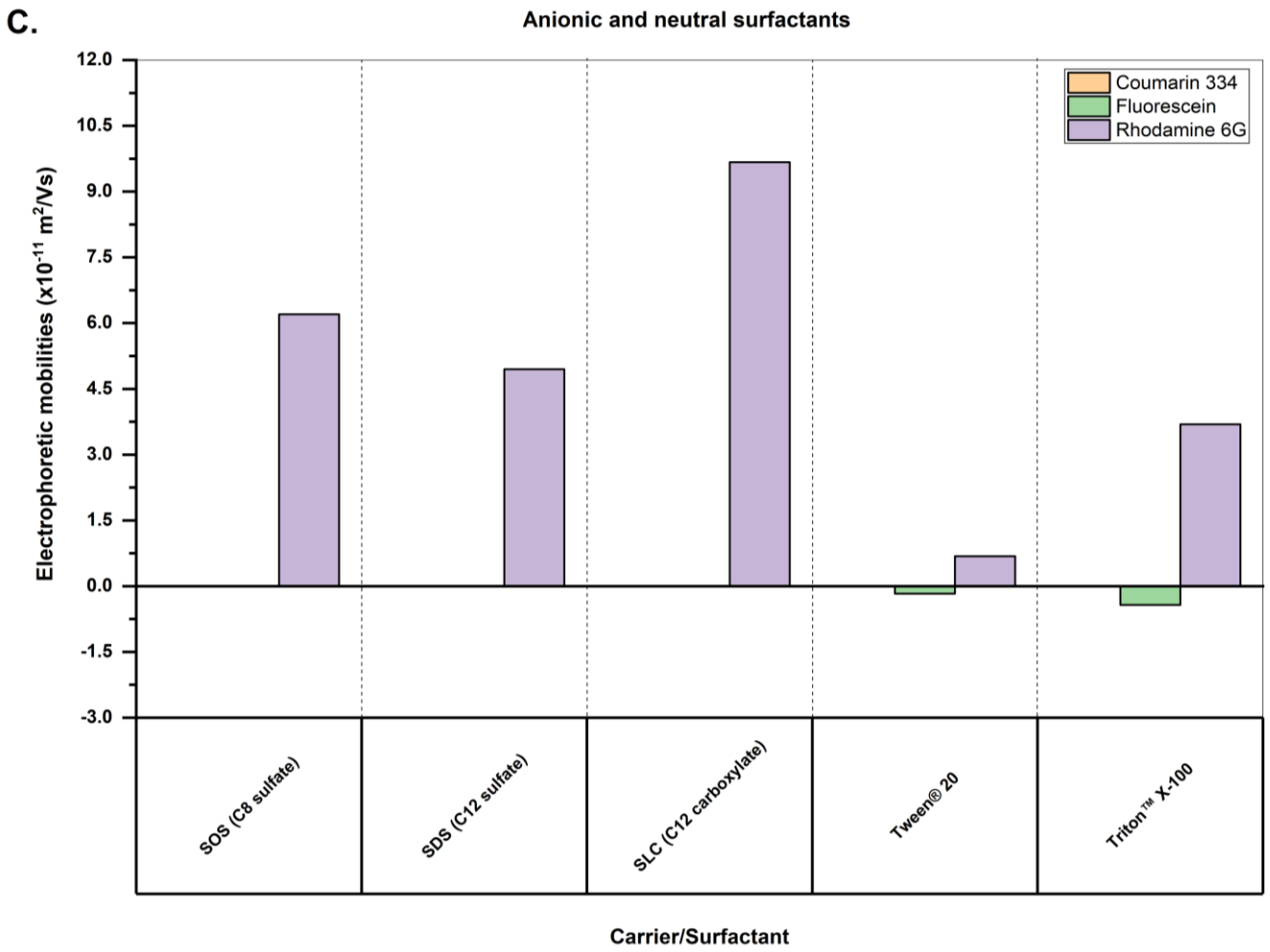

Figure 4.7. Bar graph displaying electrophoretic mobilities of Coumarin 334 (yellow), Fluorescein sodium salt (green) and R6G (purple) with (A) all carriers in which was further grouped into (B) cationic surfactants and ionic liquids and (C) anionic and neutral surfactants. The values are displayed in table 4.3.

Table 4.3. Estimation of electrophoretic mobility of fluorescent dyes on PIM containing various carriers and surfactants. Calculation parameters: PIM effective length: 40 mm (0.04 m), voltage: 2000V, and time: 60 min (3600 s). Information in the parenthesis include number of carbon units, number of branches, and functional groups.

Carriers/Surfactants	**Electrophoretic mobilities (x10^{-11} m^2/Vs)**		
	Coumarin 334 (neutral)	**Fluorescein sodium salt (anionic)**	**R6G (cationic)**
no carrier (CTA+2-NPOE)	x	x	2.65*
BTAC (C4 single)	-0.299	-0.336	0.722
BTAB (C4 single)	-0.636	x	1.380
OTAC (C8 single)	-0.006	-0.079	0.183
OTAB (C8 single)	-0.319	-0.0928	0.472
DTAC (C10 single)	-0.0317	x	0.163
DTAB (C10 single)	-0.146	x	0.469
DoTAC (C12 double)	x	x	0.122
CTAB (C16 single)	-0.173	x	0.441
BDAC (C8 double)	-0.0911	-0.0817	0.111
DDAC (C10 double)	-0.457	-0.308	0.259
AQ336 (C8+C10 triple)	-0.52	-0.469	x
CYPHOS 104	-0.128	-0.169	0.0689
SOS (C8 sulfate)	x	x	6.2
SDS (C12 sulfate)	x	x	4.95
SLC (C12 carboxylate)	x	x	9.67
Tween® 20	x	-0.171	0.683
Triton™ X-100	x	-0.428	3.69

**spot with distorted shape; x = no migration observed; negative values = migration towards anode.*

Electromigration of R6G was also found to be greater with anionic surfactants even though they cannot be compared directly due limited selection of the common functional groups and the difficulties in forming a stable PIM. Additionally, anionic surfactants showed similar selectivity towards R6G same as that of [EMIM][NTf_2], that is, there was no electromigration of Coumarin 334

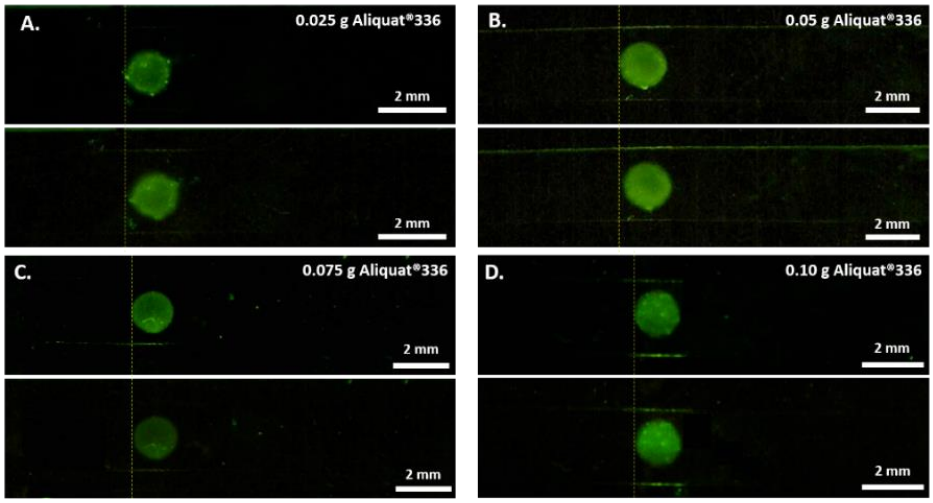

Figure 4.8. Migration of R6G on PIM containing (A) 0.025 g, (B) 0.05, (C) 0.075, and (D) 0.10 g of Aliquat®336 (based on ratio in table 4.2) before (top) and after (bottom) 60 min of electrophoresis at 2000 V. Conditions: PIM dimensions: 0.25 cm x 5 cm; length between electrodes: 4 cm. Voltage: 2000 V. Duration: 60 min. Sample(s): 10 ppm of R6G in DI. Sample volume (spot size): 0.5 µL. Drying time (before electrophoresis): 5-10 min. Dashed line marks the original location of the spot at 0 min.

and Fluorescein implying similarity of principles between anionic surfactants and [EMIM][NTf_2] governing the electromigration of R6G on PIM [42-44]. While only a limited number of neutral surfactant was used, which limits the comparisons that can be made, the electromigration of R6G suggests that there may be partitioning with Triton™ X-100 (log P = 4.15 [35]) and Tween® 20 (log P = 2.39 [35]) as the migration with the spot distorted, similar to the PIM containing only 2-NPOE shown in figure 2.4 (*chapter 2*).

For neutral and anionic molecules, Coumarin 334 and Fluorescein respectively, their electromigration behavior was similar. For single chain surfactants, the electromigration of both dyes were greatest at the lower number of carbon units. Increasing the length of the carbon chain enhanced the electromigration of both dyes, especially Fluorescein. For surfactants with two aliphatic chains, the improvement continued further and was even greater with the triple-chained Aliquat®336. Both dyes also showed deterioration in migration distance with 4-braches CYPHOS®104 IL. This finding could support the loss in mobility of Coumarin 334 with CYPHOS®104

IL as a result of larger anionic heteroconjugate/products combined with steric hindrance with this ionic liquid.

While electromigration of fluorescein directly followed the proposed trend, Coumarin 334 was found to slightly deviated as seen with BTAC, DTAC, and CTAB. Even though mobilities of Coumarin 334 was obviously detected with BTAC and BTAB, the dye was not maintained in the shape of the spot and had a similar shape to R6G with PIM containing only 2-NPOE and without carrier. Hence, it was assumed to be a result of surfactant with short number of carbon units making PIM less hydrophobic and possibly leading to more mobile environment within the PIM. However, since the mobility of Coumarin 334 in all cationic surfactants are directional (towards the anode) this suggests that there must be anionic adducts formed with Coumarin 334 and Cl^- and Br^-. The spot shape of Coumarin 334 was better retained with higher number of carbon units, such as CTAB, suggesting that increasing number of carbon units might lead to greater migration as the PIM is more hydrophobic. Alternatively, there could be higher number of Cl^- or Br^- allowing more capacity to complex with dyes; thus, preserve the spot shape. No migration can be seen with Coumarin 334 with anionic surfactants probably due to absence of heteroconjugate adducts as proposed previously. For neutral surfactants, Fluorescein showed similar findings with those PIM containing short-chained cationic surfactant with streaking of dye spots and directional migration while electromigration of Coumarin 334 was not noticeable due to severe loss of intensity.

Another finding observed for all comparable cationic surfactants with two different counter anions, chloride and bromide, was that higher electromigration of both Coumarin 334 and R6G occurred with those containing bromide anion over chloride. The reason could be the higher polarizability of bromide anion indicating a stronger ion-pair formation and binding efficiency due to smaller hydration radius [43, 45] and this may contribute to higher mobilities observed on the PIM composing of surfactants with bromide counter anion. Unexpectedly, this behavior cannot be clearly verified for Fluorescein as electromigration was not detected with BTAB and most of

increasing single-chained cationic surfactants. However, this showed evidence that there is an impact of counter anion on the electromigration of dyes on PIM.

4.8 Summary and future approach

Based on the data obtained from electromigration on PIM with various selection of surfactants and ionic liquids, Aliquat®336 was found to provide greatest electrophoretic mobilities of Fluorescein which was the focus of this chapter in determining the carriers for anionic molecules. With Aliquat®336, the electromigration of Coumarin 334 was also observed and may be due to the conjugation with the Cl^- anion of Aliquat®336 allowing mobilities of this neutral molecule. The migration of cationic of R6G was not observed as expected. These results were confirmed with membrane extraction experiment, and the extraction of Coumarin was observed even with PIM containing only Aliquat®336 supporting a theory of Coumarin adducts bearing negative charge and the unchanged absorbance of R6G agreeing with no extraction hypothesis made in *chapter 2*. Due to limited selection of anionic dyes with similar mobilities and assumption of PIM not in the best optimization, separation of these dye was not investigated. Therefore, more selection of anionic dyes would provide a better observation and more conclusive determination on the mobilities and electromigration pattern of anionic dyes and whether the concentration of PIM components used are the optimal condition for the platform.

The number of repeating carbon units, number of branches of each surfactant and their counter anion are found to have an impact not only on the electromigration but also the retainment of the dye spot, and homogeneity of the optimized PIM, in which each charged dye showed quite different trend from each other. Since the concentration of surfactants formulating PIM was used at the optimized concentration of Aliquat®336, even though some of them was used at the lower concentration due to solubility in PIM solution and physical appearances of final PIM, it is believed that optimization of PIM components is required for each carrier/surfactant to effectively monitor and compare the electromigration of dyes. However, experiment with various

surfactants and ionic liquids revealed that electromigration on PIM is likely governed by mixed mechanisms contributed by each component and differed with each variation of carrier towards each dye. Membrane extraction might also help explaining in more detail on specific mechanism how each surfactant and ionic liquid drives the electromigration of dyes; however, the experiments have not been carried out in this case due to time limit.

4.9 References

[1] M.I.G.S. Almeida, R.W. Cattrall, S.D. Kolev, Polymer inclusion membranes (PIMs) in chemical analysis-A review, Anal. Chim. Acta., 987 (2017) 1-14.

[2] M.I.G.S. Almeida, R.W. Cattrall, S.D. Kolev, Recent trends in extraction and transport of metal ions using polymer inclusion membranes (PIMs), J. Memb. Sci., 415 (2012) 9-23.

[3] L.D. Nghiem, P. Mornane, I.D. Potter, J.M. Perera, R.W. Cattrall, S.D. Kolev, Extraction and transport of metal ions and small organic compounds using polymer inclusion membranes (PIMs), J. Memb. Sci., 281 (2006) 7-41.

[4] M. Cox, Solvent extraction in hydrometallurgy, Solvent Extraction Principles and Practice, Revised and Expanded, CRC Press2004, pp. 466-515.

[5] G.W. Stevens, J.M. Perera, F. Grieser, Interfacial aspects of metal ion extraction in liquid-liquid systems, Reviews in Chemical Engineering, 17 (2001) 87-110.

[6] W. Walkowiak, M. Ulewicz, C. Kozłowski, Application of macrocycle compounds for metal ions separation and removal-a review, Ars Separatoria Acta, (2002) 87-98.

[7] T.D. Ho, C. Zhang, L.W. Hantao, J.L. Anderson, Ionic liquids in analytical chemistry: fundamentals, advances, and perspectives, Anal. Chem., 86 (2013) 262-285.

[8] A. Stojanovic, B.K. Keppler, Ionic Liquids as Extracting Agents for Heavy Metals, Sep. Sci. Technol., 47 (2012) 189-203.

[9] S. Werner, M. Haumann, P. Wasserscheid, Ionic liquids in chemical engineering, Annu. Rev. Chem. Biomol. Eng., 1 (2010) 203-230.

[10] A. Manzak, Y. Yildiz, O. Tutkun, Characterization of polymer inclusion membrane containing Aliquat 336 as a carrier, The 2014 World CongressBusan, Korea, 2014.

[11] L.J. Wang, R. Paimin, R.W. Cattrall, W. Shen, S.D. Kolev, The extraction of cadmium(II) and copper(II) from hydrochloric acid solutions using an Aliquat 336/PVC membrane, J. Memb. Sci., 176 (2000) 105-111.

[12] M. O'Rourke, R.W. Cattrall, S.D. Kolev, I.D. Potter, The extraction and transport of organic molecules using polymer inclusion membranes, Solvent Extr. Res. Dev. Jpn, 16 (2009) 1-12.

[13] E.A. Nagul, C. Fontàs, I.D. McKelvie, R.W. Cattrall, S.D. Kolev, The use of a polymer inclusion membrane for separation and preconcentration of orthophosphate in flow analysis, Anal. Chim. Acta., 803 (2013) 82-90.

[14] P. Pantůčková, P. Kubáň, P. Boček, In-line coupling of microextractions across polymer inclusion membranes to capillary zone electrophoresis for rapid determination of formate in blood samples, Anal. Chim. Acta., 887 (2015) 111-117.

[15] A. Kaya, C. Onac, H.K. Alpoguz, A novel electro-driven membrane for removal of chromium ions using polymer inclusion membrane under constant DC electric current, Journal of hazardous materials, 317 (2016) 1-7.

[16] M. Matsumoto, Y. Murakami, Y. Minamidate, K. Kondo, Separation of lactic acid through polymer inclusion membranes containing ionic liquids, Sep. Sci. Technol., 47 (2012) 354-359.

[17] Y. Cho, C. Xu, R.W. Cattrall, S.D. Kolev, A polymer inclusion membrane for extracting thiocyanate from weakly alkaline solutions, J. Memb. Sci., 367 (2011) 85-90.

[18] N.A. Mamat, H.H. See, Simultaneous electromembrane extraction of cationic and anionic herbicides across hollow polymer inclusion membranes with a bubbleless electrode, J. Chromatogr. A, 1504 (2017) 9-16.

[19] H.H. See, P.C. Hauser, Electric field-driven extraction of lipophilic anions across a carrier-mediated polymer inclusion membrane, Anal. Chem., 83 (2011) 7507-7513.

[20] J. Schmidt‐Marzinkowski, H.H. See, P.C. Hauser, Electric field driven extraction of inorganic anions across a polymer inclusion membrane, Electroanalysis, 25 (2013) 1879-1886.

[21] Y. Cho, R.W. Cattrall, S.D. Kolev, A novel polymer inclusion membrane based method for continuous clean-up of thiocyanate from gold mine tailings water, Journal of hazardous materials, 341 (2018) 297-303.

[22] K.M. White, B.D. Smith, P.J. Duggan, S.L. Sheahan, E.M. Tyndall, Mechanism of facilitated saccharide transport through plasticized cellulose triacetate membranes, J. Memb. Sci., 194 (2001) 165-175.

[23] Y.Y.N. Bonggotgetsakul, R.W. Cattrall, S.D. Kolev, Recovery of gold from aqua regia digested electronic scrap using a poly (vinylidene fluoride-co-hexafluoropropene)(PVDF-HFP) based polymer inclusion membrane (PIM) containing Cyphos® IL 104, J. Memb. Sci., 514 (2016) 274-281.

[24] M.R. Yaftian, M.I.G. Almeida, R.W. Cattrall, S.D. Kolev, Selective extraction of vanadium (V) from sulfate solutions into a polymer inclusion membrane composed of poly (vinylidenefluoride-co-hexafluoropropylene) and Cyphos® IL 101, J. Memb. Sci., 545 (2018) 57-65.

[25] M. Regel-Rosocka, M. Rzelewska, M. Baczynska, M. Janus, M. Wisniewski, Removal of palladium (II) from aqueous chloride solutions with cyphos phosphonium ionic liquids as metal ion carriers for liquid-liquid extraction and transport across polymer inclusion membranes, Physicochemical Problems of Mineral Processing, 51 (2015).

[26] M. Baczynska, M. Regel-Rosocka, M. Nowicki, M. Wisniewski, Effect of the structure of polymer inclusion membranes on zn(II) transport from chloride aqueous solutions, J. Appl. Polym. Sci., 132 (2015) 1-11.

[27] J.-P. Mikkola, P. Virtanen, R. Sjöholm, Aliquat 336®—a versatile and affordable cation source for an entirely new family of hydrophobic ionic liquids, Green Chemistry, 8 (2006) 250-255.

[28] S.D. Kolev, G. Argiropoulos, R.W. Cattrall, I.C. Hamilton, R. Paimin, Mathematical modelling of membrane extraction of gold (III) from hydrochloric acid solutions, J. Memb. Sci., 137 (1997) 261-269.

[29] G. Argiropoulos, R.W. Cattrall, I.C. Hamilton, S.D. Kolev, R. Paimin, The study of a membrane for extracting gold (III) from hydrochloric acid solutions, J. Memb. Sci., 138 (1998) 279-285.

[30] Y. Sakai, R.W. Cattrall, I.D. Potter, S.D. Kolev, R. Paimin, Transport of thiourea through an Aliquat 336/polyvinyl chloride membrane, Sep. Sci. Technol., 35 (2000) 1979-1990.

[31] J.A. Riggs, B.D. Smith, Facilitated transport of small carbohydrates through plasticized cellulose triacetate membranes. Evidence for fixed-site jumping transport mechanism, J. Am. Chem. Soc., 119 (1997) 2765-2766.

[32] N.-S. Abdul-Halim, P.G. Whitten, L.D. Nghiem, Characterising poly (vinyl chloride)/Aliquat 336 polymer inclusion membranes: Evidence of phase separation and its role in metal extraction, Separation and Purification Technology, 119 (2013) 14-18.

[33] S.D. Kolev, Y. Sakai, R.W. Cattrall, R. Paimin, I.D. Potter, Theoretical and experimental study of palladium (II) extraction from hydrochloric acid solutions into Aliquat 336/PVC membranes, Anal. Chim. Acta., 413 (2000) 241-246.

[34] R. Güell, E. Anticó, S.D. Kolev, J. Benavente, V. Salvadó, C. Fontàs, Development and characterization of polymer inclusion membranes for the separation and speciation of inorganic As species, J. Memb. Sci., 383 (2011) 88-95.

[35] ChemAxon Ltd., https://chemicalize.com/#/.

[36] C.-V. Gherasim, G. Bourceanu, Removal of chromium (VI) from aqueous solutions using a polyvinyl-chloride inclusion membrane: Experimental study and modelling, Chemical engineering journal, 220 (2013) 24-34.

[37] S. Martinez, A. Sastre, F.J. Alguacil, Gold extraction equilibrium in the system Cyanex 921-HCl・ Au (III), Hydrometallurgy, 46 (1997) 205-214.

[38] R. Navarro, I. Saucedo, A. Núñez, M. Ávila, E. Guibal, Cadmium extraction from hydrochloric acid solutions using Amberlite XAD-7 impregnated with Cyanex 921 (tri-octyl phosphine oxide), Reactive and Functional Polymers, 68 (2008) 557-571.

[39] E. Radzyminska-Lenarcik, M. Ulewicz, The use of the steric effect of the carrier molecule in the polymer inclusion membranes for the separation of cobalt (II), nickel (II), copper (II), and zinc (II) ions, Polish Journal of Chemical Technology, 17 (2015) 51-56.

[40] B. Mahanty, P.K. Mohapatra, D.R. Raut, D.K. Das, P.G. Behere, M. Afzal, W. Verboom, Polymer inclusion membrane containing a tripodal diglycolamide ligand: actinide ion uptake and transport studies, Ind. Eng. Chem. Res., 55 (2016) 2202-2209.

[41] T. Eljaddi, L. Laurent, H. Miloudi, Review on Mechanism of Facilitated Transport on Liquid Membranes, Journal of Membrane Science and Research, 3 (2017) 199-208.

[42] N. Pan, D.J. Pietrzyk, Separation of anionic surfactants on anion exchangers, J. Chromatogr. A, 706 (1995) 327-337.

[43] M.A. Woodland, C.A. Lucy, Altering the selectivity of inorganic anion separations using electrostatic capillary electrophoresis, Analyst, 126 (2001) 28-32.

[44] C. Coll, R. Martínez‐Máñez, M.D. Marcos, F. Sancenón, J. Soto, A simple approach for the selective and sensitive colorimetric detection of anionic surfactants in water, Angewandte Chemie International Edition, 46 (2007) 1675-1678.

[45] A. Ali, M. Alam, U. Farooq, S. Uzair, Effect of the nature of counterion on the micellar properties of cationic surfactants: a conductometric study, Physics and Chemistry of Liquids, 56 (2018) 528-543.

Chapter 5

Matrix-assisted laser desorption ionization-time of flight mass spectrometry (MALDI-TOF MS) as detection system for portable PIM-based electrokinetic platform

5.1 Introduction and objective

In *chapter 3*, solvent-less PIM-based electrokinetic platform was developed and used as platform to collect, extract and separate berberine chloride (BC) from a drop of blood dried on the PIM during transit. The BC on the strip was directly analysed without further sample preparation using a fluorescence microscope and quantified with calibration curves. Since the method relies on the detection of colour and fluorescence intensity, it is applicable only to compounds natively exhibiting colour or susceptible to be tagged with colour-generating molecules. With the concept of the PIM being capable of rapidly collecting whole blood from home, derivatization or staining of the sample were considered unfavourable and intentionally eliminated; hence BC with native fluorescence was used as model analyte. However, the majority of pharmaceuticals or disease markers, do not bear a self-generating colour or luminescence and this is one of the reasons why sample-pre-treatment is often required in conventional clinical diagnostic as mentioned in *chapter 1*. One of the future directions proposed in *chapter 3* was an attempt to integrate Matrix-assisted laser desorption ionization-time of flight mass spectrometry (MALDI-TOF) into the workflow anticipating that its chemical imagining feature and mass/charge-based detection would allow analysis of non-coloured compounds and expand the applicability of the PIM.

MALDI is one of the variants of MS introduced in 1988 with soft ionization where a large target molecule such as a peptide or protein is mixed with solution containing an organic energy-absorbing compound acting as matrix. The matrix is added to assist the ionization and to prevent direct ionization of the sample which could cause sample destruction [1-3]. Sample and the matrix are ionized into singly charged gaseous fractions (by adding or removing proton) by photons from

laser sources then they are separated under a magnetic or electric field and their mass/charge (m/z) ratio corresponding to the chemical structures identified with a mass analyser [3]. MALDI also allows detection with non-liquid samples as the molecules are co-crystallized and dried into solid crystals on the conductive platform. Most MALDI analysis involving microbiological detection is coupled with time-of-flight (TOF) mass analyser with the m/z of ions measured based on the time they travel to the detector at the end of the flight tube [1, 4].

Organic compounds such as α-Cyano-4-hydroxycinnamic acid (4-HCCA), 2,5-dihydroxy benzoic acid (DHB) and 3,5-dimethoxy-4-hydroxycinnamic acid (sinapinic acid) typically dissolved in mixture of DI, acetonitrile and trifluoro acetic acid (TFA), are common matrix solutions employed in MALDI-TOF for microbiological analysis [1]. Small molecules (<500 Da) are quite uncommon to be analysed using MALDI-TOF as there are detectable interference peaks from large amount of the low molecular weight matrix [5, 6]. There are several ways to address this issue including the use of sample as a matrix, i.e. matrix-free, the use of high molecular weight matrix instead of conventional ones, the use of inorganic compounds as matrix, and the use of surfactants and ionic liquids to suppress disturbing signals allowing analysis of small molecules [5, 7, 8].

Since each of our PIM-based electrokinetic strips are made up of ionic liquid and BC is the small molecule pharmaceutical model, the possibility to detect it by MALD-TOF simply by attaching PIM onto the conductive platform for MALDI, perhaps even a matrix-free approach, was investigated. With instrumentation not available at the University of Tasmania (UTAS), experiments were undertaken in collaboration with Dr. William Alexander Donald's group (Fundamental and Applied Mass Spectrometry) at Bioanalytical Mass Spectrometry Facility (UNSW Mark Wainwright Analytical Centre), University of New South Wales (UNSW).

5.2 Experimental chemicals, equipment, and methods

**Some contents and figures in this section are containing identical or similar information with materials and methods introduced in chapter 2 and chapter 3.*

5.2.1 Chemicals and equipment

Chemicals for MALDI-TOF and dyes used in this chapter are listed in table 5.1 while those for the PIM are listed in table 2.1. The acidic solvent for matrix contained 30% Acetonitrile (ACN) and 0.1% Trifluoro acetic acid (TFA) in DI, referred to as TA 30. Analysis of fluorescent dyes and BC was performed with a Bruker ultrafleXtreme MALDI-TOF/TOF mass spectrometer (Bruker Daltonics systems, Bremen, Germany) equipped with a pulsed Nitrogen laser operated at 337 nm and 25 kV. The data and mass spectra were acquired using Bruker flexAnalysis software in positive reflection ion mode. Ground steel BC targets (MTP 384, Bruker Daltonics systems, Bremen, Germany) and indium tin oxide (ITO) coated glass slide (75 x 25 mm, Bruker Pty Limited) fitted in the plate adapter (MTP Slide Adapter II, Bruker Daltonics systems, Bremen, Germany) were used as target plates for MALDI-TOF.

5.2.2 PIM preparation

PIM preparation process for this chapter is illustrated in figure 2.1 and is identical to that described in section 2.2.2 (*chapter 2*).

5.2.3 Portable electrophoresis platform

A PIM was cut into a strip with dimension of 0.25 cm x 5.0 cm for all experiments described. The portable device used in this chapter was described in section 3.3.7 and shown in figure 3.7 (*chapter 3*). All electrophoresis experiment in this chapter was performed on a portable device where the potential was supplied using batteries (24V, 6 V/cm). A handheld blue-light digital microscope and image scanner (Super COOLSCAN 4000 ED, Nikon, Sydney, Australia) were used to capture the images using DinoCapture 2.0 software and Nikon scanning software respectively. Image was then inserted and used as template in MALDI-TOF image profiling. After electrophoresis, the strips were detached from their separation platform and taped on a conductive indium tin oxide coated glass slide (ITO) prior to analysis with MALDI-TOF.

Table 5.1. List of chemicals for MALDI-TOF and dyes used in chapter 5

Chemicals/Dyes	CAS #	Formula	Structure	MW (g/mol)	Grade/Purity	Supplier
Acetonitrile (ACN)	75-05-8	C_2H_3N	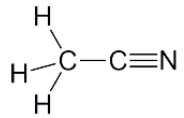	41.053	HPLC	Sigma-Aldrich
Berberine chloride (BC)	633-65-8	$C_{20}H_{18}ClNO_4$	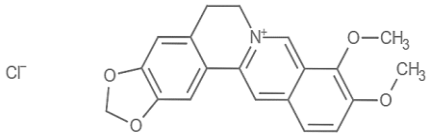	371.81	≥95%	Sigma-Aldrich
Rhodamine 123 (R123)	62669-70-9	$C_{21}H_{17}ClN_2O_3$	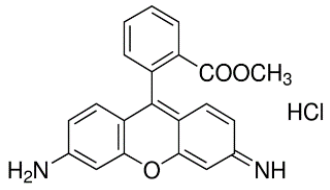	380.821	mitochondrial specific fluorescent dye	Sigma-Aldrich
Rhodamine 6G (R6G)	989-38-8	$C_{28}H_{31}ClN_2O_3$	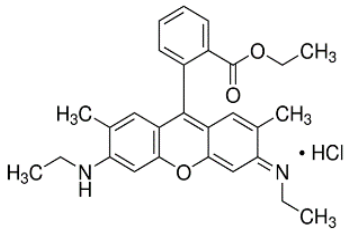	479.01	approx. 95%	Sigma-Aldrich

Chemicals/Dyes	CAS #	Formula	Structure	MW (g/mol)	Grade/Purity	Supplier
Rhodamine B (RB)	81-88-9	$C_{28}H_{31}ClN_2O_3$	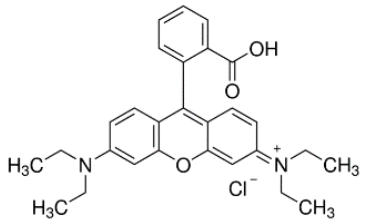	479.01	≥95%	BDH
Trifluoro acetic acid (TFA)	76-05-1	$C_2HF_3O_2$	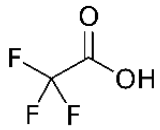	114.02	HPLC	Sigma-Aldrich
α-Cyano-4-hydroxycinnamic acid (HCCA)	28166-41-8	$C_{10}H_7NO_3$	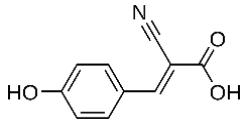	189.17	99% (HPLC)	Sigma-Aldrich

5.3 MALDI-TOF analysis of dyes and Berberine chloride on MALDI-TOF target plates

As the samples for this research involve the use of small organic dyes and drug, the first investigation was to verify the importance of matrix in contributing to the detection of these small molecules in MALDI-TOF and whether a matrix-free approach was possible. Three cationic dyes including, Rhodamine 123 (R123), Rhodamine B (RB), Rhodamine 6G (R6G) and drug standard, BC, were diluted from 1000 ppm to 50 ppm in DI and a saturated HCCA solution (7 mg/mL in TA 30) was used as a matrix without further dilution. PIM components were not involved in this experiment. The laser intensity in MALDI-TOF used was approximately 50-70% for sample without PIM components. The mass range for spectra collection was set from 200-1500 Da.

5.3.1 Ground steel BC target MTP 384

As shown in figure 5.1, one set of dye solutions was spotted (0.5 uL) directly onto the allocated wells of MALDI-TOF target plate, without HCCA while another set was immediately followed by 0.5 µL of HCCA solution and mixed gently with pipette (the total volume of the spot was 1 µL). The spots on the targets were left completely dry before inserting into MALDI-TOF instrument for analysis.

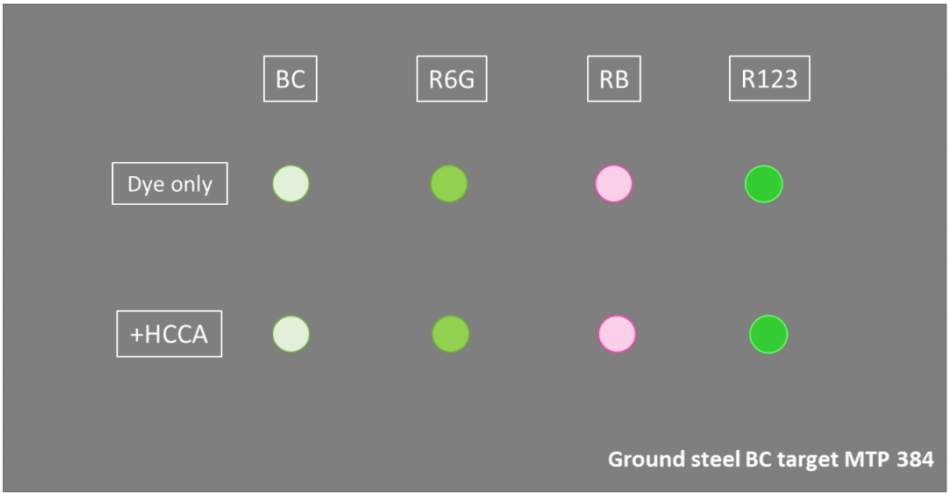

Figure 5.1. Graphic illustration showing the experimental procedure for standard solutions with and without matrix HCCA (top row and bottom row respectively) on the steel ground target plate. Total volume of each dye spot without the matrix is 0.5 uL and with matrix was 1 uL.

The spectra of all samples presented in this chapter were the highest signal intensity (from approximately more than 5 shots per sample) as the data was manually acquired via random firing of laser shots operated by user. Consequently, there was a large variation of intensity dependent on the location of the shot resulting from non-uniform distribution of self-clusters, co-crystallization with matrix, and the drying process corresponding to the abundancy of the molecules of interest [9-11].

Based on the spectra shown in figure 5.2, all analytes could be detected with MALDI-TOF with and without the matrix with the former giving higher intensity for BC (m/z 336.3 $[M + H]^+$), R6G (m/z 443.9 $[M + H]^+$), and RB (m/z 443.9 $[M + H]^+$) while opposite result was observed for R123 (m/z 345.6 $[M + H]^+$) suspecting to be a result from random shooting mentioned above. Even though the exact position of the wells on the target plate can be precisely located with engraved barcode on the plate allowing them to be electronically recognized by MALDI software, clusters or crystals on the plate surface cannot be seen with camera software as the plate was inserted into the dark vacuum tube. Samples containing HCCA generated slightly visible white grains from co-crystallization while those without HCCA were almost impossible to visualize and this could possibly be another explanation for low intensity signal. This experiment indicated that HCCA could provide better fragmentation of the small molecules generating more ions travelling to the detector; hence, higher signal intensity. However, detection of these molecules in MALDI-TOF was also possible in absence of HCCA presumably with self-fragmentation due to small molecular size and inherent charge.

5.3.2 Indium tin oxide (ITO) coated glass slide

Another target compatible for MALDI-TOF is conductive ITO glass slide (electrical resistance = 70 Ω). Similar experimental design was utilized with slight modification as illustrated in figure 5.3. Based on the sample collection on PIM described in *chapter 3*, whole blood sample containing pre-mixed BC was spotted and electrophoresis performed after the sample was dried.

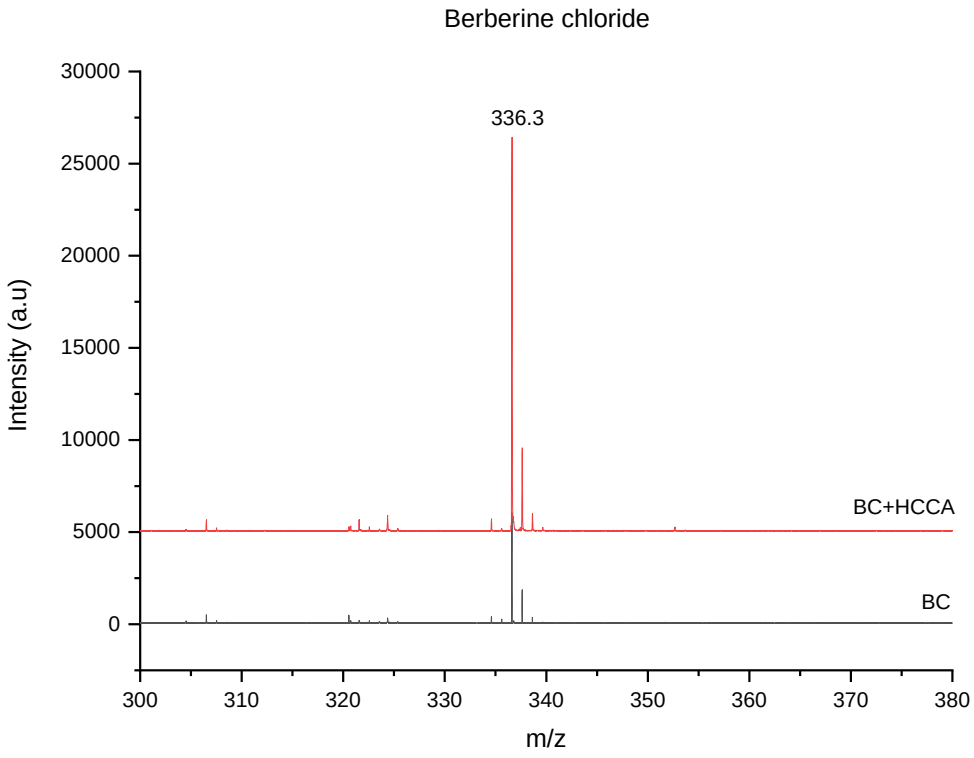
Berberine chloride
336.3
BC+HCCA
BC
Intensity (a.u)
m/z
30000
25000
20000
15000
10000
5000
0
300
310
320
330
340
350
360
370
380

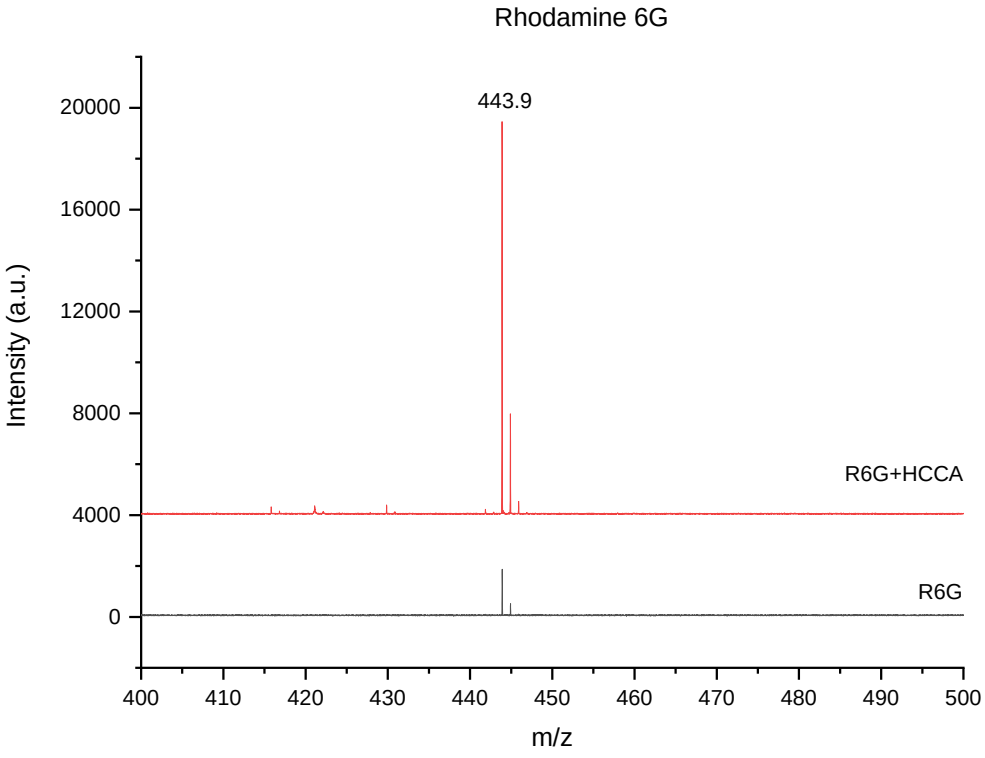
Rhodamine 6G
443.9
R6G+HCCA
R6G
Intensity (a.u.)
m/z
20000
16000
12000
8000
4000
0
400
410
420
430
440
450
460
470
480
490
500

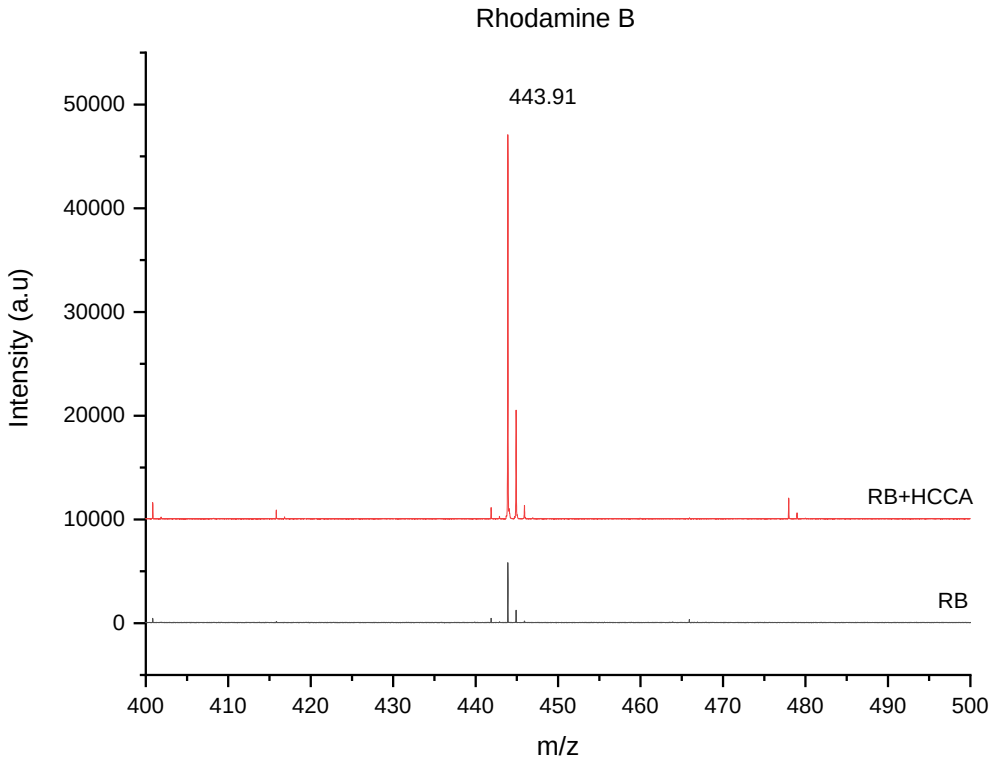

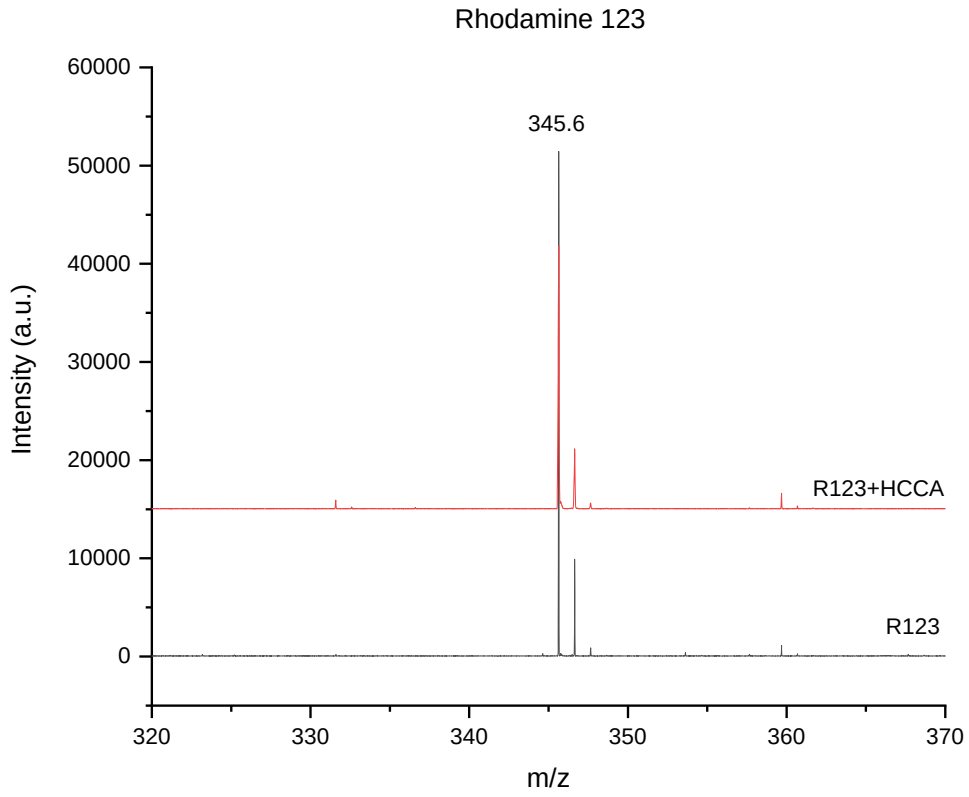

Figure 5.2. Mass spectrum of drug model, BC, and cationic dyes, R6G, RB and R123 with and without matrix (HCCA) on MALDI-TOF ground steel target plate.

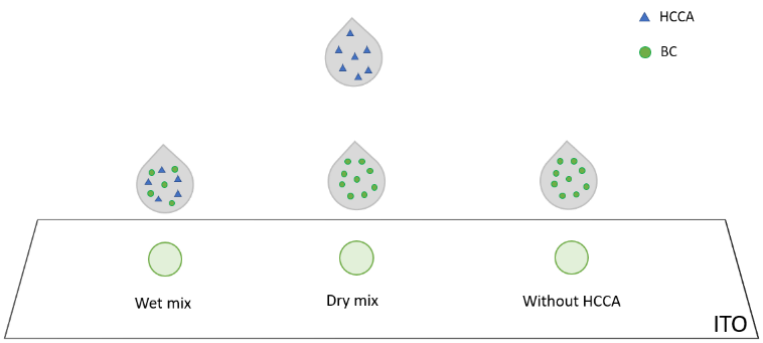

Figure 5.3. Graphic illustration showing the experimental procedure for standard solution of BC with and without matrix HCCA on the ITO glass slide. Total volume of each dye spot without the matrix is 0.5 uL and with matrix was 1 uL .

In this practical demonstration, the HCCA solution can only be applied once the device arrives at the laboratory prior to instrumental analysis. In the previous section, HCCA was mixed with BC before being spotted onto the steel ground, referring as wet mix. In this section, identical procedure was applied for ITO glass slide with HCCA added after the BC spot (0.5 µL) was completely dry on the ITO glass slide, which is referred to as dry mix, resembling in-transit portable device setting.

The result revealed acceptable signals in all three conditions with and without HCCA showing possibility of matrix-free approach on ITO glass slide (figure 5.4). Again, it was assumed that presence of HCCA might have assisted ionization of BC together with ease of locating co-crystalized crystals resulting in higher signal observed. Slight broadening of the MS peak was also observed and accumulation of ions at the laser source after multiple continuous shooting with high laser intensity was presumed a cause. Broadening was found to diminish after source cleaning.

5.4 MALDI-TOF analysis of Berberine chloride on PIM strips

5.4.1 PIM taped on ITO with carbon tape at both ends of the strips

In last section, successful analysis of small dye and drug standards from solution using MALDI-TOF was shown both in the presence and absence of matrix HCCA. However, the hypothesis

was made that the detection was possible because of the molecule crystals adhering on the surface of the plate; hence, the result might differ when they are extracted into the PIM and do not crystalize on the surface. Optimized PIM strips pre-spotted with different concentration with BC (10, 50, and 100 ppm) were analysed by MALDI-TOF. The PIM strips were taped at both ends onto the ITO glass slide using carbon tape and coated with HCCA solution using commercial electrospray coater (Image Prep™, Bruker) followed by scanning with the image scanner (the area of the scanner is limited to 20 x 25 mm) to create an image insert for MALDI imaging program as shown in figure 5.5. The ITO was locked on a plate adapter and inserted into MALDI programmed for imaging option where the laser will be automated and continuously shot through the assigned dimension with constant step size of 200 µm (horizontally and vertically) over the selected areas. An overall average spectrum and intensity profile of selected mass displayed at the end of the run could then range from hours to days depending on the area selected and step size.

A process of mass (m/z) selector will result in colour intensity profile of interested analyte in which the area where the analyte was concentrated can be located (figure 5.6). BC (m/z 336) could not be observed as shown in figure 5.6 A. When the movable mass selector (pink line)

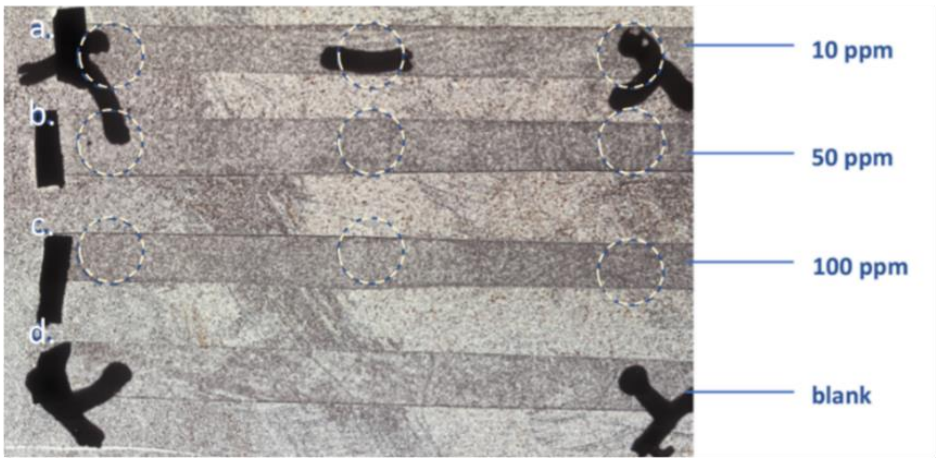

Figure 5.5. Image of optimized PIMs with (a) 10 ppm, (b) 50 ppm, (c) 100 ppm and (d) 0 ppm of BC taken with image scanner. Each PIM was containing 3 spots of BC indicated in the dashed circles. Carbon tapes are represented by black marks.

changed to m/z 379, strong colour gradient was observed (figure 5.6 B) from matrix HCCA coating all over the surface. Electrical contact between PIM and ITO was one of the main factors raised contributing to undetectable BC on the PIM as it directly correlates to amount of ionized fragments being introduced into the mass analyser [12, 13]. Even though PIM is sufficiently conductive for electromigration of BC and cations using low voltage demonstrated in *chapter 2 and 3*, this conductivity range (electrical resistance measured to be 4 MΩ) is not high enough for MALDI when compared to ITO glass. This issue was expected to be solved when the PIM were taped onto the ITO glass slide. However, since only two edges of the PIM were taped, it was further assumed that only this area with conductive tape allow direct contact between PIM and ITO while area of interest (dashed rectangle) exhibit insufficient or no conductivity during the analysis prohibiting ionization if ions.

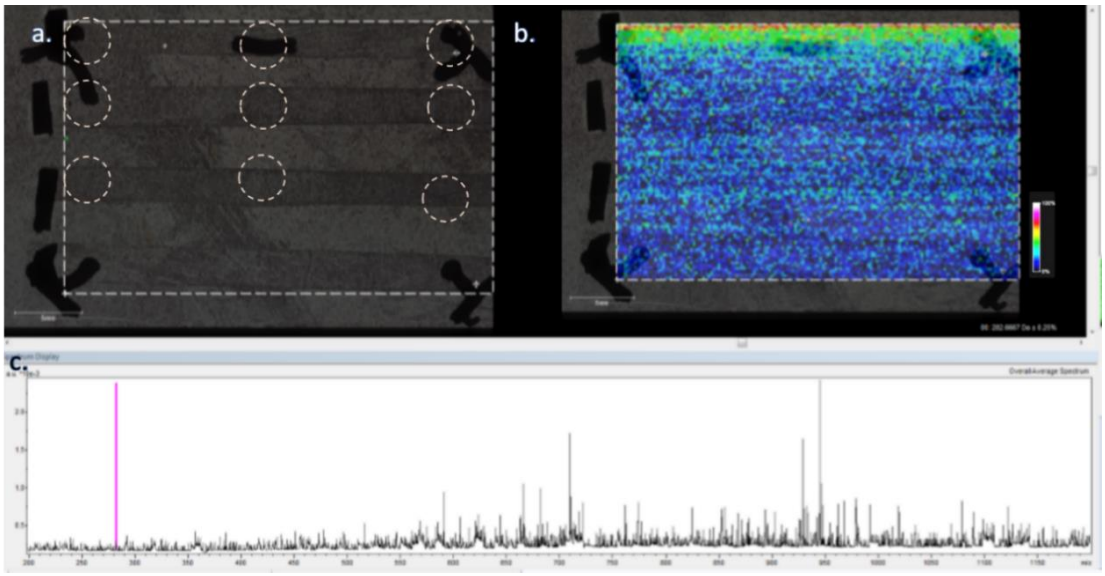

Figure 5.6. MALDI-TOF imaging result of BC sample on PIM. (A) The intensity profile of BC (m/z 336), (B) the intensity profile of HCCA (m/z 379) and (C) the overall average spectrum with mass selector (m/z 379) represented with pink line within the detected area was shown. Dashed circles indicate the locations of BC spots identical to that in figure 5.5. The scale bar indicates the intensity of the selected mass, where white and black represent 100% and 0% intensity respectively. Dashed box indicates the area selected for MALDI imaging.

Another possibility that BC was undetectable could be the excess amount of matrix HCCA crystals coated on the surface of the ITO prior to analysis. The concentration of HCCA used for MALDI is approximately 7000 ppm (7mg/mL), which is almost 100 times more concentrated than that of BC spot on the PIM. As the thickness of HCCA coating was not monitored together with unknown potential of HCCA, which is uncharged, being uptake by PIM extraction, the m/z detected was mainly corresponding with the HCCA crystals settling on the surface of PIM. Additionally, there was also a possibility that the thickness of PIM and HCCA layer could have exceeded the vertical resolution of MALDI meaning the molecules within the PIM cannot be ionized and detected as the laser cannot penetrate far enough into the PIM [14, 15].

5.4.2 PIM directly casted and dried on the ITO

In previous experiment, spots of BC on PIM with two edges being taped onto the ITO were unable to be detected with MALDI-TOF possibly due to the inadequate electrical contacts and thickness. It was then proposed that the PIM should be cast thinner than the typical thickness (which was 15-20 μm) to ensure better contact between PIM and ITO. However, casting and peeling PIM with thickness less than 10 μm was challenging as the PIM was prone to tearing. Attempts to cast different volume of PIM solution (resulting in different thickness) directly onto the ITO glass slide illustrated in figure 5.7A were then tried to maintain both the uniform contact between PIM and ITO and eliminate the peeling step allowing PIMs as thin as 5 μm to be made. However, casting PIM solution on an edge-less glass slide resulted in a non-uniform PIM as the solution did not evenly spread across the surface. There were also some heterogenous sections on PIM from uncontrollable drying which left white traces on the glass slide.

5.4.3 Entire PIM strip taped on ITO with carbon tape

Despite the positive result confirming the conductivity was the important factor for enabling analysis of BC on PIM, this method of casting PIM directly on the ITO was not an ideal approach and inapplicable for in-transit electrokinetic platform demonstrated in *chapter 3.*

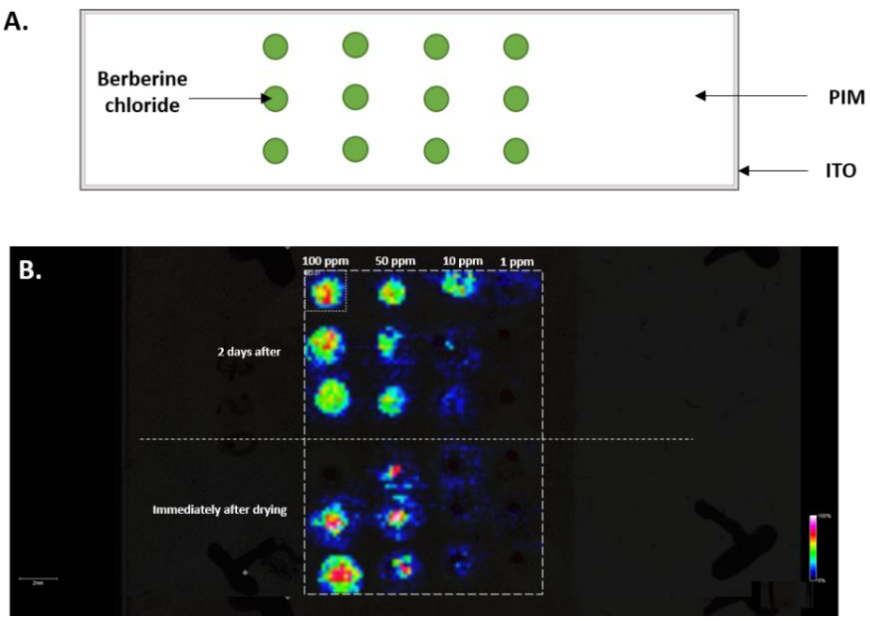

Figure 5.7. Graphic illustration of (a) MALDI preparation and (b) imaging intensity profile of 24 spots of BC with different concentration on the PIM casted directly on the ITO glass slide after 2 days of spotting (top) and immediately after the spots are dry (bottom). The scale bar indicates the intensity of the selected mass represented with pink line, where white and black represent 100% and 0% intensity respectively. Dashed box indicates the area of MALDI imaging.

Electrophoresis experiments using a PIM casted on the ITO by spotting BC solution on the PIM followed by application of voltage (2000 V) indicated no movement of the BC. It is believed that this is due to the electric current moving through the ITO rather than the PIM and that the PIM cannot be cast directly on the ITO slide. This means that the MALDI detection would have to be analysed after electrophoresis of BC in a strip format. Therefore, focus shifted to establish more uniform contact of the PIM with the ITO.

Previously, carbon tape was used to fix the PIM strips only through two edges. In this experiment carbon tape was placed along the entire length of PIM such that the entire strip is taped to the slide to make sure that all of the PIM is in contact with the ITO. The experiment includes investigation both with and without addition of matrix HCCA. BC (0.1 µL, 50 ppm) was spotted on two PIM strips: one wet-mixed and another dry-mixed with matrix HCCA and left to completely dry before taping with carbon tape. The PIM was gently pressed along its length against

the tape ensuring complete contact. The MALDI analysis was performed 1 hr later by manual operation and no imaging analysis was carried out.

As the background behind the strip is now completely opaque from the tape, it was more difficult to locate the BC spots, especially those without HCCA crystals. Selecting a large area and perform imaging with small step size (i.e. 50 µm) could resolve this problem; however, the estimated duration of the automated imaging was several hours. However, since the initial investigation was to determine if BC on PIM could be detected with this set-up (figure 5.8), a white colour marker pen was used to make the location of the spot on the ITO slide with assistance from fluorescence microscope where the green colour could be visualized. The white colour marker pen appeared opaque in the MALDI monitor against the translucent ITO so the area for laser shots could be roughly located.

The result spectra were shown in figure 5.8 in which the signal of BC could be clearly observed both with and without HCCA suggesting a successful MALDI preparation method for PIM strips. This indicate that not only the conductivity on the ITO and PIM can be effectively maintained but the thickness of layers (PIM and tape) was shown to be within the spatial resolution range of the instrument allowing ionization of molecules residing within the PIM. From a quantitative viewpoint, even though the signal intensities cannot be directly comparative due to several uncontrolled factors, a loss of signal observed for BC in PIM here may imply that the thickness of the PIM does affect the ionization efficiency when comparing to standard BC solution on the target plates. In presence of HCCA, the signals of BC observed on the steel ground (figure 5.2) and ITO (figure 5.4) were found to be approximately 5X and 40X higher than that observed in PIM respectively. On the other hand, the signal intensity of BC observed on steel ground (figure 5.2) and ITO (figure 5.4) were approximately 3X and 10X higher than in the PIM without addition of HCCA respectively. Nevertheless, this revealed that MALDI-MS might be suitable way to analyse the PIM after it is detached from the portable device.

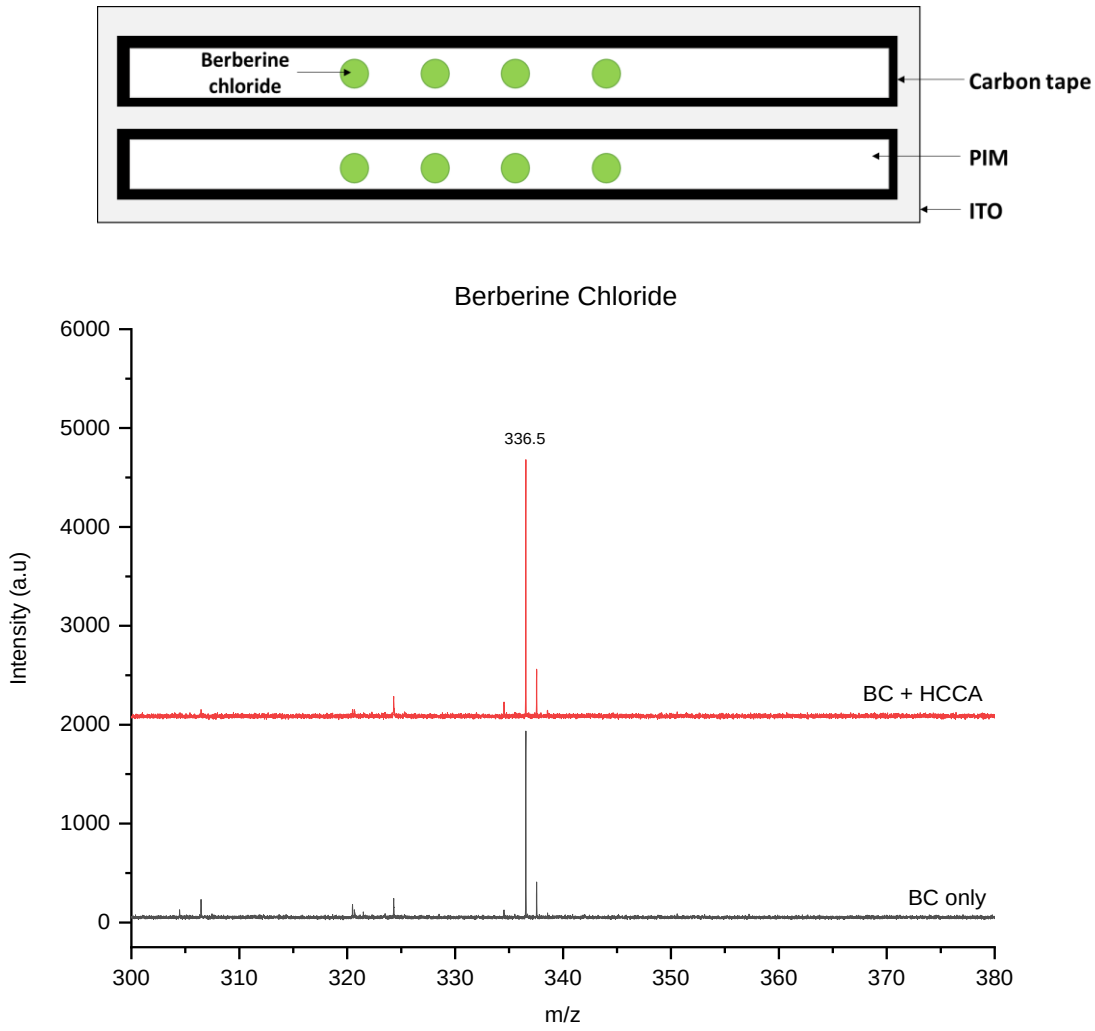

Figure 5.8. Graphic illustration of MALDI preparation and spectrum (selected from highest intensity) of BC on PIM strips being taped with carbon tape on ITO with and without matrix HCCA.

5.5 MALDI-TOF analysis of Berberine chloride on PIM strips after electrophoresis

In all previous experiments, the BC spotted on both target plates and PIM were analysed immediately after the sample was dried, 1 hour or 48 hours later; however, they were all investigated without a separation in the PIM. The next experiments were to investigate analysis of BC on the PIM strip after electrophoresis. The first experiment was to conduct electrophoresis of BC on the strip using the portable device at 24 V for 34 hours. Also, to simulate the scenario as if the drug model is non-coloured, this investigation with MALDI-TOF (100 µm step size) involved imaging feature as the location and migration distance of BC was not known.

5.5.1 MALDI imaging analysis of BC standard after its separation via in-transit electrokinetic device

The analysis of BC standard in DI (10 ppm) after electrophoresis on portable device for 34 hours was investigated. Electrophoretic process was identical to that reported for in-transit platform from *chapter 3*. After 34 hours under 24 V, the PIM was detached from the portable device and fixed with carbon tape onto the ITO as shown in grayscale image in figure 5.9. The image was taken from fluorescent microscope in this case and the white colour marker pen was used to mark location later detected and assigned within MALDI imaging program. A very bright white light in the middle of the image was a direct reflection from the fluorescent microscope against the glass slide and this has no effect with MALDI imaging.

In this situation where the spot migration distance and its location are treated as unknown, it was impossible to spot HCCA onto the exact position; therefore, HCCA solution was sprayed onto the whole surface. Instead of using commercial electrospray, with several parameter set-ups and lengthy coating time (based on the method used by Miss Liang Jiang), an off-the-shelf spray bottle was used. HCCA solution was loaded into the bottle and the ITO and PIM sprayed from approximately a single arm reach. The spraying amount was not controlled but was enough to have the whole surface of ITO covered by a small mist observable with the naked eye. The PIM on ITO was left to completely dry and automated imaging was initiated.

Assigned imaging areas were drawn as boxes (dashed yellow) based on the known migration distance of BC on PIM under 24V and to give a total scanning time of approximately 2-3 hours. Graphical illustration of the MALDI preparation, intensity profile after imaging analysis and average spectrum were shown in figure 5.9. The intensity profile revealed distribution covering a large area of the box displaying traces of detectable BC after its migration. In a typical condition, the ion source was programmed for self-cleaning at the end of each run, each dashed box for area selected, before starting the run on the area to prevent the ion accumulation from high laser power

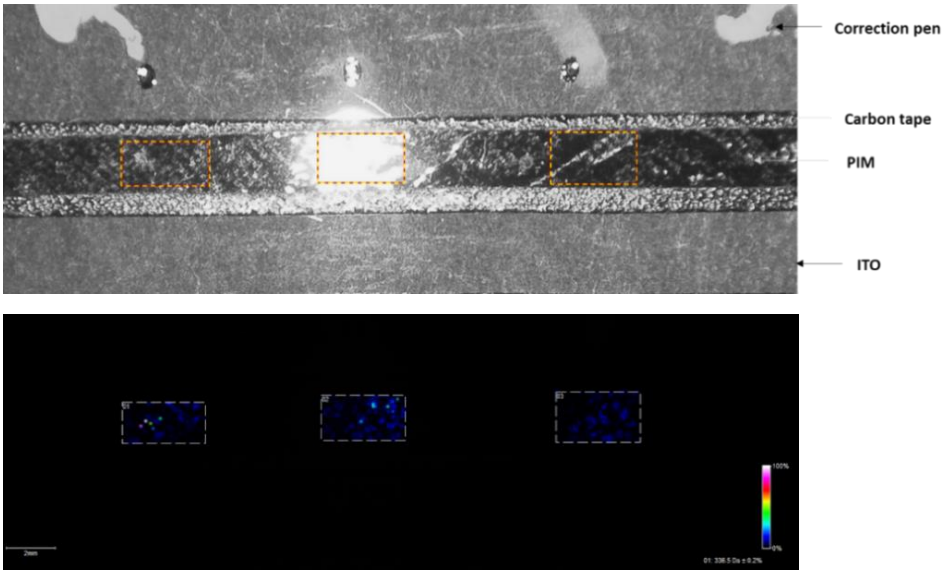

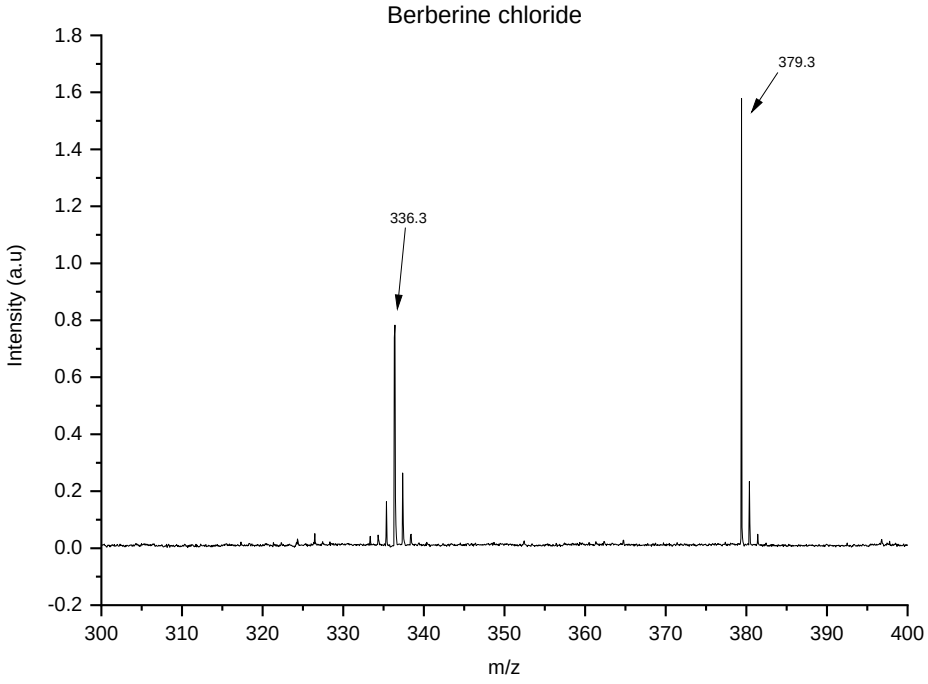

Figure 5.9. MALDI-TOF imaging result of 3 replicates of standard BC in DI on PIM after 34 hours of electrophoresis with 24V (6V/cm). The selection areas for imaging were marked in dashed yellow boxes and white boxes for original image (grayscale) and MALDI image (black) respectively. The scale bar indicates the intensity of the selected mass (336.5±0.2%) displayed in multi-colour where white and black represents 100% and 0% intensity respectively. An average spectrum detected for BC at m/z 336.3 ($[M+H]^+$) while that detected at m/z 379.3 were corresponding to HCCA ($[2M+H]^+$).

stated earlier in the chapter as possible cause of mass shift. In this case, imaging analysis for three areas were programmed to run continuously without a source cleaning step to reduce total analysis time, and this was believed to contribute to colour intensity deuteriation observed in boxes from left to right in figure 5.9. Two highest signals were observed at m/z 336.3 for BC and m/z 379.3 for matrix HCCA.

5.5.2 MALDI imaging analysis of spiked BC in whole blood sample after its separation via in-transit electrokinetic device

After the detection of the BC standard after electrophoresis, the next investigation was to perform MALDI analysis after electrophoresis of spiked BC in whole blood sample. The final concentration of spiked BC in blood matrix in this case was 10 ppm. Electrophoretic process and MALDI-TOF imaging set up were identical to those in section 5.5.1.

The intensity profile correlating to the location and distribution of BC after the electrophoresis and average spectrum were shown in MALDI image in figure 5.10. The BC was found to be located near the right end of the box indicating successful separation of molecule away from the blood spot. Furthermore, the pattern of electromigration of BC away from the blood spot correlates well with that reported in *chapter 3* (figure 3.2) with positioning distribution with the boxes agreeing well with the simultaneous diffusive enlargement of the molecules observed during electromigration.

Analysis of the spectra (figure 5.10) revealed several peaks within the selected m/z range with BC mass peaks at m/z 336.3 and the large contribution from excessive matrix HCCA at m/z 379.3 [16, 17]. The overall intensity of BC in this investigation (spiked in blood matrix) was found to be about 2X lower than that reported in section 5.5.1 with BC standard (figure 5.9) and could possibly be explained by, again, the lower concentration of BC separated from blood. In *chapter 3*, the hypothesis was made from the observation that the actual concentrations of BC observed in blood matrix were substantially lower than that in DI standards presumably due to the

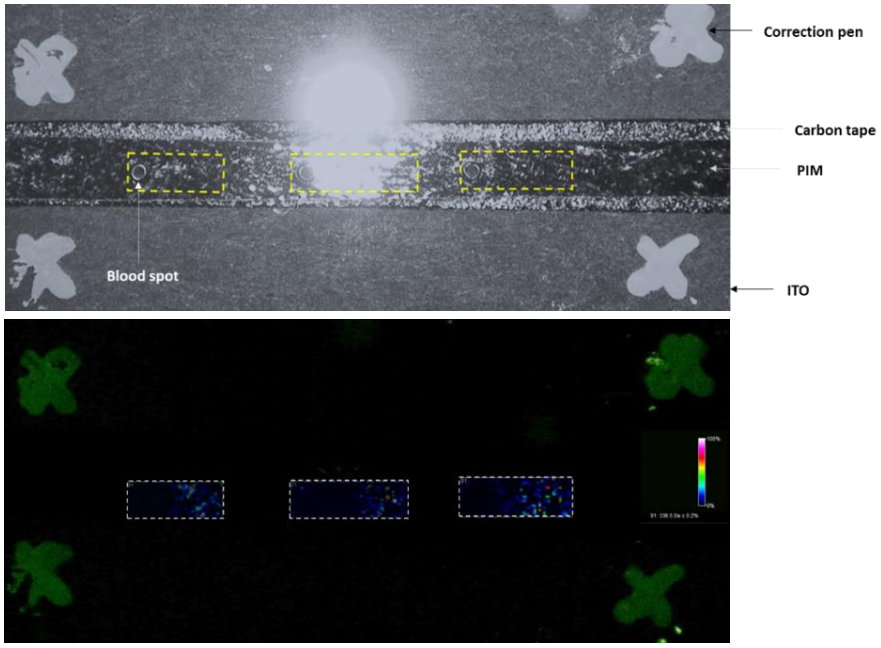

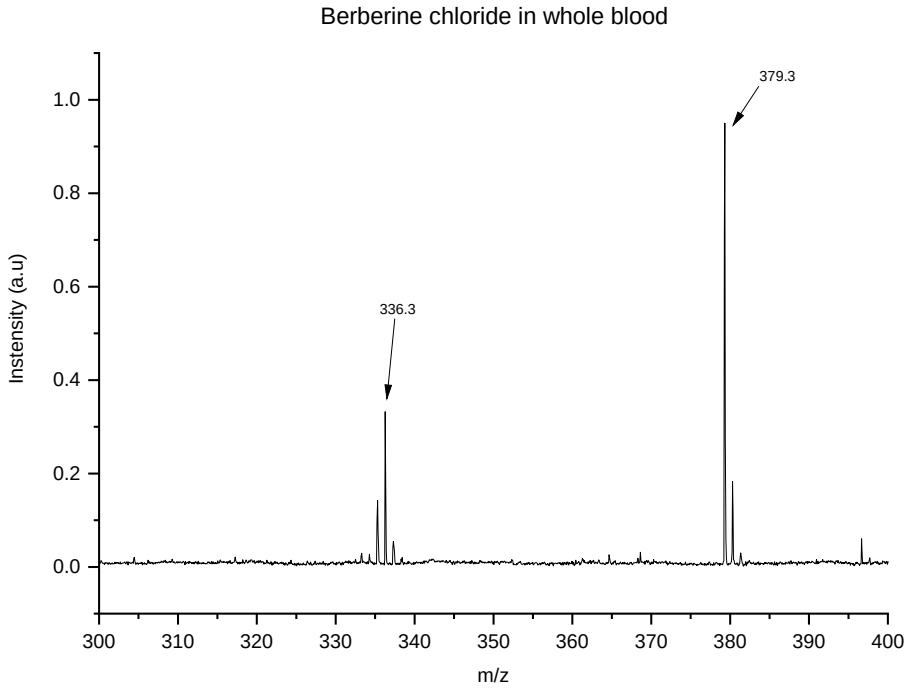

Figure 5.10. MALDI-TOF imaging result of 3 replicates of BC in whole blood sample on PIM after 34 hours of electrophoresis with 24V (6V/cm). The selection areas for imaging were marked in dashed yellow boxes and white boxes for original image (grayscale) and MALDI image (black) respectively. The scale bar indicates the intensity of the selected mass (336.5±0.2%) displayed in multi-colour where white and black represents 100% and 0% intensity respectively. An average spectrum detected for BC at m/z 336.3 ($[M+H]^+$) while that detected at m/z 379.3 were corresponding to HCCA ($[2M+H]^+$).

interaction between blood components (i.e. proteins) and BC resulting in drug-protein complex [18-21], estimated to be at least 50% based on the loss of MS signal intensity observed (figure 5.10). Here, it was also suspected that only unbound BC portions were detected by mass analyser at m/z 336.3.

In this case, it could be concluded that amount of BC molecules presented after the electrophoresis and to be detected by the mass detector decreased even though quantitative approach has not yet been fully investigated but correlates with the signal observed. Another possibility could be explained as a result from electromigration. As reported in *chapter 2*, electromigration occurs together with diffusion and dispersion resulting in molecules being less accumulated in concentrated clusters; hence; again, fewer ions to be fragmented and detected. Even though there were some issues that require further optimization to validate and effectively enhance sensitivity in analysis of BC after separation on portable platform using MALDI imaging, the result from this investigation shows the possibility of being a powerful workflow applicable for non-coloured products.

5.6 Summary and future direction

The imaging result revealed that BC at 10 ppm after separation from whole blood sample, together with their migration distance and distribution, can be analysed and detected after separation from biological sample on portable PIM platform with very simple preparation with carbon tapes and bottle sprayer for matrix solution. This concept of combining MALDI-TOF imaging analysis with portable PIM-based electrokinetic platform reported as future direction in *chapter 3* was proven possible and could potentially be applicable for practical clinical diagnostic involving non-coloured analytes. Based on this result, it was assumed that expanding m/z range window in MALDI-TOF might also allow the detection of small ions, charged electrolytes, amino acids, peptides or even proteins typically presented in blood and mainly involved in clinical blood analysis. Hence, the platform could become a very useful sample preparation for practical clinical approach.

Even though quantitation was not yet fully demonstrated and investigated, these preliminary results establish the feasibility for quantitative analysis using MALDI-TOF imaging. Therefore, it is believed that with further work, quantitative analysis would enhance sensitivity and accuracy of detection resulting in very powerful workflow for in-transit electrokinetic platform.

5.7 References

[1] N. Singhal, M. Kumar, P.K. Kanaujia, J.S. Virdi, MALDI-TOF mass spectrometry: an emerging technology for microbial identification and diagnosis, Frontiers in microbiology, 6 (2015) 791.

[2] C. Jurinke, P. Oeth, D. van den Boom, MALDI-TOF mass spectrometry, Molecular biotechnology, 26 (2004) 147-163.

[3] J.R. Yates III, A century of mass spectrometry: from atoms to proteomes, nature methods, 8 (2011) 633.

[4] A. Wieser, L. Schneider, J. Jung, S. Schubert, MALDI-TOF MS in microbiological diagnostics—identification of microorganisms and beyond (mini review), Applied microbiology and biotechnology, 93 (2012) 965-974.

[5] Z. Guo, Q. Zhang, H. Zou, B. Guo, J. Ni, A method for the analysis of low-mass molecules by MALDI-TOF mass spectrometry, Anal. Chem., 74 (2002) 1637-1641.

[6] B.M. Prentice, C.W. Chumbley, R.M. Caprioli, Absolute quantification of rifampicin by MALDI Imaging mass spectrometry using multiple TOF/TOF events in a single laser shot, Journal of The American Society for Mass Spectrometry, 28 (2017) 136-144.

[7] Y.L. Li, M.L. Gross, Ionic-liquid matrices for quantitative analysis by MALDI-TOF mass spectrometry, Journal of the American Society for Mass Spectrometry, 15 (2004) 1833-1837.

[8] C. Pan, S. Xu, L. Hu, X. Su, J. Ou, H. Zou, Z. Guo, Y. Zhang, B. Guo, Using oxidized carbon nanotubes as matrix for analysis of small molecules by MALDI-TOF MS, Journal of the American Society for Mass Spectrometry, 16 (2005) 883-892.

[9] M.W. Duncan, H. Roder, S.W. Hunsucker, Quantitative matrix-assisted laser desorption/ionization mass spectrometry, Briefings in functional genomics and proteomics, 7 (2008) 355-370.

[10] E. Szájli, T. Fehér, K.F. Medzihradszky, Investigating the quantitative nature of MALDI-TOF MS, Molecular & Cellular Proteomics, 7 (2008) 2410-2418.

[11] M. Bucknall, K.Y. Fung, M.W. Duncan, Practical quantitative biomedical applications of MALDI-TOF mass spectrometry, Journal of the American Society for Mass Spectrometry, 13 (2002) 1015-1027.

[12] T. Ozawa, I. Osaka, S. Hamada, T. Murakami, A. Miyazato, H. Kawasaki, R. Arakawa, Direct imaging mass spectrometry of plant leaves using surface-assisted laser desorption/ionization with sputter-deposited platinum film, Anal. Sci., 32 (2016) 587-591.

[13] G. McCombie, R. Knochenmuss, Enhanced MALDI ionization efficiency at the metal-matrix interface: practical and mechanistic consequences of sample thickness and preparation method, Journal of the American Society for Mass Spectrometry, 17 (2006) 737-745.

[14] A. Walch, S. Rauser, S.-O. Deininger, H. Höfler, MALDI imaging mass spectrometry for direct tissue analysis: a new frontier for molecular histology, Histochemistry and cell biology, 130 (2008) 421.

[15] C. Gregson, Optimization of MALDI tissue imaging and correlation with immunohistochemistry in rat kidney sections, Bioscience Horizons, 2 (2009) 134-146.

[16] Y. Hoyos‐Mallecot, J. Cabrera‐Alvargonzalez, C. Miranda‐Casas, M. Rojo‐Martín, C. Liebana‐Martos, J. Navarro‐Marí, MALDI‐TOF MS, a useful instrument for differentiating metallo‐β‐lactamases in Enterobacteriaceae and Pseudomonas spp, Letters in applied microbiology, 58 (2014) 325-329.

[17] K. Sparbier, S. Schubert, U. Weller, C. Boogen, M. Kostrzewa, Matrix-assisted laser desorption ionization–time of flight mass spectrometry-based functional assay for rapid detection of resistance against β-lactam antibiotics, Journal of clinical microbiology, 50 (2012) 927-937.

[18] T.C. Kwong, Free drug measurements: methodology and clinical significance, Clinica Chimica Acta, 151 (1985) 193-216.

[19] C.K. Svensson, M.N. Woodruff, J.G. Baxter, D. Lalka, Free drug concentration monitoring in clinical practice, Clinical pharmacokinetics, 11 (1986) 450-469.

[20] D.S. Hage, S.A. Tweed, Recent advances in chromatographic and electrophoretic methods for the study of drug-protein interactions, Journal of Chromatography B: Biomedical Sciences and Applications, 699 (1997) 499-525.

[21] Y.-J. Hu, Y. Liu, X.-H. Xiao, Investigation of the interaction between berberine and human serum albumin, Biomacromolecules, 10 (2009) 517-521.

Consecutive summary

A thin film made of polymer inclusion membrane (PIM) capable of performing electromigration and electrophoresis of charged molecules in an absence of electrolytes was investigated in this thesis. PIM was successfully designed and utilized as a standalone material for clinical diagnostics to address the limitations in conventional analytical techniques and clinical diagnostics such as solvent handlings, complicated sample pre-treatment procedures, expensive cost of instruments and analysis. The apparatus and application employing PIM in this lateral format and solvent-free approach has never been reported before.

PIM-based thin films were made up of cellulose triacetate (CTA) as physical film former and 2-nitrophenyl octyl ether (2-NPOE) as plasticizer enhancing flexibility of the film and ion mobility while various carriers including ionic liquids and surfactants were investigated corresponding to selectivity of different charged molecules. The “dry-to-touch” PIM was utilized in a lateral strip format to perform electromigration and electrophoresis of several dyes with different charge under an electric field. Careful optimization of PIM components revealed each constituent not only significantly contributed to the electromigration of molecules but was also essential in maintaining spot shape during migration. The principle for electromigration and electrophoresis of dyes in PIM was proposed to be combination of simultaneous mechanisms in which further investigation is still required to be conclusive. It is believed that more variations of carriers/dyes together with thorough optimization of PIM components will be able to reveal fundamental nature of both components of PIM and dyes in terms of selectivity and separation mechanisms based on their chemical structures and properties.

At the current stage, PIM can only possess single charge selector, either towards anionic or cationic molecules, based on the carrier used. A concept of a PIM strip exerting selectivity towards both anionic and cationic molecules simultaneously is one of the future perspectives to be explored using a single carrier (such as a zwitterionic surfactant) or combining two or more

carriers together. After the careful optimization, the PIM is aimed to be utilized in a therapeutic area including drug screening for overdose, toxicity, and illicit compounds as well as biomarkers and blood metabolites for health and/or disease indicator where either cation-selective or anion-selective can be selected depending on the charge of the analytes.

The PIM was successfully used as a low-voltage portable home-collection device ideal for clinical analyses where separation of drug model, Berberine Chloride (BC), from whole blood was performed while in transit. The PIM was ready to be analyzed upon arrival at the laboratory without additional treatment. This demonstrated the "in-transit electrophoresis" concept; however, several steps from PIM casting to fluorescence microscope scanning were manually operated by investigator and this sometimes results in variations between runs and reproducibility. Automation with consistent repetitive features could possibly provide more accurate and comparative results especially with microscope detection in which peak shapes and height directly corresponded to quantitative data.

In attempt to replace previous manual fluorescence intensity scanning to investigate its potential as detection aiming for more practical workflow for in-transit electrokinetic platform, portable PIM was combined with Matrix-assisted laser desorption ionization-time of flight mass spectrometry (MALDI-TOF). The integration of PIM and MALDI system was found to extend the analysis to non-colored target molecules by displaying a distribution imaging profile correlating to the mass/charge (m/z) ratio. It was suggested that quantitative data could also be obtained through MALDI; however, proper procedures for sample preparation and instrument parameters are required be able to provide very reliable quantitative data regarding the concentration of the target analytes. Since analysis in MALDI-TOF being performed automatically based on the instrument system input, the reproducibility of the runs is expected to improve; thus, better accuracy and reliable readouts. Furthermore, an in-transit electrokinetic concept coupled with MALDI-TOF could also reveal blood components such as amino acids and proteins. This might

become helpful for determination, or even quantitation, of suspected blood-binding reaction correlating to final concentration of free analyte. We believe that these proposed plans would will remarkably improve PIM electrokinetic capability together with a step closer for the platform to become applicable for pragmatic clinical analysis.